Master of Science in
Cultural Heritage Materials & Technologies

Department of History, Archaeology
& Cultural Resources Management
University of the Peloponnese

UNIVERSITY OF THE PELOPONNESE

PANAGOPOULOU AIKATERINI
(R.N. 1012201502008)

DIPLOMA THESIS:

THE MINOAN PEAK SANCTUARY AT AYIOS YEORYIOS STO VOUNO, KYTHERA: TECHNOLOGICAL INVESTIGATIONS OF BRONZE FINDS

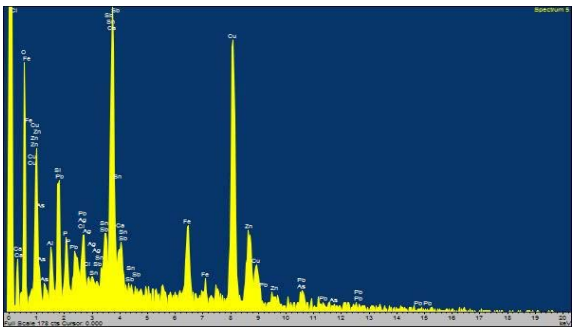

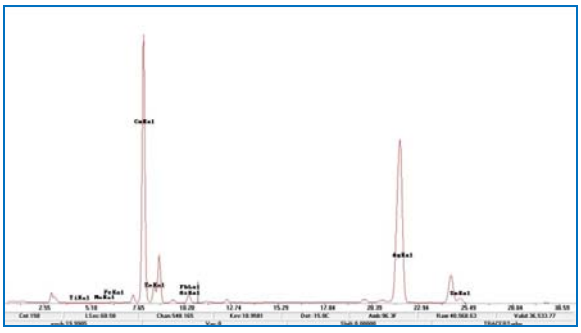

SUPERVISING COMMITTEE:
- Assistant Professor Aimilia Banou
- Associate Professor Nikolaos Zacharias

EXAMINATION COMMITTEE:
- Assistant Professor Aimilia Banou
- Associate Professor Nikolaos Zacharias
- Dr. Charilaos Tselios, Ministry of Culture

KAΛAMATA, SEPTEMBER 2016

Copyright©: Aikaterini Panagopoulou, Kalamata 2016

CONTENTS

Foreword.....4

Introduction……..6

1. The Archaeological evidence.....9

1.1 The location of the sanctuary……9

1.2 The excavation and the finds…….……..10

1.3 Objects selected for investigation…….……...11

2. Technological Investigation……13

2.1 Recording of Selected Finds…….…13

2.2 Chemical Analyses…….23

2.2.1 XRF analysis……...24

2.2.2 SEM-EDS analysis……..26

2.3 Inspection under the Optical Microscope……...27

2.4 Elemental analysis using pXRF…….44

2.5 Chemical analysis using SEM-EDS……..48

2.6 Results……52

3. Conclusions…….87

Appendix Figures.....93

Appendix I XRF Analysis: Tables and Spectra ……....98

Appendix II SEM-EDS Analysis: Tables, Spectra and Microphotographs130

Bibliography……..……193

Foreword

The current study constitutes a diploma thesis for the Master of Science in Cultural Heritage Materials and Technologies, Department of History, Archaeology and Cultural Resources Management of the University of the Peloponnese.

My engagement with the bronze finds from the peak sanctuary at Ayios Yeoryios sto Vouno, Kythera started in 1994, when metal finds from the site were transferred to the laboratory of the Archaeological Museum of Piraeus for conservation. As their details were being gradually revealed during the cleaning process, my interest in them grew and prompted me to look for new data and information which could be associated with them. This study is a starting point for the analysis of bronze finds from the peak sanctuary and the study of issues related to their technology and origin.

I would like to express my thanks to my supervisors and members of the Examination Committee, Assistant Professor Aimilia Banou, Associate Professor Nikolaos Zacharias and Dr. Charilaos Tselios, Ministry of Culture, for their constant valuable advice, targeted comments and support. I also thank the late Professor Yiannis Sakellarakis, excavator of the 1992-1994 season, for entrusting the conservation of the metal finds to me and Aimilia Banou, excavator of the 2011-2015 season who, as excavator, gave me the opportunity to deal with this very interesting topic. I like to give my special thanks to the professors of the master class for sharing their knowledge with me and to the administrative staff for the continuous support. Many thanks are due to the Laboratory of Archaeometry of the University of the Peloponnese provided the equipment for all the analyses included in the present study. I would like to express my thanks to the members of the Laboratory and especially to Mrs. Eleni Palamara for her

valuable assistance. Last but not least I would like to thank my family for their moral support throughout my effort.

Introduction

The sanctuary at Ayios Yeoryios sto Vouno, Kythera, is the only Minoan peak sanctuary, identified with certainty, so far outside Crete and one of the two Minoan peak sanctuaries found unplundered (Fig.1). It was founded in the MMIB period and reached its acme in the Neopalatial period, especially in the MMIIIB-LMIA period (Sakellarakis2011:63,167-168,200-203,261-268,281-287,289-291,298,303,323-329,333, Banou2012:1). The variety and quality of its votives, confirm the importance of the sanctuary, which not only was the peak sanctuary of the Minoan colony at Kastri, but also it was very probably frequented by Minoans travelling across the Aegean in search for metals. The most impressive category of offerings consists of bronze statuettes of Minoan adorants (113), while, a bronze figurine of a scorpion constitutes one of the most interesting finds (Banou2012:1, Banou2014:7). Other significant bronze votive offerings include human limbs, a rare cut-out of a man and another larger of a woman, a small bronze votive double axe as well as various miniature blade cut-outs and votives in form of bronze sheet[1] (Sakellarakis1996:86, Banou2012:5) (Fig.2). It is obvious that at the peak sanctuary of Ayios Yeoryios sto Vouno there is a significant peculiarity in connection to the votive offerings: the number and the variety of the bronze finds. While the bronze votive offerings found at the metropolitan Minoan peak sanctuaries are rarer than the terracotta figurines, at Ayios Yeoryios the proportion of bronze to clay offerings is reversed. In addition, the large number of bronze dedications indicates that the overseas visitors of the sanctuary were involved in metal exploitation and trade across the Aegean and with the mainland and possibly engaged in copper processing and manufacturing (Banou2007, Banou2012:4-5). Hence, they

[1] Some finds of Ayios Yeoryios, such as figurines of scorpions made of bronze or clay and clay libation tables, were not previously known from other peak sanctuaries, while other finds like clay building models, a black steatite ladle with carved inscription and mainly the bronze statuettes of Minoan adorants are extremely rare (Banou2012:1, Banou2014:2).

might have offered bronze objects in order to please or to beg the deity, requesting their protection during the trip and their safe return.

At the Cretan peak sanctuaries the cheap material used for the majority of votive offerings indicates the popular nature of cult practice, in contrast with the peak sanctuary at Ayios Yeoryios where the wealth of dedications is noteworthy (Sakellarakis1996:88-89). As copper was the base metal of this period, it was directly connected with the economy of societies and was an indication of wealth and prestige. The visitors of the sanctuary therefore, might have belonged to a wealthy class or to a high social elite group directly associated to a palatial center, which accumulated the metal and controlled their manufacturing and trade (Banou2014:8). It is worth mentioning that features indicating authority is shown in some votives. In two bronze statuettes of adorants the clothing indicates priests, while the caps in two heads indicate leading persons (Sakellarakis2013:119).

Due to its important location, the island of Kythera might have been especially included in a cyclic voyage from west Crete to the western Cyclades and back to Crete, aiming at the exploitation of the rich metallic sources of the islands (Fig.3). Any center or polity intending to establish its power in Crete by trying to exercise control also beyond the island, would be interested in the control of sea and trade routes and therefore for the island of Kythera, which, in this way and according to the archaeological evidence, became fully “minoanised” already in the MMIB period (Broodbank and Kiriatzi2007:241-243). Beyond the evidence of the metal offerings at the peak sanctuary, the archaeometallurgical investigation of copper finds from the Second Palace Period at Kastri, most likely represent semi-finished metal, probably ingots. However, the sources of the copper imported to Kythera have not, at present, established. The copper could have been introduced either as finished objects or locally manufactured ones made from imported metal which, in turn, would be ready for recycling, and

may have already gone through an earlier remelting stage, indicating the high value of this metal. Despite what this evidence is (how many objects are and of what kind), it remains possible that Kythera acted as enter-point and distribution center for raw metals, certainly for copper, as well as a location for the manufacture of objects, although there is no clear evidence for metallurgy activities at present (Broodbank et al.2007:227-235).

The aim of this thesis is to investigate issues relating to the trade network and the origin of metal findings from the peak sanctuary of Ayios Yeoryios sto Vouno, as well as, to examine the possible particularities concerning their technological characteristics. Through the investigation of bronze finds, the circulation of metals and metal objects and consequently the possible interaction of sociopolitical structures between Kythera and Crete could be estimated. By means of analytical techniques, the chemical composition of copper-based finds could be clarified, and the type of the alloy used identified, resulting to a possible estimation of the correlation of finds with other of similar composition.

For this purpose, nineteen small objects from the sanctuary were analyzed with the methods of X-ray Fluorescence and Scanning Electron Microscope coupled with Energy Dispersive X-ray Spectroscopy in the laboratory of Archaeometry of the University of the Peloponnese[2]. The results of the measurements were recorded, classified, correlated, evaluated and they are presented in the following chapters. In the first chapter, the location of the sanctuary, the excavation and the findings as well as the selection of finds for this research are presented. In the second chapter the methods of the investigation, the measurements and the selected objects and their results are

[2] The bronze finds were analyzed in accordance with a permission (protocol number: ΥΠΠΟΑ/ΓΔΑΠΚ/ΔΣΑΝΜ/ΤΕΕ/Φ77/168075/101301/2735) granted by the Directorate of Conservation of Ancient and Modern Monuments of the Hellenic Ministry of Culture and Sports.

discussed, followed by the conclusions. Finally, all measurements and their spectra are included in the Appendix.

1. The Archaeological evidence

1.1 The location of the sanctuary

Ayios Yeoryios sto Vouno is located in the southeast of the island of Kythera on a hill named after one of the two byzantine churches standing on its top, namely Ayios Georyios and Panayia Myrtidiotissa (Fig.4). The peak sanctuary rises to an altitude of about 350 m and within a short distance, just four kilometers, from the Minoan settlement in Kastri (Banou2012:2). Moreover, the top of the hill offers a panoramic view stretching from Kavo-Malias and Taygetos in the Southeastern Peloponnese, to the South-Western Aegean and Crete. It is noteworthy that, in clear days, to the South, not only Antikythera and the mountains of Crete are seen, but also the White Mountains and the Psiloreitis, while to the East, the Cyclades are seen (Banou2012:2, Banou2014:2). In this way, the sanctuary at Ayios Yeoryios sto Vouno overviews not only a large part of Kythera but also, more importantly, a large portion of southeastern Aegean, crucial for the Minoan sea routes, shared by all Minoan peak sanctuaries, which not only overlook palaces and important settlements but also act like guarding points (Sakellarakis2013:8-12) (Fig.5). As a site, therefore, Ayios Yeoryios presents all typical topographical characteristics of peak sanctuaries: accessibility, proximity to the main settlement of the area, general prominence and visibility (Sakelarakis2013:138).

More specifically, Ayios Yeoryios, still nowadays, represents a benchmark to sailors approaching Kythera either from the south or from southeast, as it is visible mainly from the south. It constitutes one of the special spaces that,

somehow, control, supervise and guard large marine areas in the eastern Mediterranean (Kourkoumelis2011: 97-98). The access to the highest point of the Ayios Yeoryios peak, nowadays, is from the east. The abundant deposits of Minoan pottery which have been revealed during the surface survey and the excavation of the site on the South slope, indicate however, that in the past the access to the sanctuary was probably from the West, in constant view with the settlement of Kastri and its surrounding area. (Banou2014:3,Banou2015:2). Excavation concentrated on the top, in front of the two churches, on the northern but mainly on the southern slope. Cult activity, however, must have taken place mostly on the top, from where, finds were fallen in the course of time. (Sakallarakis2011:148-149,Banou2014:3, Banou2015:2).

1.2 The excavation and the finds

The sanctuary was firstly excavated by Yannis Sakellarakis, from 1992 to 1994 (Sakellarakis2011:147). The archaeologicfal investigation of the site was resumed from 2011 to 2015, by Emilia Banou, of the Department of History, Archaeology and Cultural Resources Management, of the University of the Peloponnese.

Bronze Age material was recovered from all terraces, from north to south, despite the fact that the site was in use also in later periods, even with internals. Unmixed Bronze Age material was mainly found in cavities of the rock (Sakellarakis2011:333-334). No architectural remains certainly associated with the sanctuary have been found, but other finds associated with it are abundant, mostly pottery and votives typical of Minoan peak sanctuaries. Bronze figurines of adorants are the most important category of offerings, while the significance of the sanctuary is demonstrated further by the large number of other votives, made of bronze or clay such as figurines

of animals, human limbs, bronze miniature blades, bronze sheets, fragments of building models, fragments with landscape representations, parts of stone tools and vessels, mainly libation tables and ladles, while a black steatite ladle that bears a Linear A inscription carved on the lip constitutes one of the most interesting and unique finds[3]. Other finds typical of Minoan cult practice that came to light are miniature clay pairs of horns of consecration and a small bronze votive double axe the prime symbol of Minoan Crete (Sakellarakis2013:70-79, Banou2012:5) (Fig.6,7). Additionally, the discovery of unworked pieces of lapis lacedaimonius and rosso antico, as well as pieces of ingots and bronze casting residue are worth mentioning (Sakellarakis2013:150).

The peak sanctuary at Ayios Yeoryios sto Vouno stands out for the number of copper finds, in contrast with the rest of Minoan peak sanctuaries, where the majority of votives is of clay. The bronze figurines of adorants in particular, as valuable offerings and not marketable products were related to the religious - political influence and propaganda of Crete at key points of the Aegean (Sapouna-Sakellaraki2012: 5-6). This fact, combined with the prominent place of the sanctuary, confirms that Kythera participated in the Aegean metals trade network and suggests that the peak sanctuary at Ayios Yeoryios sto Vouno might have been connected with an important Cretan centre, maybe Knossos, in its Neopalatial phase (Banou2012:1).

1.3 Objects selected for investigation

The selected objects were uncovered in 2011 and 2012 and they are seven objects or fragments made from bronze sheets, one bronze figurine base,

[3] The inscription bears three signs of Linear A, transliterated as *da-ma-te*, on the basis of phonetic values of Linear B assigned to them. This transliteration is reminiscent of the name of the goddess Demeter (Sakellarakis, Olivier1994:347-351).

four vessel fragments and seven pieces of casting residues. We tried to include fragments from different types of finds in order to arrive at conclusion regarding the alloys which have been used in the manufacture of objects intended for different uses. Moreover, since there is a correlation between the composition and the intended use of artefacts, and their properties, apart from the manufacturing technique, largely depend on the type of the alloy used for their manufacture, we thought that the study of fragments from different types of articles could provide a clearer picture of the source of the raw materials used in their manufacture.

Through the chemical analysis, we tried to identify the alloys which have been used for the manufacture of objects and to investigate issues related to the provision so such raw materials, and the way they reached Ayios Yeoryios sto Vouno, either as manufactured objects or as ingots. Furthermore, taking into consideration that different types of copper alloys were used in the course of time, and since the site was used not only during the prehistoric but also during the Byzantine and post-Byzantine period, we tried to estimate chronologically some finds, based on the chemical analysis of their composition. It should be noted here that the selection of the sheet bearing an incised representation (catalogue number: KYT_AYV_BS_19) was based on the difference of its appearance in relation to all other bronze finds of the sanctuary. We tried therefore to recognize its composition, to clarify its authenticity, and possibly, to look for other artefacts made of similar alloys in the prehistoric time. The assemblage of casting residues which has been selected, is interesting not only for the investigation of potential sources of raw materials, but also for the elucidation that they are related to metal spills, and hence, they might indicate a local production of offerings.

2. Technological Investigation

2.1 Recording of Selected Finds

To facilitate the study and the evaluation of results, the objects were divided into four categories based on their typology: seven pieces of bronze sheets, seven pieces of bronze wastes, one metal fragment from the base of a figurine and four bronze vessel fragments from the rim, body and handle of vessels. Cut-outs, miniature blades, shapeless copper-based sheets as well as a copper-based sheet with a leg incision compose the bronze sheets group. The characterization "waste" was given to the amorphous metal lumps, which, based on their small size and lack of defined shape, are probably metal spills. The objects were first visually inspected for their morphology, corrosion pattern and general appearance. The description of the artefacts (after the cleaning treatment) and contextual information are presented in the following catalogue. Abbreviations used are KYT: Kythera, AYV: Ayios Yeorgios sto Vouno, BW: bronze wastes, BS: bronze sheets, FB: figurine base, VF: vessel fragment, 01-19: sequence number.

CATALOGUE

<table>
<tr><td>KYT_AYV_BS_01</td><td colspan="3">Bronze Sheet</td></tr>
<tr><td rowspan="2"> 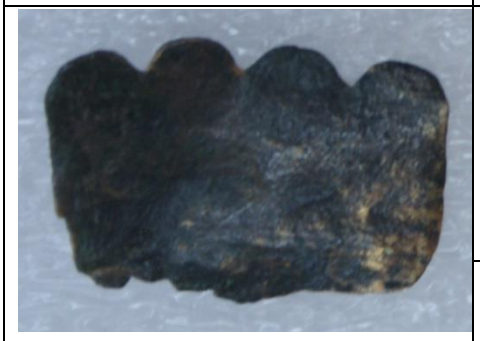 </td><td>Weight: 1.5gr</td><td>Dimensions (max.)
Length: 2.7cm
Width: 1.9cm
Thickness: 0.1cm</td><td>Excavation date: 22/07/2011</td></tr>
<tr><td colspan="3">Excavation data:
From rubble of retaining wall</td></tr>
<tr><td colspan="4">Macroscopic description:
Copper-based metal cut-out sheet; covered by thin, dark green patina; formed with curved notches at one end; both surfaces almost flat; light bending in the middle; free corroded metal appears locally.</td></tr>
</table>

KYT_AYV_BS_02	Bronze Sheet		
	Weight: 2.8gr	Dimensions (max.) Length: 4.2cm Width: 2.5cm Thickness: 0.2cm	Excavation date: 22/07/2011
	Excavation data: From rubble of retaining wall		
Macroscopic description: Small, shapeless copper-based metal sheet with a hole on the edge; covered by thin, dark green patina; partially bended; both surfaces almost flat; metal released from corrosion products appears locally.			

KYT_AYV_BS_06	Bronze Sheet		
	Weight: 0.4gr	Dimensions (max.) Length: 3.0cm Width: 0.7cm Thickness: ≤0.1cm	Excavation date: 22/07/2011
	Excavation data: From rubble of retaining wall		
Macroscopic description: Miniature blade; copper-based metal sheet; ripped at one end - cut at the other; both surfaces almost flat; slightly bended; covered by green corrosion products; flaking of corrosion layers occurs locally on one side; free corroded metal appears locally.			

KYT_AYV_BS_07	Bronze Sheet		
	Weight: 2.3gr	Dimensions (max.) Length: 3.2cm Width: 2.4cm Thickness: 0.2cm	Excavation date: 19/07/2011
	Excavation data: From rubble of retaining wall		
Macroscopic description: Small shapeless copper-based sheet; both surfaces almost flat; partially bended; covered by green corrosion products; flaking of corrosion layer appears locally, released un-corroded bulk metal.			

KYT_AYV_BS_08	Bronze Sheet		
	Weight: 1.6gr	Dimensions (max.) Length: 3.0cm Width: 2.5cm Thickness: 0.1cm	Excavation date: 25/07/2011
	Excavation data: From rubble of retaining wall		
Macroscopic description: Small shapeless copper-based sheet; both surfaces almost flat; bended perpendicularly in the middle; covered by green corrosion layers; free corroded metal appears locally.			

KYT_AYV_BS_10	Bronze Sheet		
	Weigh: 0.9gr	Dimensions (max.) Length:2.6cm Width: 0.8cm Thickness: 0.1cm	Excavation date: 19/07/2011
	Excavation data: From soil sieving - Trench IA		
Macroscopic description: Miniature blade; copper-based metal sheet; slightly bended in the middle; both surfaces almost flat; covered by green patina; one end turned upwards; metal released from corrosion products appear locally.			

KYT_AYV_BS_19	Bronze Sheet		
	Weight: 2.1gr	Dimensions (max.) Length:5.3cm Width: 3.2cm Thickness: 0.1cm	Excavation date: 21/07/2011
	Excavation data: From rubble of retaining wall		
Macroscopic description: Rectangular copper-based sheet with a probable leg incision on the center; on the perimeter repoussé dot decoration; suspension hole in the middle of upper edge; yellowish color on the front - silver appearance on the back; greenish and gray-black corrosion products appear locally in very thin layers; black spots unevenly distributed mainly on the back.			

KYT_AYV_FB_03	Figurine Base		
	Weight: 15.35gr	Dimensions (max.) Length: 2.6cm Width: 1.7cm Thickness: 0.9cm	Excavation date: 19/07/2011
	Excavation data: Section IA - Pass		
Macroscopic description: Copper-based metal fragment from a figurine base; covered by corrosion layers; circular shaped and broken by nearly half; both surfaces smoothed; encrustations of soil impurities and corrosion products formation remain locally; free corroded metal in the place of the figurine.			

KYT_AYV_BW_04	Bronze Waste		
	Weight: 10.5gr	Dimensions (max.) Length: 2.4cm Width: 1.5cm Thickness: 1.75cm	Excavation date: 22/07/2011
	Excavation data: From soil sieving - Trench I		
Macroscopic description: Amorphous copper-based metal lump; one surface almost plane; covered by green corrosion product; encrustations of soil impurities appear in some cavities; surface morphology probably indicates a spill.			

KYT_AYV_BW_05	Bronze Waste		
	Weight: 5.8gr	Dimensions (max.) Length: 2.2cm Width: 1.5cm Thickness: 1.75cm	Excavation date: 25/07/2012
	Excavation data: South side - Trench III - Pass 8B		
Macroscopic description: Amorphous copper-based metal lump; rounded but rough surfaces; covered by green corrosion products; soil impurities appear in cavities; surface morphology probably indicates copper prills.			

KYT_AYV_BW_14	Bronze Waste		
	Weight: 6.55gr	Dimensions (max.) Length:2.1cm Width:2.0cm Thickness: 0.7cm	Excavation date: 19/07/2011
	Excavation data: From soil sieving Section IA		
Macroscopic description: Amorphous copper-based metal lump; crude surfaces; covered by dark green corrosion products; calcareous and soil conglomerates in cavities; surface morphology probably indicates a spill.			

KYT_AYV_BW_15	Bronze Waste		
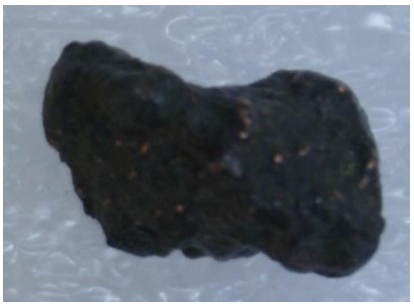	Weight: 5.6gr	Dimensions (max.) Length:1.8cm Width: 1.1cm Thickness: 1.0cm	Excavation date: 19/07/2011
	Excavation data: From soil sieving - Trench IA		
Macroscopic description: Amorphous copper-based metal lump; one surface almost plane, crude the others; covered by dark green corrosion products; soil encrustations appear in cavities; surface morphology probably indicates a spill.			

KYT_AYV_BW_16	Bronze Waste		
	Weight: 13.75gr	Dimensions (max.) Length:2.8cm Width: 1.8cm Thickness: 1.7cm	Excavation date: 18/07/2012
	Excavation data: Trench IIB - Pass 5		
Macroscopic description: Amorphous copper-based metal lump; two plane surfaces; covered by dark green corrosion products; encrustations of soil impurities appear locally in cavities; small holes on the surface due probably to steam export during melting process.			

KYT_AYV_BW_17	Bronze Waste		
	Weight: 2.4gr	Dimensions (max.) Length:1.6cm Width: 1.0cm Thickness: 0.5cm	Excavation date: 18/07/2012
	Excavation data: Trench IIB - Pass 5		
Macroscopic description: Amorphous copper-based metal lump; covered by dark green corrosion products; one surface almost plane, crude the others; surface morphology probably indicates a spill.			

KYT_AYV_BW_18	Bronze Waste		
	Weight: 1.3gr	Dimensions (max.) Length: 1.0cm Width: 0.7cm Thickness: 0.7cm	Excavation date: 18/07/2012
	Excavation data: Trench IIB - Pass 5		
Macroscopic description: Amorphous copper-based metal lump; rough surfaces; covered by dark green corrosion products; calcareous and soil conglomerates in cavities; surface morphology probably indicates a spill.			

KYT_AYV_VF_09	Vessel Fragment		
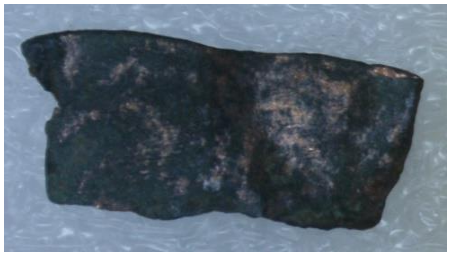	Weight: 1.6gr	Dimensions (max.) Length:3.2cm Width: 1.3cm Thickness: 0.1cm	Excavation date: 19/07/2011
	Excavation data: From soil sieving - Trench IA		
Macroscopic description: Copper-based fragment, probably from vessel rim; both surfaces almost flat; bended partially; covered by green patina; free corroded metal appears locally.			

KYT_AYV_VF_11	Vessel Fragment		
	Weight: 3.9gr	Dimensions (max.) Length:4.0cm Width: 2.0cm Thickness: 0.1cm	Excavation date: 19/07/2011
	Excavation data: Terrace 5 - Surface find		
Macroscopic description: Copper-based fragment from vessel rim; covered by green patina; smoother outside than inside; two engraved parallel grooves externally denote the start of outcurved rim; metal turns inwards to form the rim; free corroded metal appears locally.			

KYT_AYV_VF_12	Vessel Fragment		
	Weight: 2.5gr	Dimensions (max.) Length:2.5cm Width: 1.8cm Thickness: 0.1cm	Excavation date: 19/07/2011
	Excavation data: Terrace 5 - Surface find		
Macroscopic description: Copper-based fragment from vessel body; covered by green patina; smoothed both surfaces; parallel grooves inside, maybe imitating wheel; parallel grooves externally in the beginning of the base; free corroded metal appears locally.			

KYT_AYV_VF_13	Vessel Fragment		
	Weight: 4.1gr	Dimensions (max.) Length:1.6cm Width: 2.2cm Thickness: 0.3cm	Excavation date: 19/07/2011
	Excavation data: Terrace 5 - Surface find		
Macroscopic description: Copper-based fragment, probably from vessel handle; on the outside start of embossed decorative elements; almost flat inside; covered by green corrosion layers; free corroded metal appears locally.			

2.2 Chemical Analyses

X-ray Fluorescence and Scanning Electron Microscope coupled with Energy Dispersive X-ray Spectroscopy are the selected chemical analysis methods for this research. These methods aim mainly to the study of chemical composition of metals. They can provide quick results with considerable accuracy, while they do not cause any damage to the objects being examined which, if necessary, can be re-examined in the future by other methods. They are sensitive to most elements which exist in the copper alloys and they enable to more than one element to be determined from a single measurement. Their main advantage, however, is that they are non-destructive methods. The selected objects can to be introduced within the analysis area of the SEM instrument without prior sampling since their dimensions are small. The non-destructiveness and non-invasiveness make these methods an irreplaceable tool for analyzing copper alloys objects. Consequently, they have become standard methods used to the investigation of copper alloys, regarding their composition, their production technologies, their origin and also their authenticity (Musilek et al. 2012:1193-1194, 1200).

The application of a non-destructive technique aims to the examination of a metal object without the removal of a sample, in a few seconds without further preparation. In this way, the qualitative and quantitative results are obtained from the metal surface. Nevertheless, it should be pointed out that the analytical data may be influenced by several factors such as the heterogeneity of metal alloys, the presence of corrosion layers and the conservation processes. Once any corrosion or patina product is removed, the X-rays can be directed to the pure metal phase, however in case that only the surface coatings are analyzed, the accuracy of the results regarding the composition of the metal bulk under the surface patina is questionable

(Liritzis and Zacharias2011:123). Therefore, the surface layers have to be removed before applying the aforementioned methods.

The metal objects under study underwent a conservation treatment at the laboratory of the Archaeological Museum in Piraeus by the writer. Because the patina may be protective and prevent further corrosion, this operation was performed according to the principles of the metallic objects conservation. The removal of corrosion products was carried out by mechanical way, using dental wheel, scalpel and glass-brush, excluding the use of chemical substances. The layers of corrosion products were decreased as much as possible, preventing any damage of the surface. In the course of treatment, the cleaned surface examined periodically, since a shiny appearance does not guarantee that uncorroded metal has been reached.

In the following chapters the XRF and SEM-EDS methods are briefly described, in order that the possibilities of each method but also their limits become apparent. These are important factors to be taken into account for the interpretation and evaluation of the analyses results.

2.2.1 XRF analysis

The X-ray fluorescence technique has been one of the most successful techniques used for the investigation of ancient metal objects. The portability of XRF spectrometers makes them suitable for in situ investigation and extends their use to the analysis of objects of any shape and size (Ferretti 2014:1753-1754). The XRF spectrometers allow the completely non-destructive examination of the artefacts, simultaneous multi-elemental detection, wide analytical range, high analytical sensitivity and fully implemented quantitative analysis, whenever necessary. The analytical range of the spectrometer extends from the atomic number Z=13

(Aluminum), in the case of high concentration (~1-2%), but practically from Z= 14 (Silicon) up to Z=92 (Uranium), under two operation modes, the unfiltered one, with the high voltage set at 15kV and the filtered one, with the high voltage set at 40kV. The filter improves the sensibility in the detection of trace or minor elements and allows the efficient excitation of medium Z elements. The filter mode is used for the analysis of metal alloys (Karydas 2007:419-421). The XRF method is not effective for the analysis of low atomic number elements, which, when present in small amounts, are undetectable by XRF spectrometer (Ferretti 2014:1755-1756). Some trace elements can be detected in concentrations up to 10-100ppm, depending on the material and the element which is detected. In general, when the measurement time is increased, the detection limit is reduced, but this does not mean that trace elements in extremely small concentrations can be detected (Lyritzis2007:152). As far as copper alloys are concerned, however, several minor elements occur in sufficiently high amounts to be detected by XRF spectrometers. Given that these minor elements have larger variation ranges, they are more effective discriminators than major elements. The elemental composition can be an indicator of the manufacturing technique, for example hammer parts of an object always contain less lead than the cast parts (Ferretti 2014:1755-1756). Nevertheless, lead can vary widely within large sculptures due to separation by gravity during the casting process. Such variations can be correctly identified by XRF analysis allowing a non-destructive spots examination, and so, a representative result can obtained. This is a significant advantage over methods that require sampling, since the result from a single analysis may not be indicative of the alloy composition of an entire object (Smith2012:40).

The analytical XRF signal, namely the characteristic X-rays of the constituent elements, originate mostly from a thin surface layer extending to

a few microns, depending on the metal composition and the detected X-ray energy. (Karydas et al. 2004:16). Since it concerns a surface analytical method, only a thin layer on the surface of an artefact can be analyzed, whereas variations in the surface roughness and heterogeneities can cause a measurement error. (Musilek et al. 2012:1200). It should be noted, finally, that for a quantitative investigation with the XFR method a calibration with standard samples is required, while the measurements accuracy depends on the morphology of the sample and object, their solid geometry, and also placement in XRF device, since the angle formed between the investigated surfaces and the direction of the beam affects the measurements (Lyritzis2007:152).

2.2.2 SEM-EDS analysis

Examination of the objects at high magnifications and elemental analysis can be conducted under Scanning Electron Microscope (SEM) with Energy Dispersive Spectroscopy (EDS) bulk analyses from surface to core and semi-quantitative line scanning that is performed under the SEM (Tselios et al.2015:82). It uses electron beams, instead of light, and thus magnifications up to 30000 (1μm) are achieved. Its operation is based on the interactions of an electron beam with the area being examined. The large focusing ability and the magnification change possibility, combined with the fact that no sampling is required, have established SEM-EDS as a basic and essential research instrument. The intensity of the emitted electrons is influenced by the composition (backscattered electrons) and surface topography (secondary electrons). The interactions between beam and object are recorded by the sensors and converted into an image. By applying a system of detection and dispersion of X-ray energies, semi-quantitative elemental analysis of the material can be acquired (Lyritzis2007:206-209).

Backscattered electron images in the SEM display compositional contrast that result from different atomic number elements and their distribution. EDS allows the identification of these particular elements and their relative proportions. SEM-EDS are not a surface analysis technique and it provides qualitative and quantitative elemental bulk analysis, while it can provide spot analysis of inclusions and micro phases, which is very important for the study of alloys. Due to the fact that X-rays are generated from very deep in the interaction volume, the units of spatial resolution are microns. The size of the interaction volume increases with accelerating voltage and thus it is common to use intermediate accelerating voltage to ensure the peaks which are considerable to record (Hafner 0000:1-5). I should be noted, however, that in the SEM-EDS analysis, a difficulty occurs in the discrimination of some peaks, belonging to common elements of copper alloys such as arsenic, lead and sulfur (Georgakopoulou and Basiakos2015:348).

2.3 Inspection under the Optical Microscope

The objects were first inspected and photographed using an optical microscope at magnifications 15X and 50X and internally lit LED, without further treatment, while examination at 200X magnification was executed, when necessary. A portable optical microscopy device was used, made by the i-Scope-Moritex Company, with a source of Light Emitting Diodes (LED) system, in visible light. The additional possibility of using polarized light to refute the refraction of natural light was available. The device was connected to a portable computer for the digital recording and management of photos. By means of magnification, the morphology of the surface is examined and details on the composition and texture are sought, while micro-photographs of particularities and material phases were obtained (Lytitzis2007:212).

Initially by using X15 and X50 magnifying lenses, the effects of the cleaning treatment were evaluated, namely, if free corroded areas beneath the layers of corrosion products, from which could be taken accurate measurements, have been appeared. These areas were then pointed for analysis. Moreover, areas of particular interest, such as discontinuities or other elements that would merit further investigation, were sought.

It was found that, in general, the state of preservation of all the objects is good. There is metal core and areas where the bulk metal has been disclosed. The rest of the metal surface is covered by thin layers of corrosion, patina, which as estimated, could be penetrated by the beam of X-rays during the analysis process. Limited soil remains embedded within surface's micro-cracks and micro-cavities were distinguished on the bronze sheets and on the figurine base, while on the wastes, encrustations or/and agglomerates, due to either adhesion of soil and salts impurities or formation of corrosion products, were distinguished into the roughest surfaces and where there are surface's deep and abrupt anomalies.

Further examination at magnification 200X was performed where needed, as in the case of metal wastes. Since their surface morphology maybe indicate copper prills, features which confirm that it concerns solidified molten metal, were looked for. Indeed, the existence of copper prills is established, which sometimes are corroded, or surrounded by copper oxides (for instance in the cases of KYT_AYV_BW_04, KYT_AYV_BW_05, KYT_AYV_BW_14 and KYT_AYV_BW_18), whilst, in some cases copper prills were surrounded also by iron oxides (e.g. KYT_AYV_BW_15 and KYT_AYV_BW_16). Moreover, calcareous conglomerates were localized, which may be present in the ore or produced by the erosion of furnace material due to the use of calcium during smelting (for example KYT_AYV_BW_04, KYT_AYV_BW_16 and KYT_AYV_BW_17). A characteristic porosity formed during the flow and cooling of the metal was

also observed. This porosity is caused by gases and forms holes due to the steam export during the melting process. The steam could be produced, as a combustion gas, by the firing of the used wood and the void spaces arose from air and steam trapped during the casting of the molten metal (for instance in the cases of KYT_AYV_BW_04, KYT_AYV_BW_05, KYT_AYV_BW_14 and KYT_AYV_BW_17). The grand and deep voids indicate no further manufacturing processing from smelting (probably in the cases of KYT_AYV_BW_17 and KYT_AYV_BW_18) (Mangou and Ioannou2000:212). Additionally, carbon residues caused by the combustion were observed in some cases (for example KYT_AYV_BW_05, KYT_AYV_BW_14 and KYT_AYV_BW_15).

The observations and microphotographs of objects during the inspection under the Optical Microscope at magnifications X10, X50 and X200 are cited in the following catalogue.

OPTICAL MICROSCOPY CATALOGUE

KYT_AYV_BS_01	REMARKS
001 002 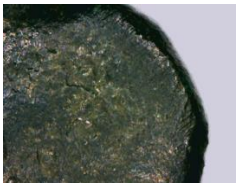 003 004 005 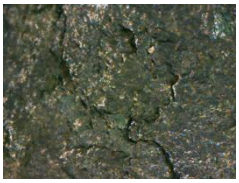 006	001-002: general view of the two surfaces at magnification X15. 003-004: magnification X50. Details. Possible traces of cutting tool at the edges. 005-006: magnification X50. Details. Area with smoother patina (left). Probable incomplete surface treatment during manufacture (right). Sufficient cleaning treatment.

KYT_AYV_BS_02	REMARKS
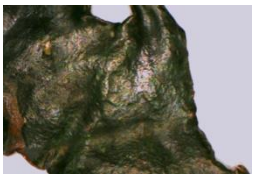 007 008 009 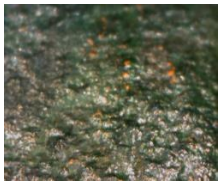 010	007-008: partial view of the two surfaces at magnification X15. 009-010: magnification X50. Details. Areas with smoother patina. Appearance of free corroded areas. Sufficient cleaning treatment.

KYT_AYV_BS_06	REMARKS
031 032 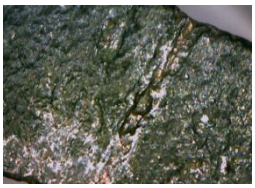 033 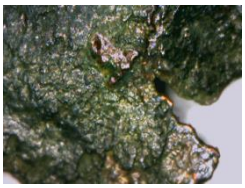 034 035	031: general view of one surface at magnification X15(left). 032: magnification X50. Detail of the marking area of the figure 031. Exfoliation of corrosion products. 033-034: magnification X50. Details. Areas covered by corrosion layers and exfoliations. 035: magnification X50- polarized light. Detail. Free corroded area suitable for examination.

KYT_AYV_BS_07	REMARKS
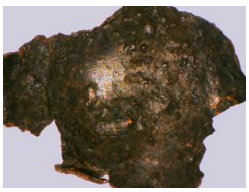 036 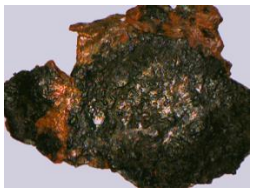 037 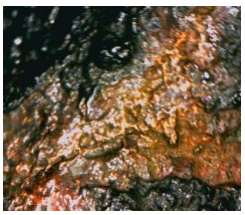 038 039	036-037: general view of the two surfaces at magnification X15. 038-039: magnification X50. Details. Exfoliation of corrosion products with the bulk metal underneath. Probable use of different alloy type, due to the color of the bulk metal.

KYT_AYV_BS_08	REMARKS
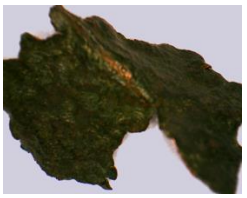 040 041 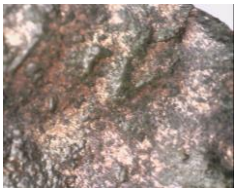 042 043	040: magnification X15. General view. 041: magnification X50- polarized light. Detail. Thin corrosion layer on the surface. 042-043: magnification X50- polarized light. Details. Cleaned area suitable for examination.

KYT_AYV_BS_10	REMARKS
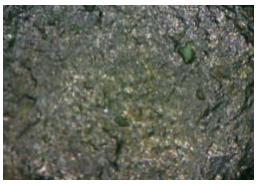 048 049 050 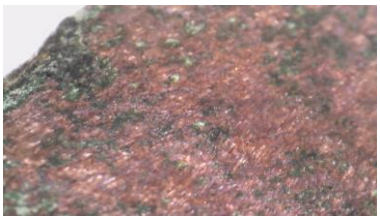 051	048-049: magnification X50. Details. Surfaces covered by corrosion layers. Polarized light (right). 050: magnification X50- polarized light. Detail. Cleaned area with occasional soil and corrosion encrustations. 051: magnification X200- polarized light. Detail. Free corroded area suitable for examination.

KYT_AYV_BS_19	REMARKS
096 097 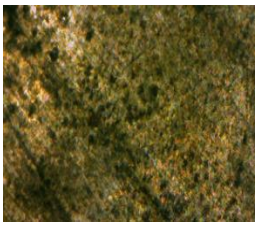 098 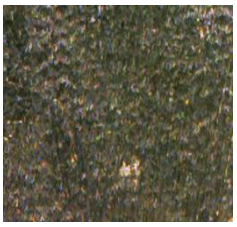 099 100 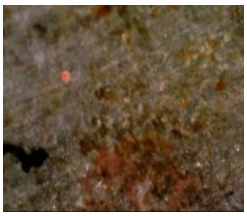 101 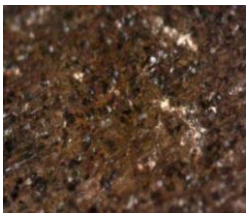 102	096-097: part figures of the two surfaces at magnification X15. 098-099: magnification X50-polarized light. Details. Greenish corrosion products on the front view (left). Green-gray corrosion products on the back view (right). Probable coexistence of silver and copper in the alloy. The different appearance of the two views is probably due to the burial conditions. 100: magnification X200-polarized light. Silver appearance on the back view after cleaning treatment. 101-102: magnification X200-polarized light. Locally gray-black and red – green appearance, showing both silver and bronze corrosion products (left). Black spots were unevenly distributed showing silver erosion (right).

KYT_AYV_FB_03	REMARKS
011 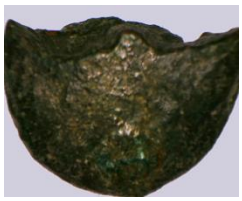 012 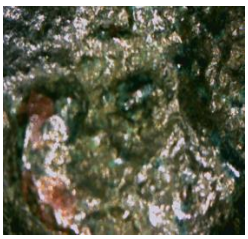 013 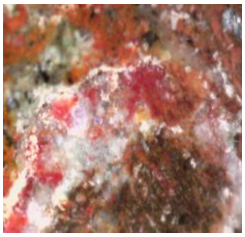 014 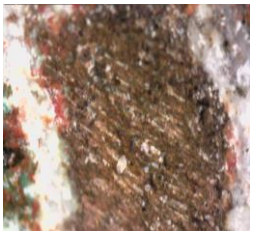 015 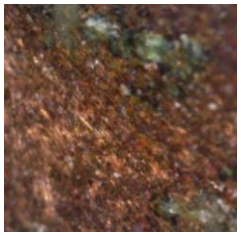 016	011-012: general view of the two surfaces at magnification X15. 013: magnification X50. Detail. The region where the figurine was placed on and area covered by cuprite. 014: magnification X200 - polarized light. Distinct presence of cuprite and calcareous encrustations (part of the same area as on 013). 015-016: magnification X200 - polarized light. Free corroded area and calcareous encrustations (left). Cleaned area suitable for examination (right).

KYT_AYV_BW_04	REMARKS
017 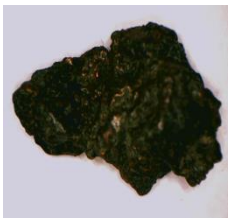 018 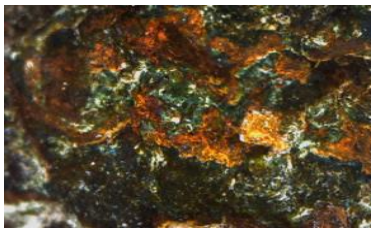 019 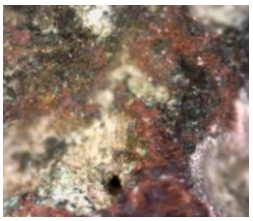 020 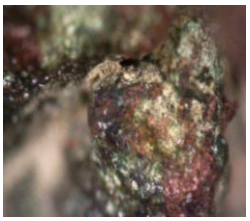 021 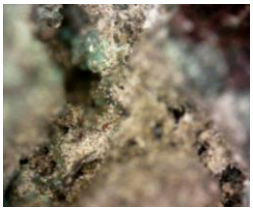 022 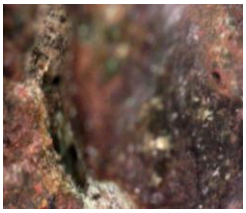 023	017-018: general view of two surfaces at magnification X15. Plane surface (left) - Crude surface (right). 019: magnification X50. Detail. Areas where free corroded metal between copper oxides occurs. 020-021: magnification X200 - polarized light. Copper prills surrounded by copper oxides, gas holes and calcareous residues. 022: magnification X200 - polarized light. Calcareous residues in the light colored areas. Porous appearance caused by gases. 023: magnification X200 - polarized light. Porous appearance caused by gases and copper prills.

KYT_AYV_BW_05	REMARKS
024 025 026 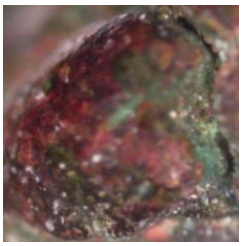 027 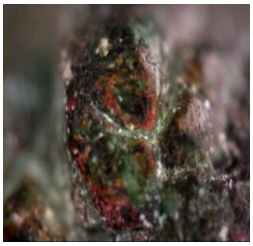 028 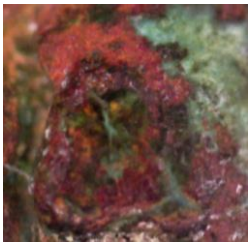 029 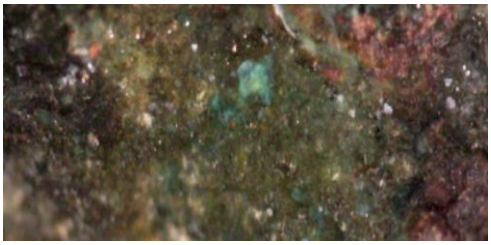 030	024-025: general view of the two surfaces at magnification X15. 026: magnification X50. Detail. Cuprite (red) and green copper oxides. Appearance of copper prills. 027: magnification X200-polarized light. Solidified molten metal indicating metal flow. Voids caused during melting are also visible. 028-029: magnification X200-polarized light. Copper oxides and corroded copper prills. 030: magnification X200-polarized light. Copper prills, copper oxides and black layers probably due to carbon residues. Possible appearance of atacamite (existence of Cl) in the light green areas of the figures 029 and 030.

KYT_AYV_BW_14	REMARKS
069 070 071 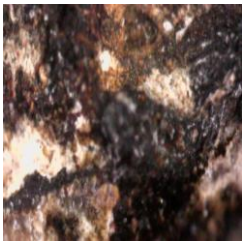 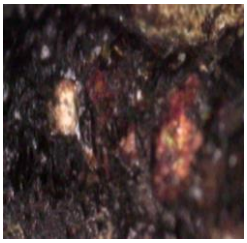 072 073 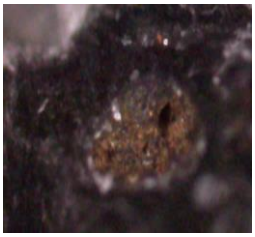 074 075	069: magnification X15. General view. 070: magnification X50- polarized light. Detail. Free corroded area with a porous appearance. 071: magnification X50- polarized light. Detail. Free corroded area and voids. Distinct dark-black areas probably caused by carbon residues and soil agglomerates. 072-073: magnification X200- polarized light. Black layer probably due to carbon residues and iron oxides. Copper prills (right). 074-075: magnification X200- polarized light. Deep gas holes and probable iron oxides (left). Calcareous and soil agglomerates and porosity caused by gas (right).

KYT_AYV_BW_15	REMARKS
076 077 078 079 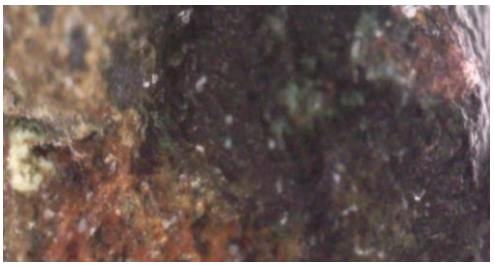 080	076-077: magnification X50-polarized light. Details. Copper prills and gas holes. Green-gray corrosion layer (left). Cleaned area (right). 078-079: magnification X200-polarized light. Copper prills and copper oxides. Copper prills surrounded, probably, by iron oxides (right). 080: magnification X200-polarized light. Copper prills and gas holes. Probable iron impurities on the left part and carbon residues on the dark layers.

KYT_AYV_BW_16	REMARKS
081 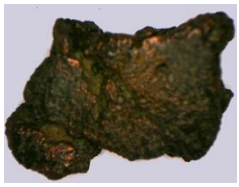 082 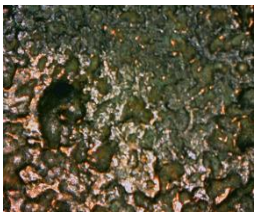 083 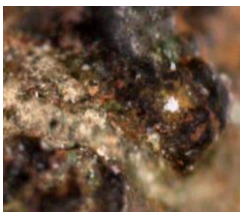 084 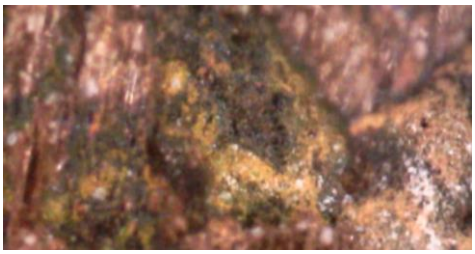 085 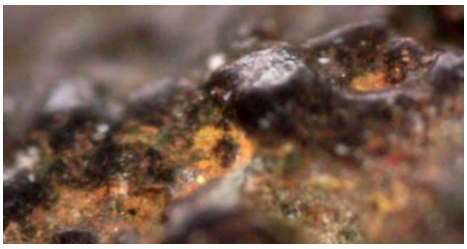 086	081-082: general view of the two surfaces at magnification X15. 083: magnification X50. Detail. Crude surface covered by corrosion layers and occasional appearance of free corroded metal. 084: magnification X200-polarized light. Soil and calcareous conglomerates; dark layer, possibly due to iron oxides. 085: magnification X200-polarized light. Porous appearance caused by gases with small holes; copper prills surrounded, probably, by iron oxides. 086: magnification X200-polarized light. Gas holes on the surface and probable iron impurities.

KYT_AYV_BW_17	REMARKS
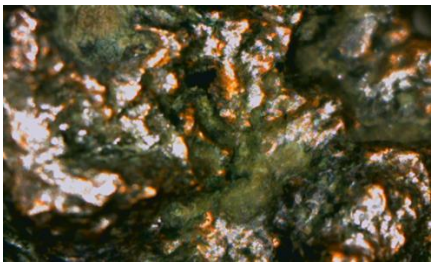 087 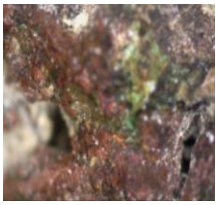 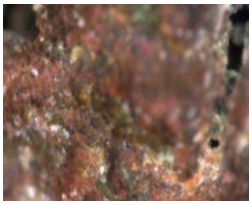 088 089 090	087: magnification X50. Detail. Copper prills surrounded by copper oxide, gas holes appeared on the surface. 088-089: magnification X200-polarized light. Porosity formed during the flow and cooling of the metal. Copper prills surrounded by copper oxides. 090: magnification X200-polarized light. Calcareous conglomerates entrapped in big gas holes.

KYT_AYV_BW_18	REMARKS
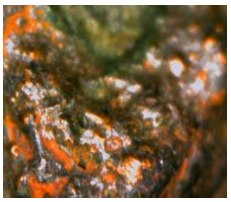 091 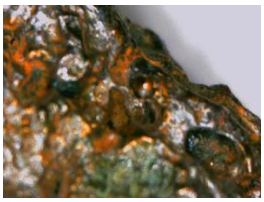 092 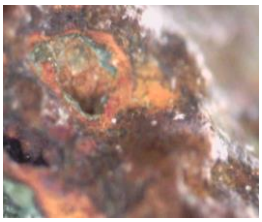 093 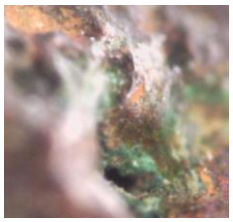 094 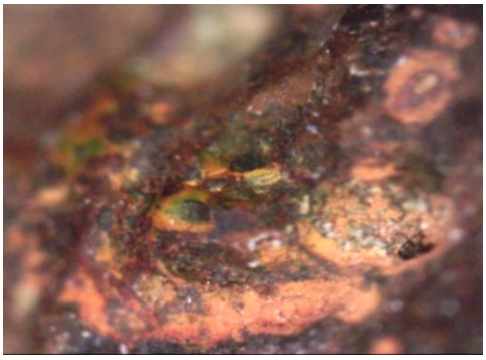 095	091-092: magnification X50. Details. Copper prills surrounded by copper and iron oxides. Crude surface caused by gas holes (right). 093-094: magnification X200-polarized light. Porous appearance caused by gases and surface with grand and deep voids. 095: magnification X200-polarized light. Copper prills surrounded by copper oxides and corroded copper prills. Possibly presence of iron oxides. Porous appearance caused by gases during melting.

KYT_AYV_VF_09	REMARKS
044 045 046 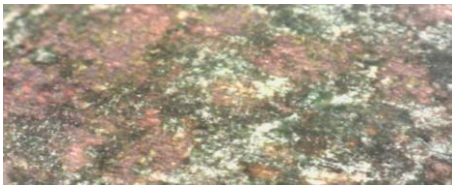 047	044-045: partial view of the two surfaces at magnification X15. 046: magnification X50- polarized light. Detail. Free corroded area on the rim. The rest surface covered by thin corrosion layers 047: magnification X50- polarized light. Detail. Area cleaned or covered by thin corrosion layer suitable for examination.

KYT_AYV_VF_11	REMARKS
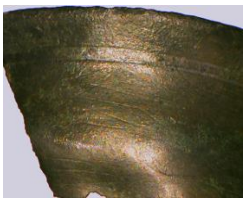 052 053 054 055 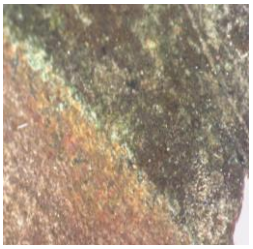 056 057	052-053: partial view of the two surfaces at magnification X15. Sheet inturned to form the rim (right). 054-055: magnification X50- polarized light. Details. Grooves on the exterior and thin patina (left). Inturned end of the sheet and free corroded area (right). 056-057: magnification X50- polarized light. Details. Free corroded and corroded areas on the exterior (left). Free corroded area on the interior (right).

KYT_AYV_VF_12	REMARKS
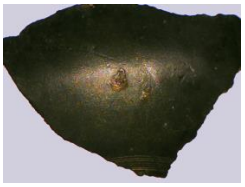 058 059 060 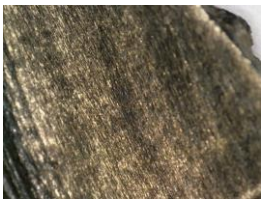 061 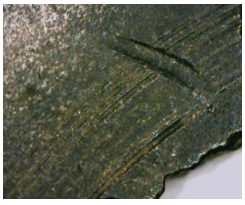 062 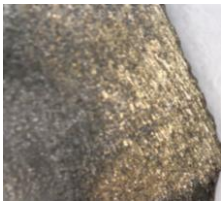 063	058-059: general view of the two surfaces at magnification X15. 060-061: magnification X50- polarized light. Details. Parallel grooves on the interior and thin corrosion layer (left). Free corroded area (right). 062-063: magnification X50- polarized light. Details. External surface. Parallel grooves in the beginning of the base (left). Free corroded area (right).

KYT_AYV_VF_13	REMARKS
064 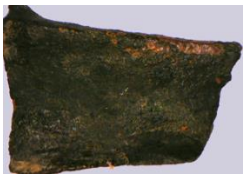 065 066 067 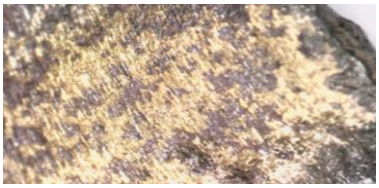 068	064-065: general view of the two surfaces at magnification X15. 066-067: magnification X50- polarized light. Details. Areas covered by corrosion layers. Decorative element (right). 068: magnification X50- polarized light. Detail. Free corroded area on the back.

2.4 Elemental analysis using pXRF

A portable X-ray fluorescence device (pXRF) was employed for the determination of the chemical composition of the selected copper-based finds from Ayios Yeoyios sto Vouno. X-ray fluorescence is a well-established technique for the identification of key features of metal objects, which aims to the recognition of their elemental characterization. It is a highly sensitive technique for performing rapid and non-destructive detection of chemical elements. It determines the identity and quantity of elements and distinguishes them from background radiation. Moreover, the portable XRF device offers the possibility to acquire the maximum possible information in one operational action (Liritzis, Zacharias 2011:109-112). It can detect amounts of major, minor, and trace chemical elements and in particular, it is capable of detecting trace amounts of heavy elements, such as antimony (Sb) and lead (Pb), elements of special interest for the current research. This technique is able to contribute to the provenance studies, based on the identified elements and their concentrations and by comparing metal and analyzed objects (Liritzis, Zacharias 2011:109-112).

For the purpose of the present study a portable instrument was used with a detector of the Bruker Company, model Tracer III-SD, accompanied by a portable mini-pump vacuum and a portable computer for the storage and processing of the obtained spectra (Fig.8). The system includes software for quantitative analysis, depending on the nature of the measured material; consequently, the metal/alloys program was selected. The used settings are: yellow filter Al-Ti, accelerating voltage 40kV and current 12μA. The diameter of the X-rays beam was 3X3mm and the measurement time for each spot analysis was 60 seconds. Since metals, usually, exhibit heterogeneity, multiple measurements were obtained from several areas of each object, avoiding surface heterogeneities. The number of the measurements taken for each object depended on the size of the object, for

example, if the available surface is small, the object cannot be moved onto the surface analysis of the device, and the available free-corroded areas, which had been detected during the previous microscopic examination. The recorded composition for each object is the mean value of two to five measurements. Another value that was calculated is the standard deviation. It is considered statistically important because it contributes to the clearer evaluation of the results and indicates whether there are significant variations between measurements. All elements are presented in weight percentage (wt. %) and the data are normalized to 100% by the instrumentation.

The accuracy of the applied analytical technique was checked by analyzing the certified reference copper alloys CDA 360 with a set of determinations: 60.99% Cu, 35.88% Zn, 0.15% Fe and 2.98% Pb. Three measurements were taken from the standard and the mean values are: 61.70% Cu, 35.55% Zn, 0.08% Fe and 2.17% Pb. Since other elements are also detected in very low quantities, we conclude that there are no significant deviations from the default values of the elements which we are interested for. All measurements of the certified reference copper alloy CDA 360 using pXRF are cited on Table 1 - Appendix I.

The chemical analyses of the copper-based objects from Ayios Yeoryios sto Vouno using pXRF are presented on Tables 1-3. The percentage of each element is recorded as the mean value (average) of all the measurements taken. It should be mentioned here that the XRF analysis for the object KYT_AYV_BW_14 has been estimated only qualitatively, because of the errors arisen during the measurements, relating to its size and shape and thus, they are not included on the tables.

Bronze Sheets

Table 1: Concentration of the elements (mean values) detected with XRF method expressed in % wt. (n.d.: non detected).

KYT_AYV	BS_01	BS_02	BS_06	BS_07	BS_08	BS_10	BS_19
CuO	86,10	93,35	79,04	79,43	98,83	82,84	31,33
As_2O_3	0,63	0,32	0,05	0,00	0,13	0,01	1,14
SnO_x	1,38	1,93	0,27	0,06	0,24	0,21	9,35
PbO	2,81	1,72	0,26	0,04	n.d.	0,21	0,13
Fe_2O_3	0,82	0,74	1,16	0,04	0,18	1,21	0,33
ZnO	7,74	1,31	15,88	26,01	0,48	12,72	4,49
Ni	0,03	0,20	0,55	n.d.	0,05	0,64	1,79
Sb_2O_5	0,11	0,11	0,26	0,02	0,04	0,18	0,17
Ag	0,10	0,06	0,31	0,01	0,04	0,25	50,47
MnO	0,06	0,05	0,20	n.d.	n.d.	0,17	0,04
Co_3O_4	0,04	0,04	0,27	n.d.	n.d.	0,22	n.d.
ZrO_2	0,09	0,12	0,87	0,02	n.d.	0,69	0,20
Nb_xO_x	0,07	0,07	0,72	0,10	n.d.	0,52	n.d.
Bi_2O_3	n.d.	0,02	0,16	n.d.	0,02	0,12	0,56

Bronze Wastes

Table 2: Concentration of the elements (mean values) detected with XRF method expressed in % wt. (n.d.: non detected).

KYT_AYV	BW_04	BW_05	BW_15	BW_16	BW_17	BW_18
CuO	77,88	72,25	73,35	85,94	83,82	87,57
As_2O_3	0,01	0,20	1,15	0,33	0,17	0,08
SnO_x	0,30	0,73	0,54	0,12	0,16	0,16
PbO	0,28	0,09	5,85	3,68	n.d.	0,10
Fe_2O_3	0,80	5,04	2,44	0,39	3,68	0,10
ZnO	17,05	17,87	13,50	6,92	9,89	10,88
Ni	0,68	0,24	0,35	0,27	0,73	0,63
Sb_2O_5	0,29	0,55	0,48	0,31	0,14	0,11
Ag	0,34	0,64	0,54	0,17	0,06	0,06
MnO	0,22	0,32	0,25	0,10	0,18	0,12
Co_3O_4	0,28	0,62	0,35	0,12	0,08	n.d.
ZrO_2	0,93	0,75	0,61	0,46	n.d.	0,06
Nb_xO_x	0,76	0,39	0,37	0,40	n.d.	n.d.
Bi_2O_3	0,17	0,32	0,21	0,79	0,23	0,13

Figurine Base and Vessel Fragments

Table 3: Concentration of the elements (mean values) detected with XRF method expressed in % wt. (n.d.: non detected).

KYT_AYV_	FB_03	KYT_AYV_	VF_09	VF_11	VF_12	VF_13
CuO	76,05	CuO	79,10	71,54	67,35	83,92
As_2O_3	1,20	As_2O_3	0,08	0,93	1,68	0,02
SnOx	0,62	SnO_x	0,23	0,52	0,59	0,13
PbO	6,33	PbO	0,93	5,75	4,75	0,33
Fe_2O_3	3,47	Fe_2O_3	1,04	1,73	3,02	0,42
ZnO	8,91	ZnO	16,23	16,03	19,83	13,70
Ni	0,45	Ni	0,75	1,24	0,87	0,41
Sb_2O_5	0,29	Sb_2O_5	0,22	1,17	0,45	0,12
Ag	0,56	Ag	0,21	0,26	0,28	0,08
MnO	0,28	MnO	0,19	0,15	0,21	0,01
Co_3O_4	0,38	Co_3O_4	0,13	0,22	0,37	0,09
ZrO_2	0,65	ZrO_2	0,43	0,25	0,33	0,38
Nb_xO_x	0,30	Nb_xO_x	0,29	0,18	0,26	0,41
Bi_2O_3	0,12	Bi_2O_3	0,17	0,03	0,01	0,01

The detailed results of the analytical work for each object and the related spectra are presented on Tables 2-19, Spectra 1-54 - Appendix I.

2.5 Chemical analysis using SEM-EDS

Chemical analysis for major and trace elements was made by SEM-EDS Spectroscopy. SEM-EDS allows the chemical analysis of specific alloy phases and of components of size up to few microns. Analyses can be performed without the material embedding in the resin, by the introduction of the entire object into the analysis area. The possibility of a simultaneous

chemical analysis of the observation point makes the SEM-EDS a key tool for the study of metal alloys (Georgakopoulou and Basiakos2010:434).

Bulk compositional analysis was performed using a SEM JEOL system (JSM-6510LV), coupled with an EDS by Oxford Instruments and software by INCA (Fig.9). The device provides the possibility of a three dimensional imaging and recording of the observation point. Analysis was done in high vacuum, with secondary electrons, in a small spot size (40). The settings of the analysis are: accelerating voltage 20kV, working distance 15mm and collection time 90sec. The analyses were performed in magnifications 200X and 1400X. The objects were mounted onto a specimen holder and a double-sided carbon tape was used, which improves conductivity and permits analysis. Taking advantage of the presence of the carbon tape for the distinction of free-corroded areas, five to eight measurements of each object were taken from corroded and cleaned areas. The recorded composition is the mean value of the measurements, while the standard deviation was also calculated (see above). All elements are presented in weight percentage (wt. %) and the data are normalized to 100% by the instrumentation.

The accuracy of the applied analytical technique was checked by analyzing the same certified reference copper alloy CDA 360. Three measurements were taken from the standard and the mean values are: 61.80% Cu, 35.70% Zn, 0.31% Fe and 2.21% Pb. The results from all measurements and the related spectra are displayed on Table 1, Spectra 1-3 - Appendix II. It is concluded that no significant deviations from the default values exist. However, small variances in the values, regarding iron in particular, that are noticed between the two analytical techniques, could be due to the device normalization and were taken into consideration in the discussion of the results.

The chemical analyses of the copper-based objects from Ayios Yeoryios sto Vouno using SEM-EDS are presented on Tables 4-6. The percentage of each element is recorded as the mean value (average) of all the taken measurements.

Bronze Sheets

Table 4: Concentration of the elements (mean values) detected with SEM-EDS method expressed in % wt. (n.d.: non detected).

KYT_AYV_	BS_01	BS_02	BS_06	BS_07	BS_08	BS_10	BS_19
CuO	81,00	96,21	87,68	55,60	89,42	58,70	8,64
As_2O_3	0,60	0,40	0,76	2,21	0,42	1,50	0,51
SnO_x	2,92	0,64	0,67	2,88	0,55	0,30	0,83
PbO	2,49	0,31	0,90	1,86	0,62	0,79	0,84
FeO	0,79	0,48	0,43	0,87	0,59	1,49	0,66
ZnO	6,41	0,39	0,80	25,13	0,44	1,10	1,42
Ni	0,44	0,55	n.d.	5,29	n.d.	n.d.	1,43
Sb_2O_5	n.d.	n.d.	n.d.	n.d.	n.d.	n.d.	n.d.
Ag	0,24	0,17	0,86	2,24	0,29	1,77	78,80
S	n.d.	n.d.	1,75	n.d.	n.d.	n.d.	0,69
MgO	n.d.	n.d.	n.d.	n.d.	n.d.	n.d.	1,02
Al_2O_3	2,14	1,31	n.d.	6,32	2,13	12,00	2,95
SiO_2	5,32	1,73	n.d.	13,20	5,72	33,46	3,24
P_2O_5	2,14	1,70	n.d.	n.d.	1,03	n.d.	n.d.
Cl	2,00	n.d.	8,70	10,06	2,85	4,11	n.d.
K_2O	n.d.	n.d.	n.d.	n.d.	n.d.	n.d.	n.d.
CaO	3,81	n.d.	n.d.	10,76	2,27	7,36	3,33

Bronze Wastes

Table 5: Concentration of the elements (mean values) detected with SEM-EDS method expressed in % wt. (n.d.: non detected).

KYT_AYV	BW_04	BW_05	BW_14	BW_15	BW_16	BW_17	BW_18
CuO	84,75	64,03	47,12	73,49	88,98	83,74	93,57
As_2O_3	0,50	0,61	1,60	0,36	0,94	0,84	0,57
SnO_x	0,29	5,70	0,81	1,53	0,25	0,78	0,60
PbO	0,23	n.d.	0,35	5,40	0,37	0,96	1,08
FeO	0,50	3,89	28,82	1,59	0,34	6,61	0,40
ZnO	0,17	1,29	0,53	1,19	2,45	0,38	0,46
Ni	0,46	n.d.	0,97	n.d.	n.d.	n.d.	n.d.
Sb_2O5	n.d.	n.d.	1,86	n.d.	0,53	n.d.	n.d.
Ag	0,22	n.d.	n.d.	n.d.	0,14	0,30	0,59
S	n.d.	0,85	n.d.	n.d.	n.d.	n.d.	n.d.
MgO	n.d.	2,45	n.d.	n.d.	n.d.	n.d.	n.d.
Al_2O_3	3,57	8,04	4,99	4,90	1,79	n.d.	n.d.
SiO_2	10,80	18,33	11,32	14,92	9,63	2,80	n.d.
P_2O_5	n.d.	n.d.	n.d.	2,59	n.d.	n.d.	n.d.
Cl	2,14	4,12	n.d.	0,65	1,04	6,07	3,80
K_2O	n.d.	n.d.	n.d.	1,62	n.d.	n.d.	n.d.
CaO	2,06	11,73	12,51	3,58	1,79	n.d.	n.d.

Figurine Base and Vessel Fragments

Table 6: Concentration of the elements (mean values) detected with SEM-EDS method expressed in % wt. (n.d.: non detected).

KYT_AYV	FB_03	KYT_AYV_	VF_09	VF_11	VF_12	VF_13
CuO	64,13	CuO	54,87	58,27	55,16	94,63
As_2O_3	2,43	As_2O_3	0,89	1,19	1,17	0,28
SnO_x	0,58	SnO_x	1,39	14,17	5,90	0,15
PbO	14,18	PbO	1,22	4,23	6,89	0,46
FeO	n.d.	FeO	0,64	0,65	2,95	0,29
ZnO	0,22	ZnO	1,07	12,47	10,68	4,33
Ni	n.d.	Ni	0,92	0,72	0,86	n.d.
Sb_2O_5	0,75	Sb_2O_5	n.d.	7,66	4,08	n.d.
Ag	n.d.	Ag	0,43	0,13	0,27	0,26
S	n.d.	S	1,77	n.d.	n.d.	n.d.
MgO	n.d.	MgO	n.d.	n.d.	n.d.	n.d.
Al_2O_3	1,37	Al_2O_3	11,11	1,98	4,11	n.d.
SiO_2	16,53	SiO_2	34,08	5,40	6,74	n.d.
P_2O_5	1,91	P_2O_5	n.d.	n.d.	2,89	n.d.
Cl	4,81	Cl	3,00	1,43	1,65	n.d.
K_2O	n.d.	K_2O	1,76	n.d.	n.d.	n.d.
CaO	3,25	CaO	3,95	4,77	9,30	n.d.

The detailed results of the analytical work for each object and the related spectra, as well as indicative images of backscattered electron in the SEM are presented on Tables 2-20, Spectra 4-119, Images 1-38 - Appendix II.

2.6 Results

It should be noted in advance that variances in the measurements between the two methods are expected, taking into account the different measuring techniques, the variance of particle distribution in objects, and the

measurement from different parts of them. As far as XRF analysis is referred, errors related to the shape of the objects may arise, in cases of crude or curved surfaces, if the objects cannot be in direct contact with the examination area of the device or if the objects are too thin or smaller than the examination area (Georgakopoulou and Bassiakos2015:348). Moreover, an Aluminum-Titanium filter in the XRF analysis excluded the lighter elements from the measurements; thus, elements such as Aluminum, Silicon, Sulfur, Chlorine and Calcium which may be present in the objects, either naturally or as a result of corrosion (corrosion products and solid residues) could not be detected. This also lead to an overestimation of the presence of other elements, detected though in the SEM-EDS. On the other hand, elements in trace concentrations have been detected. Also, the quantification of lead and arsenic, which are very important for the identification of copper alloys, is problematic with both methods, because of the difficulty in the distinction of their peaks (Georgakopoulou and Bassiakos2015:349). Finally, the penetration depth of the two techniques differs, as, X-rays penetrate to a greater depth than the electron beam. As a result, the normalization of the measurements to 100% may raise the concentration of some elements against others. In the discussion of the results that follows, the element ratios and not the absolute values have been taken into account.

The two analytical used methods showed that the objects are made of copper-based alloys which contain both arsenic and tin, apart from the sheet KYT_AYV_BS_19 which is manufactured by a silver-copper alloy, containing amounts of arsenic and tin as well. Figure 1 shows the relative presence of the elements Copper, Arsenic, Tin, Lead, Iron, Zinc, Nickel, Antimony and Silver measured by both XRF and SEM-EDS techniques. The high copper content indicates that in most cases the metal used should be considered as pure. The XRF analysis recorded copper presence in a

percentage more than 70% w.t. in almost all objects, while SEM-EDS analysis in ten. Since copper without alloying may be the only component from which objects were made, the presence of arsenic in a percentage lower than 1% w.t. may be due to the fact that copper and arsenic are mineralogically joined, as we shall see below, although the presence of arsenic makes also copper alloy harder in comparison to tin (the same quantity), especially during cold forging (Tselios2008:78-79). The detected elements Iron, Lead, Zinc, Nickel, Antimony and Silver are considered as impurities into the alloys. The concentration of Zinc, though, is significant in some cases.

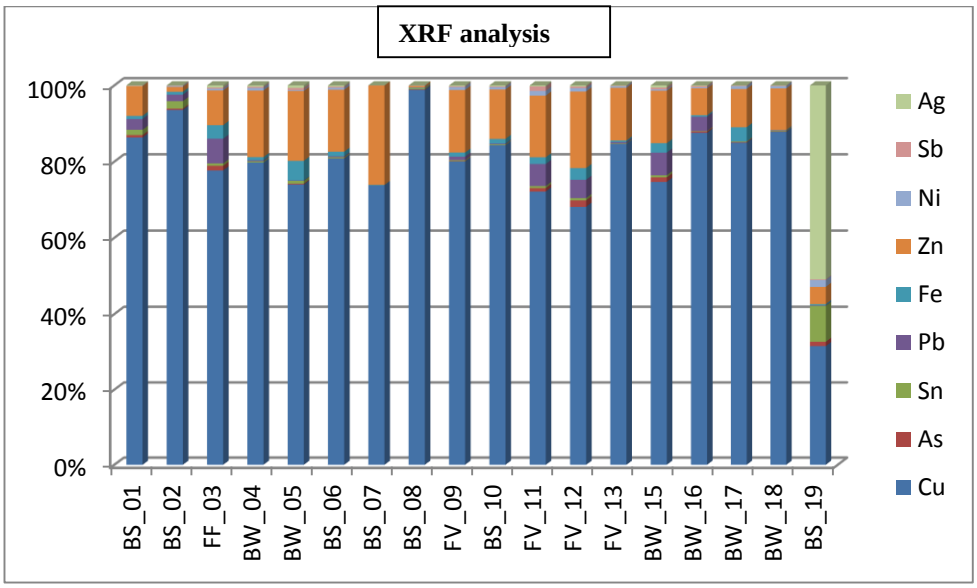

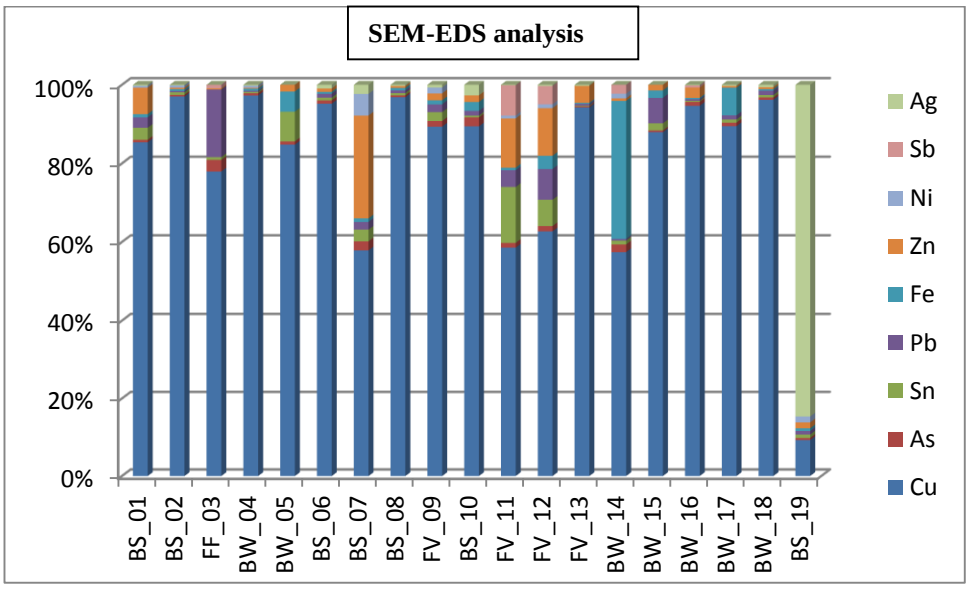

Fig.1: Histograms showing the relative abundance of the elements Cu, As, Sn, Pb, Fe, Zn, Ni, Sb and Ag measured by the XRF and SEM-EDS analyses.

Arsenic occurs in low concentrations in all objects. Figure 2 displays the distribution of Copper and Arsenic in the four groups of objects by both analytical techniques. Since there are ores naturally rich in arsenic, it is considered that the minimum presence of arsenic indicating an intentional addition of the specific element is 1-1.2 % w.t. However, many researchers suggest a higher level of 2 or 2.5% w.t. while other maintain that arsenical coppers were the result of the use in the furnace charge of copper ores with naturally occurring arsenic rather than of truly deliberate alloys. However, copper rich in arsenic might also have been intentionally selected (Webb et al.2006:274, Georgakopoulou and Bassiakos2015:347).

The improving of the alloy properties occurs with an addition of arsenic in the copper in concentrations higher than 2% w.t., resulting in the increase of its ductility and hardness. However, only after hammering may arsenical copper become advantageous as compared to copper, while in casting both have almost the same hardness. Additionally, arsenic acts as de-oxidant in

casting, suppressing brittleness due to the presence of copper oxide inclusions in the metal (Papadimitriou2008:277).

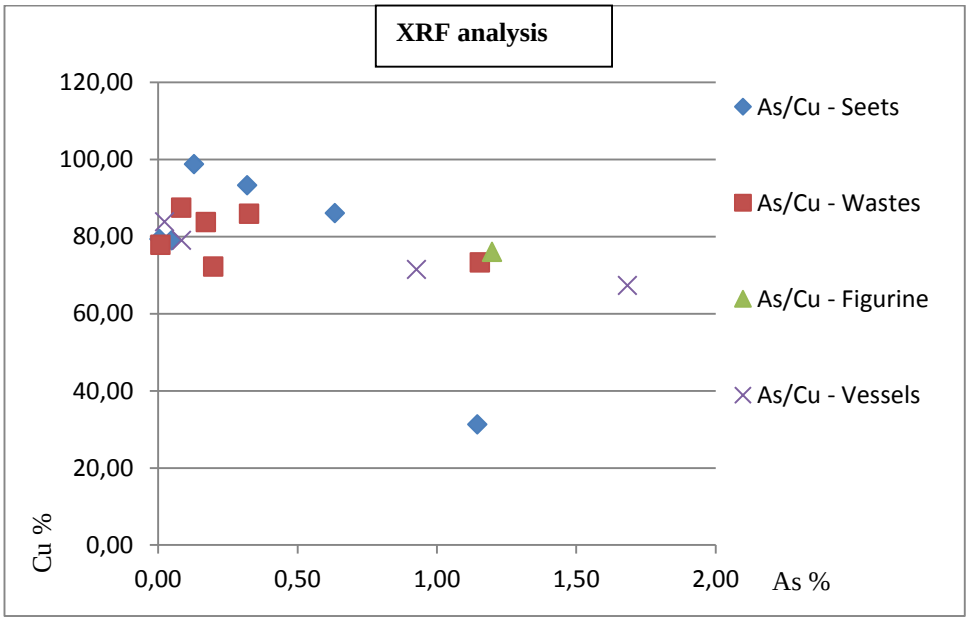

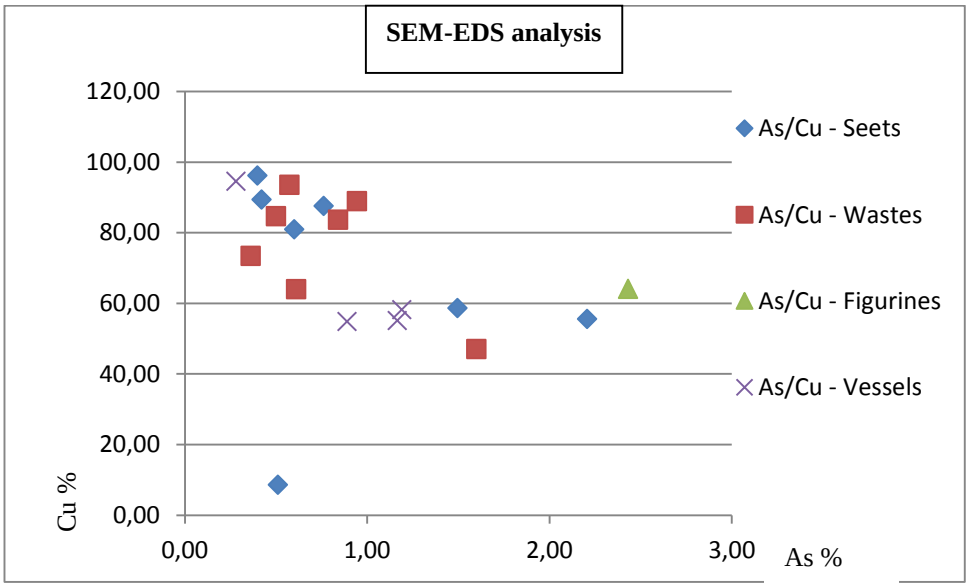

Fig. 2: Distribution of Copper and Arsenic in the four groups of objects in the XRF and SEM-EDS analyses.

It should be mentioned also that the final amount of arsenic in the alloy may be decreased because of its easy evaporation, as metal or as arsenious oxide, during the melting, heating or forging process and thus, the deliberate addition of arsenic could not be ascertained (Papadimitriou2008:281, Tselios2008:78). In our case only few objects seem to have an arsenic content, which could lead to the conclusion of an intentional addition, and it is worth noting that the fragment of figurine may be one of them. However, taking into account the problems of methods related to the identification of the arsenic peaks, and the fact that its content could be reduced during the manufacturing, we could say that the arsenic concentrations in some of the analyzed objects might be more enhanced.

Arsenical copper ores, such as enargite [Cu_3AsSn], tennantite [Cu_3AsS_x, where x = 3-4] or basic copper arsenates may have been used in the in the manufacture of objects in the 3rd millennium. The Cycladic copper ores are often mixed with arsenical minerals which provided an ideal raw material for the production of arsenical copper, while high arsenic ores exist in Lavrion and Cyprus (Mangou and Ioannou1997:64-67, Stos-Gale 2000:61, Webb et al. 2006: 274). In particular, chalcopyrite and oxidized ores, like azurite and malachite, from Kamariza and Sounion in the Lavrion region, when smelted, produced metallic copper containing considerable amounts of arsenic, a fact that may result at the accidental production of arsenical copper; other rich arsenical copper ores from Lavrion are olivenite [$Cu_2(OHAsO_4)$] and konichalcite [CaCu[(OH)(AsO4)]]. Furthermore, it is remarkable that the easy production of copper from Lavrion can yield a copper metal above 90% w.t. (Gale et al.2009:158,165,170). On the other hand, various arsenic sulfide minerals could also have been added to the copper or could have been present already in certain types of copper ores that, upon smelting, would have produced an arsenical copper alloy. Slags from the Skouries smelting site on Kythnos proved to contain appreciable

amounts of arsenic. It is also possible that complex sulfide and arsenide ores were being smelted in the Aegean or both copper and arsenic-rich ores have been used (Muhly2006:164,167, Georgakopoulou2004:8). In the Early Bronze Age, high levels of arsenic have been found in copper prills embedded in slags at Crysokamino, for which, mixing of arsenic and copper ores has been suggested. At this site though, only imported copper ores were smelted (Katapotis and Bassiakos2007:74, Muhly2004:287). Addition of arsenical minerals to copper metal has been proposed for Poros- Katsampas, where, the study of metalworking provides the first direct evidence for the intentional production of arsenic-copper alloys, since analyses of the majority of copper prills inclusions in crucible slags found that these contained between 1 and 6% w.t. arsenic, whilst there are prills with arsenic concentration up to 52% w.t. (Georgakopoulou2004:8, Doonan et al.2007:111).

Tin occurs also in low concentrations in all assemblages of the objects from Ayios Yeoryios sto Vouno. Figure 3 shows the distribution of Copper and Tin in the four groups of objects by both analytical techniques. Analyses of copper based artefacts from the Aegean have shown that that during the Late Bronze Age the arsenic ratio to copper is low, whilst, when tin is introduced, the copper ratio decreases; thus an arsenical copper alloy requires 97% w.t. of pure copper, while tin bronze requires less amount of copper, approximately 86-89% w.t. (Mangou and Ioannou1997: 67-68, Bassiakos and Tselios2012:160). However, although the addition of tin in any amount into the alloys is considered deliberate, its presence alters the properties of the alloy only at concentrations above 2% w.t. and then the alloy is called bronze (Tselios2008:78-79).

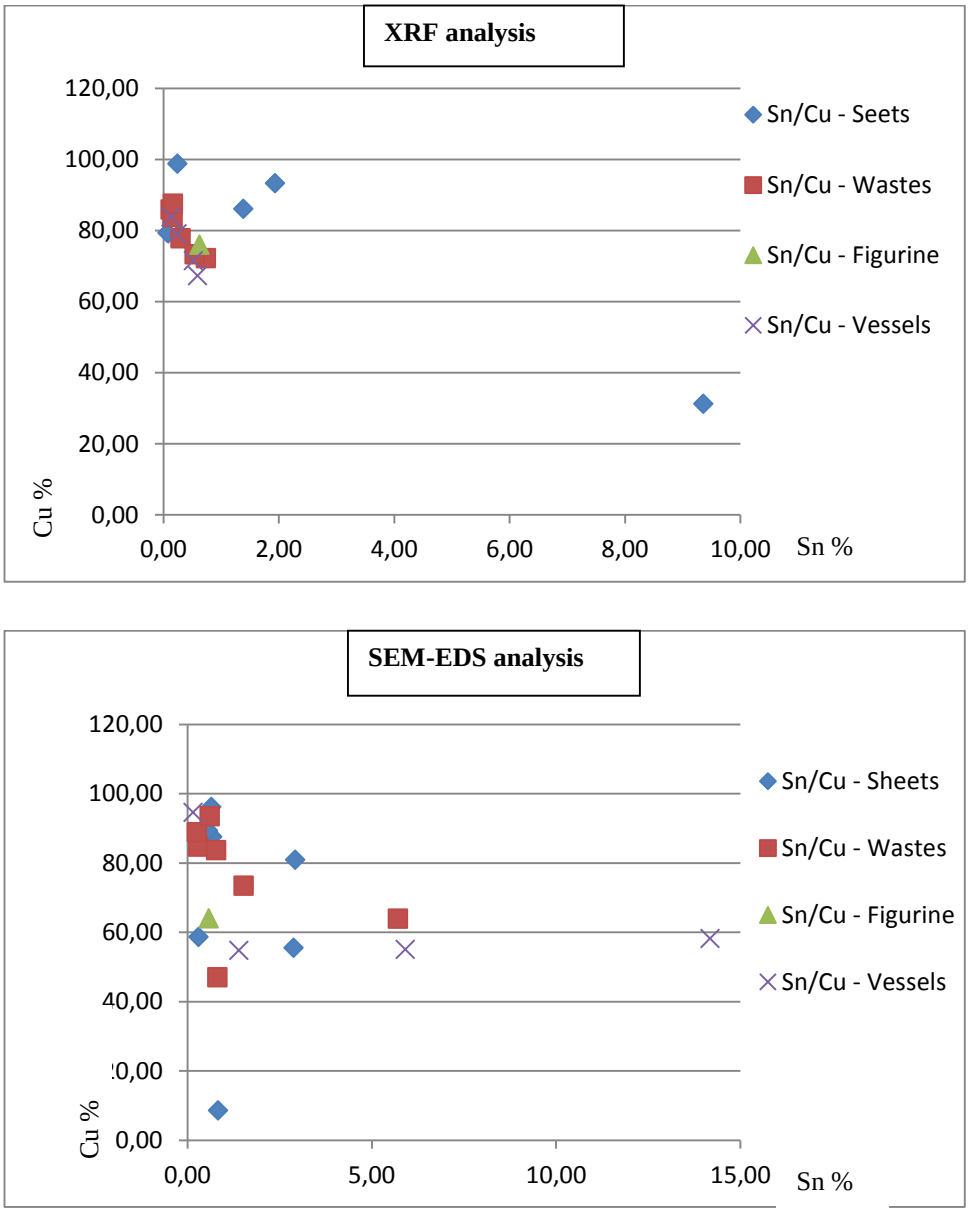

Fig. 3: Distribution of Copper and Tin in the four groups of objects in the XRF and SEM-EDS analyses.

At Kastri on Syros, analyses have documented that metallurgy involved a combination of arsenical copper and bronze, with the addition of tin to arsenical copper. Moreover, the coexistence of the two elements has been attested in analyzed artefacts from Anatolia, where it occurs both in jewelry

and in bronze manufacturing. It is noteworthy in this respect that, the sites Kastri on Syros and Troy seem important metallurgical associations (Muhly2006:172,175). Concerning tin, it is not indigenous to the Aegean and had to be imported. The tin for bronze objects might have come from central Asia, Afghanistan, western and eastern Anatolia and transferred by sea from one or more Syrian ports to the Aegean, namely, along a long-distance trade route (Muhly2006:169-171, Gillis, Clayton2008:134). Should be mentioned that the coexistence of arsenical copper and bronze could also be attributed to the recycling of metals from different periods as a result of local production, of the persistence of a strong metallurgical tradition involving the use of arsenical copper or of restricted access to mineral resources (Papadimitriou2008:281).

As stated above, extremely low percentage of tin is generally observed in the case of Ayios Yeoryios sto Vouno, while the copper remains at high concentrations. Quantities above 2% w.t. were only detected in two objects in the assemblage of sheets, in one waste and in one vessel fragment in the SEM-EDS examination. Furthermore, it is worth noting that both elements, arsenic and tin, coexist in the alloys, in low concentrations, with the copper quantity remaining at high levels. A first estimation of the distribution of arsenic and tin concentrations versus copper concentration, as it has been measured by the SEM-EDS technique in the four groups of objects, is shown in Figure 4. We conclude that the majority of objects under study are made from pure copper with a low arsenic content, probably from the ore or from scrap, examination which is expected in a sanctuary where the waste of the expensive tin is not needed for the manufacturing of simple votives.

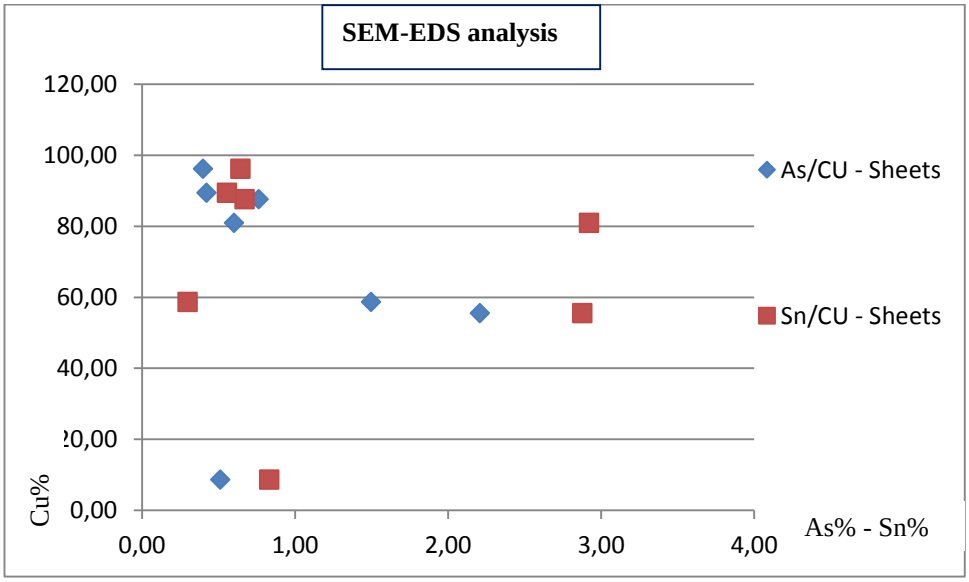
SEM-EDS analysis
120,00
100,00
80,00
60,00
40,00
0,00
0,00
1,00
2,00
3,00
4,00
Cu%
As% - Sn%
As/CU - Sheets
Sn/CU - Sheets

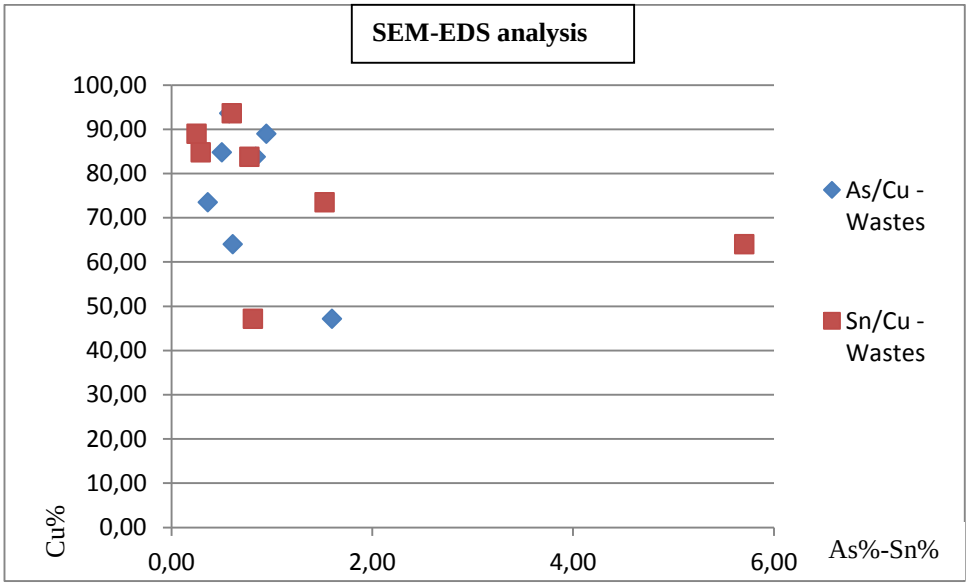
SEM-EDS analysis
100,00
90,00
80,00
70,00
60,00
50,00
40,00
30,00
20,00
10,00
0,00
0,00
2,00
4,00
6,00
Cu%
As%-Sn%
As/Cu - Wastes
Sn/Cu - Wastes

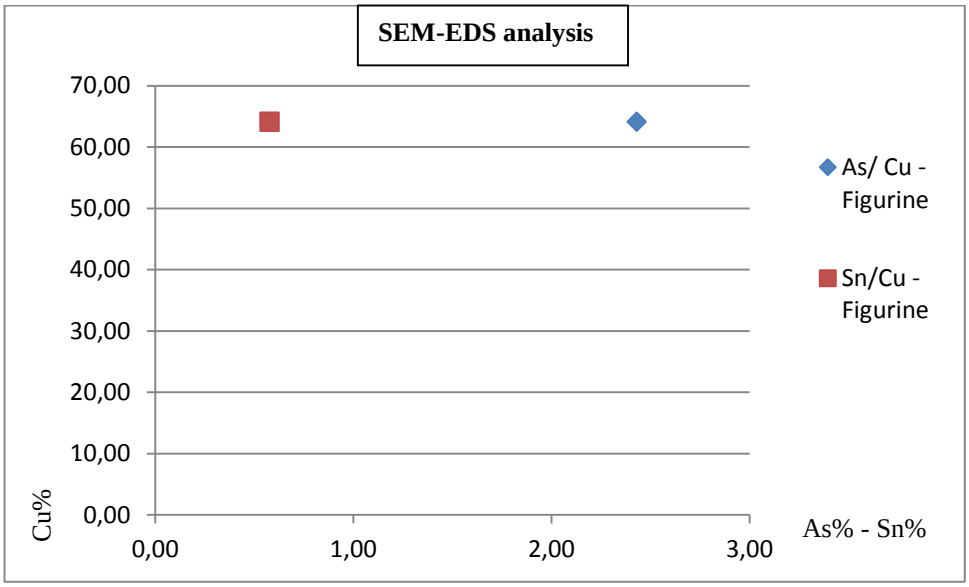

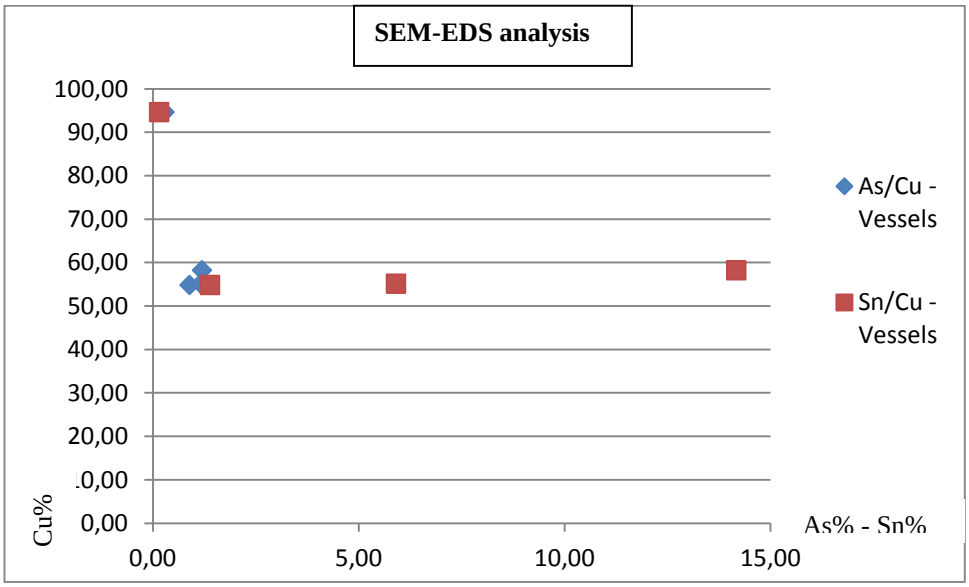

Fig. 4a-d: Distribution of Arsenic and Tin versus Copper in each assemblage of objects by SEM-EDS analysis.

The presence of Lead is confirmed by both analytical techniques in almost all objects from Ayios Yeoryios sto Vouno. The distribution of copper and

lead in the four groups of objects, by both analytical techniques, is shown in Figure 5.

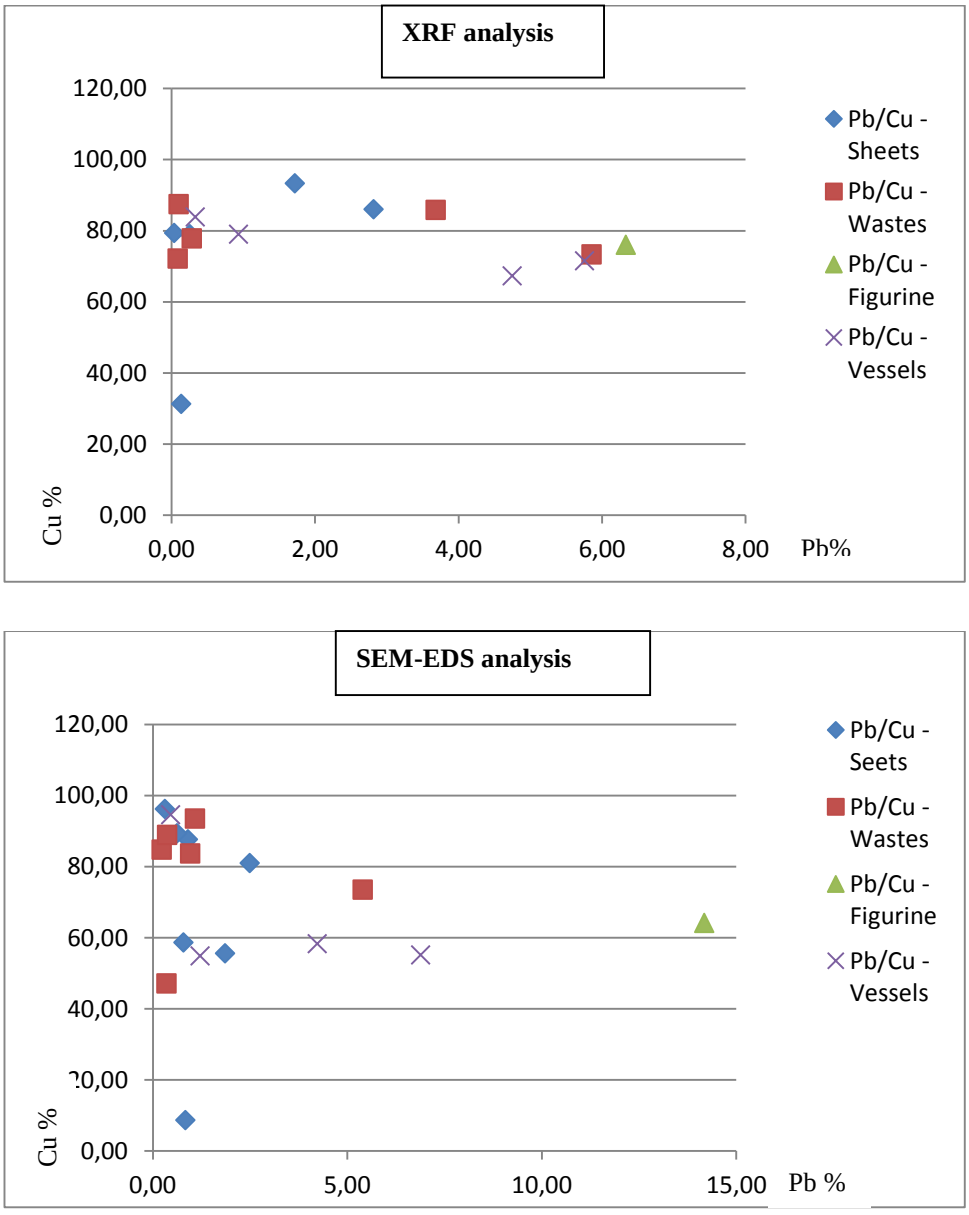

Fig. 5: Distribution of Copper and Lead in the four groups of objects, by both analytical techniques.

Concentrations above 2% w.t. that facilitates the casting of copper and copper alloys are detected in some sheets and wastes and in the assemblage

of vessels. The lead concentration occurring in the fragment of figurine is notable and leads to the assumption of a deliberate addition in order to improve castability. Given that when lead exists in hammered or forged alloys should be considered as impurity, in contrast to casted alloys where it is considered as a deliberate addition because it lowers the melting point of the alloy and improves castability (Papadimitriou2008:282,286). However, lead concentrations up to 4% w.t. could be considered as coming from the ore and low levels of lead are common in copper smelting slags (Mangou and Ioannou1997:68-69, Georgakopoulou2004:9). Moreover, lead segregates in copper alloys and may be concentrated in some parts by the action of gravity, when the alloy is still in a liquid state and thus, areas exceptionally rich in lead are formed. In other words, lead creates areas of heterogeneity into the alloy, a fact that would result in a higher lead to copper ratio in the measurements, related to the examined area (Georgakopoulou and Bassiakos2015:349, Papadimitriou2008:286). Lead arsenate ores commonly mixed with oxidized copper ores and other leaded copper ores such as bournonite [PbCuSbS3] occur in Lavrion. The most important lead sulfide mineral, the galena, occurs in marbles and schists at Kamariza, often together with chalcopyrite ore (Gale et al.2009:163,174, Gale et al. 2008:93). Cycladic copper also contain also lead as impurity often at per cent level (Webb et al. 2006:271). In the EM period, lead and copper ores and lead slags existed in Sifnos, while at the copper smelting site Skouries on Kythnos, lead occurs in a variable content, as trace element in arsenic copper prills and slags. (Stos-Gale2000:61, Muhly2006:167, Gale et al.1985:89).

Iron was found in all analyzed objects by both analytical techniques, with only one exception concerning the figurine fragment, in which iron was not detected with the SEM-EDS method. The vast majority of the objects have iron content below 1.5% w.t. and only a small number exceeds this

concentration. Figure 6 displays the distribution of copper and iron in both analytical techniques. The significant iron concentration in one waste, as well as the low iron content in the assemblage of sheets is worth mentioning.

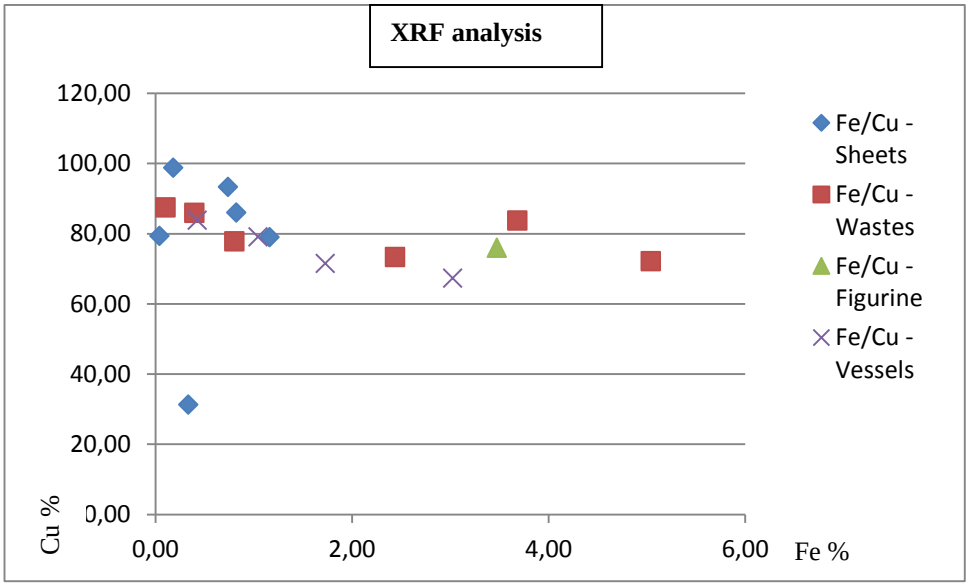

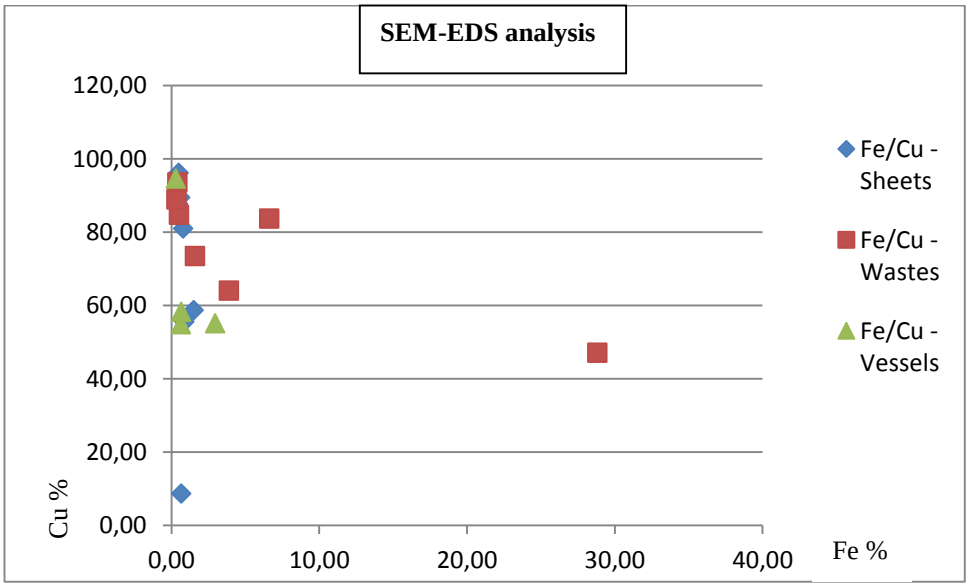

Fig. 6: Distribution of Copper and Iron in the four groups of object by both analytical techniques.

The presence of iron in the copper alloys could be explained by the the deliberate use of iron minerals as a fluxing agent during smelting or by their accidental existence in the used copper ore (Mangou, Ioannou2000:215). Moreover, the iron concentration can rise due to corrosion. The multimetallic ore deposits at Lavrion contain, among others, also iron minerals. Pure chalcopyrite [CuFeS2] occurs there in high concentrations, while chalcopyrite in the calcschists occurs mainly in the Kamariza deposits (Gale et al.2009:162-163). Outcrops of oxidized ores, azurite and malachite within a ferruginous matrix occur also on Crete, where the most of the ingots contain amounts of iron ranging up to 4% w.t. (Doonan et al.2007:100, Mangou and Ioannou2000: 215). It concerns primary ingots, before cleaning during melting. In the 3rd millennium BC, at the Chrysokamino smelting place on Crete fragments of slags contain crystals of the iron oxides magnetite and wustite as well as copper oxidation products, with a small amount of arsenic. However, copper ores were brought there from elsewhere to be smelted, since copper mineralization has not been identified in the vicinity of Crysokamino, and lead isotope analysis of slags has revealed variability, associated probably with the use of ores from various deposits. Nevertheless, it should be noticed that Crysokamino is the only case where calc-ferrous flux was used in copper smelting resulting to significant levels of iron-oxide and lime in the slags (Betancourt2008:107-108,110, Katapotis and Bassiakos2007: 69,71-72). The copper-iron mineralization is usually attested in quartz veins hosted in schists and marbles, while copper-iron ores occur at Milyes on Kythnos (Webb et al. 2006:271, Gale et al.1985:89, Katapotis and Bassiakos2007:70). Copper minerals containing iron occurs in Cyprus where the dominant ores are the primary sulphidic ores of chalcopyrite and pyrite, which are associated with a variety of secondary copper sulfide and oxide minerals, including chalcocite, bornite, covellite and cuprite. (Gale and Stos-Gale2012:77-78, Charalambous et al.2015:97).

The presence of Zinc is confirmed by both analytical techniques in all the objects, either in very low concentrations or in significant amounts. However, high zinc concentrations, which may indicate an intentional addition, are probably connected with a later period of manufacture. The distribution of Copper and Zinc in the four assemblages of objects is seen in Figure 7.

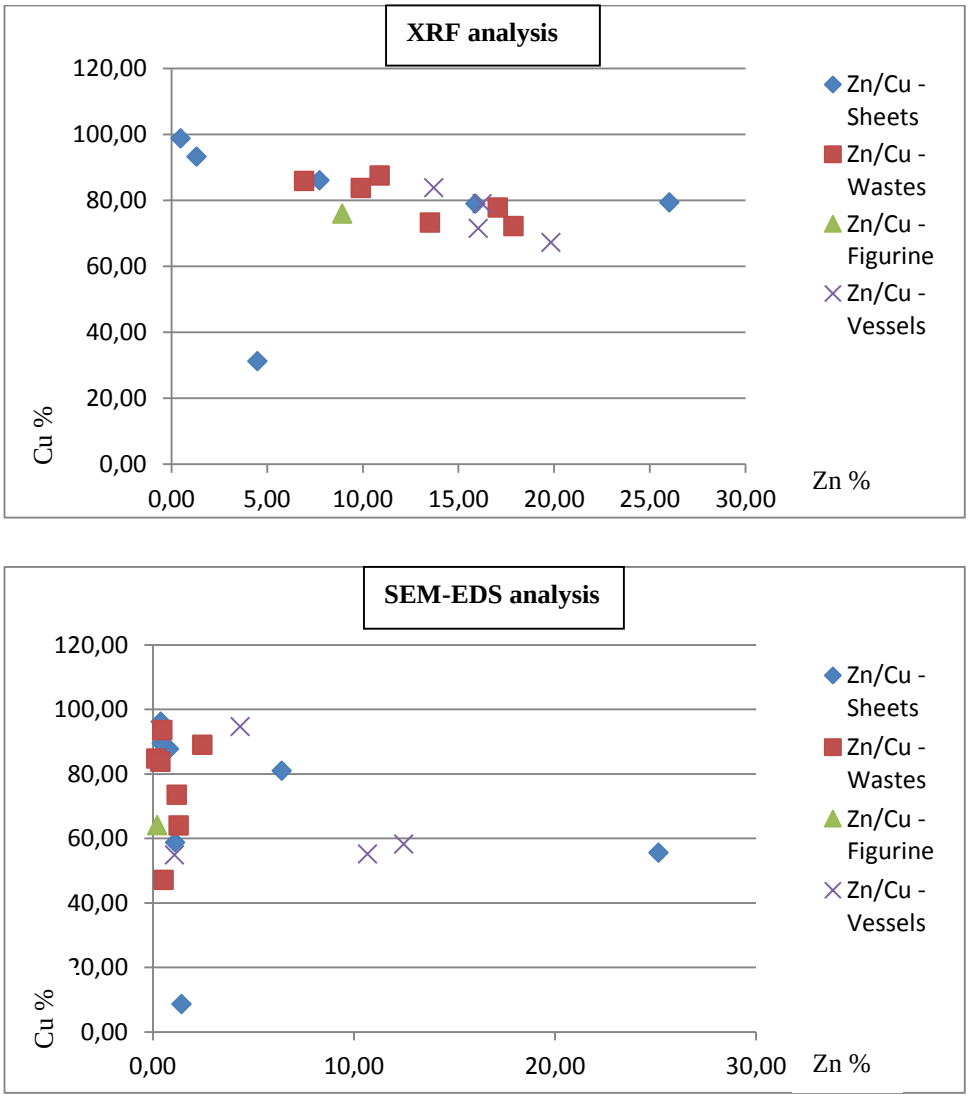

Fig. 7: Distribution of Copper and Zinc in the four groups of objects, by both analytical techniques.

The occurrence of zinc should be probably considered accidental in prehistoric alloys, since zinc is not introduced to the composition of copper alloys and remains unknown in the Aegean region up to Hellenistic or Roman period (Papadimitriou2008:271). The multimetallic ore deposits on Lavrion contain a number of arsenic, lead and zinc complex copper minerals. Sphalerite [(Zn,Fe)S] is the chief ore of zinc, which consists of zinc sulfide and almost always contains variable amounts of iron. This mineral occurs in marbles and schists in the Kamariza, often together with chalcopyrite ores (Gale et al. 2009:161-163). Zinc in low amounts has been detected in most of the Cretan ingots, while it occurs also in the copper sulphide ores on Cyprus (Mangou and Ioannou2000:215, Charalambus et al. 2015:97). Moreover, it occurs in substantial amounts in slags from Kythnos, where it co-exists with arsenic and lead (Gale et al. 1985:86). It should be mention here that the presence of corrosion leads to an overestimation of zinc in measurements.

The presence of silver in trace concentrations was documented in all the objects by XRF and in most of them by SEM-EDS, suggesting its occurrence as impurity. However, the extremely high content of silver in one sheet indicates that it is the dominant element. Figure 8 displays the distribution of copper and silver in both analytical techniques. The Silver / Copper ratio for the sheet KYT_AYV_BS_19 is shown separately in the upper right part of the diagram.

In Lavrion ore deposits there are significant amounts of silver. Galena deposits in Kamariza often include silver sulfide mineral and occur within marble and schist horizons. This argentiferous galena is the most important ore of silver (Gale et al. 2009:162-163). Apart from Lavrion, silver and lead were produced locally in the Cyclades, for instance on Kea, Kythnos and Siphnos. The lead/silver mining and smelting site at Ayios Sostis on Siphnos and the copper smelting site at Skouries on Kythnos are the most

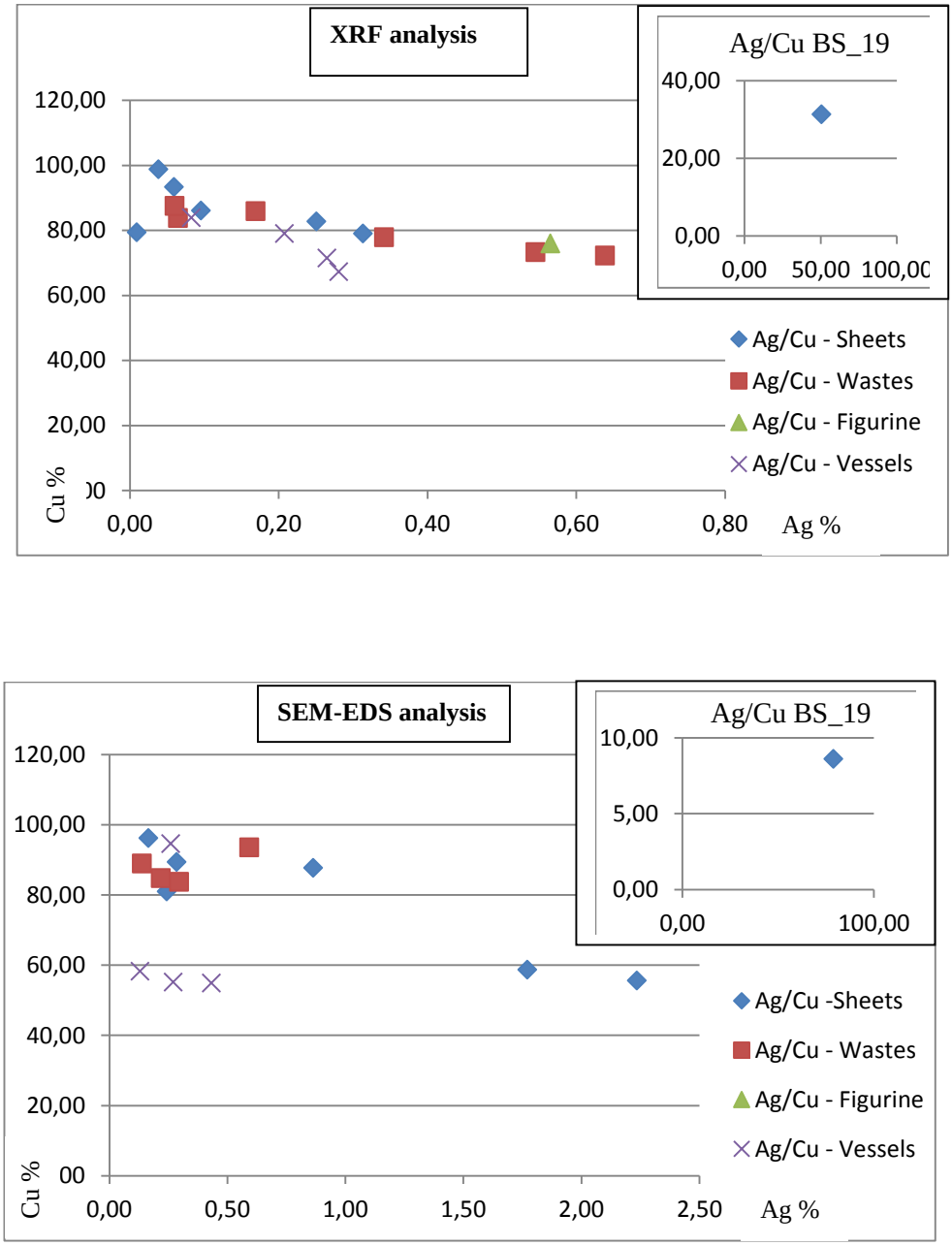

Fig. 8: Distribution of copper and silver in the four groups of objects, with both analytical techniques. Upper right, the Ag/Cu ratio in the sheet KYT_AYV_BS_19.

well-known, while at Daskaleio-Kavos on the islet of Keros metallurgical remains include copper and lead metal, iron minerals and litharge (Gale et al.1985:82, Georgakopoulou2004:3- 4).

These sources, however, indicate the production of metal silver, or the presence of silver as impurity into the alloy. The bronze sheet KYT_AYV_BS_19 represents a different composition from the rest of the analyzed objects as it consists of silver and copper, an alloy uncommon in the Aegean. Apart from the deliberate addition of copper to silver, aiming to a falsification, silver-copper alloys may have been used because of the different appearance and properties which give to the items. An artefact made by a similar copper-silver alloy, with silver content of about 35% w.t., has been found at Mochlos on Crete, whilst, equivalent silver-copper alloys have been found in Anatolia, where the copper metallurgy involves the use of silver (Tselios2008:79, Muhly2006:167). In Eastern Anatolia, at the site Arslantepe on Malatya, objects of silver-copper alloys, with silver contents ranging between 16% and 70% w.t., have been found in a royal tomb (Palmieri et al.2002:52-53). This composition on the one hand results to a lower melting point of the alloy making it easier to handle for melting and casting and on the other hand, upon solidification, allows the alloy to acquire a bright silvery color. The metal luster and hardness increase by heating below the melting point and silver emerges on the surface by hammering and annealing. In this way, these metal alloys have a bright silvery color after having been hammered into shape. These objects, such as the sheet KYT_AYV_BS_19, show a brilliant silvery color after removing the corrosion layer and restoring the original surface; besides, the color, hardness and exceptionally good preservation of BS_19 distinguish it from the other objects under study (Palmieri et al.2002:52-53, Tselios2008:79).

Nickel and Antimony were detected in trace amounts mainly by the XRF method, as the use of the Aluminum - Titanium filter enabled the

examination of such concentrations. The SEM-EDS has recorded these elements only in few cases. Figures 9 and 10 display the distribution of nickel and antimony versus copper by the XRF technique.

Nickel is common in arsenide and sulpharsenide copper ores. Elevated level of nickel concentration has been noted in Crete, while, in most of the Cretan ingots, nickel has been detected in amounts up to 3.0% w.t. (Mangou and Ioannou2000: 215, Doonan et al.2007:106). Moreover, nickel has been detected in slags on Kythnos, where there are copper sources containing significant amounts of nickel. Analyses of copper prills from this place have shown that nickel and arsenic content resulting accidentally from the smelting of oxidized ores (Gale et al.1985:81,89). At Crysokamino, copper ores and prills are characterized by similar arsenic/copper and nickel/copper ratios (Katapotis and Bassiakos2007:72-73).

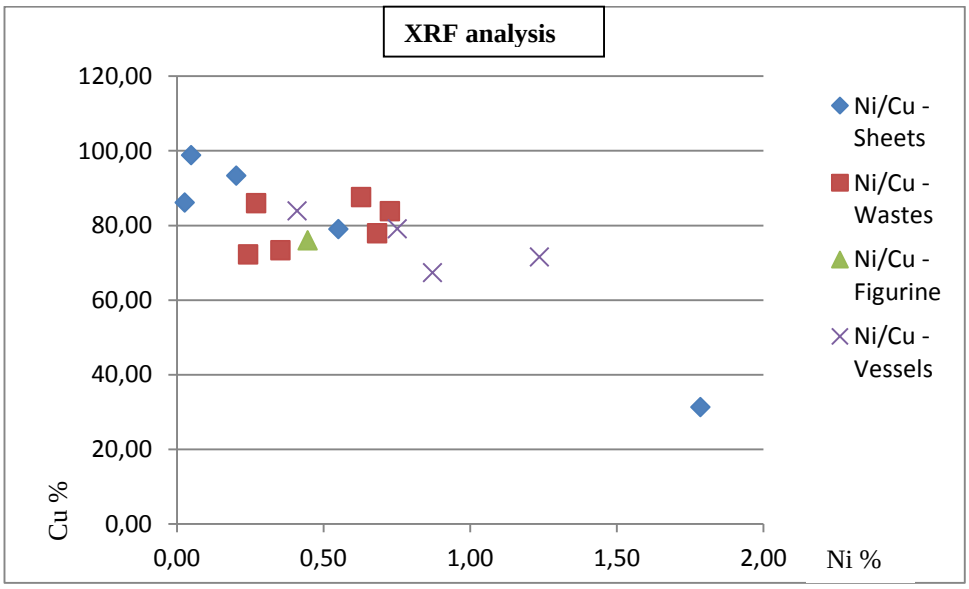

Fig. 9: Distribution of Copper and Nickel in the four groups of objects, by XRF analysis.

The antimony at trace concentrations is regarded as coming from ores like the antimonial copper sulphides (Mangou and Ioannou1997:64). However, it is generally considered as common impurity in the copper alloys (Papadimitriou2008:272). Antimony also co-exists with lead in copper leaded minerals, such as bournonite [PbCuSbS3], occurring in Lavrion (Gale et al.2009:165).

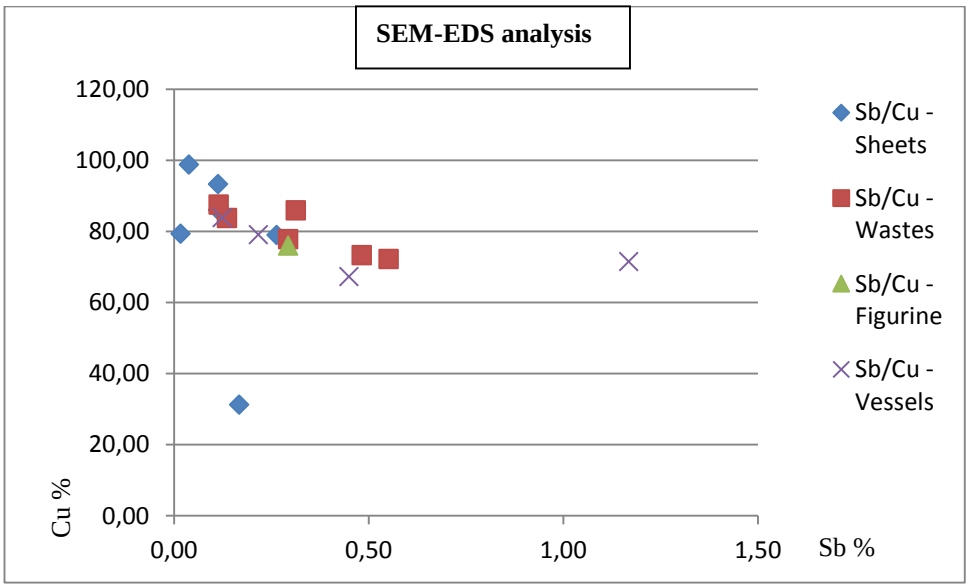

Fig. 10: Distribution of Copper and Antimony in the four groups of objects, by XRF analysis.

Calcium was detected in almost all the objects under study by the SEM-EDS technique and its distribution is shown in Figure 11. Calcium may be used during smelting process, to fuel ash, or may exist as eroded furnace material. Moreover, the presence of calcium may arise from the ores. For instance, slags on Kythnos contain calcium at medium-high concentrations, at a mean of 8% w.t., fluctuating up to 17% w.t. This level is too high to have come from the charcoal or to have been added as a flux and thus, it may have come from the ores which predominantly occur in veins of

marbles and schist (Gale et al.1985:86, Stos-Gale and Gale2006:305). In our case, significant calcium concentrations are recorded in some objects, while the presence of calcium had been also observed during the aforementioned microscopic examination. However it must be taken into account that the encrustations, due to either adhesion of soil residues or formation of corrosion products, may lead to a higher content of calcium. Therefore, both, corroded and free of corrosion areas, have been analyzed during the examination of objects.

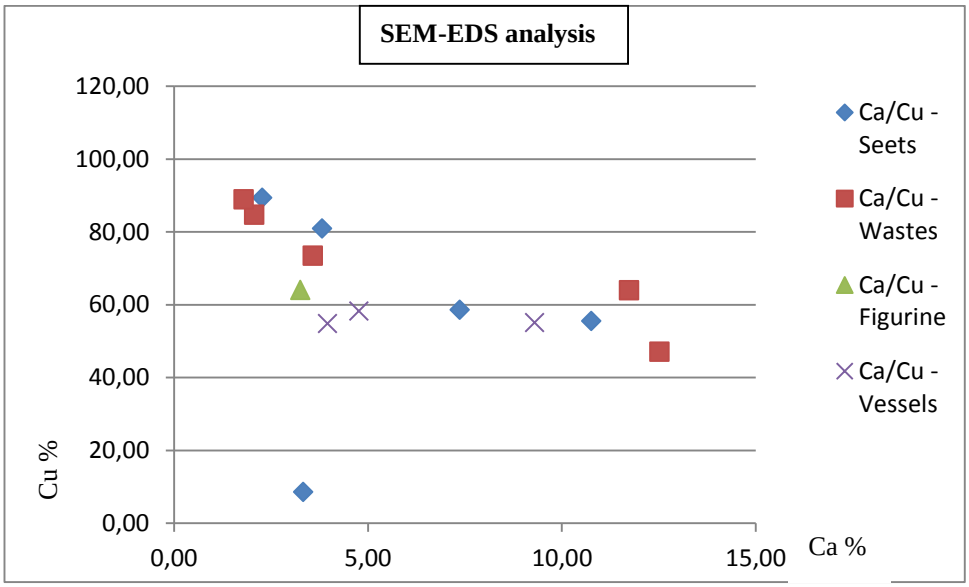

Fig. 11: Distribution of Copper and Calcium in the four groups of objects by SEM-EDS technique.

Sulfur was detected by SEM-EDS in the objects BS_06, BW_05, VF_09 and BS_19. The existence of sulphur characterizes the rich cupriferous sulphides minerals of Cyprus which contain also significant amounts of iron, as mentioned before, because of the common mineral chalcopyrite [Cu FeS2]. Additionally, sulfur occurs in the sulfides copper ores in Lavrion. However, it is worth mentioning that the ores on Cyprus are unusually free of lead, a fact that probably distinguishes them from the chalcopyrite

occurring at Lavrion (Bassiakos and Tselios2012:159, Charalambous et al.2015:96). We could say, therefore, that two different ores containing sulfur have been investigated, a first one without lead detected in the waste KYT_AYV_BW_05, which could possibly come from Cyprus and a second one with a lead content detected in the sheet KYT_AYV_BS_06 and in the vessel KYT_AYV_BV_09, which could possibly come from Lavrion. Copper alloys though, could have been produced by a co-smelting using copper oxide ores together with either copper sulpharsenide or iron sulpharsenide (Muhly2006:167).

It is interesting at this point to observe the element ratios versus copper in the waste KYT_AYV_BW_05, which is one of the three objects with sulfur content (fig.12). This object contains sulfur as well as a significant content of iron, while lead has not been detected. This reminds Cypriot ore and may lead to a possibly Cyprus origin.

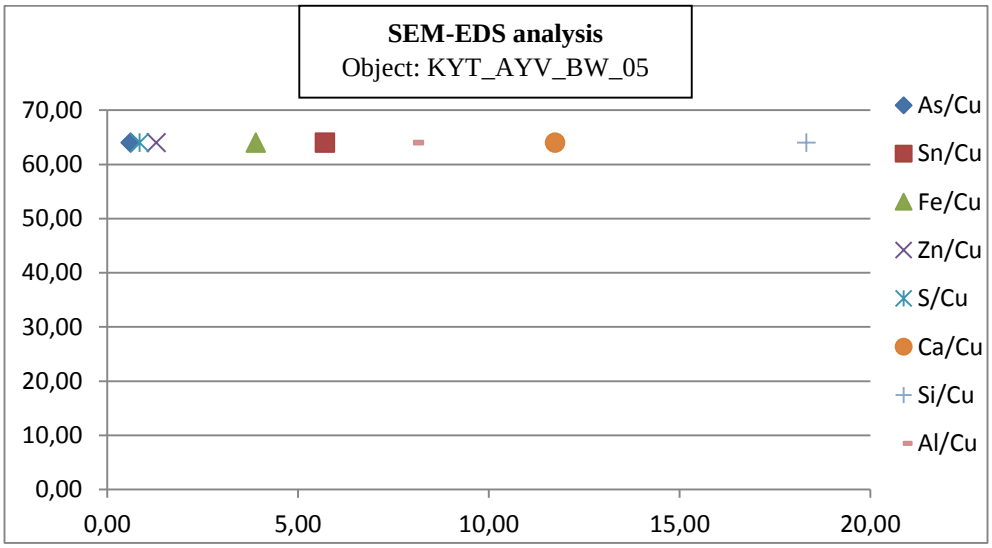

Fig.12: Element ratios versus Copper in the object KYT_AYV_BW_05, measured by SEM-EDS (mean values of measurements).

The existence of Aluminum, Silicon and Magnesium, elements detected by SEM-EDS in some cases, may be related to the smelting procedure or to the

presence of soil remains, entrapped to corrosion encrustations. Aluminum-silicate melts of various chemical compositions affect the slag melting points and furnace temperatures as well as the efficiency of separation of metal from the slag phase in the furnace. Especially, the existence of quartz (SiO_2) within the copper slags suggests that copper most likely was entered to the charge as a mineral rather than in its metallic form (Georgakopoulou2004:9). Figure 13 shows the distribution of silicon and copper in the four groups of objects by SEM-EDS technique. We see that in the assemblage of wastes the SEM-EDS analysis have attested an appreciable amount of silicon that may be due to the used copper minerals, given that, attached calcareous rock or soil conglomerates were also entrapped between copper oxides in the aforementioned microscopic examination.

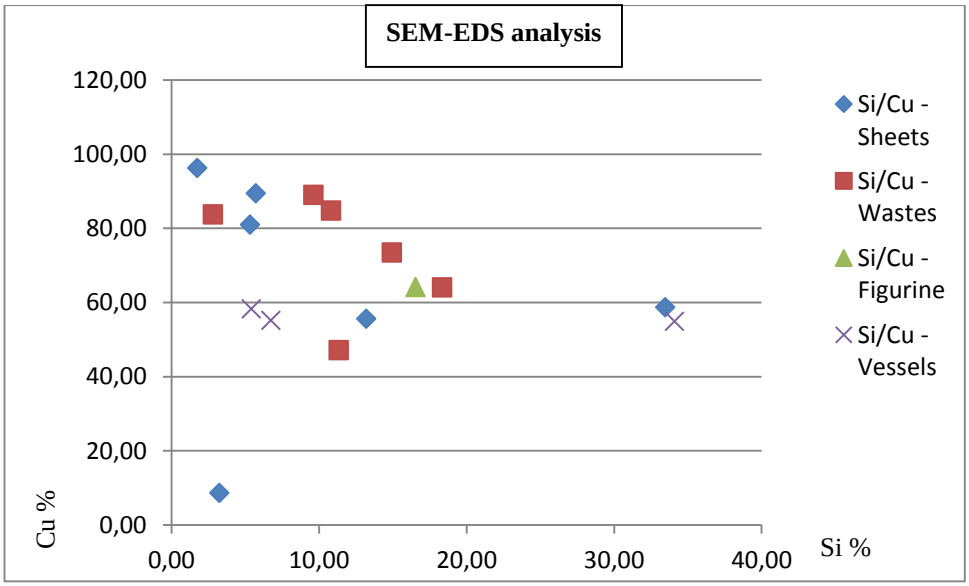

Fig. 13: Distribution of Silicon and Copper in the four groups of objects by SEM-EDS technique.

The detected Chlorine is due to the corrosion of copper, as copper oxides, malachite, azurite and cuprite, have been weathered to atakamite

[$Cu_2Cl(OH)_3$]. This formation is favored by the presence of Chlorine and humidity, which are prevalent in costal environments such as that at Ayios Yeoryios sto Vouno in Kythera.

The measurements of the sheet assemblage taken by both XRF and SEM-EDS techniques concerning the elements Cu, As, Sn, Pb, Fe, Zn, Ni, Sb and Ag are recorded on Tables 7 and 8. The elements Al, Si and Ca, detected by SEM-EDS, are not included here, because their vast majority is probably related to the existed corrosion layers. Since the deliberate addition of zinc to the copper alloys was unknown in prehistoric periods, the sheet KYT_AYV_BS_07 has been excluded from the group because of its extremely high concentration of zinc. The distribution of the elements arsenic, tin, lead, iron, zinc and silver versus copper for the rest of the objects of this assemblage are shown in Figure 14, while the distribution of the elements copper, arsenic, tin, lead, iron and zinc versus silver for the sheet KYT_AYV_BS_19 is shown separately in Figure 15, because of the different composition of the alloy.

Bronze Sheets

Table 7: Concentration of the elements (mean values) Cu, As, Sn, Pb, Fe, Zn, Ni, Sb and Ag expressed in % wt (n.d.: non detected). Measurements taken by **XRF**.

KYT_AYV	BS_01	BS_02	BS_06	BS_07	BS_08	BS_10	BS_19
CuO	86,10	93,35	79,04	79,43	98,83	82,84	31,33
As_2O_3	0,63	0,32	0,05	0,00	0,13	0,01	1,14
SnO_x	1,38	1,93	0,27	0,06	0,24	0,21	9,35
PbO	2,81	1,72	0,26	0,04	n.d.	0,21	0,13
Fe_2O_3	0,82	0,74	1,16	0,04	0,18	1,21	0,33
ZnO	7,74	1,31	15,88	26,01	0,48	12,72	4,49
Ni	0,03	0,20	0,55	n.d.	0,05	0,64	1,79
Sb_2O_5	0,11	0,11	0,26	0,02	0,04	0,18	0,17
Ag	0,10	0,06	0,31	0,01	0,04	0,25	50,47

Bronze Sheets

Table 8: Concentration of the elements (mean values) Cu, As, Sn, Pb, Fe, Zn, Ni, Sb and Ag expressed in % w.t. (n.d.: non detected). Measurements taken by **SEM-EDS**.

KYT_AYV	BS_01	BS_02	BS_06	BS_08	BS_10	BS_19	BS_07
CuO	81,00	96,21	87,68	89,42	58,70	8,64	55,60
As_2O_3	0,60	0,40	0,76	0,42	1,50	0,51	2,21
SnO_x	2,92	0,64	0,67	0,55	0,30	0,83	2,88
PbO	2,49	0,31	0,90	0,62	0,79	0,84	1,86
Fe	0,79	0,48	0,43	0,59	1,49	0,66	0,87
ZnO	6,41	0,39	0,80	0,44	1,10	1,42	25,13
Ni	0,44	0,55	n.d.	n.d.	n.d.	1,43	5,29
Sb_2O_5	n.d.	n.d.	n.d.	n.d.	n.d.	n.d.	n.d.

In general, a relatively low impurity level was observed which improved the ability of the metal to be forged or hammered without cracking (Papadimitriou2008:279). The addition of tin made the alloys harder, but the concentration of tin is appreciable only in the sheet KYT_AYV_BS_01, which also has a high lead ratio. Thus, we could suppose that possibly the coppersmiths were not particularly interested on the production of a strong alloy but, primarily, of a stable one, since, significant amounts of arsenic and lead, elements which can destabilize an alloy, are not observed[4]. Additionally, in this group, a low iron concentration was observed, maybe due to the fact that in the case of forming by hammering, the presence of iron is harmful and can be manifested as various surface defects such as the cracks. We could speak, therefore, of a sufficient control of the metallurgical process and an advanced technology.

[4] Lead liquefies within the solid mass of the alloy when heated above 330^0C and thus cracking occurs during forging or hammering, while arsenic may evaporate during hot forging causing softening of the alloy (Papadimitriou2008:276).

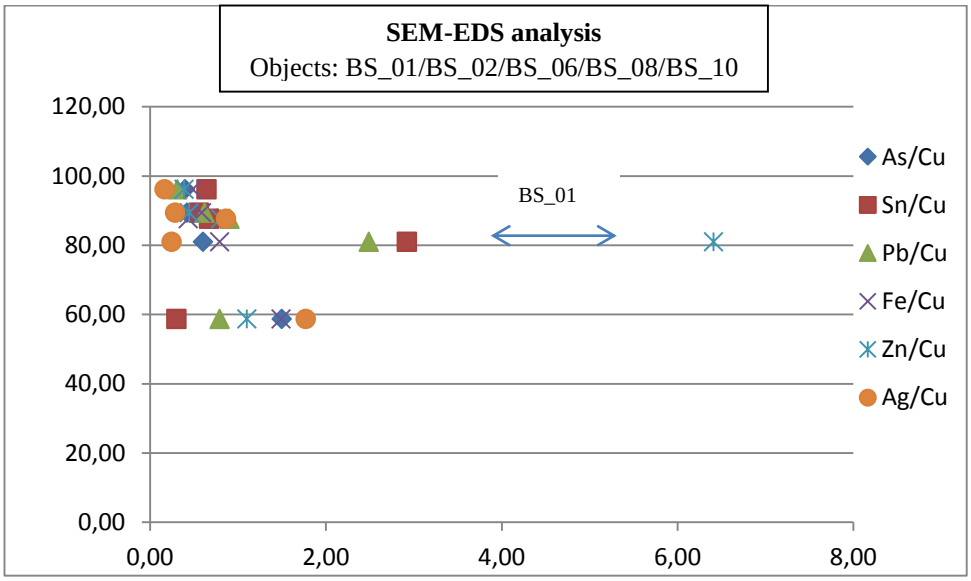

Fig. 14: Distribution of the elements Arsenic, Tin, Lead, Iron, Zinc and Silver versus Copper measured by SEM-EDS.

Regarding the object KYT_AYV_BS_19, the low impurities level is worth mentioning. It is, possibly, an intentionally made alloy rather than a falsification product and its manufacturing presents similarities with silver-copper alloys from Anatolia. The manufacturing of such alloys aimed to the production of artifacts with a rich silvery and lustrous appearance. This item could have been imported, since other imported 'exotic' finds in the Late Minoan period have been found on Crete, especially at Mochlos[5], a fact showing the relations of the Minoans with Anatolia and the trade route, from where, the tin came. It is worth mentioning that an appreciable tin ratio occurs also in the object KYT_AYV_BS_19.

[5] Apart from the before mentioned artefact made by a similar silver-copper alloy, the excavation at Mochlos has uncovered a sistrum probably manufactured in Egypt and a trident probably from the Syrian coast (Tzachili2004:22, Soles2004:148,153).
In Messenia, analyses have revealed the presence of silver plating objects, for funerary purpose, however, the object KYT_AYV_BS_19 seems that is made from a silver-copper alloy (Tselios et al2015:83-84).

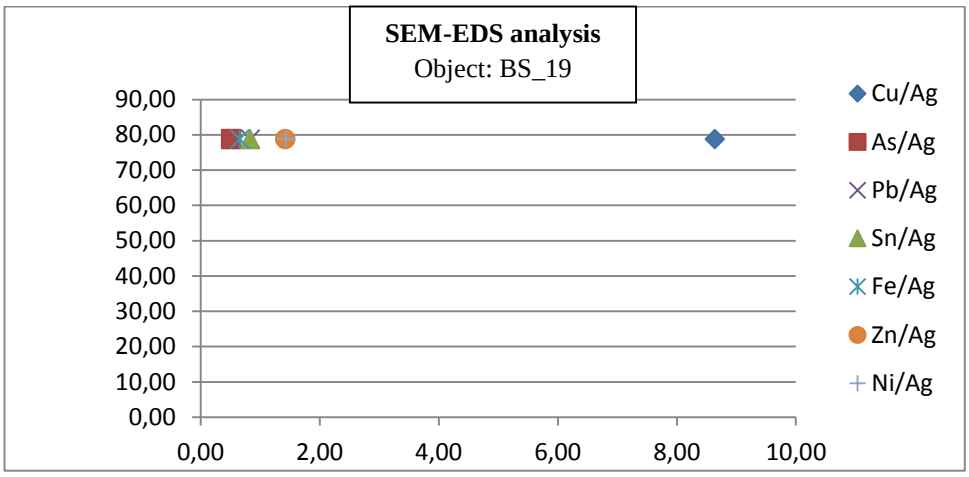

Fig. 15: Distribution of the elements Copper, Arsenic, Tin, Lead, Iron and Zinc versus Silver for the sheet KYT_AYV_BS_19.

The measurements of the waste assemblage, concerning the elements Cu, As, Sn, Pb, Fe, Zn, Ni, Sb and Ag, taken by XRF and the elements Cu, As, Sn, Pb, Fe, Zn, Ni, Sb, Ag, S, Ca, Si and Al taken by SEM-EDS are recorded on Tables 9 and 10.

Bronze Wastes

Table 9: Concentration of the elements (mean values) Cu, As, Sn, Pb, Fe, Zn, Ni, Sb and Ag expressed in % w.t. Measurements taken by XRF (n.d.: non detected).

KYT_AYV	BW_04	BW_05	BW_15	BW_16	BW_17	BW_18
CuO	77,88	72,25	73,35	85,94	83,82	87,57
As_2O_3	0,01	0,20	1,15	0,33	0,17	0,08
SnO_x	0,30	0,73	0,54	0,12	0,16	0,16
PbO	0,28	0,09	5,85	3,68	n.d.	0,10
Fe_2O_3	0,80	5,04	2,44	0,39	3,68	0,10
ZnO	17,05	17,87	13,50	6,92	9,89	10,88
Ni	0,68	0,24	0,35	0,27	0,73	0,63
Sb_2O_5	0,29	0,55	0,48	0,31	0,14	0,11
Ag	0,34	0,64	0,54	0,17	0,06	0,06

Bronze Wastes

Table 10: Concentration of the elements (mean values) Cu, As, Sn, Pb, Fe, Zn, Ni, Sb, Ag, S, Ca and Si expressed in % w.t. Measurements taken by SEM-EDS (n.d.: non detected).

KYT_AYV	BW_04	BW_05	BW_14	BW_15	BW_16	BW_17	BW_18
CuO	84,75	64,03	47,12	73,49	88,98	83,74	93,57
As_2O_3	0,50	0,61	1,60	0,36	0,94	0,84	0,57
SnO_x	0,29	5,70	0,81	1,53	0,25	0,78	0,60
PbO	0,23	n.d	0,35	5,40	0,37	0,96	1,08
FeO	0,50	3,89	28,82	1,59	0,34	6,61	0,40
ZnO	0,17	1,29	0,53	1,19	2,45	0,38	0,46
Ni	0,46	n.d.	0,97	n.d.	n.d.	n.d.	n.d.
Sb_2O_5	n.d.	n.d.	1,86	n.d.	0,53	n.d.	n.d.
Ag	0,22	n.d.	n.d.	n.d.	0,14	0,30	0,59
S	n.d.	0,85	n.d.	n.d.	n.d.	n.d.	n.d.
CaO	2,06	11,73	12,51	3,58	1,79	n.d.	n.d.
SiO_2	10,80	18,33	11,32	14,92	9,63	2,80	n.d.
Al_2O_3	3,57	8,04	4,99	4,90	1,79	n.d.	n.d.

Taking into account the limitations of both methods related to the calculation of arsenic concentration as well as the easy evaporation of arsenic during melting, we could say that in the wastes KYT_AYV_BW_14 and KYT_AYV_BW_16, the arsenic content shows that these may have come from the recycling of arsenical copper. A different composition presents the waste KYT_AYV_BW_05, which is a metal spill and contains the higher level of tin, probably from tin copper melting, while significant tin ratios occur also in KYT_AYV_BW_15. Thus, we could say that various types of alloys may have been used according to the produced objects and the desired properties. Moreover, since tin was a rare and possibly expensive material, compared to arsenic, which may also come from the

recycling of old metals, we could suppose that different kinds of alloys might have been used. Additionally, the high copper concentration in the wastes may indicate that pure copper metal was intended for the manufacturing of objects.

Moreover, the choice of the alloy might have depended on the available sources. The waste KYT_AYV_BW_05 represents a peculiarity, since it is the only that contains sulfur. The existence of sulfur combined with the absence of lead and the significant ratio of iron may lead to the conclusion that it possibly came from Cyprus, where cupriferous sulphides minerals occur. The distribution of the elements arsenic, tin and sulfur versus copper in the waste assemblage is shown in Figure 16, while Figure 17 displays the distribution of the elements sulfur, lead, iron and calcium.

The extremely high iron and calcium ratios in the waste KYT_AYV_BW_14 could have derived from the occurrence of corrosion and soil residues. The high lead concentration may be due to the intended casting, where higher amounts of lead were used. Since lead has a low melting point, it often occurs in low concentrations in copper wastes. Thus, the waste KYT_AYV_BW_15 possibly represents a pure leaded copper, maybe for casting, since it comprises a significant amount of lead combined with a high copper ratio. The extremely low iron concentration in the wastes KYT_AYV_BW_04, KYT_AYV_BW_16 and KYT_AYV_BW_18 combined to a high copper ratio may indicate fragments of an oxide ingot, namely a product of secondary admixture.

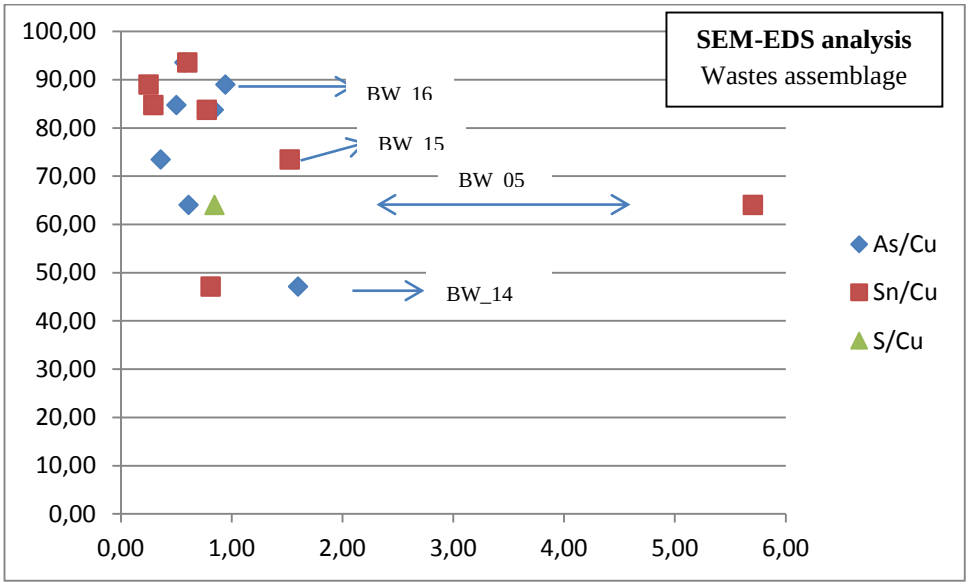

Fig. 16: Distribution of the elements Arsenic, Tin and Sulfur versus Copper in the waste assemblage.

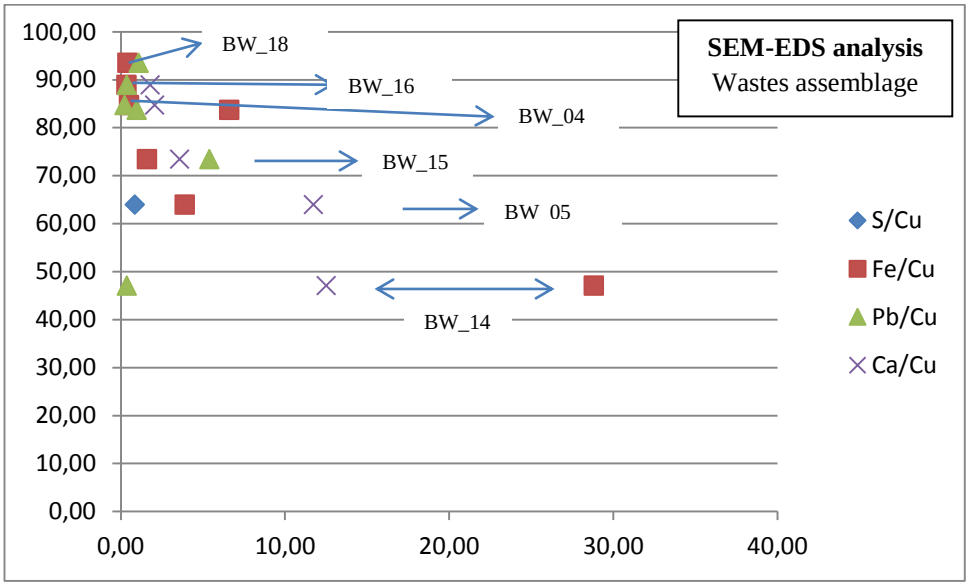

Fig. 17: Distribution of the elements Sulfur, Lead, Iron and Calcium versus Copper in the waste assemblage.

The measurements of the figurine base taken by both XRF and SEM-EDS techniques concerning the elements Cu, As, Sn, Pb, Fe, Zn, Ni, Sb and Ag are recorded on Tables 11 and 12. The elements Al, Si and Ca, detected by SEM-EDS are not included here, because their vast majority is probably related to the existed corrosion layers.

Figurine Base

Table 11: Concentration of the elements (mean values) Cu, As, Sn, Pb, Fe, Zn, Ni, Sb and Ag expressed in % w.t. Measurements taken by XRF (n.d.: non detected).

KYT_AYV	CuO	As_2O_3	SnO_x	PbO	Fe_2O_3	ZnO	Ni	Sb_2O_5	Ag
FB_03	76,05	1,20	0,62	6,33	3,47	8,91	0,45	0,29	0,56

Figurine Base

Table 12: Concentration of the elements (mean values) Cu, As, Sn, Pb, Fe, Zn, Ni, Sb and Ag expressed in % w.t. Measurements taken by SEM-EDS (n.d.: non detected).

KYT_AYV	CuO	As_2O_3	SnO_x	PbO	FeO	ZnO	Ni	Sb_2O_5	Ag
FB_03	64,13	2,43	0,58	14,18	n.d.	0,22	n.d.	0,75	n.d.

The significant concentration of arsenic, which has been recorded with both techniques, leads to the conclusion that the figurine base is possibly the only case of intentional addition of arsenic. Nevertheless, an alloy deriving from recycling of old metals might have been used, since the advantageous properties of arsenical copper are not necessary for the manufacturing of figurines, more so as arsenical copper and copper have almost the same hardness in casting and only after hammering arsenical copper may become advantageous.

The presence of lead in casted objects is explained by the fact that it promotes castability and lowers the melting point of the alloy. Arsenic also

acts as deoxidant in casting, suppressing brittleness, due to the presence of copper oxide inclusions in the metal (Papadhmitriou2008:277). But even more important is the fact that the addition of arsenic to the alloy gives to the object a wanted silvery appearance. The presence of iron is indifferent to casting and may be tolerated up to 5% w.t., as at higher contents it may increase the melting point of the alloy (Papadimitriou2008:287). In the objects under study the iron concentration is very low and we could suggest that coppersmiths knew the consequences of iron in the alloy. The low iron concentration combined with the high lead concentration would lead us to suggest that the coppersmiths were able to control the melting point of the produced alloy and, thus, were able to select the alloys according to the manufacturing technique, the concentration of impurities and the desired properties of the objects to be produced. The distribution of the elements arsenic, tin, lead and iron versus copper in the figurine base, with both techniques, is shown in Figure 18.

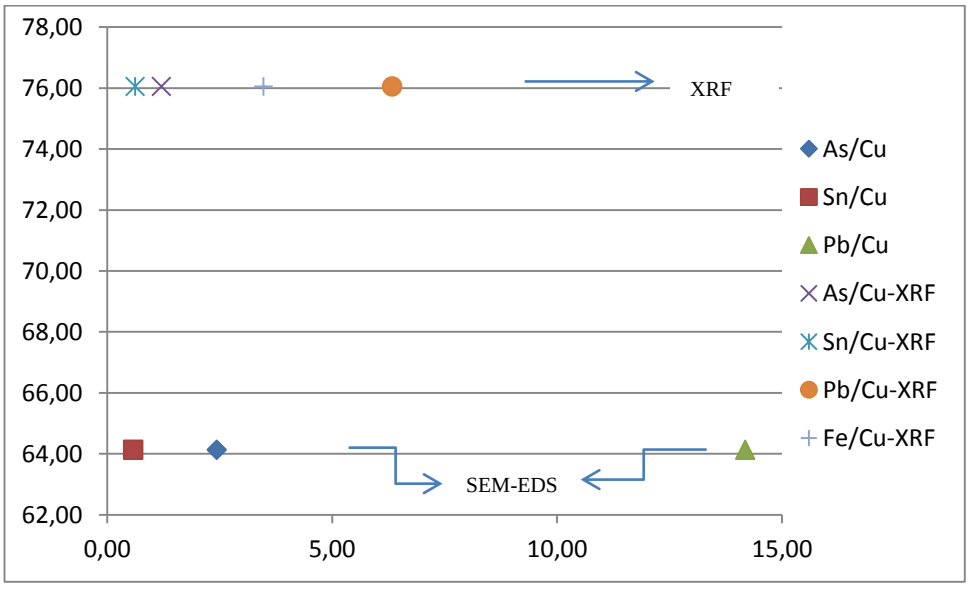

Fig. 18: Distribution of the elements As, Sn, Pb and Fe versus Cu in the figurine base by both techniques.

On Tables 13 and 14 the measurements of the vessel assemblage taken by both XRF and SEM-EDS techniques concerning the elements Cu, As, Sn, Pb, Fe, Zn, Ni, Sb and Ag are presented. The extremely high concentration of zinc, detected by both techniques, in the fragments of vessels KYT_AYV_FV_11 and KYT_AYV_FV_12, leads us to suggest that they probably come from a later period, since in the prehistoric copper alloys the deliberate addition of zinc was unknown. As far as the fragment KYT_AYV_FV_13 is concerned, which contains a lower amount of zinc, the different composition may have been resulted by the manufacturing technique, since the lower amount of zinc combined with the very pure copper metal is a common composition of vessel handles in later periods.

Vessel Fragments

Table 13: Concentration of the elements (mean values) Cu, As, Sn, Pb, Fe, Zn, Ni, Sb and Ag expressed in % w.t. Measurements taken by XRF (n.d.: non detected).

KYT_AYV_	VF_09	VF_11	VF_12	VF_13
CuO	79,10	71,54	67,35	83,92
As_2O_3	0,08	0,93	1,68	0,02
SnO_x	0,23	0,52	0,59	0,13
PbO	0,93	5,75	4,75	0,33
Fe_2O_3	1,04	1,73	3,02	0,42
ZnO	16,23	16,03	19,83	13,70
Ni	0,75	1,24	0,87	0,41
Sb_2O_5	0,22	1,17	0,45	0,12
Ag	0,21	0,26	0,28	0,08

Vessel Fragments

Table 14: Concentration of the elements (mean values) Cu, As, Sn, Pb, Fe, Zn, Ni, Sb and Ag expressed in % w.t. Measurements taken by SEM-EDS (n.d.: non detected).

KYT_AYV_	VF_09	VF_11	VF_12	VF_13
CuO	54,87	58,27	55,16	94,63
As_2O_3	0,89	1,19	1,17	0,28
SnO_x	1,39	14,17	5,90	0,15
PbO	1,22	4,23	6,89	0,46
FeO	0,64	0,65	2,95	0,29
ZnO	1,07	12,47	10,68	4,33
Ni	0,92	0,72	0,86	n.d.
Sb_2O_5	n.d.	7,66	4,08	n.d.
Ag	0,43	0,13	0,27	0,26
S	1.77	n.d.	n.d.	n.d.

However, the composition of fragment KYT_AYV_VF_09 shows similarities to that of the sheet KYT_AYV_BS_01, including a significant amount of tin and lead it may thus represent a prehistoric alloy with similar characteristics to that described above. In comparison to KYT_AYV_BS_01, however, the copper ratio is lower, while a significant sulfur concentration has been detected. This may be due to the use of sulfide minerals, which, taken together with the co-existence of lead and silver, could may suggest a provenance from Lavrion. Since the concentration of lead is significant, we may also suppose a deliberate addition of this element to the object. Figure 19 displays the distribution of the elements arsenic, tin, lead, iron, nickel, silver and sulfur versus copper in the fragment KYT_AYV_VF_09 by SEM-EDS and XRF techniques.

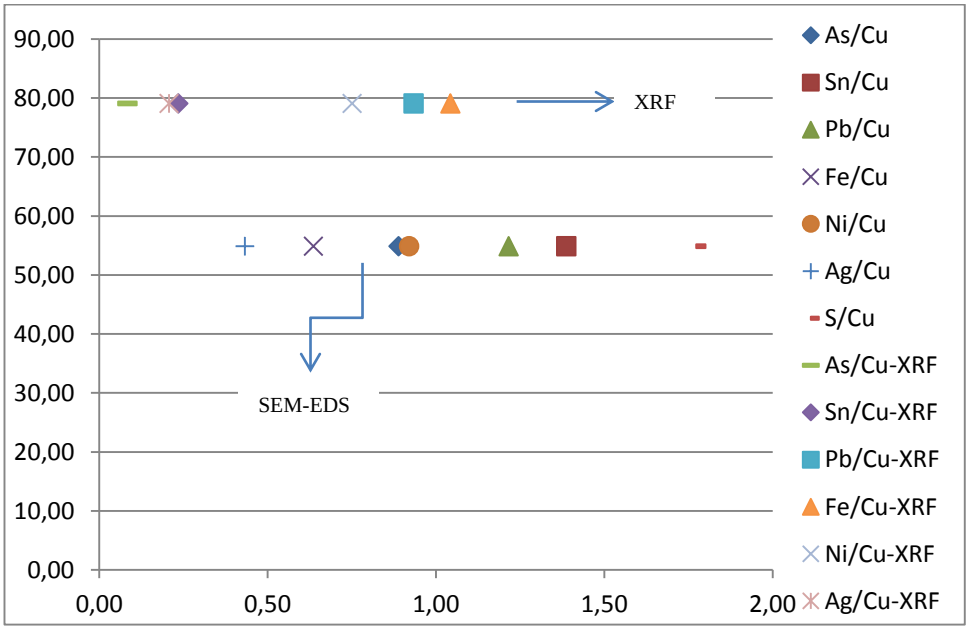

Fig. 19: Distribution of the elements As, Sn, Pb, Fe, Ni, Ag and S versus copper in the fragment VF_09, by SEM-EDS and XRF techniques.

3. Conclusions

From the investigation of bronze objects of the peak sanctuary at Ayios Yeorgios sto Vouno on Kythera, we could conclude that the copper-based objects vary in their elemental composition. Copper is the dominant component and arsenic, tin, lead and iron are present as minor constituents. A copper manufacture therefore, containing minor constituents due either to recycling or their presence in the ore, probably indicates a local production. Other minor or trace elements detected are zinc, silver, nickel and antimony. As far as the object KYT_AYV_BS_19 is especially concerned, this is highly differentiated through the alloy used for its manufacture having silver as its dominant component. The vessel fragments KYT_AYV_VF_11, KYT_AYV_VF_12 and the sheet KYT_AYV_BS_07, which contain a

significant amount of zinc, are connected with a later period, Hellenistic or Roman, when bras was in use (bras is the alloy of copper with zinc).

The variation in composition of objects shows that they do not all come from a single source or production. Additionally, the detection of low tin contents is remarkable, since tin was added in considerable amounts in copper alloys during the Late Bronze Age. Moreover, the presence of small amounts of other metals together with arsenic and tin indicate that in most cases, recycled metals have been used. The low arsenic content may be also due to the recycling of older metals because of the evaporation of an arsenic quantity during the re-melting and the addition of tin for the manufacturing of new objects. However, the possibility of an intentional alloy including both arsenic and tin could not be excluded. The intension of such an admixture would have been either the enhancement of the properties of the objects or the presence of arsenic in recycled metal.

A further remark should also be made concerning the fluctuations in the quantities of tin and arsenic in the analyzed objects. Taking into consideration some peculiarities of the arsenical copper, such as its superior properties for hot-working and also the property of arsenic to act as de-oxidant in casting, the silver appearance that gives to objects as well as the fact that for the manufacturing of bronze votives the mechanical advantages of tin bronze were not necessary, we conclude that probably different alloys were used depending on the type of object that would be manufactured. The coppersmiths who visited the sanctuary of Ayios Yeorgios sto Vouno therefore, were possibly aware of the necessary techniques and could possess the means for the selection of the more suitable alloy and manufacture process for any type of object. Thus, while repeated analyses of areas by SEM-EDS determine that the figurine base KYT_AYV_FB_03 is made of arsenical copper alloy, with an arsenic ratio 2.43% wt. ± 0.4, the concentration of tin in the sheet KYT_AYV_BS_01 is 2.92 wt. ±0.75;

regarding wastes, KYT_AYV_BW_05 has a tin ratio of 5.7% wt. ±0.42 and KYT_AYV_BW_14 an arsenic ratio of 1.60 wt. ±0.57. We could therefore suggest a preference for arsenic addition in the case of the casted objects, versus a tin addition in hammered objects, whilst, regarding wastes a fluctuation in the use of both arsenic and tin is observable depending on their intended use.

Arsenical copper could have derived from recycled metal hoards or indicate easier access to sources of copper containing arsenic. Minoans were familiar with the manufacturing of arsenic-copper alloys from the 3rd millennium already, as the study of copper melting sites at Crysokamino and Poros Katsambas has established. The similarities of the objects from Ayios Yeoryios sto Vouno with materials and slags from these sites could therefore be related to the use of recycled metals. It should be noted, however, that the concentrations of arsenic in the wastes KYT_AYV_BW_14 and KYT_AYV_BW_16, which range from 1% to 1.5% w.t., could lead to the conclusion that they come from arsenical copper manufacturing.

Based on the used chemical analyzes, our conclusions concerning the potential source of raw materials could not be considered definite. Other combined analytical methods are also necessary, in order to resolve issues related to provenance. However, the presence of the metals arsenic, lead and silver as well as of smaller amounts of other basic metals such as iron, nickel and antimony suggest that polymetallic ores were probably used for the manufacture of the objects from Ayios Yeoryios sto Vouno. This kind of ores occurs both at region of Lavrion and in the Cyclades, but the Cyclades, are considered as a probable copper source in the Early Bronze Age mainly. However, and the use of polymetallic ores in the case of Ayios Yeoryios sto Vouno could be due to the deliberate admixture of various materials in the furnace charge during smelting, or from the re-melting of recycled metals.

On the other hand, the documented high content of copper may also be connected with copper ores at Lavrion, the easy process of which can yield minerals with a copper content up to 90% w.t. This fact combined with the detection of lead, zinc, silver and iron in the objects from Ayios Yeoryios sto Vouno suggests that raw materials from Lavrion might have been used. Another indication for the use of ores from Lavrion, in this case of sulfide ores, arises from the analysis of fragment KYT_AYV_VF_09, in which, trace amounts of silver and nickel as well as significant amounts of lead has been detected. Lavrion was one of the ore sources supplying copper to the Minoans, especially in the Late Bronze Age and high copper concentrations have generally been documented in artefacts found in Crete.

A probable provenance from Cyprus may be assigned in the case of waste KYT_AYV_BW_05 only, in which a composition of cupriferous sulphides minerals typical for Cyprus has been detected. Additionally the bronze sheet KYT_AYV_BS_19 could be related to Anatolia, either as finished artefact or as manufacturing technique. Cyprus was in contact with the Anatolian mainland, exporting and receiving both imported raw materials and finished artefacts, while metalsmiths from Anatolia went to Cyprus for metal prospecting (Webb et al.2006:282).

Chemical analyses of oxhide ingots of the LBA[6] period found in Crete have shown that copper was very pure, usually containing 99% w.t. or more of copper and with arsenic impurity of about 0.3% w.t. (Gale and Stos-Gale1986:85, Papadimitriou2008:283). Thus, the amorphous metal lumps KYT_AYV_BW_04, KYT_AYV_BW_16, and KYT_AYV_BW_18 of the waste assemblage may be fragments of ingots since their composition

[6] Similar ingots belonging to previous periods have not be found because probably does not exist. Then raw copper was available as small pieces and prills since the level of metallurgical production was small leading to the division and cutting of the material into small pieces for melting purpose (Papadimitriou2008:283).

indicates pure bronze. These fragments, combined with the detection of lead, may have been intended as votives per se or for the manufacture[7]. However, one waste, the KYT_AYV_BW_05, may be a bronze prill residue indicating manufacture in situ.

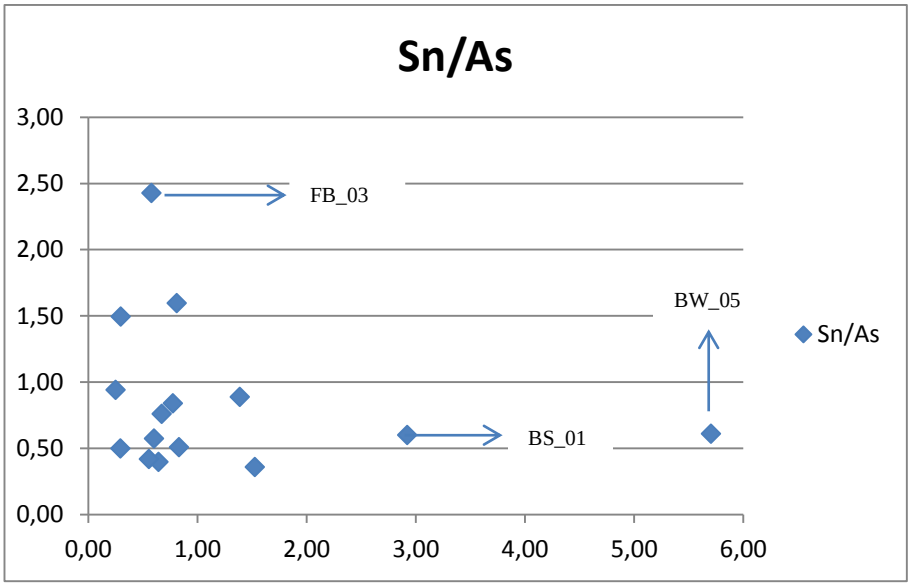

Fig. 20: Distribution of Sn and As by SEM-EDS technique.

In a period when tin bronze was already used, significant tin concentrations have not been detected, while, a high copper content has been documented by the analyses. Thus, the objects were probably made by pure copper with a low amount of impurities. From the distribution of tin and arsenic (fig. 20) we could conclude that the only cases where a deliberate alloying occurs are the arsenical coper of KYT_AYV_FB_03 and the tin bronzes KYT_AYV_BS_01 and KYT_AYV_BW_05.

The metallurgical study of the object sample from Ayios Yeoryios sto Vouno strengthens the hypothesis that the peak sanctuary was frequented by

[7] For the presence of a broken miniature ingot in a cultic context at Alassa, Cyprus, Hadsisavvas 2011, 23-24; for the interpretation of miniature ingots as cultic artifacts in general, see Giumlia-Mair, Kassianidou and Papasavvas 2011.

Minoans engaged in metal exploitation and trade is strengthened. The overseas visitors of the sanctuary not only knew the metal sources of the Aegean but very possibly also those in more distant areas. They possessed the knowledge of alloying methods and of the process of copper alloy objects. Furthermore, they were interested on rare manufacturing techniques or objects made by different alloys. Both raw materials and finished objects are present in the sanctuary while scrap ingots and the bronze spill may indicate local production.

Much work is still needed for a thorough understanding of the provenance and manufacturing of the bronze votives from the peak sanctuary at Ayios Yeorgios sto Vouno on Kythera. This study can only form a basis for further investigation, for which not only chemical analyses but also the application of other combined techniques may be used. The great number and the variety of bronze objects from Ayios Yeoryios sto Vouno are very promising in this respect.

APPENDIX

Figures

Fig.1: View of Ayios Yeoryios sto Vouno, photo taken from south (Sakellarakis 2011:149).

Fig.2: Piraeus, Archaeological Museum: adorants statuettes, scorpion's figurine, human limbs, a black steatite ladle with carved inscription and miniature blades from the Peak Sanctuary at Ayios Yeoryios sto Vouno.

Fig.3: Photo of the eastern Mediterranean by satellite (Kourkoumelis2011:77).

Fig.4: View of Ayios Yeoryios sto Vouno, photo taken from northwest (https://hellenicum.wordpress.com).

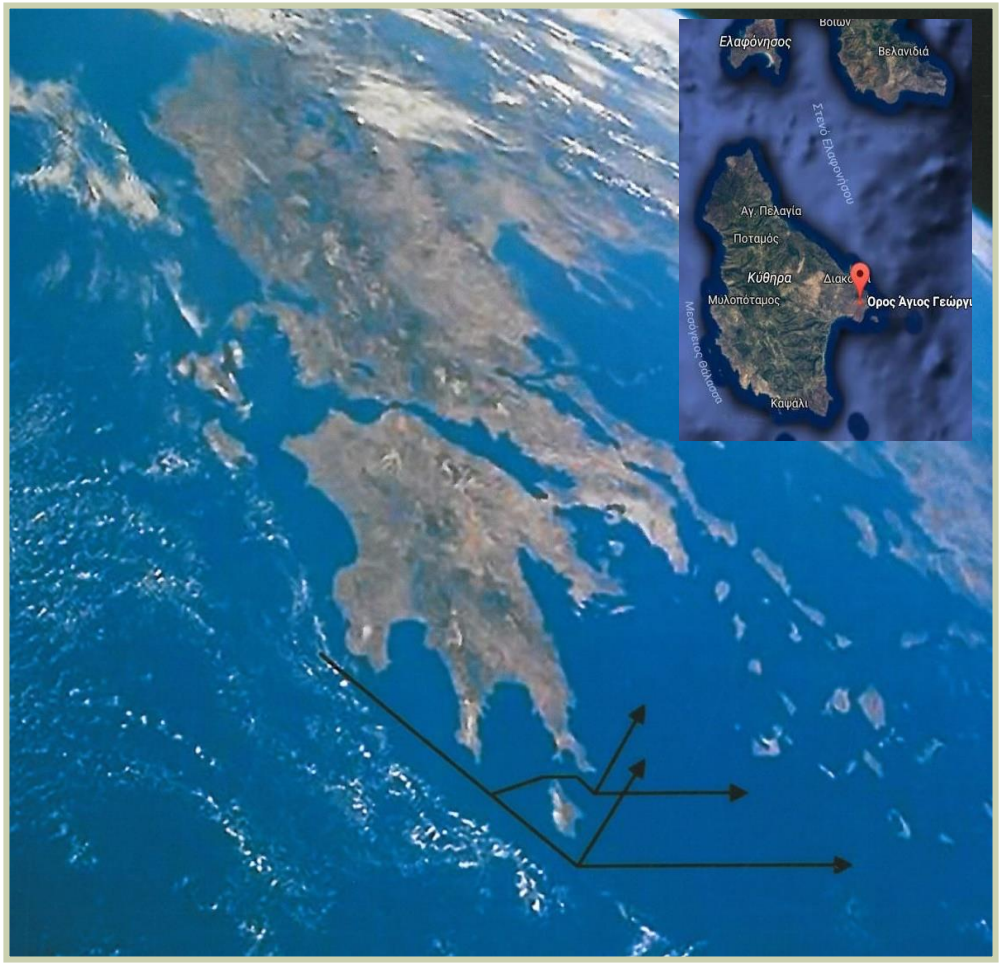

Fig.5: Kythira by satellite. The ship paths from west to east are marked (NASA file) (Kourkoumelis2011:79). The smaller map shows the island of Kythera and the location of Ayios Yeoryios sto Vouno.

Fig.6: Kythera, New Archaeological Museum: statuettes of Minoan adorants, human limbs and cut-outs from the Peak Sanctuary at Ayios Yeoryios sto Vouno.

Fig.7: Piraeus, Archaeological Museum: display case containing adorants statuettes, double axe, a woman cut-out and other finds from the Peak Sanctuary.

Fig.8: The portable X-ray fluorescence device (pXRF) which was employed for this study.

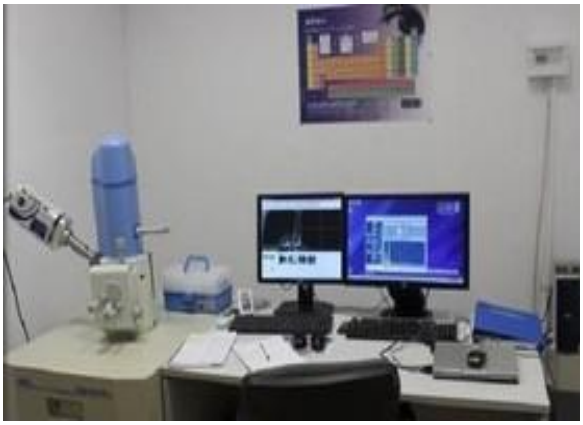

Fig.9: The SEM JEOL system coupled with an EDS by Oxford Instruments and software by INCA which was employed for the bulk compositional analysis in this study (http://kalamata.uop.gr/~archaeolab).

APPENDIX I

XRF Analysis: Tables and Spectra

Table 1: The measurements of the certified reference copper alloy **CDA 360** using pXRF expressed in % wt. (m.: measurement, St. Dev.: Standard Deviation, n.d.: non detected).

CDA360	m.1	m.2	m.3	Average	St. Dev.
MnO	n.d.	n.d.	n.d.	-	-
Fe_2O_3	0,08	0,08	0,08	0,08	0,00
Co	0,02	0,02	0,02	0,02	0,00
Ni	0,11	0,10	0,11	0,10	0,00
CuO	61,68	61,74	61,69	61,70	0,03
ZnO	35,52	35,54	35,59	35,55	0,04
As_2O_3	n.d.	0,01	0,01	0,01	0,00
ZrO_2	0,01	0,01	0,01	0,01	0,00
Nb	0,19	0,20	0,19	0,20	0,01
Ag	n.d.	n.d.	n.d.	-	-
SnO_x	0,16	0,17	0,16	0,16	0,01
Sb2O5	n.d.	n.d.	0,01	0,00	-
PbO	2,23	2,14	2,14	2,17	0,05
Bi_2O_3	n.d.	n.d.	n.d.	-	-

Bronze Sheet assemblage

Table 2: The performed measurements of the object **KYT_AYV_BS_01** using pXRF expressed in % wt. (m.: measurement, St. Dev.: Standard Deviation, n.d.: non detected).

BS_01	m.1	m.2	m.3	m.4	m.5	Average	St. Dev.
MnO	0,06	0,07	0,04	0,06	0,04	0,06	0,01
Fe_2O_3	0,82	1,03	0,71	0,86	0,68	0,82	0,14
Co	0,04	0,05	0,04	0,04	0,04	0,04	0,01
Ni	0,03	0,01	0,02	0,02	0,05	0,03	0,01
CuO	87,23	86,12	85,96	85,41	85,81	86,10	0,68
ZnO	7,05	7,84	7,81	8,01	7,98	7,74	0,40
As_2O_3	0,56	0,61	0,67	0,64	0,69	0,63	0,05
ZrO2	0,10	0,10	0,08	0,10	0,08	0,09	0,01
Nb	0,09	0,09	0,06	0,09	0,05	0,07	0,02
Ag	0,07	0,10	0,10	0,09	0,11	0,10	0,01
SnO_x	1,42	1,39	1,33	1,42	1,35	1,38	0,04
Sb_2O_5	0,10	0,11	0,11	0,11	0,13	0,11	0,01
PbO	2,42	2,47	3,06	3,14	2,99	2,81	0,34
Bi_2O_3	n.d.	0,01	n.d.	n.d.	n.d.	0,00	0,00

KYT_AYV_BS_01

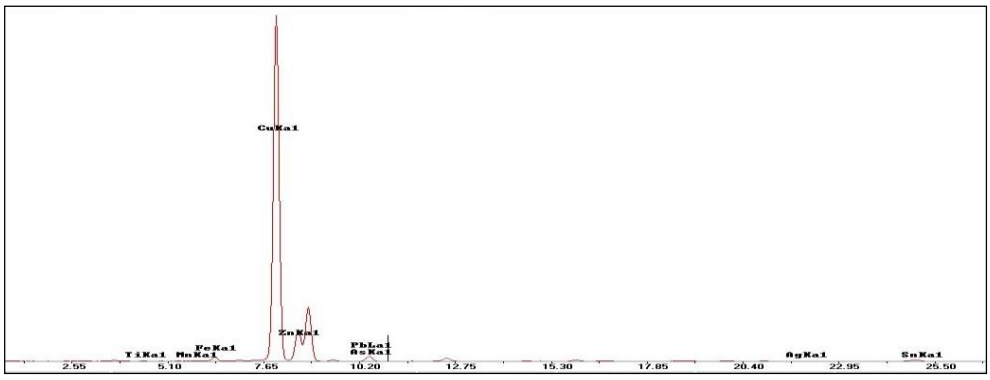

Spectra 1: First measurement of the object BS_01.

Spectra 2: Second measurement of the object BS_01.

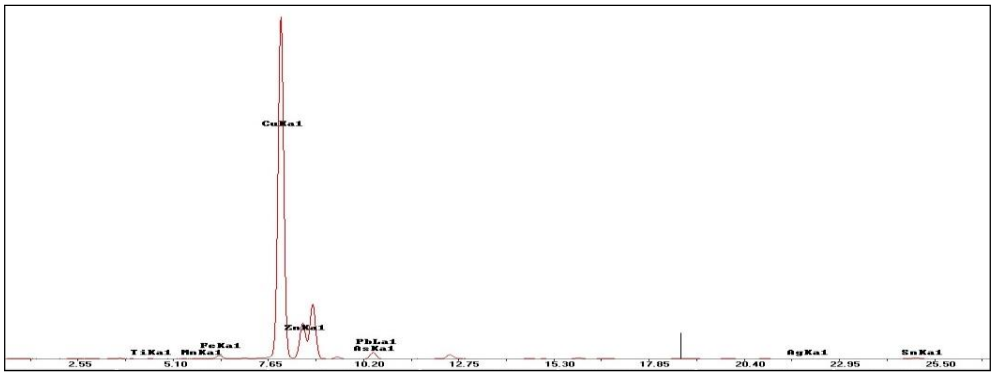

Spectra 3: Third measurement of the object BS_01

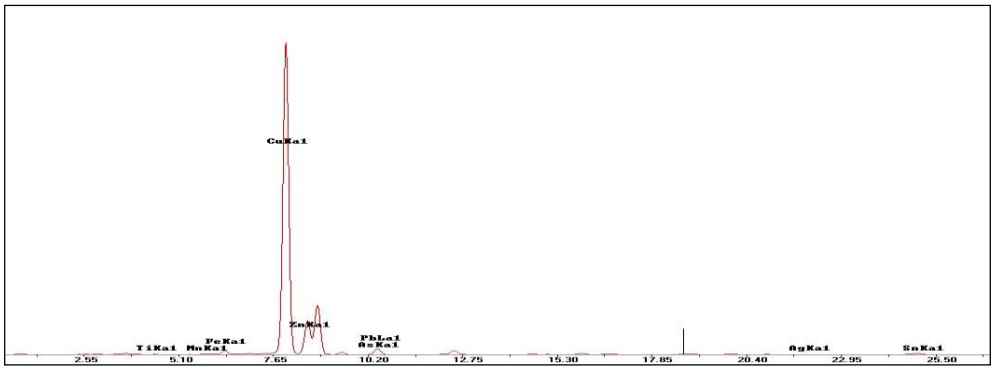

Spectra 4: Fourth measurement of the object BS_01.

Spectra 5: Fifth measurement of the object BS_01.

Table 3: The performed measurements of the object **KYT_AYV_BS_02** using pXRF expressed in % wt. (m.: measurement, St. Dev.: Standard Deviation, n.d.: non detected).

BS_02	m.1	m.2	m.3	m.4	Average	St. Dev.
MnO	0,06	0,05	0,07	0,04	0,05	0,01
Fe_2O_3	0,76	0,74	0,82	0,62	0,74	0,08
Co	0,04	0,04	0,05	0,03	0,04	0,01
Ni	0,18	0,19	0,24	0,21	0,20	0,03
CuO	96,80	96,64	96,42	83,52	93,35	6,55
ZnO	1,33	1,30	1,33	1,27	1,31	0,02
As_2O_3	0,08	0,11	0,10	0,99	0,32	0,45
ZrO_2	0,13	0,11	0,13	0,10	0,12	0,01
Nb	0,08	0,06	0,08	0,05	0,07	0,02
Ag	0,03	0,05	0,04	0,11	0,06	0,04
SnO_x	0,24	0,26	0,32	6,89	1,93	3,31
Sb_2O_5	0,05	0,07	0,04	0,17	0,08	0,06
PbO	0,19	0,35	0,34	5,99	1,72	2,85
Bi_2O_3	0,03	0,03	0,02	n.d.	0,02	0,01

KYT_AYV_BS_02

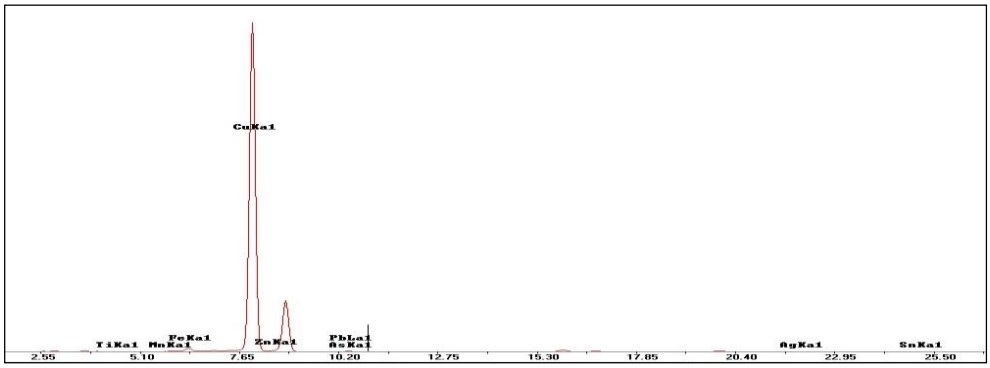

Spectra 6: First measurement of the object BS_02.

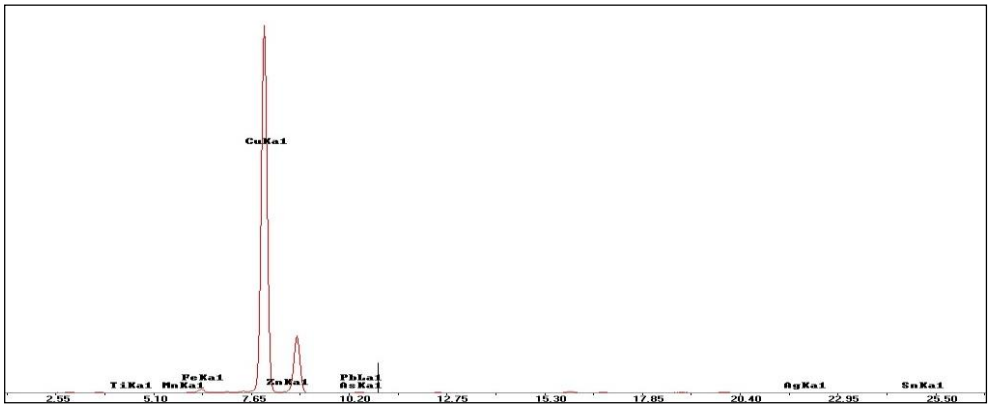

Spectra 7: Second measurement of the object BS_02.

Spectra 8: Third measurement of the object BS_02.

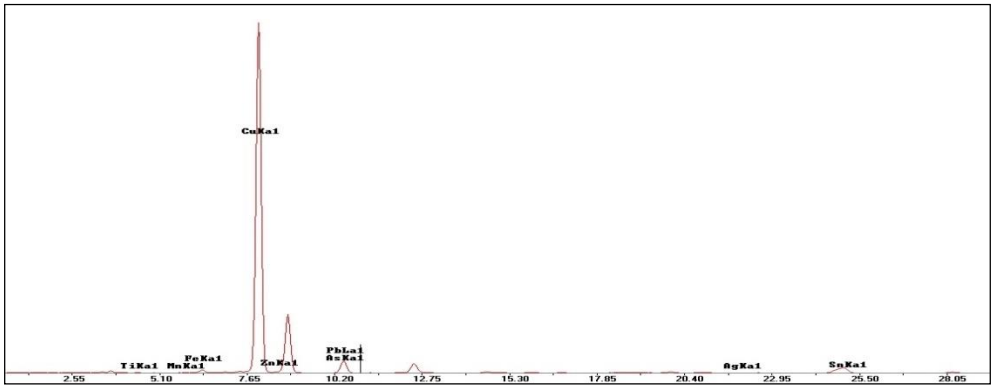

Spectra 9: Fourth measurement of the object BS_02.

Table 4: The performed measurements of the object **KYT_AYV_BS_06** using pXRF expressed in % wt. (m.: measurement, St. Dev.: Standard Deviation).

BS_06	m.1	m.2	m.3	Average	St. Dev.
MnO	0,21	0,19	0,22	0,20	0,01
Fe_2O_3	1,12	1,29	1,07	1,16	0,12
Co	0,26	0,27	0,26	0,27	0,01
Ni	0,57	0,51	0,57	0,55	0,04
CuO	79,04	79,23	78,85	79,04	0,19
ZnO	15,93	15,70	16,02	15,88	0,16
As_2O_3	0,05	0,04	0,05	0,05	0,01
ZrO_2	0,90	0,71	1,00	0,87	0,15
Nb	0,76	0,55	0,85	0,72	0,15
Ag	0,29	0,35	0,30	0,31	0,04
SnO_x	0,25	0,33	0,23	0,27	0,05
Sb_2O_5	0,23	0,32	0,24	0,26	0,05
PbO	0,24	0,32	0,20	0,26	0,06
Bi_2O_3	0,15	0,19	0,14	0,16	0,03

KYT_AYV_BS_06

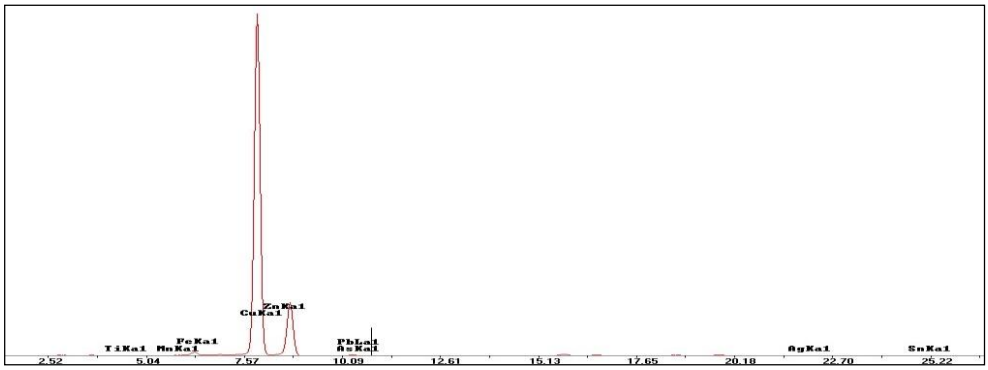

Spectra 10: First measurement of the object BS_06.

Spectra 11: Second measurement of the object BS_06.

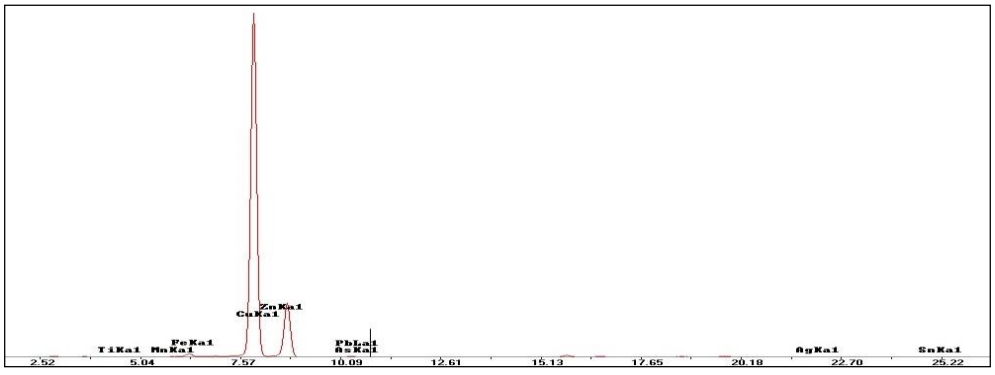

Spectra 12: Third measurement of the object BS_06.

Table 5: The performed measurements of the object **KYT_AYV_BS_07** using pXRF expressed in % wt. (m.: measurement, St. Dev.: Standard Deviation, n.d.: non detected).

BS_07	m.1	m.2	m.3	m.4	Average	St. Dev.
MnO	0,01	n.d	n.d.	n.d.	0,00	0,00
Fe2O3	n.d	0,04	n.d.	0,04	0,02	0,02
Co	n.d.	0,01	n.d.	n.d.	0,00	0,00
Ni	n.d.	n.d.	n.d.	n.d.	-	-
CuO	71,91	62,15	81,33	79,43	73,71	8,71
ZnO	28,02	37,43	18,37	20,22	26,01	8,68
As2O3	0,01	n.d.	n.d.	n.d.	0,00	0,00
ZrO2	n.d.	0,01	0,03	0,02	0,02	0,01
Nb	n.d.	0,15	0,13	0,13	0,10	0,07
Ag	n.d.	0,02	0,01	0,01	0,01	0,01
SnOx	n.d.	0,09	0,07	0,09	0,06	0,04
Sb2O5	0,01	0,04	0,01	0,01	0,02	0,02
PbO	0,04	0,04	0,03	0,03	0,04	0,01
Bi2O3	n.d.	0,01	n.d.	n.d.	0,00	0,00

KYT_AYV_BS_07

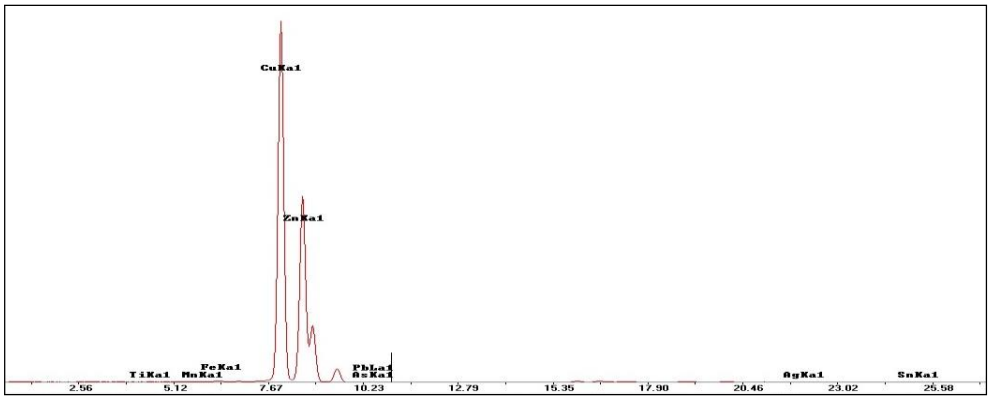

Spectra 13: First measurement of the object BS_07.

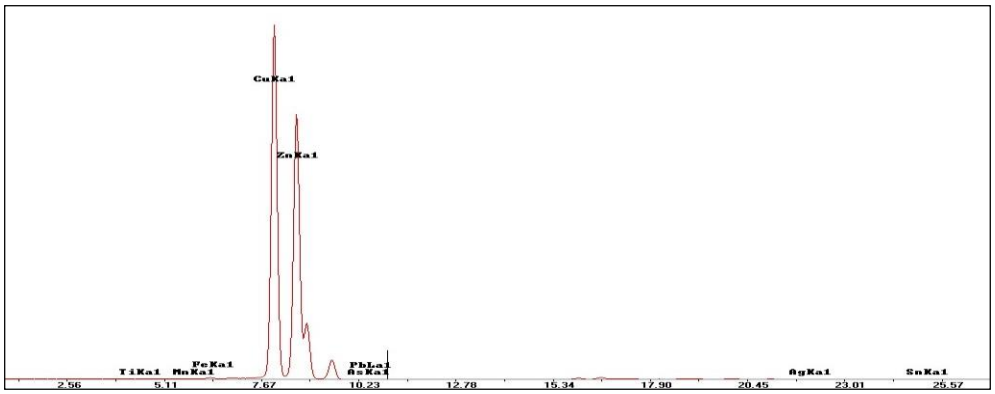

Spectra 14: Second measurement of the object BS_07.

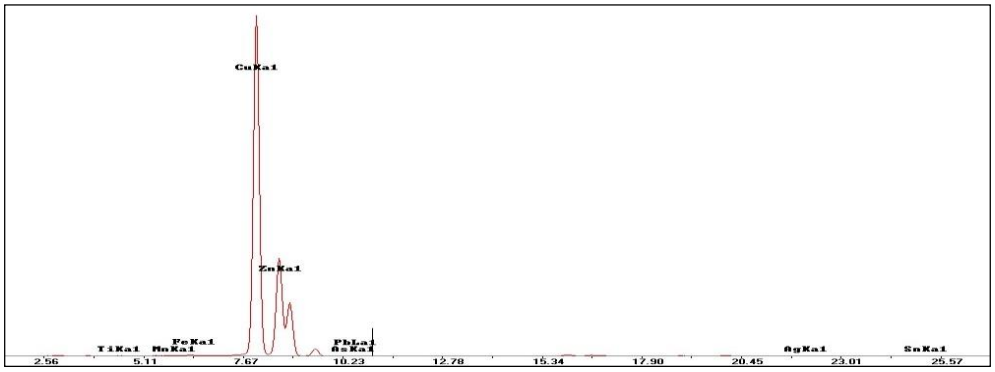

Spectra 15: Third measurement of the object BS_07.

Spectra 16: Fourth measurement of the object BS_07.

Table 6: The performed measurements of the object **KYT_AYV_BS_08** using pXRF expressed in % wt. (m.: measurement, St. Dev.: Standard Deviation, n.d.: non detected).

BS_08	m.1	m.2	m.3	Average	St. Dev.
MnO	n.d.	n.d.	n.d.	-	-
Fe_2O_3	0,17	0,22	0,15	0,18	0,04
Co	n.d.	n.d.	n.d.	-	-
Ni	0,06	0,03	0,05	0,05	0,01
CuO	98,85	98,78	98,85	98,83	0,04
ZnO	0,48	0,47	0,48	0,48	0,01
As_2O_3	0,13	0,12	0,13	0,13	0,00
ZrO_2	n.d.	n.d.	0,01	0,00	0,00
Nb	n.d.	n.d.	n.d.	-	-
Ag	0,03	0,05	0,03	0,04	0,01
SnO_x	0,22	0,25	0,24	0,24	0,02
Sb_2O_5	0,03	0,05	0,03	0,04	0,01
PbO	n.d.	n.d.	n.d.	-	-
Bi_2O_3	0,02	0,02	0,02	0,02	0,00

KYT_AYV_BS_08

Spectra 17: First measurement of the object BS_08.

Spectra 18: Second measurement of the object BS_08.

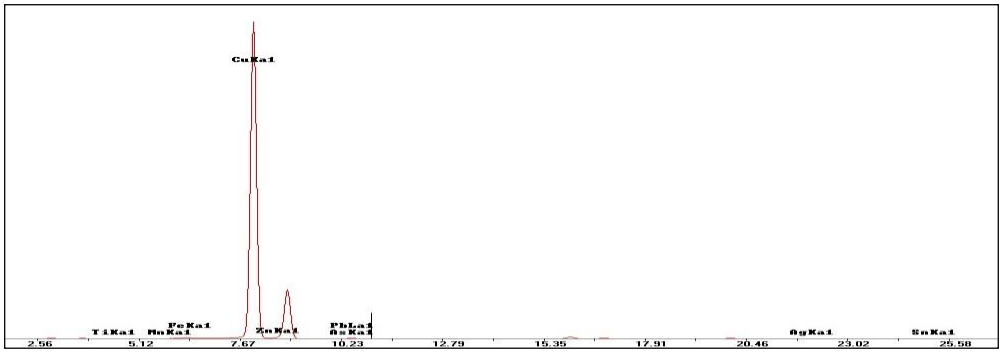

Spectra 19: Third measurement of the object BS_08.

Table 7: The performed measurements of the object **KYT_AYV_BS_10** using pXRF expressed in % wt. (m.: measurement, Av.: Average, St. Dev.: Standard Deviation, n.d.: non detected).

BS_10	m.1	m.2	Av.	St.Dev.	BS_10	m.1	m.2	Av.	St.Dev.
MnO	0,28	0,07	0,17	0,15	ZrO_2	1,27	0,12	0,69	0,81
Fe_2O_3	1,50	0,92	1,21	0,41	Nb	0,96	0,07	0,52	0,63
Co	0,40	0,03	0,22	0,26	Ag	0,44	0,06	0,25	0,27
Ni	1,04	0,24	0,64	0,56	SnO_x	0,31	0,12	0,21	0,13
CuO	68,87	96,80	82,84	19,74	Sb_2O_5	0,29	0,07	0,18	0,16
ZnO	24,11	1,34	12,72	16,10	PbO	0,33	0,10	0,21	0,16
As_2O_3	n.d.	0,03	0,01	0,02	Bi_2O_3	0,20	0,05	0,12	0,11

KYT_AYV_BS_10

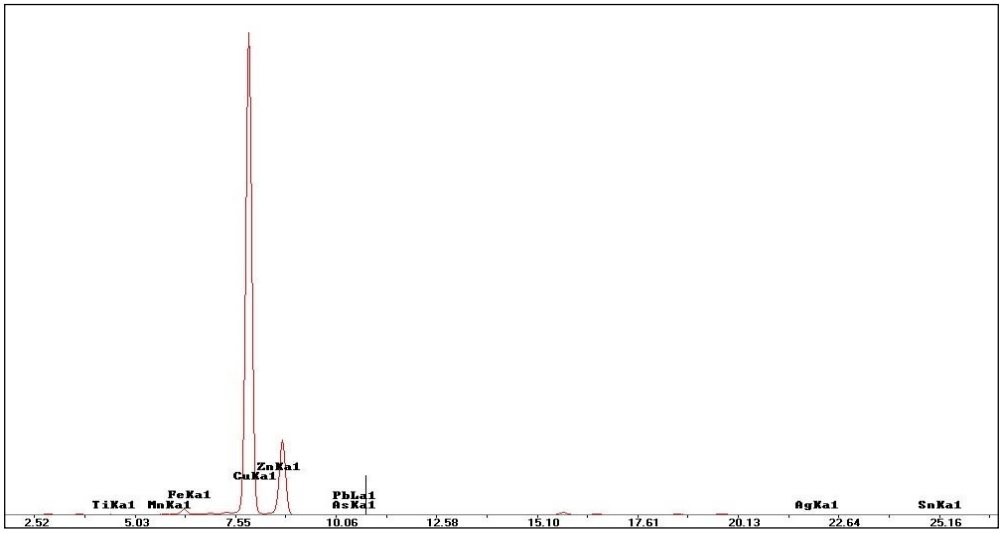

Spectra 20: First measurement of the object BS_10.

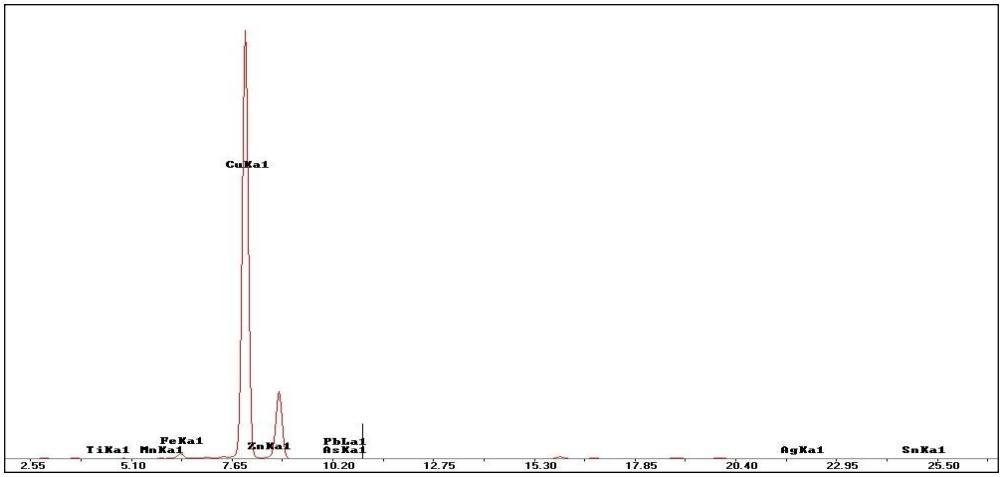

Spectra 21: Second measurement of the object BS_10.

Table 8: The performed measurements of the object **KYT_AYV_BS_19** using pXRF expressed in % wt. (m.: measurement, St. Dev.: Standard Deviation, n.d.: non detected).

BS_19	m.1	m.2	m.3	Average	St. Dev.
MnO	0,03	0,06	0,02	0,04	0,02
Fe_2O_3	0,16	0,78	0,06	0,33	0,39
Co	n.d.	0,01	n.d.	0,00	0,00
Ni	1,81	1,77	1,77	1,79	0,03
CuO	27,71	25,43	40,84	31,33	8,32
ZnO	4,45	4,48	4,53	4,49	0,04
As_2O_3	1,22	1,37	0,84	1,14	0,27
ZrO_2	0,23	0,22	0,14	0,20	0,05
Nb	n.d.	n.d.	n.d.	-	-
Ag	52,93	54,47	44,02	50,47	5,64
SnO_x	10,40	10,50	7,16	9,35	1,90
Sb_2O_5	0,18	0,22	0,10	0,17	0,06
PbO	0,27	n.d.	0,13	0,13	0,13
Bi_2O_3	0,60	0,69	0,39	0,56	0,16

KYT_AYV_BS_19

Spectra 22: First measurement of the object BS_19.

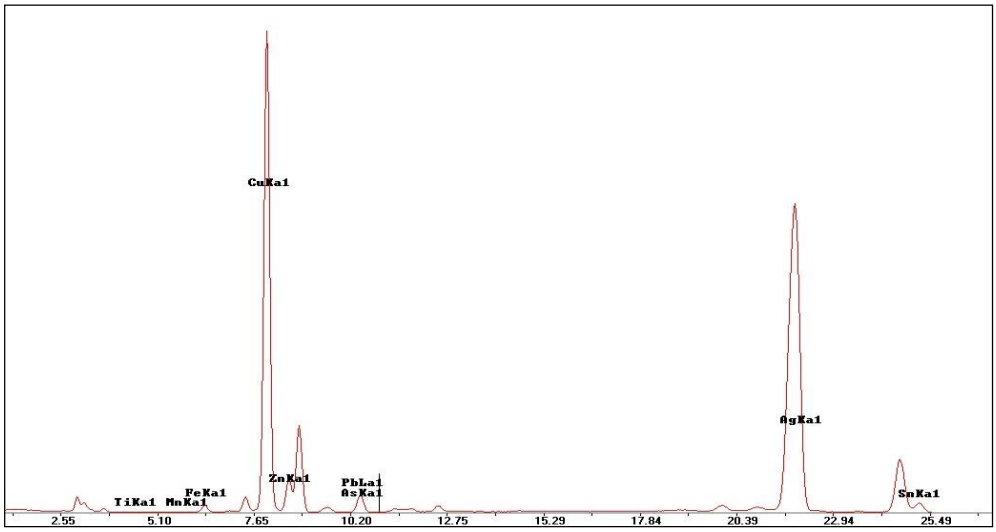

Spectra 23: Second measurement of the object BS_19.

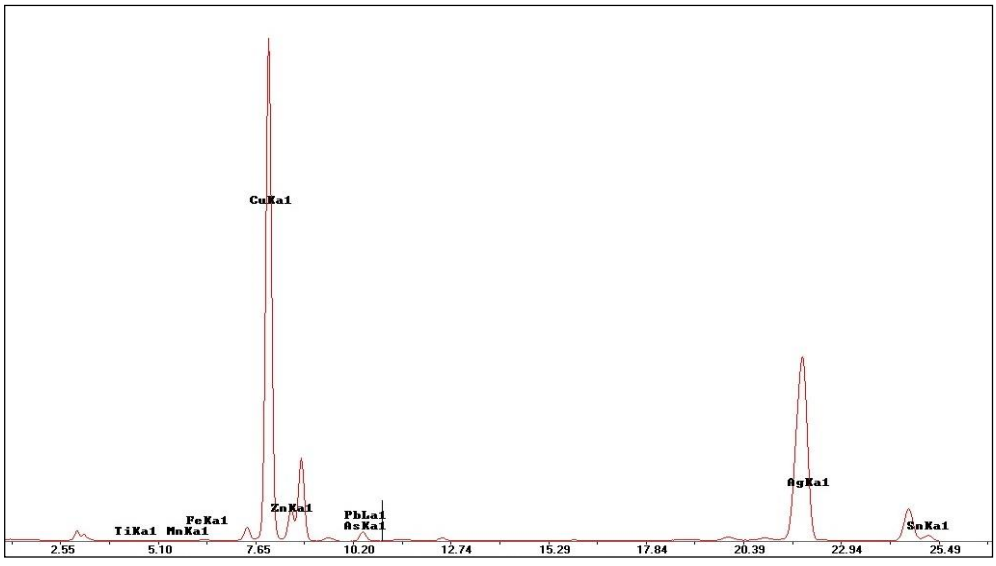

Spectra 24: Third measurement of the object BS_19.

Figurine Base assemblage

Table 9: The performed measurements of the object **KYT_AYV_FB_03** using pXRF expressed in % wt. (m.: measurement, St. Dev.: Standard Deviation, n.d.: non detected).

FB_03	m.1	m.2	m.3	m.4	m.5	Average	St. Dev.
MnO	0,09	0,62	0,18	0,36	0,13	0,28	0,22
Fe_2O_3	1,23	8,18	1,69	5,93	0,33	3,47	3,40
Co	0,03	0,92	0,18	0,68	0,10	0,38	0,40
Ni	n.d.	1,64	0,15	0,10	0,34	0,45	0,68
CuO	86,25	62,45	81,62	63,95	85,98	76,05	11,88
ZnO	1,18	12,70	6,10	16,69	7,90	8,91	5,99
As_2O_3	0,15	0,75	1,01	0,71	3,37	1,20	1,25
ZrO_2	0,12	1,69	0,38	0,57	0,50	0,65	0,60
Nb	0,06	0,72	0,29	n.d.	0,41	0,30	0,29
Ag	0,14	0,96	0,28	1,15	0,30	0,56	0,45
SnO_x	0,23	1,25	0,35	0,91	0,37	0,62	0,44
Sb_2O_5	0,17	1,57	0,29	1,08	0,29	0,68	0,61
PbO	10,36	6,48	7,47	7,35	n.d.	6,33	3,83
Bi_2O_3	n.d.	0,08	n.d.	0,53	n.d.	0,12	0,23

KYT_AYV_FB_03

Spectra 25: First measurement of the object FB_03.

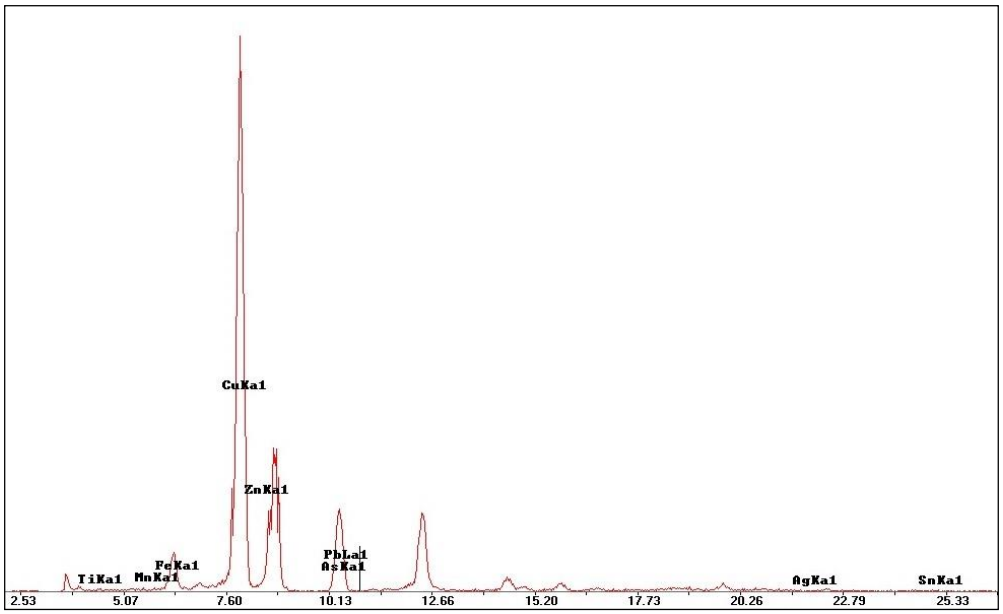

Spectra 26: Second measurement of the object FB_03.

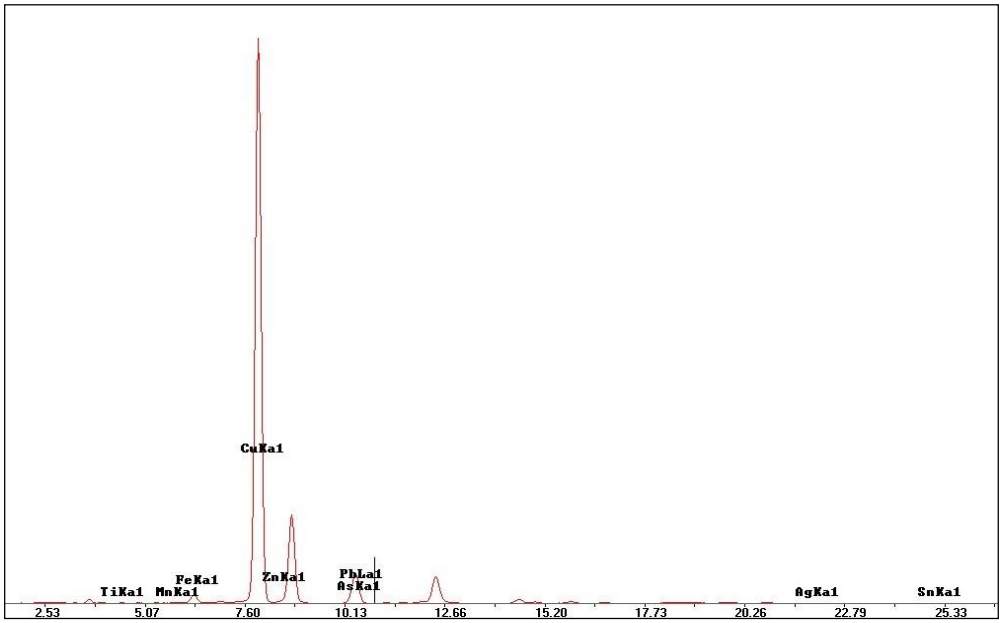

Spectra 27: Third measurement of the object FB_03.

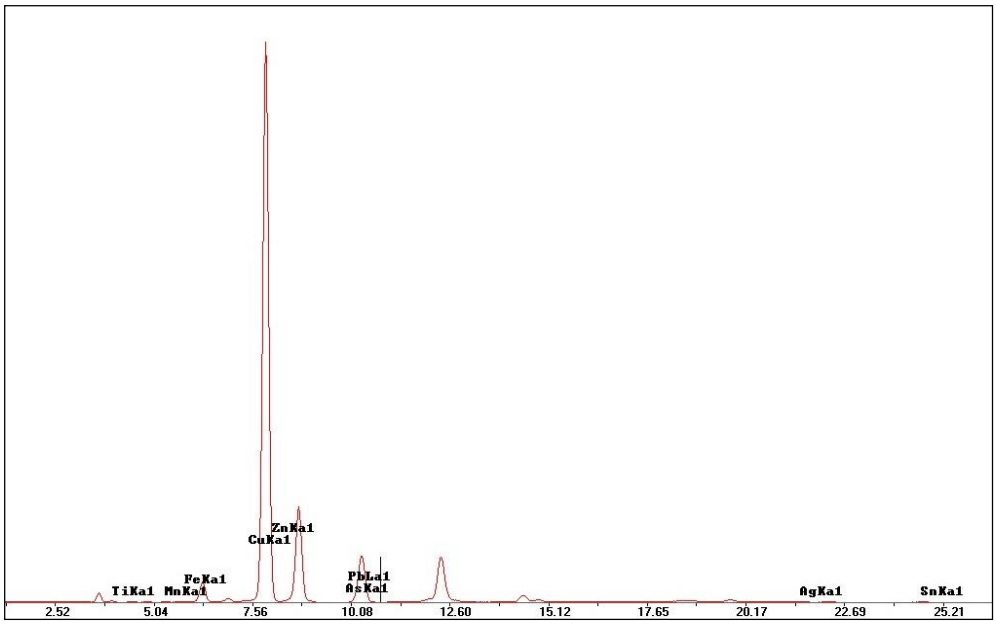

Spectra 28: Fourth measurement of the object FB_03.

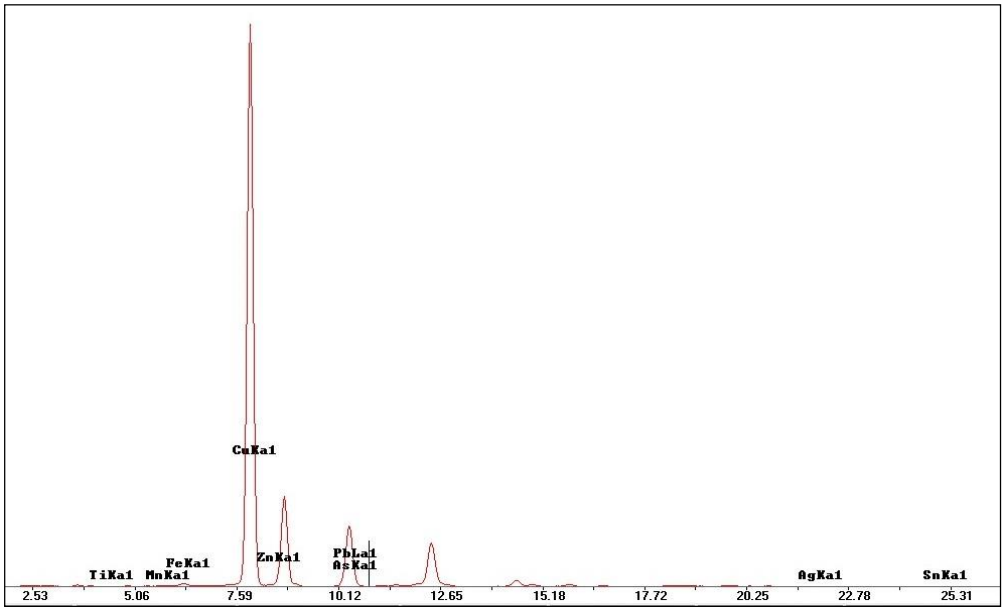

Spectra 29: Fifth measurement of the object FB_03.

Bronze Waste assemblage

Table 10: The performed measurements of the object **KYT_AYV_BW_04** using pXRF expressed in % wt. (m.: measurement, St. Dev.: Standard Deviation, n.d.: non detected).

BW_04	m.1	m.2	m.3	m.4	m.5	m.6	Average	St. Dev.
MnO	0,23	0,21	0,23	0,23	0,20	0,23	0,22	0,01
Fe_2O_3	0,55	0,47	0,89	1,04	0,65	1,20	0,80	0,29
Co	0,26	0,26	0,30	0,31	0,24	0,32	0,28	0,03
Ni	0,71	0,73	0,69	0,67	0,68	0,62	0,68	0,04
CuO	77,52	77,72	77,79	77,79	79,01	77,44	77,88	0,57
ZnO	17,40	17,33	16,96	17,01	16,51	17,06	17,05	0,32
As_2O_3	0,01	n.d.	n.d.	0,02	n.d.	0,02	0,01	0,01
ZrO_2	1,16	1,07	1,01	0,90	0,65	0,82	0,93	0,18
Nb	0,98	0,89	0,84	0,73	0,50	0,61	0,76	0,18
Ag	0,31	0,33	0,31	0,33	0,36	0,41	0,34	0,04
SnO_x	0,24	0,28	0,27	0,28	0,34	0,37	0,30	0,05
Sb_2O_5	0,25	0,28	0,25	0,26	0,33	0,39	0,29	0,06
PbO	0,24	0,29	0,29	0,27	0,32	0,29	0,28	0,03
Bi_2O_3	0,14	0,15	0,16	0,16	0,19	0,22	0,17	0,03

KYT_AYV_BW_04

Spectra 30: First measurement of the object BW_04.

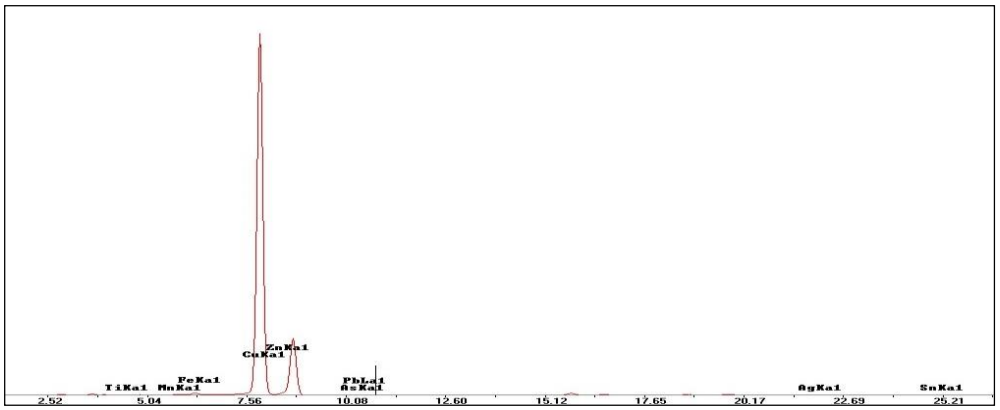

Spectra 31: Second measurement of the object BW_04.

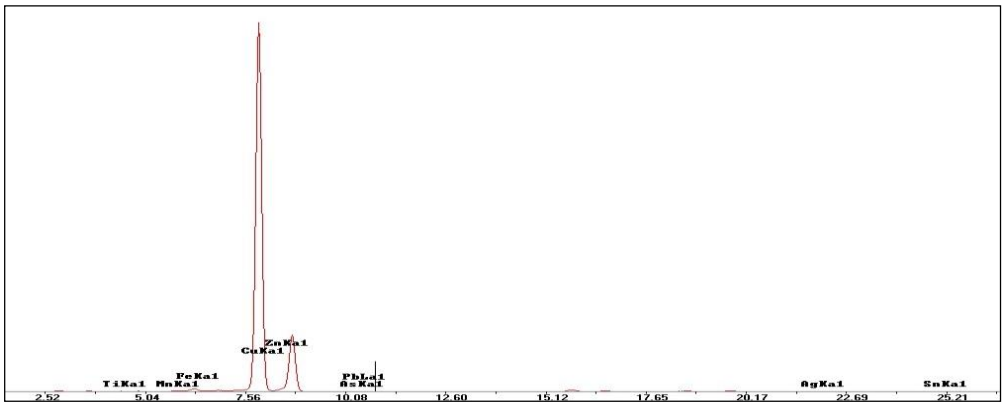

Spectra 32: Third measurement of the object BW_04.

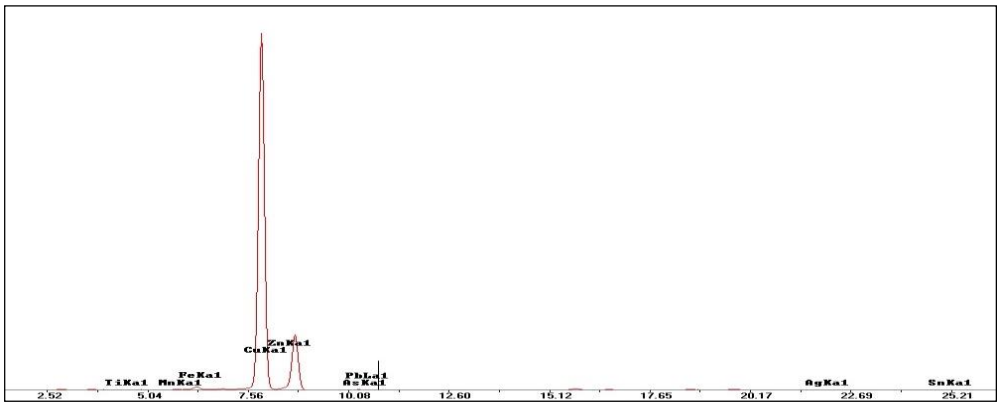

Spectra 33: Fourth measurement of the object BW_04.

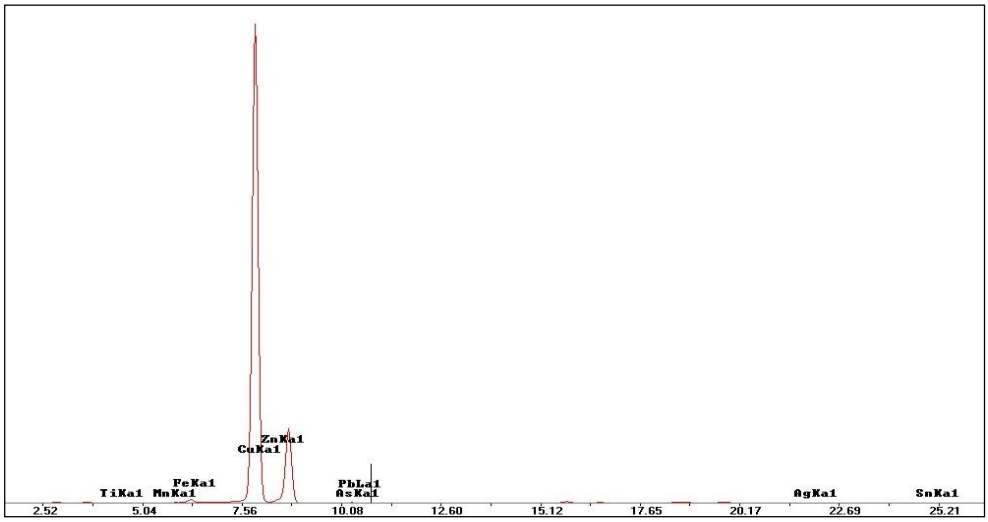

Spectra 34: Fifth measurement of the object BW_04.

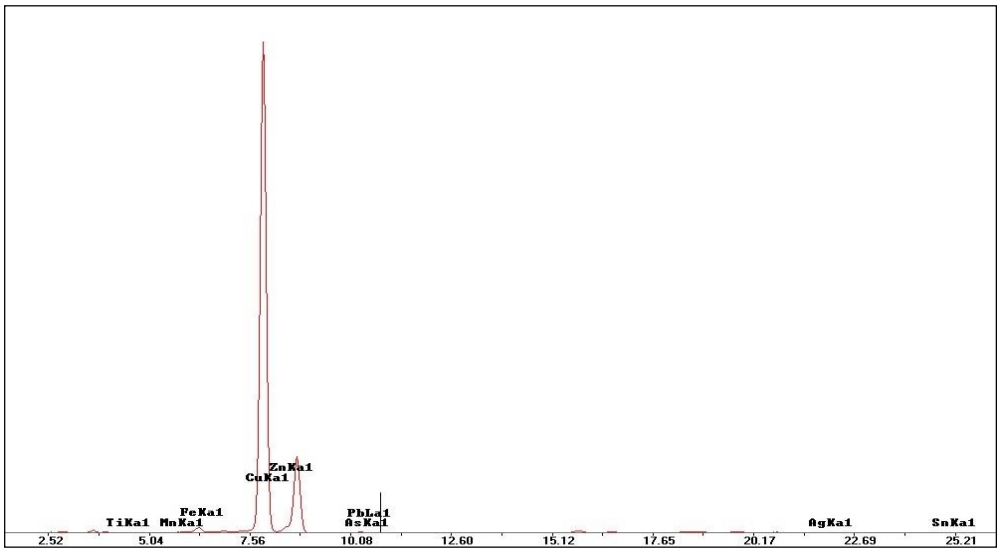

Spectra 35: Sixth measurement of the object BW_04.

Table 11: The performed measurements of the object **KYT_AYV_BW_05** using pXRF expressed in % wt. (m.: measurement, St. Dev.: Standard Deviation, n.d.: non detected).

BW_05	m.1	m.2	m.3	Average	St. Dev.
MnO	0,33	0,28	0,35	0,32	0,04
Fe_2O_3	4,01	3,57	7,53	5,04	2,17
Co	0,63	0,47	0,76	0,62	0,15
Ni	0,47	0,26	n.d.	0,24	0,24
CuO	67,69	77,65	71,41	72,25	5,03
ZnO	22,79	14,58	16,24	17,87	4,34
As_2O_3	0,13	0,20	0,26	0,20	0,07
ZrO_2	0,95	0,73	0,56	0,75	0,19
Nb	0,48	0,49	0,18	0,39	0,18
Ag	0,70	0,47	0,75	0,64	0,15
SnO_x	0,68	0,64	0,87	0,73	0,12
Sb_2O_5	0,58	0,44	0,63	0,55	0,10
PbO	0,23	n.d.	0,04	0,09	0,12
Bi_2O_3	0,32	0,24	0,41	0,32	0,09

KYT_AYV_BW_05

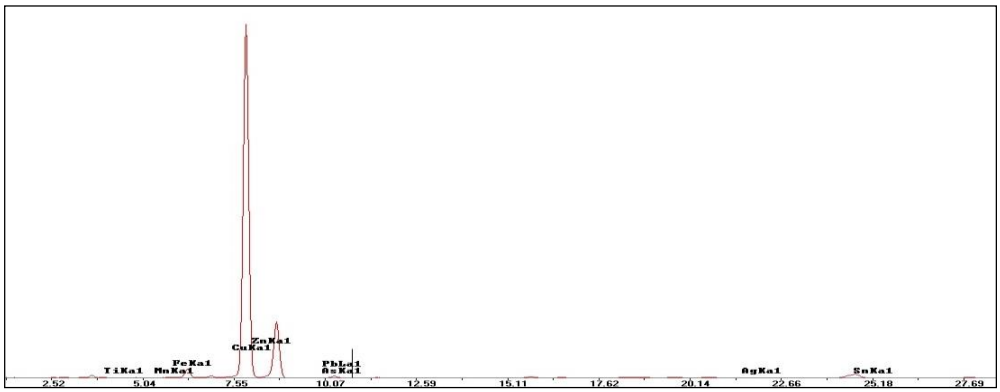

Spectra 35: First measurement of the object BW_05.

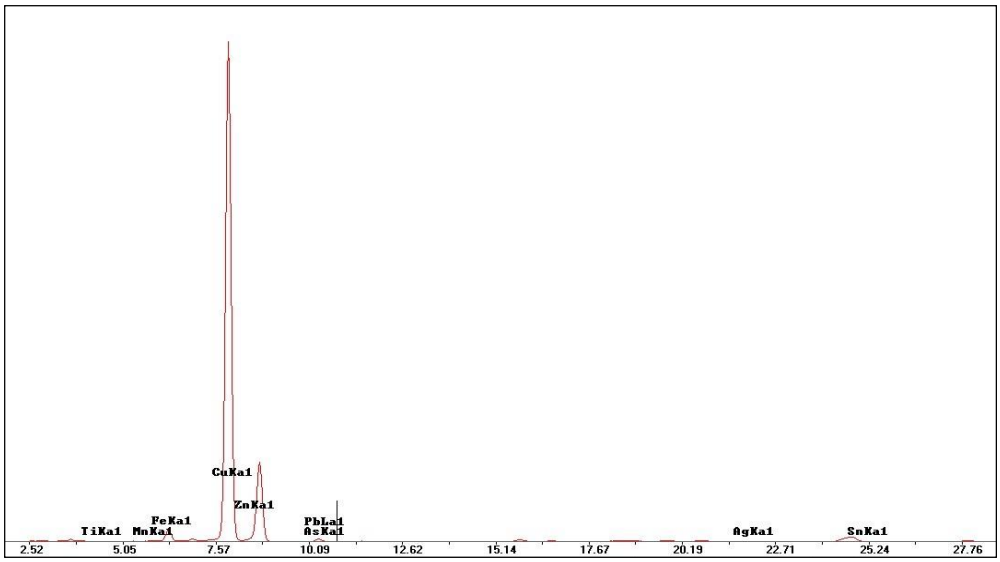

Spectra 36: Second measurement of the object BW_05.

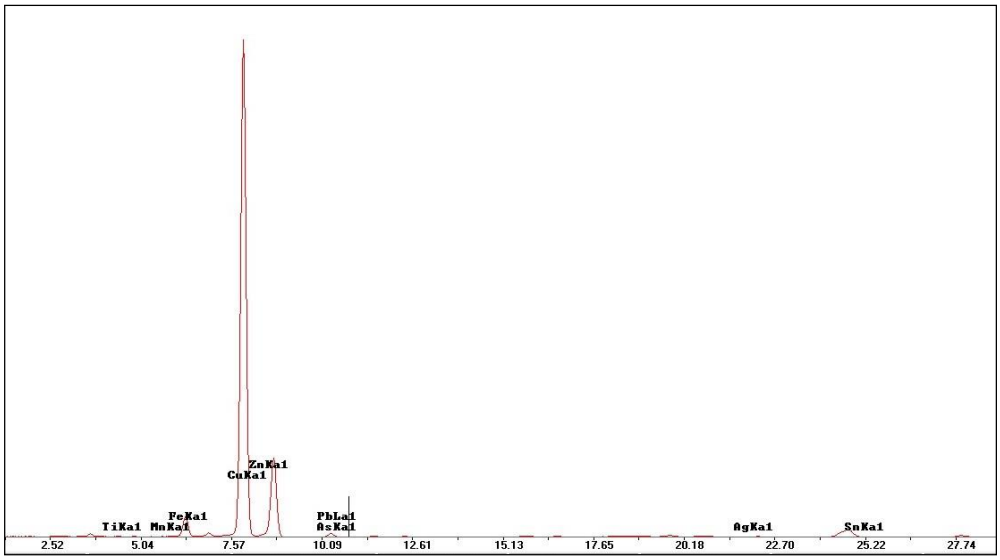

Spectra 37: Third measurement of the object BW_05.

Table 12: The performed measurements of the object **KYT_AYV_BW_15** using pXRF expressed in % wt. (m.: measurement, Av.: Average, St. Dev.: Standard Deviation, n.d.: non detected).									
BW_15	m.1	m.2	Av.	St. Dev.	BW_15	m.1	m.2	Av.	St. Dev.
MnO	0,22	0,29	0,25	0,05	ZrO_2	0,69	0,54	0,61	0,11
Fe_2O_3	1,58	3,30	2,44	1,22	Nb	0,50	0,23	0,37	0,19
Co	0,28	0,42	0,35	0,10	Ag	0,42	0,67	0,54	0,18
Ni	0,42	0,29	0,35	0,09	SnO_x	0,44	0,64	0,54	0,14
CuO	74,99	71,71	73,35	2,32	Sb_2O_5	0,37	0,60	0,48	0,16
ZnO	13,54	13,46	13,50	0,06	PbO	5,19	6,51	5,85	0,93
As_2O_3	1,20	1,11	1,15	0,07	Bi_2O_3	0,16	0,25	0,21	0,06

KYT_AYV_BW_15

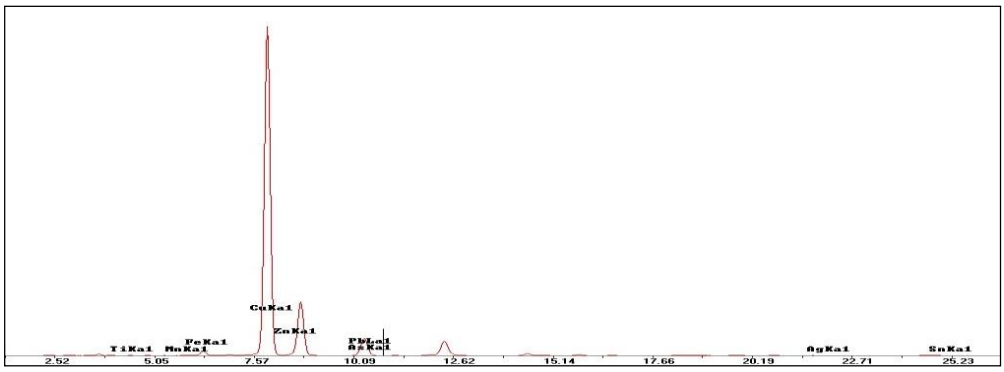

Spectra 38: First measurement of the object BW_15.

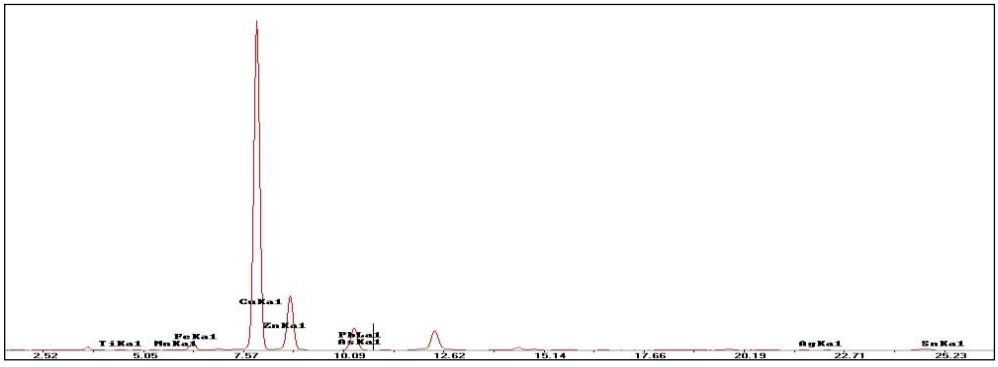

Spectra 39: Second measurement of the object BW_15.

Table 13: The performed measurements of the object **KYT_AYV_BW_16** using pXRF expressed in % wt. (m.: measurement, Av.: Average, St. Dev.: Standard Deviation, n.d.: non detected).

BW_16	m.1	m.2	Av.	St. Dev.	BW_16	m.1	m.2	Av.	St. Dev.
MnO	0,20	n.d.	0,10	0,14	ZrO_2	0,91	n.d.	0,46	0,64
Fe_2O_3	0,71	0,08	0,39	0,44	Nb	0,79	n.d.	0,40	0,56
Co	0,24	n.d.	0,12	0,17	Ag	0,25	0,09	0,17	0,12
Ni	0,54	n.d.	0,27	0,38	SnO_x	0,24	n.d.	0,12	0,17
CuO	81,35	90,54	85,94	6,50	Sb_2O_5	0,24	0,38	0,31	0,10
ZnO	13,84	n.d.	6,92	9,79	PbO	0,00	7,36	3,68	5,21
As_2O_3	0,37	0,28	0,33	0,07	Bi_2O_3	0,32	1,26	0,79	0,67

KYT_AYV_BW_16

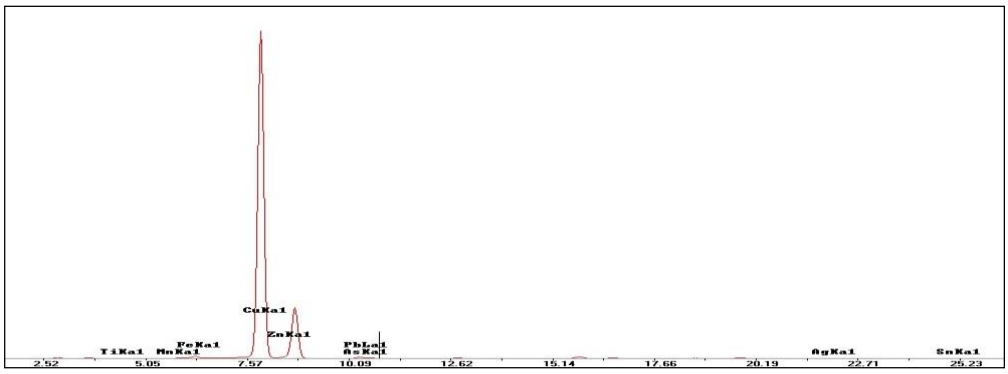

Spectra 40: First measurement of the object BW_16.

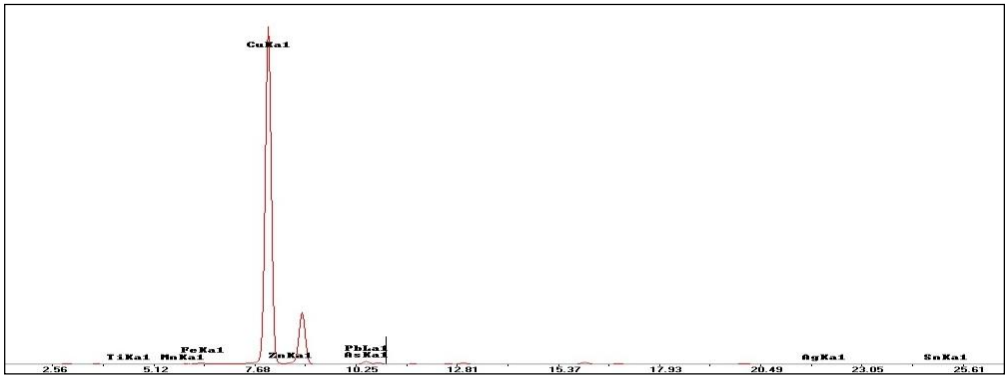

Spectra 41: Second measurement of the object BW_16.

Table 14: The performed measurements of the object **KYT_AYV_BW_17** using pXRF expressed in % wt. (m.: measurement, St. Dev.: Standard Deviation, n.d.: non detected).

BW_17	m.1	m.2	m.3	m.4	Average	St. Dev.
MnO	0,15	0,20	0,18	0,19	0,18	0,02
Fe_2O_3	0,44	6,12	5,50	6,17	4,56	2,76
Co	n.d.	n.d.	n.d.	n.d.	-	-
Ni	0,63	0,78	0,72	0,78	0,73	0,07
CuO	87,49	82,27	83,35	82,16	83,82	2,51
ZnO	10,54	9,76	9,38	9,88	9,89	0,48
As_2O_3	0,15	0,18	0,18	0,18	0,17	0,01
ZrO_2	0,08	0,08	0,07	0,08	0,08	0,00
Nb	n.d.	n.d.	n.d.	n.d.	-	-
Ag	0,06	0,07	0,06	0,07	0,06	0,00
SnO_x	0,14	0,18	0,15	0,15	0,16	0,01
Sb_2O_5	0,12	0,13	0,15	0,14	0,14	0,01
PbO	n.d.	n.d.	n.d.	n.d.	-	-
Bi_2O_3	0,20	0,24	0,25	0,25	0,23	0,02

KYT_AYV_BW_17

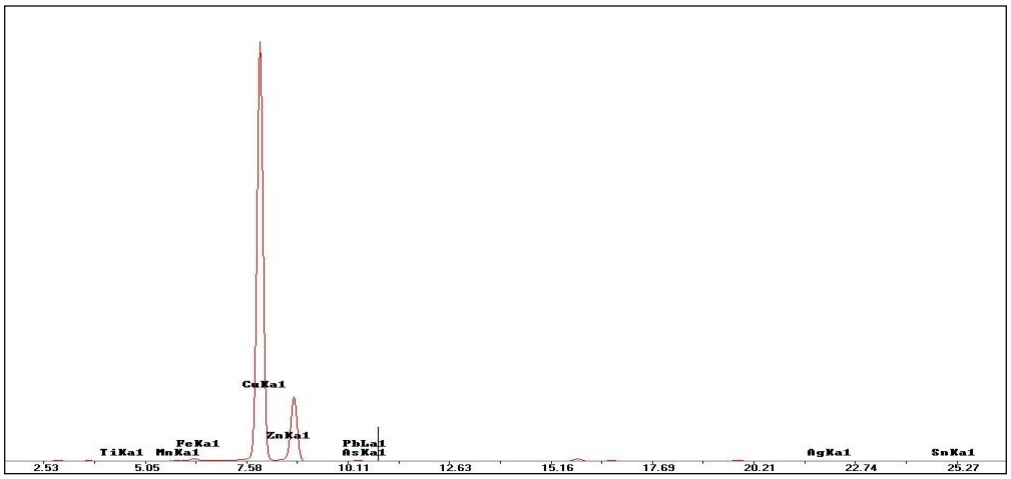

Spectra 42: First measurement of the object BW_17.

Table 15: The performed measurements of the object **KYT_AYV_BW_18** using pXRF expressed in % wt. (m.: measurement, Av.: Average, St. Dev.: Standard Deviation, n.d.: non detected).									
BW_18	m.1	m.2	Av.	St. Dev.	BW_18	m.1	m.2	Av.	St. Dev.
MnO	0,12	0,12	0,12	0,00	ZrO2	0,06	0,05	0,06	0,01
Fe_2O_3	0,12	0,08	0,10	0,03	Nb	n.d.	n.d.	-	-
Co	n.d.	n.d.	-	-	Ag	0,06	0,06	0,06	0,00
Ni	0,62	0,64	0,63	0,01	SnO_x	0,16	0,16	0,16	0,00
CuO	87,24	87,90	87,57	0,46	Sb_2O_5	0,10	0,12	0,11	0,01
ZnO	11,11	10,66	10,88	0,32	PbO	0,20	0,00	0,10	0,14
As_2O_3	0,08	0,09	0,08	0,01	Bi_2O_3	0,13	0,13	0,13	0,00

KYT_AYV_BW_18

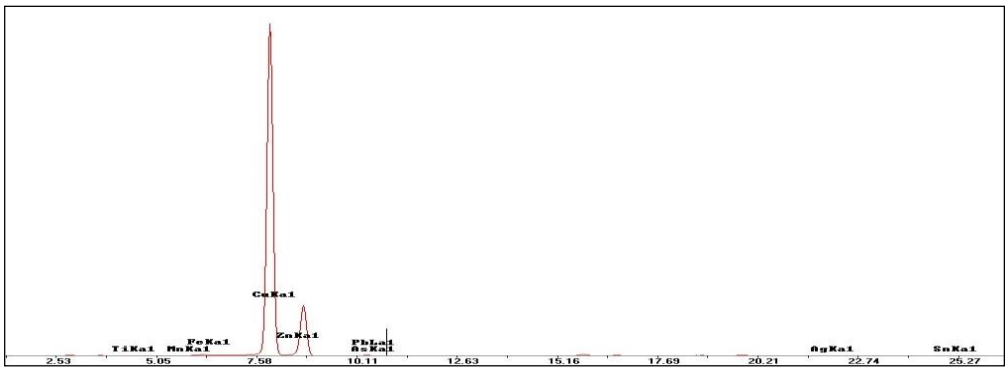

Spectra 43: First measurement of the object BW_18.

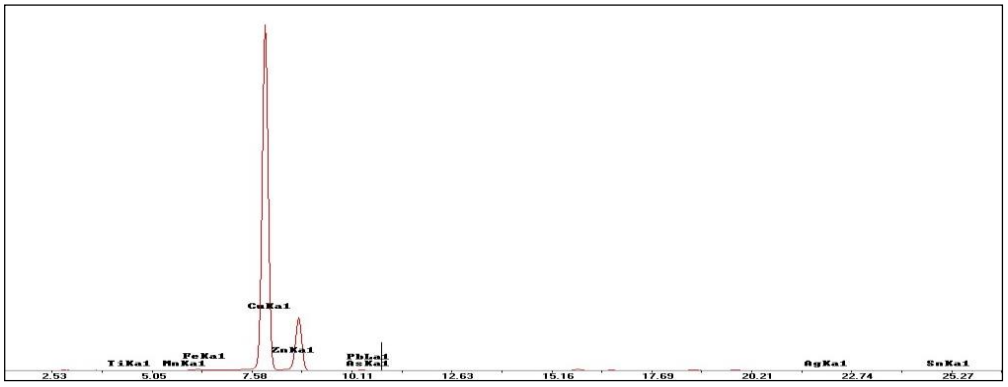

Spectra 44: Second measurement of the object BW_18.

Vessel Fragment assemblage

Table 16: The performed measurements of the object **KYT_AYV_VF_09** using pXRF expressed in % wt. (m.: measurement, St. Dev.: Standard Deviation, n.d.: non detected).

VF_09	m.1	m.2	m.3	Average	St. Dev.
MnO	n.d.	0,30	0,28	0,19	0,17
Fe_2O_3	0,43	1,38	1,32	1,04	0,53
Co	n.d.	n.d.	0,38	0,13	0,22
Ni	0,20	1,14	0,91	0,75	0,49
CuO	98,69	69,63	68,97	79,10	16,97
ZnO	0,40	23,79	24,48	16,23	13,71
As_2O_3	0,16	0,05	0,05	0,08	0,06
ZrO_2	0,01	0,10	1,18	0,43	0,65
Nb	n.d.	n.d.	0,87	0,29	0,50
Ag	0,00	0,16	0,46	0,21	0,23
SnO_x	0,08	0,30	0,33	0,23	0,14
Sb_2O_5	0,01	0,28	0,36	0,22	0,18
PbO	n.d.	2,61	0,19	0,93	1,46
Bi_2O_3	0,02	0,26	0,23	0,17	0,13

KYT_AYV_VF_09

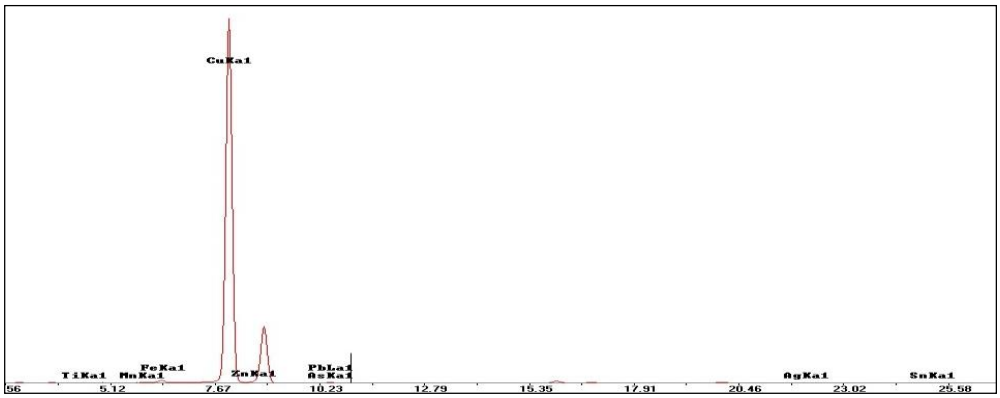

Spectra 45: First measurement of the object VF_09.

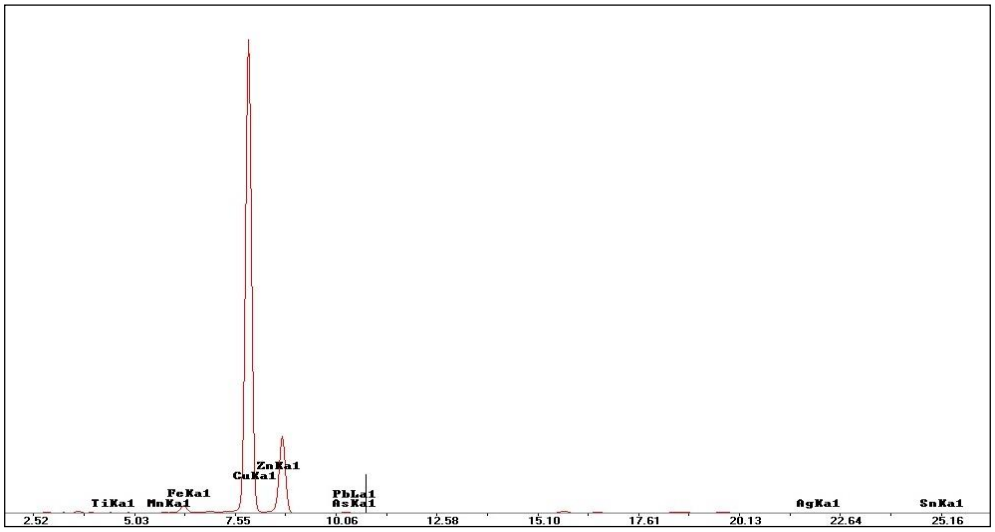

Spectra 46: Second measurement of the object VF_09.

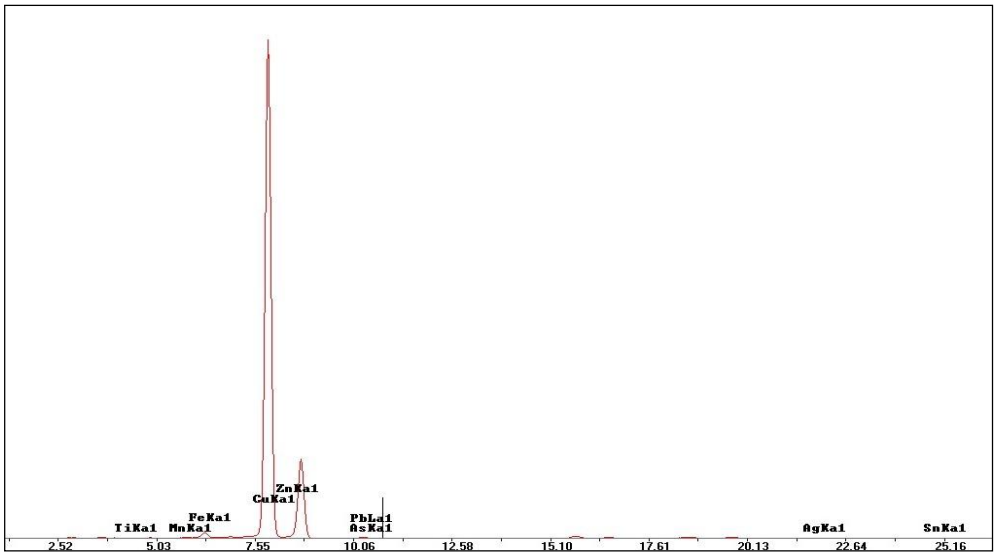

Spectra 47: Third measurement of the object VF_09.

Table 17: The performed measurements of the object **KYT_AYV_VF_11** using pXRF expressed in % wt. (m.: measurement, St. Dev.: Standard Deviation, n.d.: non detected).					
VF_11	m.1	m.2	m.3	Average	St. Dev.
MnO	0,09	0,16	0,19	0,15	0,06
Fe_2O_3	1,13	1,59	2,47	1,73	0,68
Co	0,09	0,25	0,32	0,22	0,12
Ni	1,06	1,32	1,33	1,24	0,15
CuO	73,81	70,54	70,27	71,54	1,97
ZnO	12,50	17,71	17,88	16,03	3,06
As_2O_3	0,95	0,90	0,93	0,93	0,03
ZrO_2	0,07	0,33	0,35	0,25	0,15
Nb	0,03	0,26	0,26	0,18	0,13
Ag	0,21	0,28	0,30	0,26	0,05
SnO_x	0,62	0,44	0,49	0,52	0,09
Sb_2O_5	2,38	0,51	0,62	1,17	1,05
PbO	7,06	5,69	4,51	5,75	1,28
Bi_2O_3	n.d.	0,02	0,08	0,03	0,04

KYT_AYV_VF_11

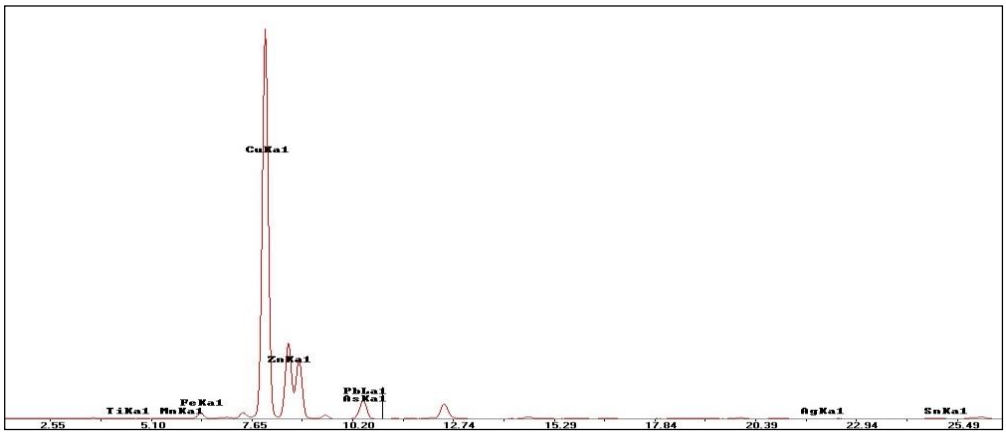

Spectra 48: First measurement of the object VF_11.

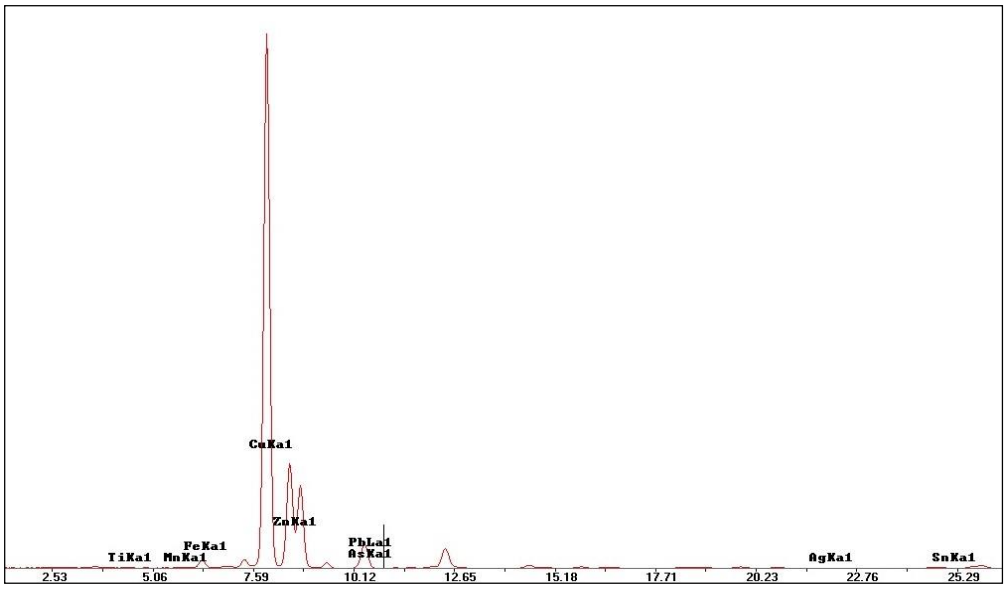

Spectra 49: Second measurement of the object VF_11.

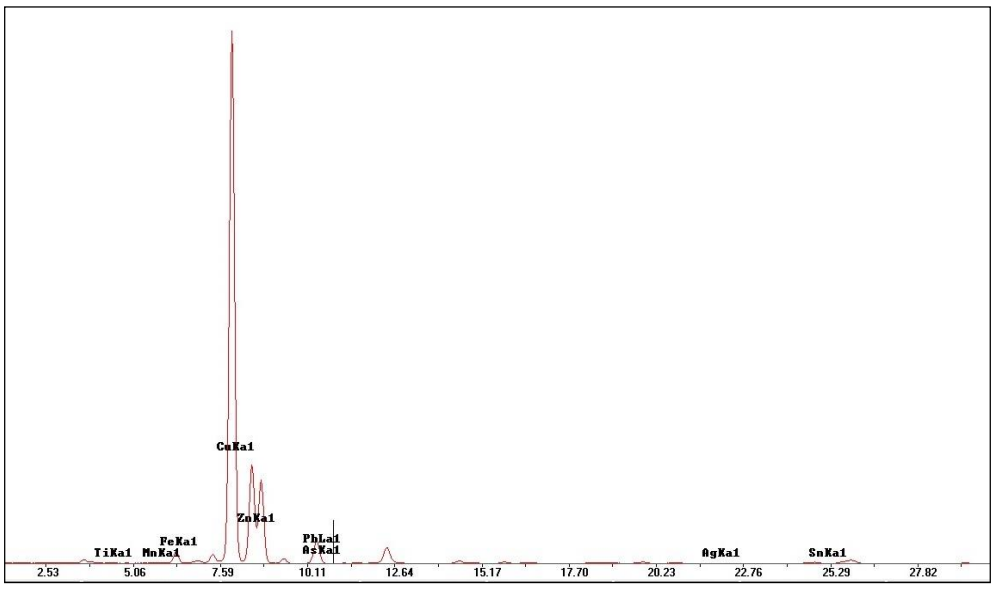

Spectra 50: Third measurement of the object VF_11.

Table 18: The performed measurements of the object **KYT_AYV_VF_12** using pXRF expressed in % wt. (m.: measurement, Av.: Average, St. Dev.: Standard Deviation, n.d.: non detected).									
VF_12	m.1	m.2	Av.	St. Dev.	FV_12	m.1	m.2	Av.	St. Dev.
MnO	0,23	0,19	0,21	0,03	ZrO_2	0,36	0,30	0,33	0,04
Fe_2O_3	3,38	2,66	3,02	0,51	Nb	0,29	0,24	0,26	0,04
Co	0,40	0,33	0,37	0,05	Ag	0,29	0,27	0,28	0,01
Ni	0,85	0,89	0,87	0,03	SnO_x	0,60	0,59	0,59	0,01
CuO	66,72	67,97	67,35	0,89	Sb_2O_5	0,44	0,46	0,45	0,02
ZnO	19,96	19,70	19,83	0,19	PbO	4,54	4,96	4,75	0,29
As_2O_3	1,95	1,41	1,68	0,38	Bi_2O_3	n.d.	0,02	0,01	0,01

KYT_AYV_VF_12

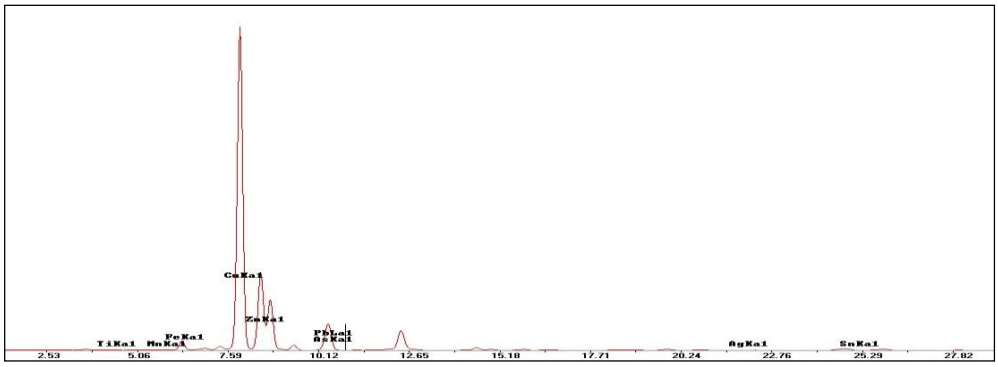

Spectra 51: First measurement of the object VF_12.

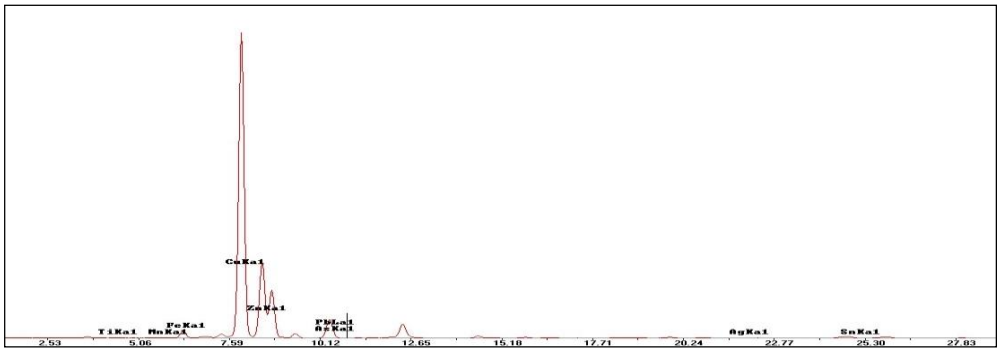

Spectra 52: Second measurement of the object VF_12.

Table 19: The performed measurements of the object **KYT_AYV_VF_13** using pXRF expressed in % wt. (m.: measurement, Av.: Average, St. Dev.: Standard Deviation, n.d.: non detected).									
VF_13	m.1	m.2	Av.	St. Dev.	FV_13	m.1	m.2	Av.	St. Dev.
MnO	0,11	0,12	0,11	0,01	ZrO_2	0,06	0,59	0,33	0,38
Fe_2O_3	0,40	0,45	0,42	0,04	Nb	n.d.	0,59	0,29	0,41
Co	n.d.	0,12	0,06	0,09	Ag	0,04	0,13	0,08	0,06
Ni	0,48	0,33	0,41	0,11	SnO_x	0,09	0,16	0,13	0,05
CuO	84,63	83,21	83,92	1,00	Sb_2O_5	0,10	0,15	0,12	0,03
ZnO	13,44	13,96	13,70	0,36	PbO	0,54	0,11	0,33	0,31
As_2O_3	0,03	0,02	0,02	0,01	Bi_2O_3	0,08	0,06	0,07	0,01

KYT_AYV_VF_13

Spectra 53: First measurement of the object VF_13.

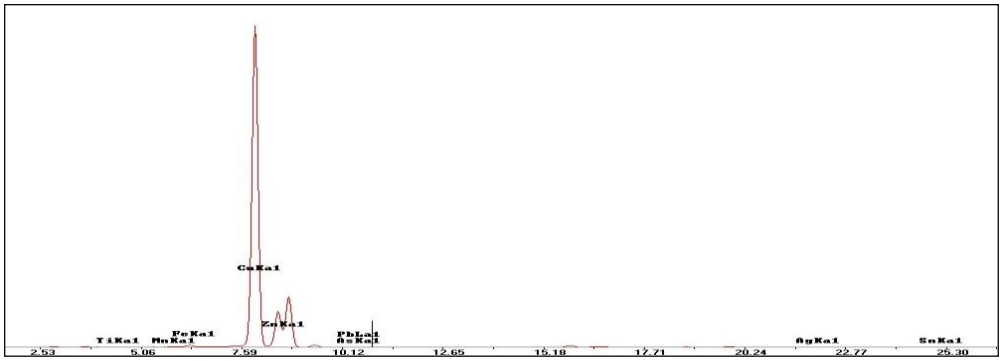

Spectra 54: Second measurement of the object VF_13.

APPENDIX II

SEM-EDS Analysis: Tables, Spectra and Microphotographs

Table 1: The measurements of the certified reference copper alloy **CDA 360** using SEM-EDS, expressed in % wt. (m.: measurement, Av.: Average, St. Dev.: Standard Deviation).

CDA 360	m. 1	m. 2	m. 3	Av.	St. Dev.
FeO	0,39	0,43	0,10	0,31	0,18
CuO	62,33	62,02	61,04	61,80	0,67
ZnO	35,21	35,04	36,82	35,69	0,98
PbO	2,07	2,51	2,03	2,21	0,27

CDA 360

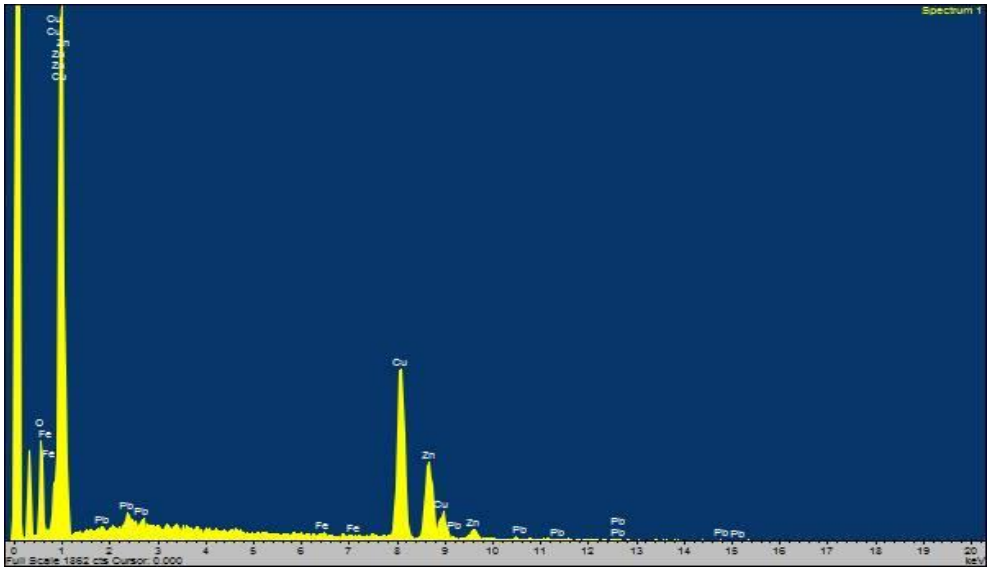

Spectra 1: First measurement of the certified reference copper alloy CDA 360.

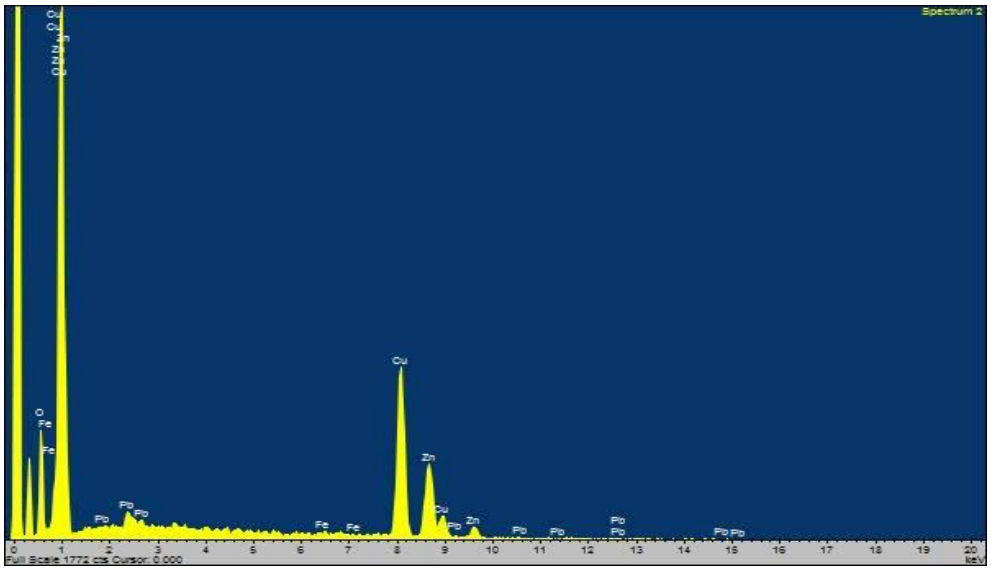
Spectrum 2
O
Fe
Fe
Cu
Zn
Pb
Fe
Cu
Zn
Pb
Pb
Pb

Bronze Sheet assemblage

Table 2: The performed measurements of the object **KYT_AYV_BS_01** using SEM-EDS expressed in % wt. (m.: measurement, Av.: Average, St. Dev.: Standard Deviation, n.d.: non detected).

BS_01	m.1	m.2	m.3	m.4	m.5	m.6	Av.	St.Dev.
Al_2O_3	n.d.	n.d.	n.d.	n.d.	2,14	n.d.	2,14	-
SiO_2	n.d.	n.d.	n.d.	1,69	8,94	n.d.	5,32	5,13
P_2O_5	n.d.	n.d.	n.d.	1,06	3,22	n.d.	2,14	1,53
Cl	0,56	0,77	1,30	2,11	6,31	0,92	2,00	2,18
CaO	n.d.	n.d.	n.d.	n.d.	3,81	n.d.	3,81	-
FeO	0,48	0,51	0,52	1,13	1,88	0,21	0,79	0,61
Ni	0,55	n.d.	0,38	n.d.	n.d.	0,39	0,44	0,10
CuO	86,83	87,34	89,06	78,06	58,09	86,64	81,00	11,87
ZnO	7,90	7,53	4,73	5,91	6,84	5,54	6,41	1,22
As_2O_3	0,46	0,33	n.d.	0,33	1,10	0,78	0,60	0,33
Ag	n.d.	0,05	0,03	0,52	0,34	0,27	0,24	0,21
SnO_x	1,93	2,58	2,82	4,21	2,87	3,11	2,92	0,75
PbO	1,28	0,90	1,16	4,98	4,46	2,14	2,49	1,79

KYT_AYV_BS_01

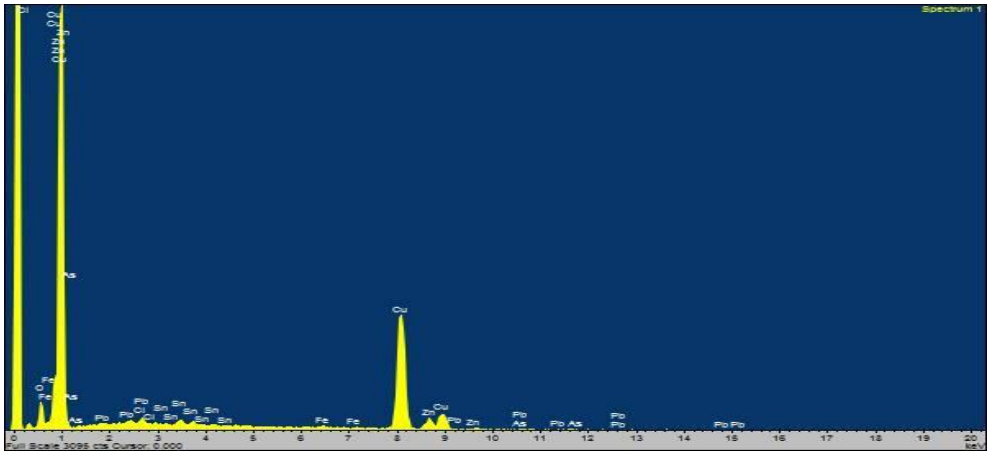

Spectra 4: First measurement of the object BS_01.

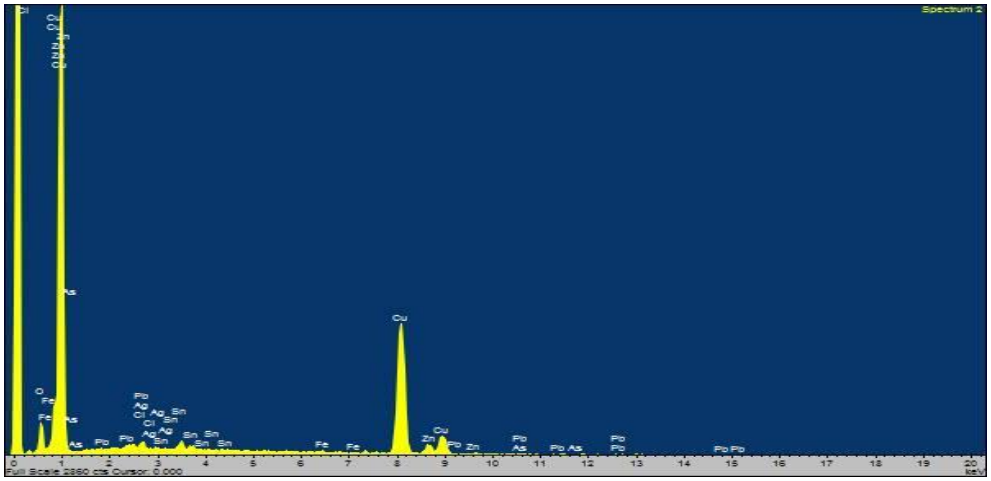

Spectra 5: Second measurement of the object BS_01.

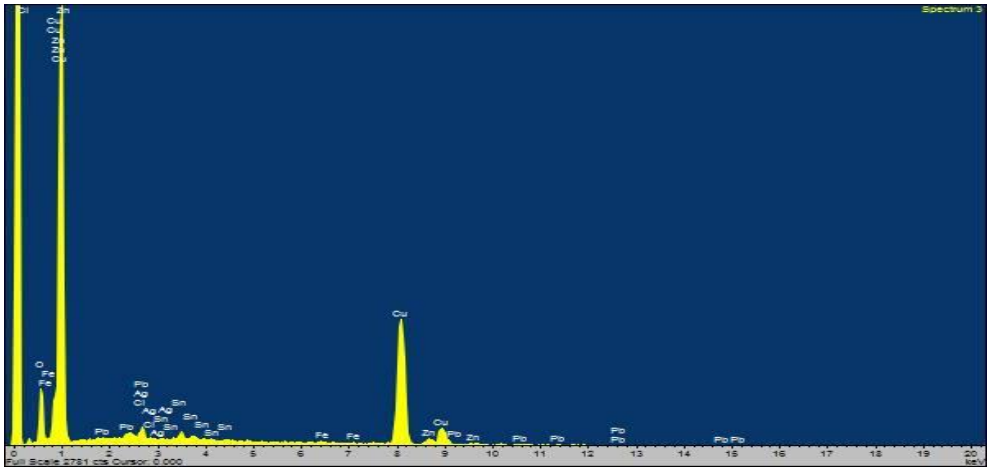

Spectra 6: Third measurement of the object BS_01.

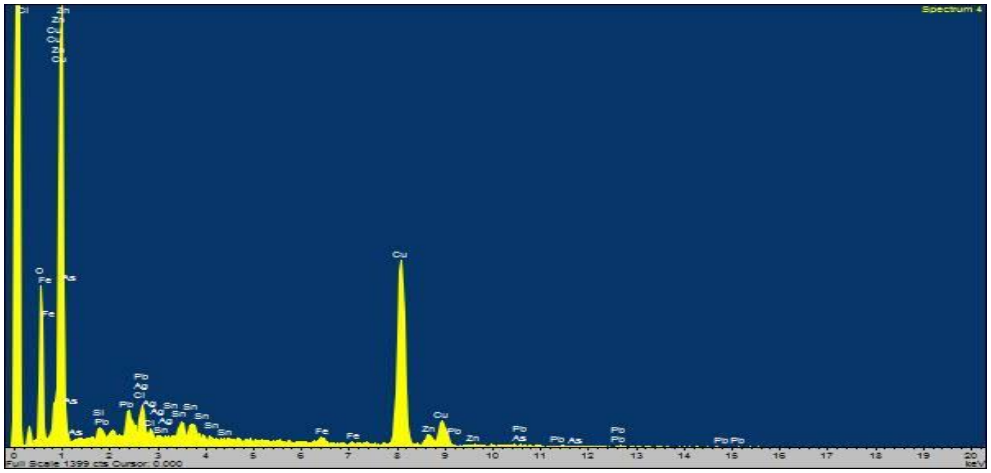

Spectra 7: Fourth measurement of the object BS_01.

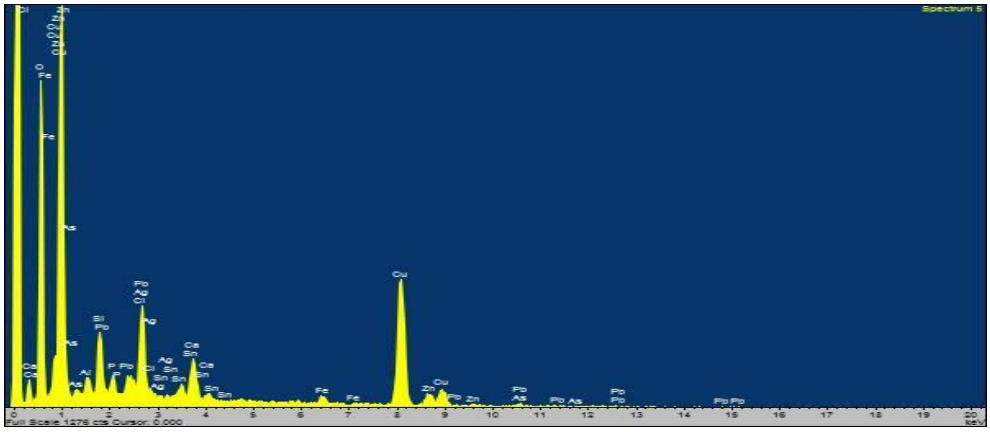

Spectra 8: Fifth measurement of the object BS_01.

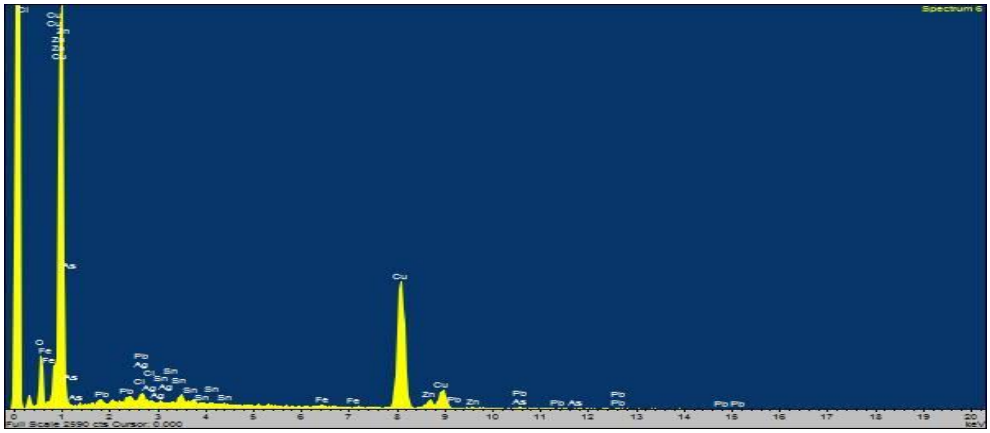

Spectra 9: Sixth measurement of the object BS_01.

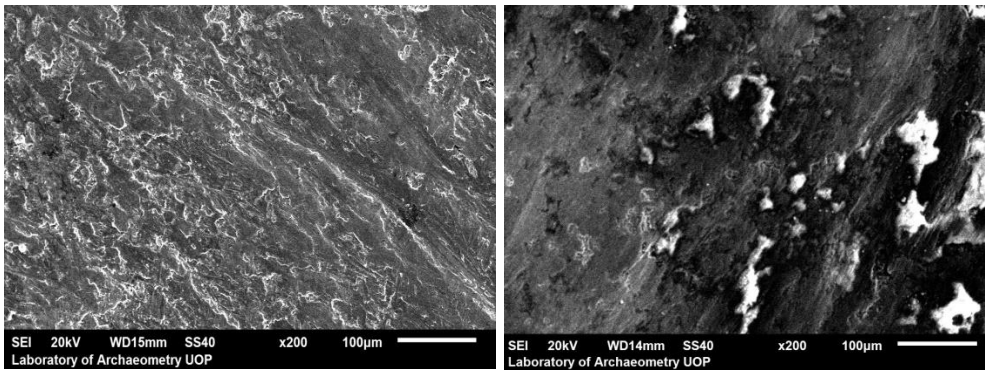

Images 1-2: Backscattered electron images in the SEM for the object BS_01. Magnification 200X. Compositional contrast that results from different atomic number elements and their distribution are displayed.

Left: cleaned area (measurement 2 – spectra 5). Right: partially cleaned area (measurement 4 – spectra 7).

Table 3: The performed measurements of the object **KYT_AYV_BS_02** using SEM-EDS expressed in % wt. (m.: measurement, Av.: Average, St. Dev.: Standard Deviation, n.d.: non detected).

BS_02	m.1	m.2	m.3	m.4	m.5	m.6	Av.	St.Dev.
SiO_2	n.d.	n.d.	n.d.	n.d.	n.d.	1,73	1,73	-
P_2O_5	n.d.	n.d.	n.d.	n.d.	1,70	n.d.	1,70	-
Cl	n.d.	0,64	1,40	0,66	1,80	2,04	1,31	0,64
FeO	0,52	0,32	0,36	0,53	0,70	0,47	0,48	0,14
Ni	0,65	n.d.	0,36	0,63	n.d.	n.d.	0,55	0,16
CuO	97,96	98,32	96,02	96,61	93,59	94,76	96,21	1,83
ZnO	n.d.	0,12	0,80	n.d.	0,60	0,02	0,39	0,38
As_2O_3	0,35	n.d.	0,54	0,22	0,48	n.d.	0,40	0,14
Ag	n.d.	n.d.	n.d.	0,33	n.d.	n.d.	0,33	-
SnO_x	0,53	0,50	0,52	0,83	1,13	0,34	0,64	0,29
PbO	n.d.	0,10	n.d.	0,20	n.d.	0,63	0,31	0,28

KYT_AYV_BS_02

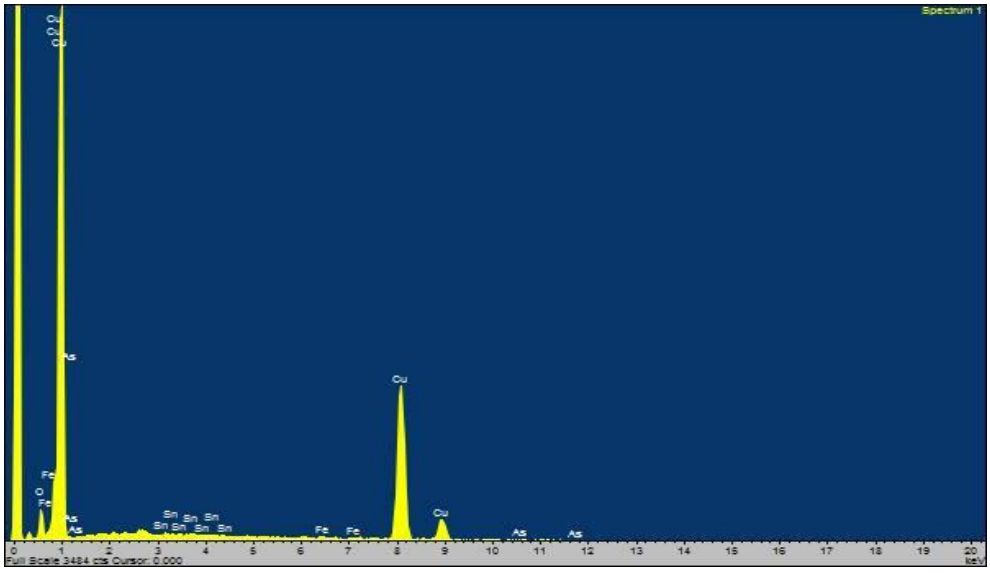

Spectra 10: First measurement of the object BS_02.

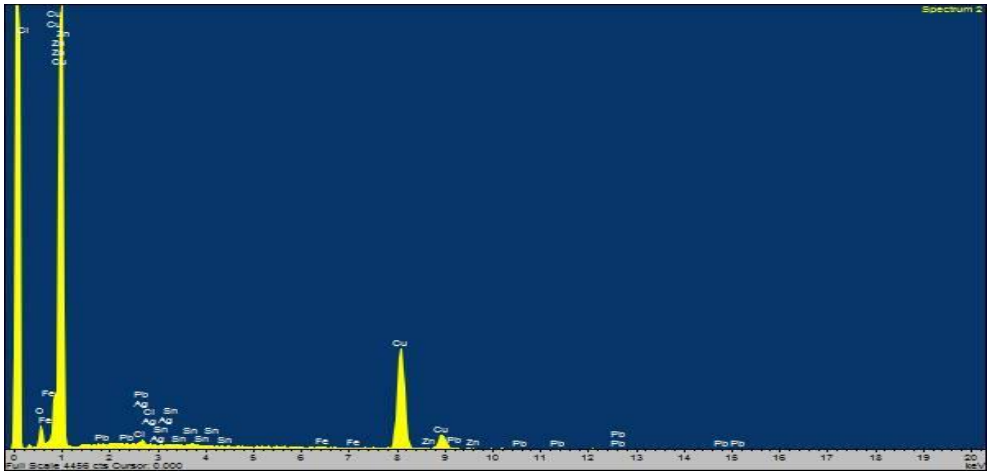

Spectra 11: Second measurement of the object BS_02.

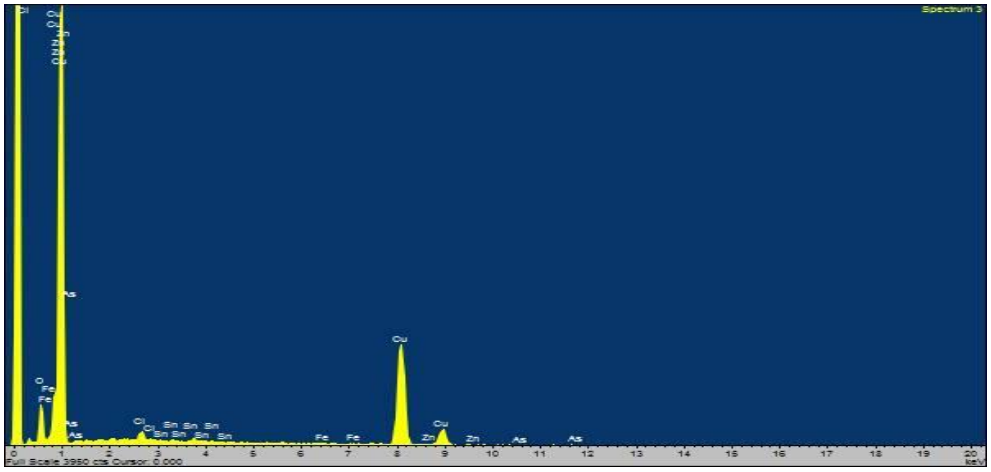

Spectra 12: Third measurement of the object BS_02.

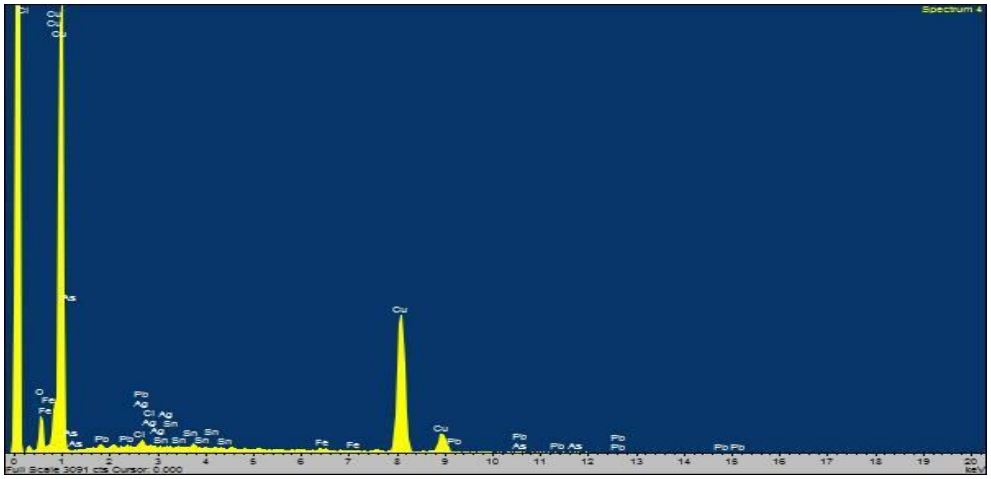

Spectra 13: Fourth measurement of the object BS_02.

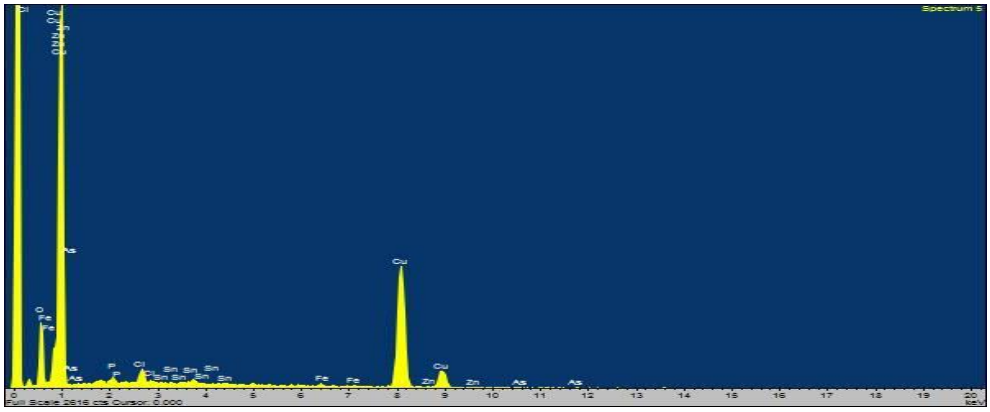

Spectra 14: Fifth measurement of the object BS_02.

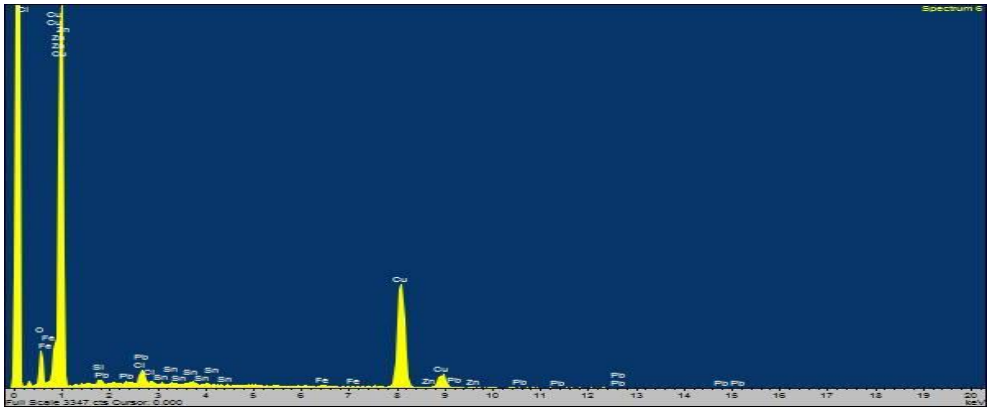

Spectra 15: Sixth measurement of the object BS_02.

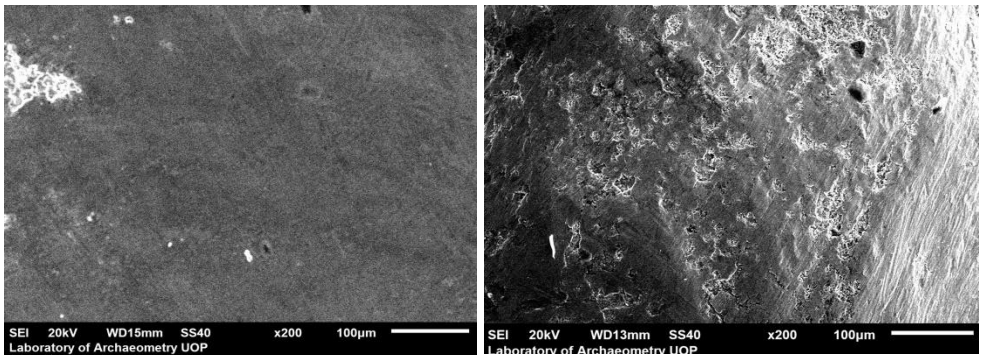

Images 3-4: Backscattered electron images in the SEM for the object BS_02. Magnification 200X. Compositional contrast that results from different atomic number elements and their distribution are displayed.

Left: cleaned area (measurement 1 - spectra 10). The high copper content is obvious and forms an almost homogeneous area. Right: partially cleaned area (measurement 6 - spectra 15).

Table 4: The performed measurements of the object **KYT_AYV_BS_06** using SEM-EDS expressed in % wt. (m.: measurement, Av.: Average, St. Dev.: Standard Deviation, n.d.: non detected).

BS_06	m.1	m.2	m.3	m.4	m.5	m.6	m.7	m.8	Av.	St.Dev
S	n.d.	1,47	1,53	1,98	2,14	1,29	n.d.	2,07	1,75	0,36
Cl	6,95	8,93	13,12	2,96	6,14	14,61	9,26	7,61	8,70	3,75
FeO	0,63	n.d.	0,34	0,33	n.d.	n.d.	n.d.	n.d.	0,43	0,17
CuO	91,25	88,53	81,85	94,39	89,86	80,74	87,84	86,97	87,68	4,57
ZnO	n.d.	0,24	n.d.	n.d.	1,36	n.d.	n.d.	n.d.	0,80	0,79
As_2O_3	0,73	n.d.	1,34	0,65	n.d.	0,87	0,40	0,58	0,76	0,32
Ag	n.d.	n.d.	n.d.	n.d.	n.d.	n.d.	1,30	1,29	0,86	0,75
SnO_x	n.d.	0,27	0,78	n.d.	0,34	n.d.	1,20	0,76	0,67	0,38
PbO	0,43	0,56	1,05	n.d.	0,16	2,49	n.d.	0,72	0,90	0,83

KYT_AYV_BS_06

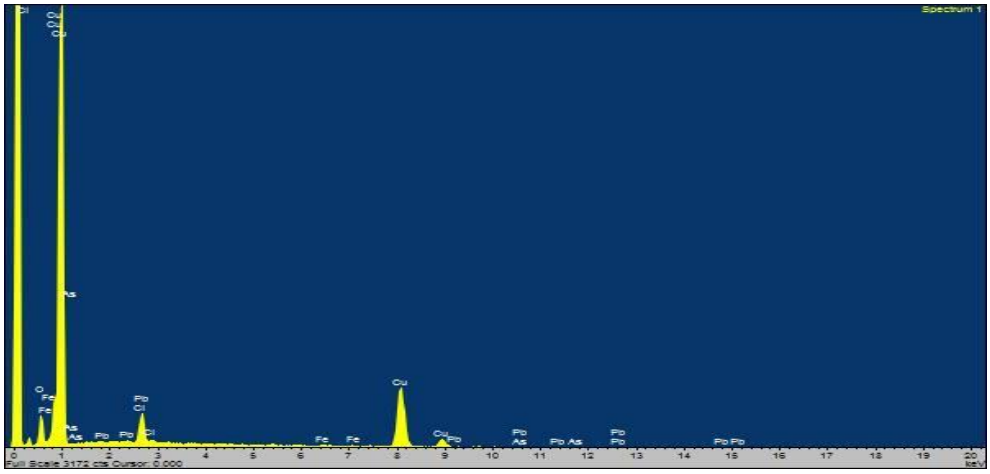

Spectra 16: First measurement of the object BS_06.

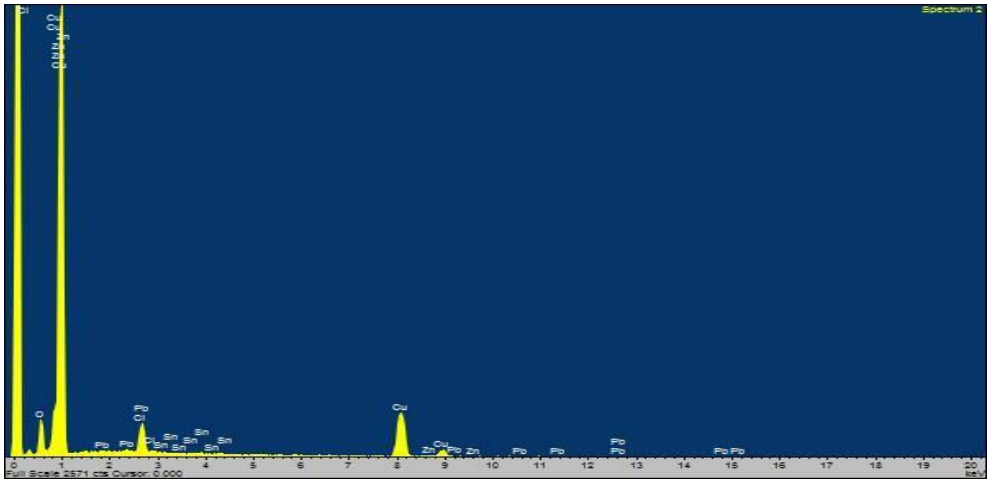

Spectra 17: Second measurement of the object BS_06.

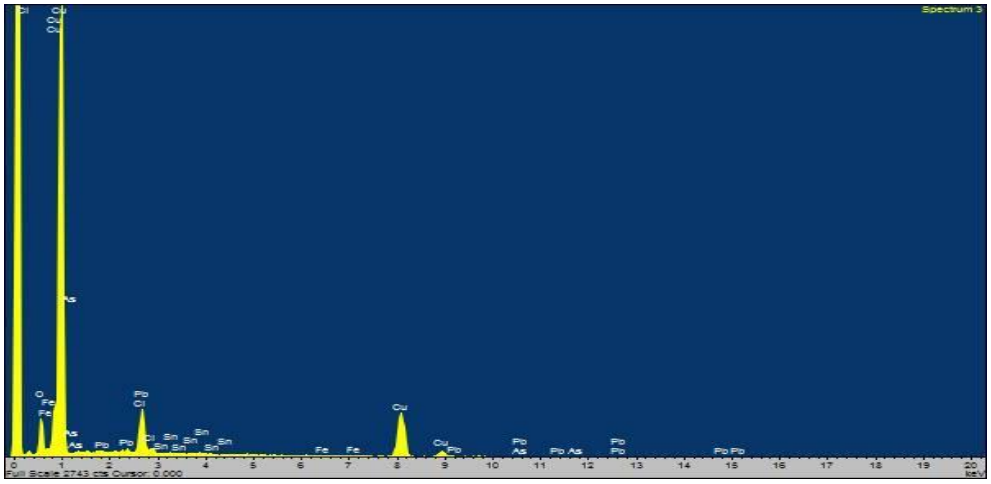

Spectra 18: Third measurement of the object BS_06.

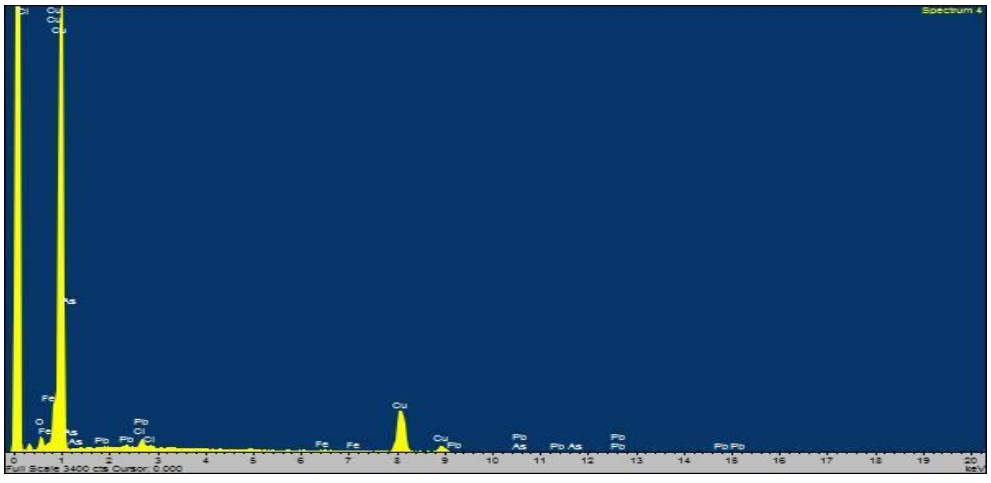

Spectra 19: Fourth measurement of the object BS_06.

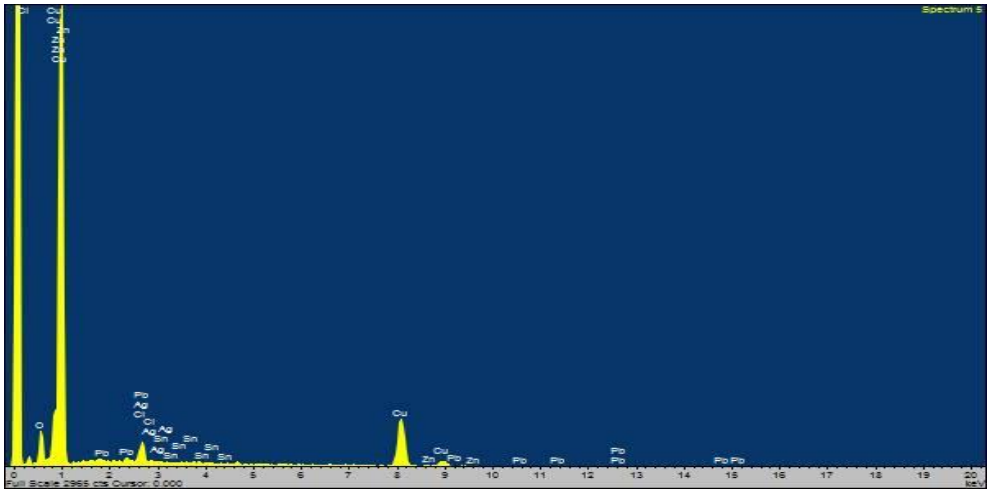

Spectra 20: Fifth measurement of the object BS_06.

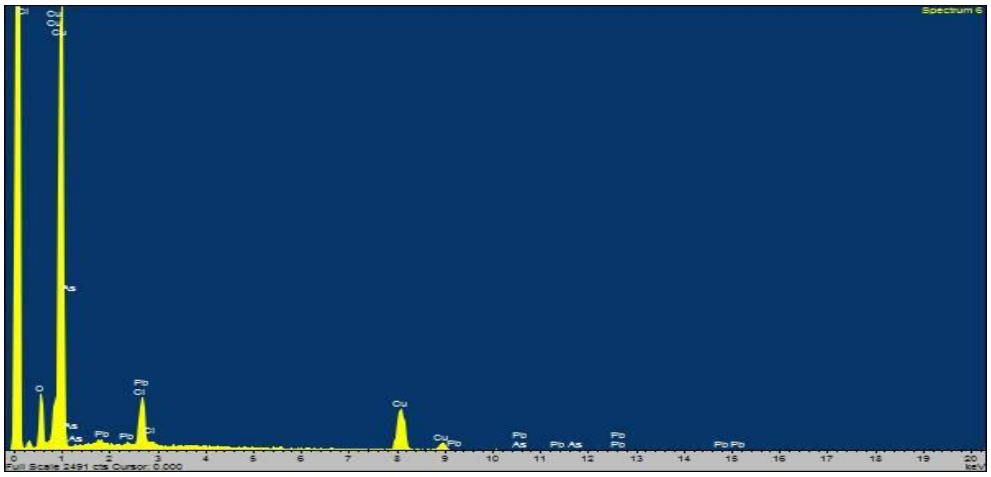

Spectra 21: Sixth measurement of the object BS_06.

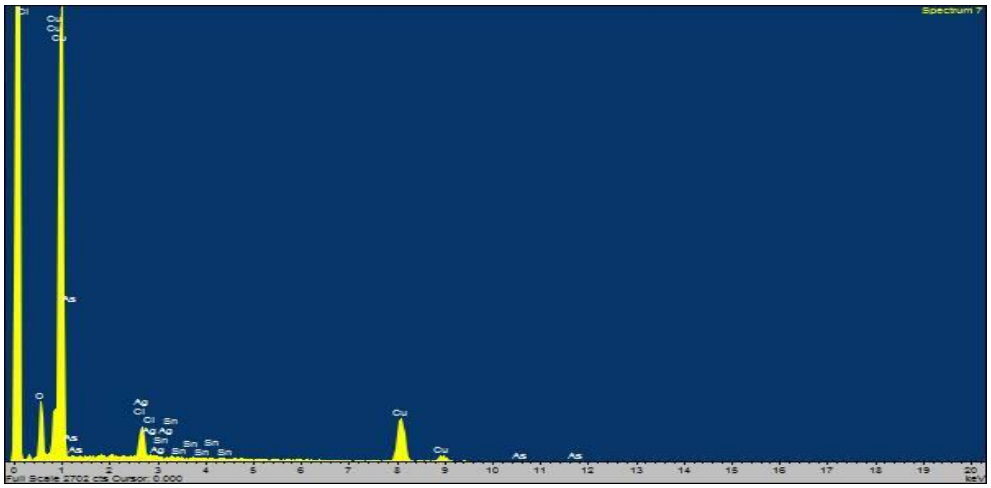

Spectra 22: Seventh measurement of the object BS_06.

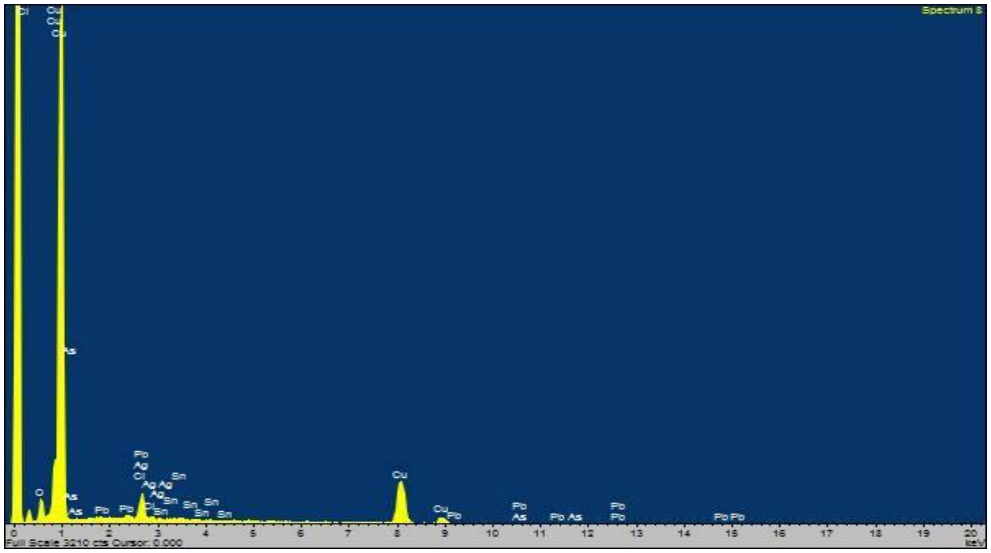

Spectra 23: Eighth measurement of the object BS_06.

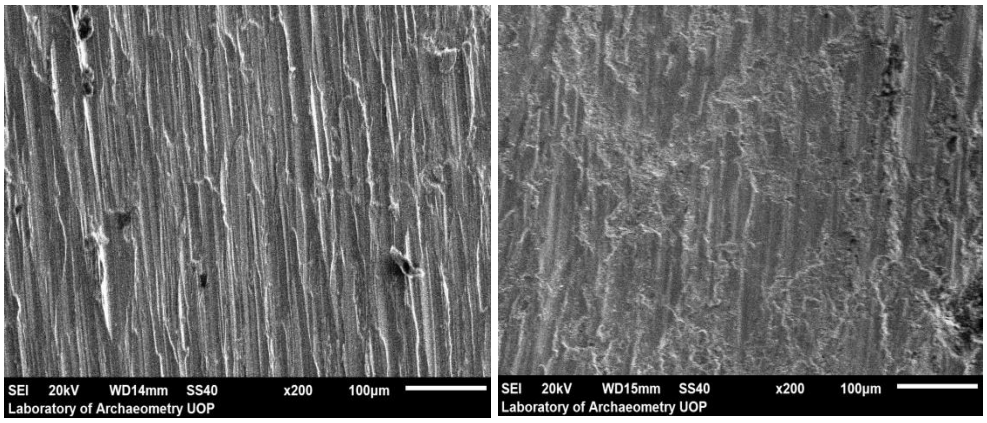

Images 5-6: Backscattered electron images in the SEM for the object BS_06. Magnification 200X. Compositional contrast that results from different atomic number elements and their distribution are displayed.

Left: the highest copper content cleaned area, shown as almost homogeneous (measurement 4 - spectra 19). Right: the highest chlorine (caused by corrosion) and lead content area (measurement 6 - spectra 21).

Table 5: The performed measurements of the object **KYT_AYV_BS_07** using SEM-EDS expressed in % wt. (m.: measurement, Av.: Average, St. Dev.: Standard Deviation, n.d.: non detected).

BS_07	m.1	m.2	m.3	m.4	m.5	m.6	Av.	St.Dev.
Al_2O_3	6,32	n.d.	n.d.	n.d.	n.d.	n.d.	6,32	-
SiO_2	13,20	n.d.	n.d.	n.d.	n.d.	n.d.	13,20	-
Cl	2,37	6,22	n.d.	4,10	5,80	31,80	10,06	12,25
CaO	10,76	n.d.	n.d.	n.d.	n.d.	n.d.	10,76	-
FeO	0,90	n.d.	0,32	n.d.	n.d.	1,40	0,87	0,54
Ni	n.d.	n.d.	n.d.	n.d.	n.d.	5,29	5,29	-
CuO	37,26	77,16	70,49	67,01	48,53	33,12	55,60	18,48
ZnO	24,37	14,03	28,35	26,35	29,93	27,77	25,13	5,76
As_2O_3	3,09	n.d.	n.d.	n.d.	2,91	0,62	2,21	1,38
Ag	n.d.	1,03	n.d.	n.d.	3,44	n.d.	2,24	1,70
SnO_x	n.d.	n.d.	0,45	2,53	5,65	n.d.	2,88	2,62
PbO	1,73	1,57	0,39	n.d.	3,74	n.d.	1,86	1,39

KYT_AYV_BS_07

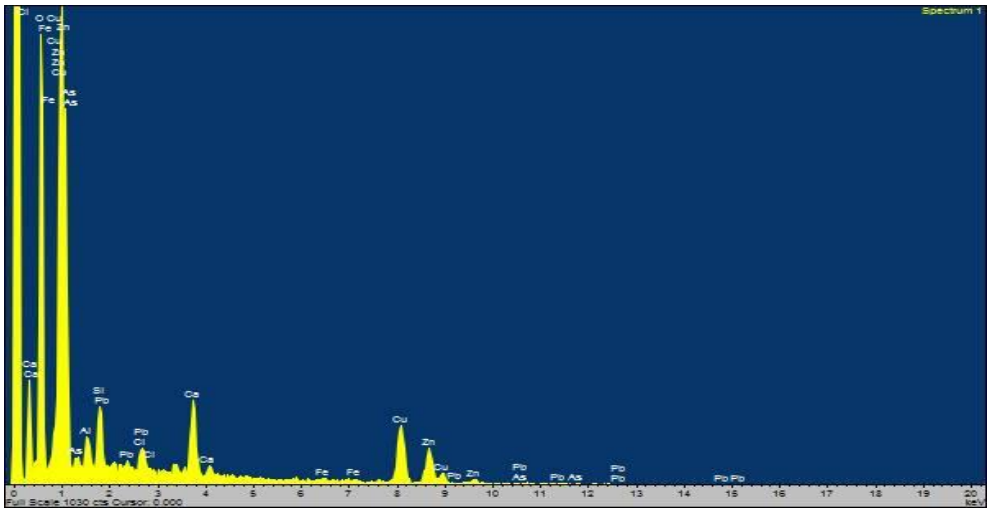

Spectra 24: First measurement of the object BS_07.

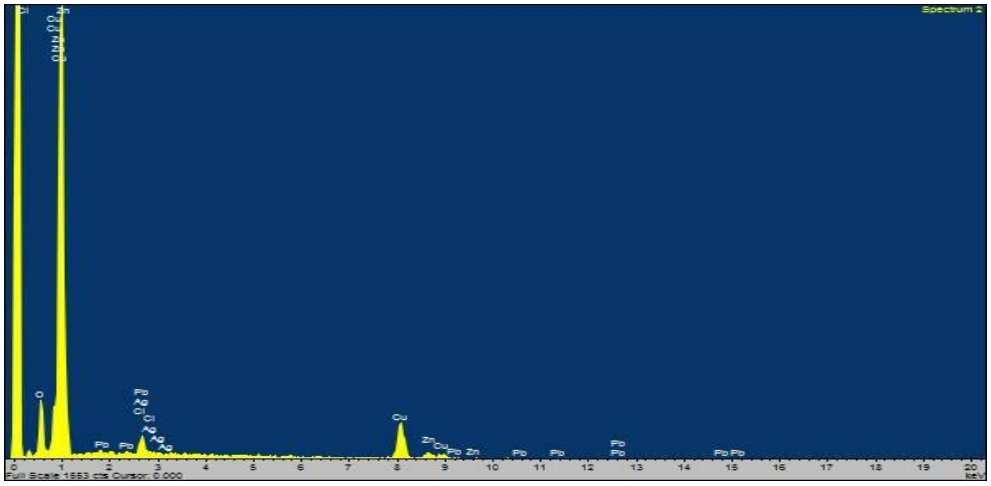

Spectra 25: Second measurement of the object BS_07.

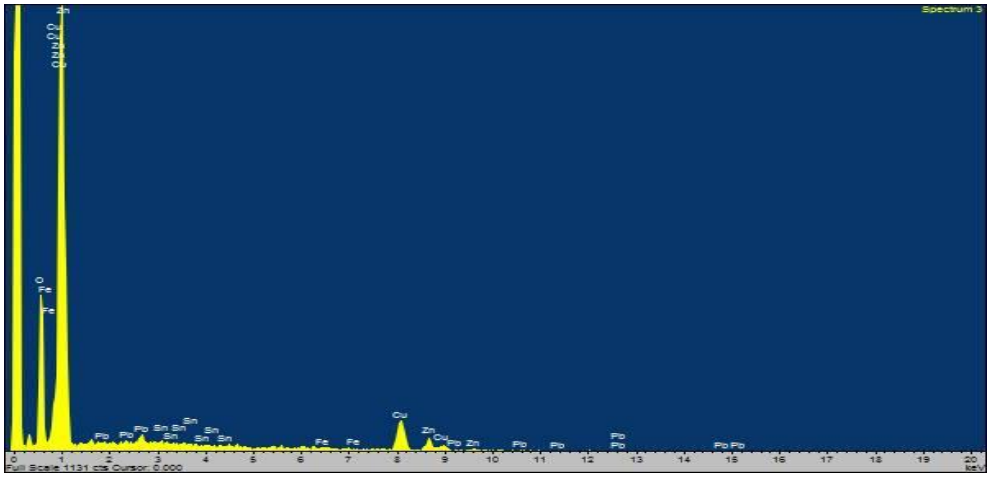

Spectra 26: Third measurement of the object BS_07.

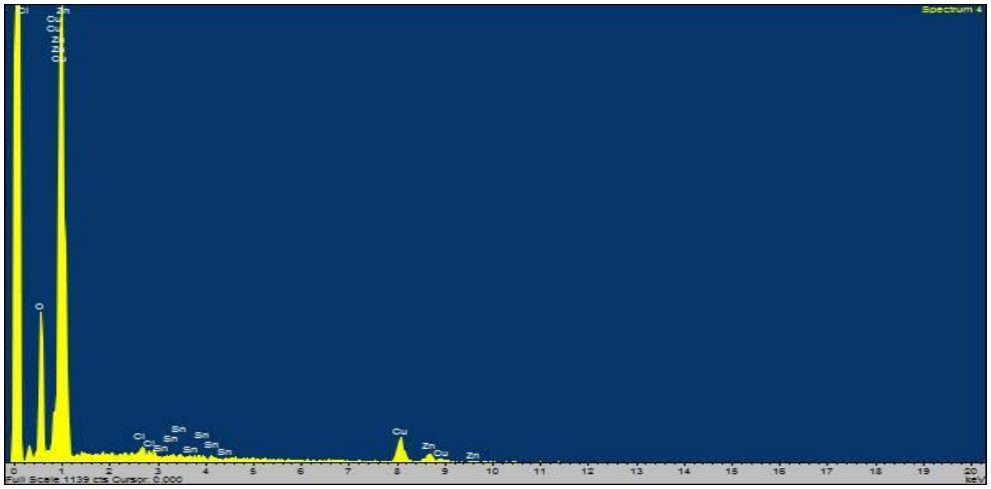

Spectra 27: Fourth measurement of the object BS_07.

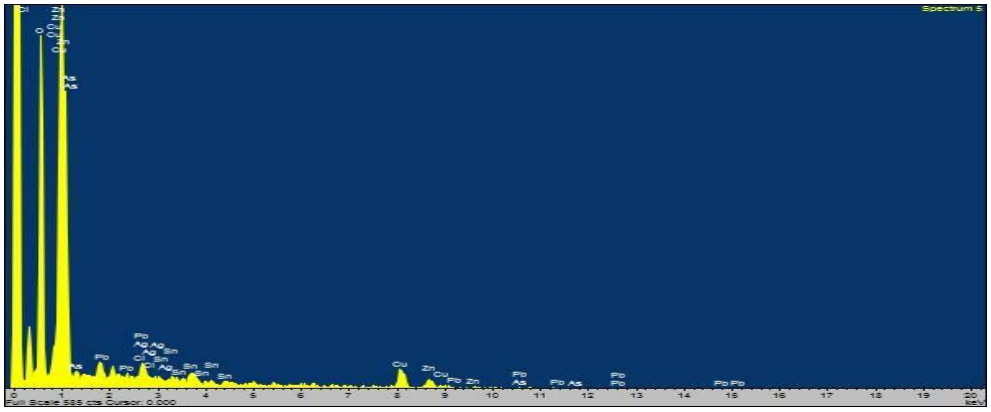

Spectra 28: Fifth measurement of the object BS_07.

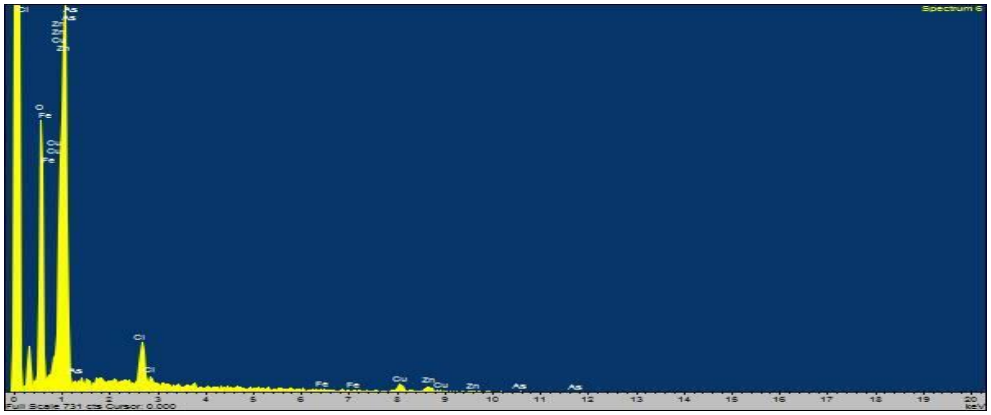

Spectra 29: Sixth measurement of the object BS_07.

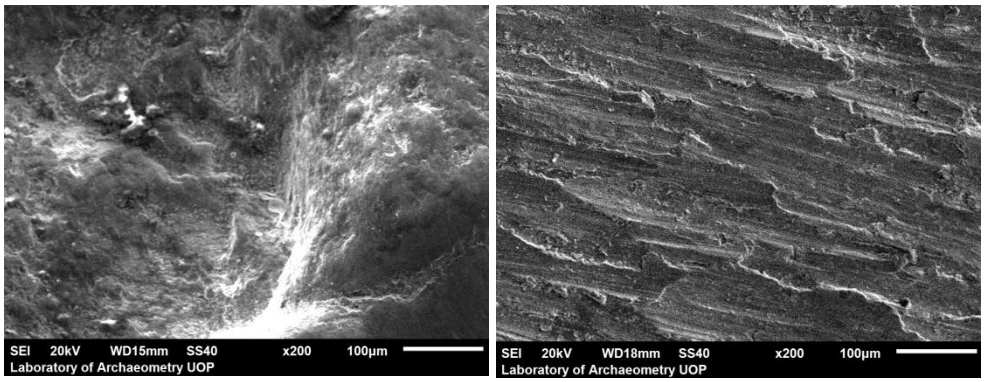

Images 7-8: Backscattered electron images in the SEM for the object BS_07. Magnification 200X. Compositional contrast that results from different atomic number elements and their distribution are displayed.

Left: partially cleaned area (measurement 1 - spectra 24). Right: the highest copper content area (measurement 2 - spectra 25).

Table 6: The performed measurements of the object **KYT_AYV_BS_08** using SEM-EDS expressed in % wt. (m.: measurement, Av.: Average, St. Dev.: Standard Deviation, n.d.: non detected).

BS_08	m.1	m.2	m.3	m.4	m.5	Av.	St. Dev.
Al_2O_3	n.d.	n.d.	n.d.	2,13	n.d.	2,13	-
SiO_2	1,71	n.d.	n.d.	9,71	5,73	5,72	4,00
P_2O_5	0,99	0,17	0,21	1,78	2,57	1,14	1,03
Cl	1,44	1,16	n.d.	4,26	4,53	2,85	1,79
CaO	n.d.	n.d.	n.d.	2,49	2,05	2,27	0,31
FeO	n.d.	0,04	n.d.	0,93	0,79	0,59	0,48
CuO	93,71	96,41	97,89	76,87	82,24	89,42	9,33
ZnO	0,51	0,34	0,73	0,23	0,40	0,44	0,19
As_2O_3	0,31	0,81	0,18	0,34	0,46	0,42	0,24
Ag	0,26	0,12	0,41	n.d.	0,35	0,29	0,13
SnO_x	0,81	0,50	0,35	n.d.	n.d.	0,55	0,23
PbO	0,26	0,45	0,24	1,26	0,88	0,62	0,44

KYT_AYV_BS_08

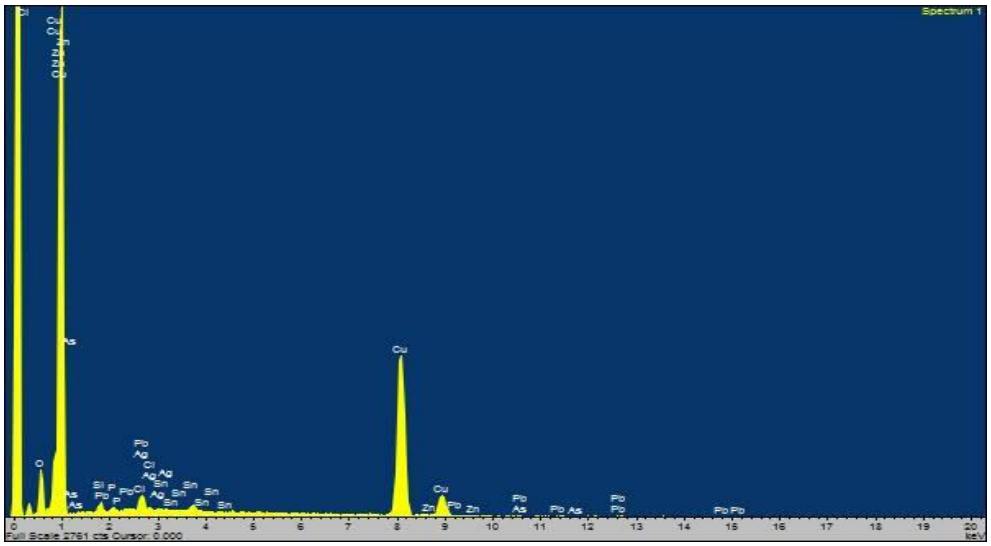

Spectra 30: First measurement of the object BS_08.

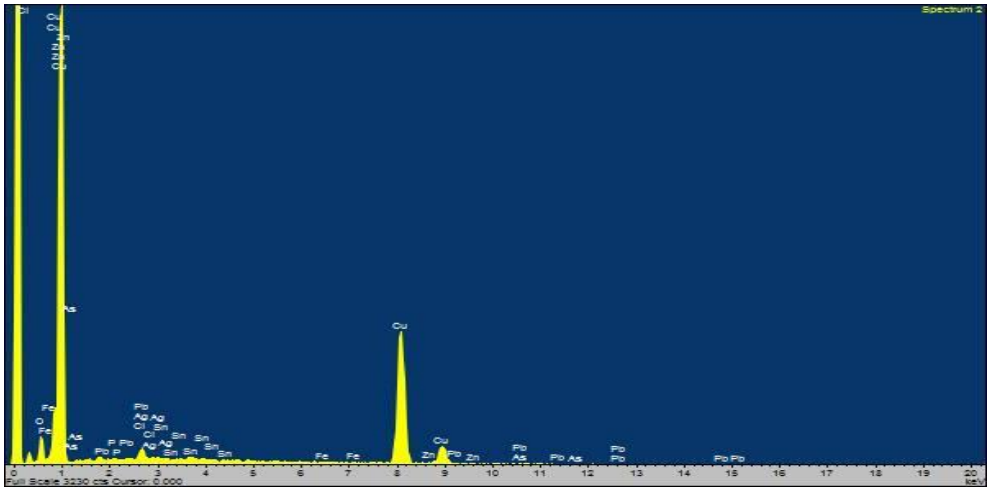

Spectra 31: Second measurement of the object BS_08.

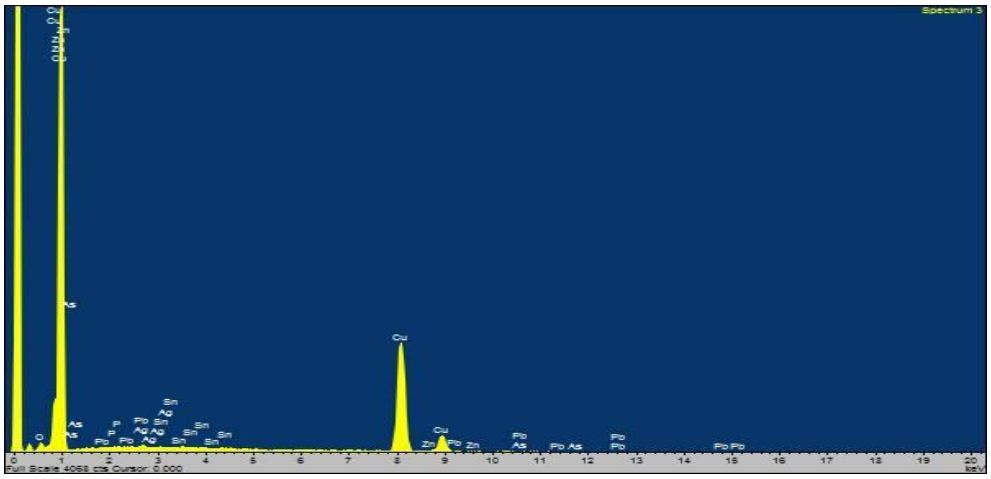

Spectra 32: Third measurement of the object BS_08.

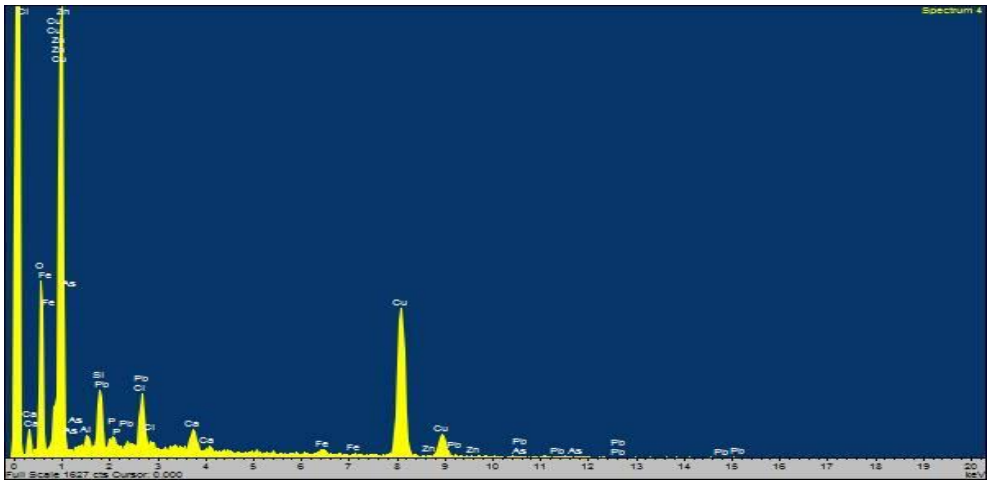

Spectra 33: Fourth measurement of the object BS_08.

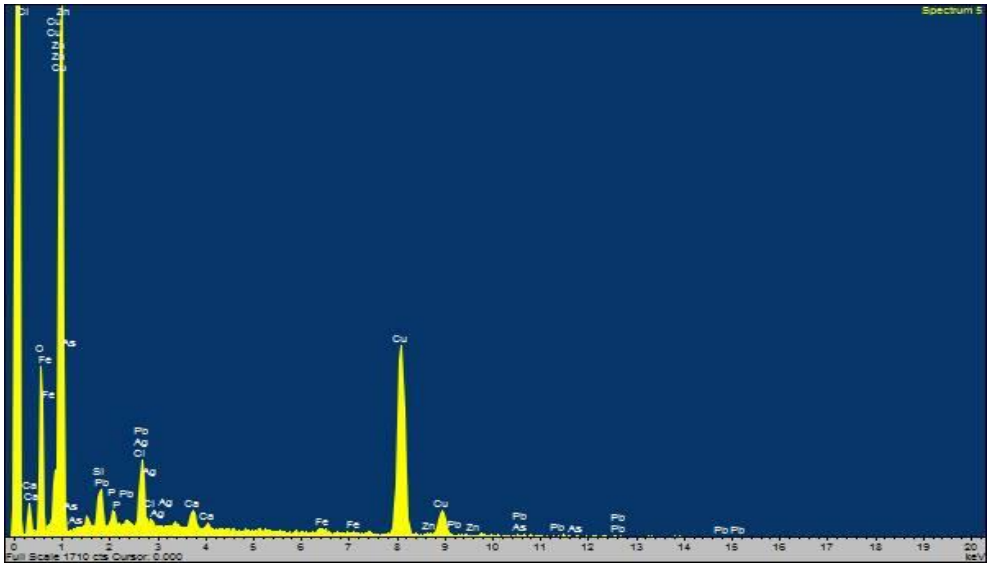

Spectra 34: Fifth measurement of the object BS_08.

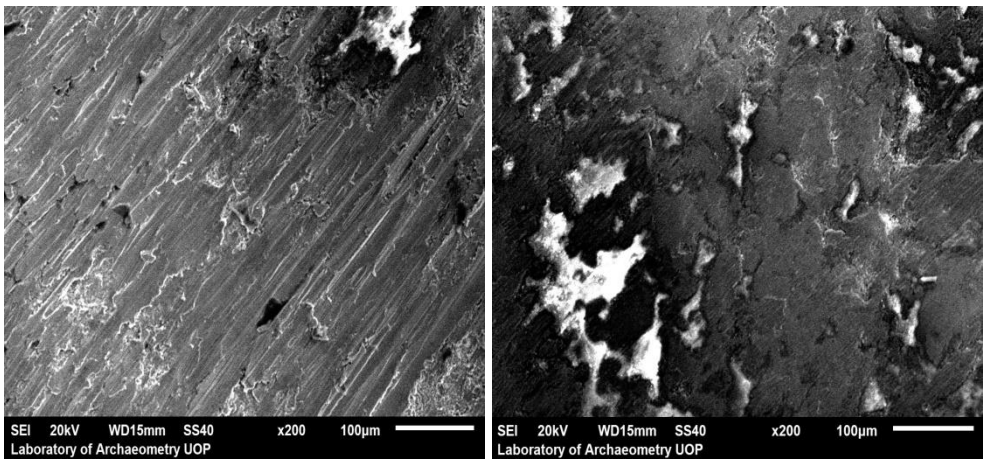

Images 9-10: Backscattered electron images in the SEM for the object BS_08. Magnification 200X. Compositional contrast that results from different atomic number elements and their distribution are displayed.

Left: high copper content cleaned area (measurement 2 - spectra 31). Right: partially cleaned area with residues of soil encrustations and chlorine caused by corrosion (measurement 4 - spectra 33).

Table 7: The performed measurements of the object **KYT_AYV_BS_10** using SEM-EDS expressed in % wt. (m.: measurement, Av.: Average, St. Dev.: Standard Deviation, n.d.: non detected).

BS_10	m.1	m.2	m.3	m.4	m.5	m.6	Av.	St.Dev.
Al_2O_3	n.d.	n.d.	n.d.	10,30	13,70	n.d.	12,00	2,40
SiO_2	4,66	19,95	20,62	69,51	52,55	n.d.	33,46	26,65
Cl	2,42	3,73	6,79	n.d.	n.d.	3,49	4,11	1,88
CaO	n.d.	n.d.	n.d.	6,61	8,11	n.d.	7,36	1,06
FeO	0,55	1,15	n.d.	1,09	3,17	n.d.	1,49	1,15
CuO	90,57	74,72	70,80	6,20	20,32	89,57	58,70	36,33
ZnO	0,40	n.d.	n.d.	n.d.	1,00	1,90	1,10	0,75
As_2O_3	0,09	n.d.	n.d.	2,41	0,33	3,15	1,50	1,52
Ag	n.d.	n.d.	1,66	1,85	n.d.	1,80	1,77	0,10
SnO_x	0,36	n.d.	0,13	0,40	n.d.	n.d.	0,30	0,15
PbO	0,96	0,45	n.d.	1,62	0,82	0,09	0,79	0,58

KYT_AYV_BS_10

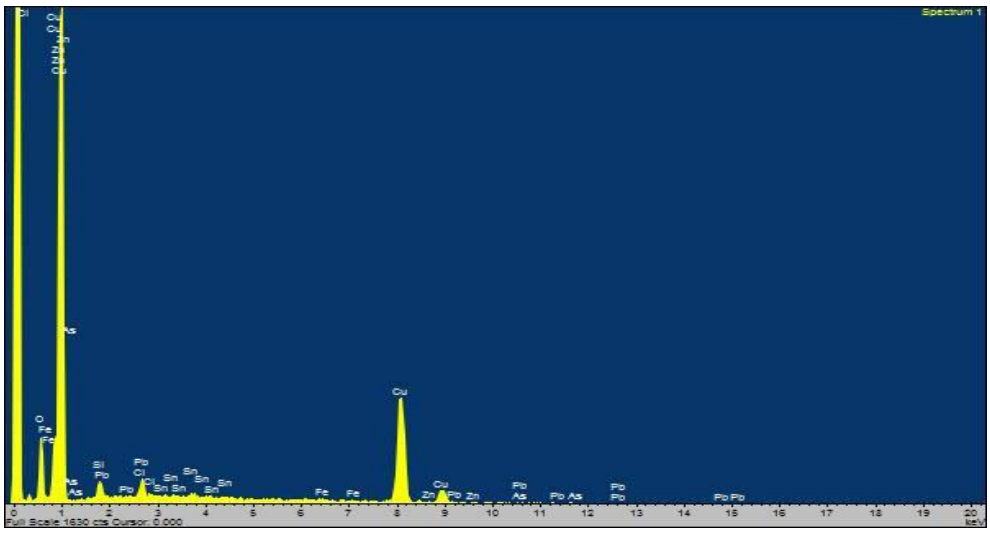

Spectra 35: First measurement of the object BS_10.

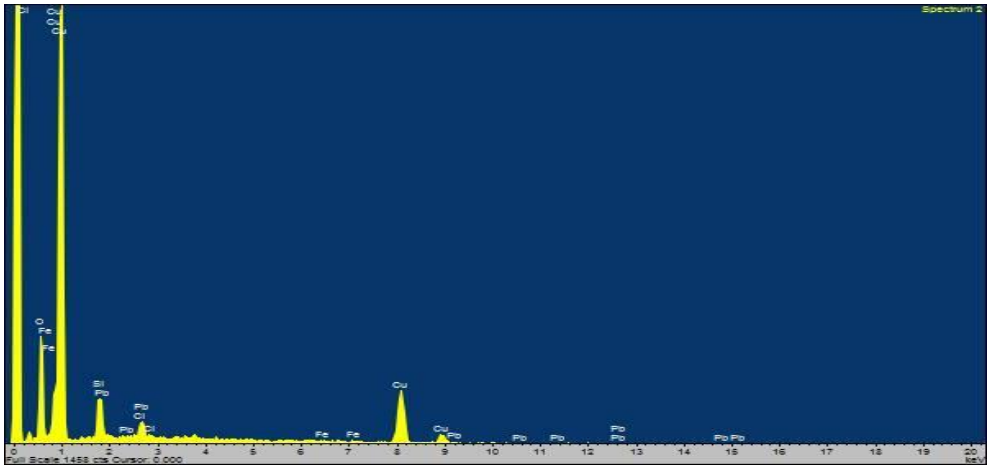

Spectra 36: Second measurement of the object BS_10.

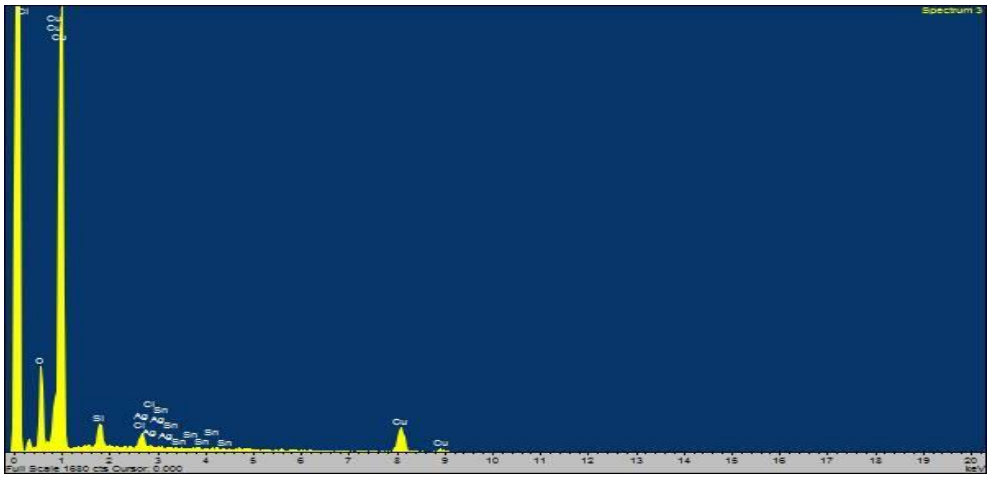

Spectra 37: Third measurement of the object BS_10.

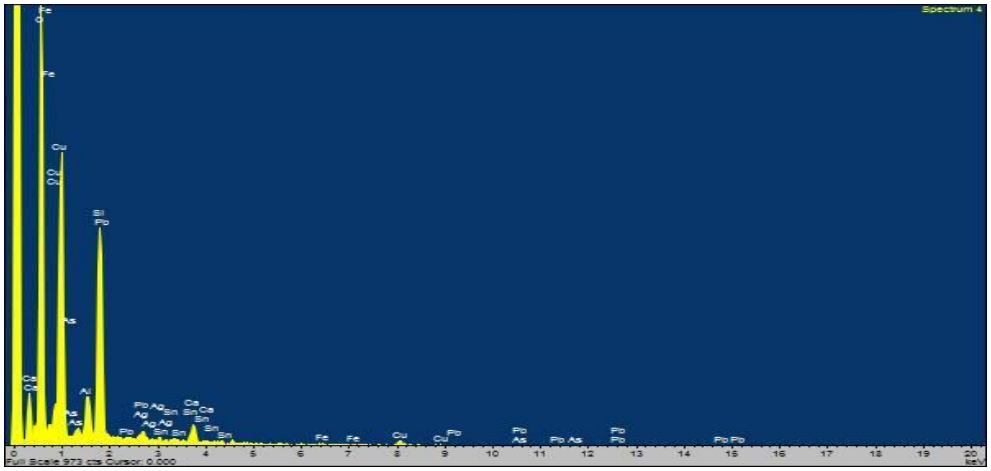

Spectra 38: Fourth measurement of the object BS_10.

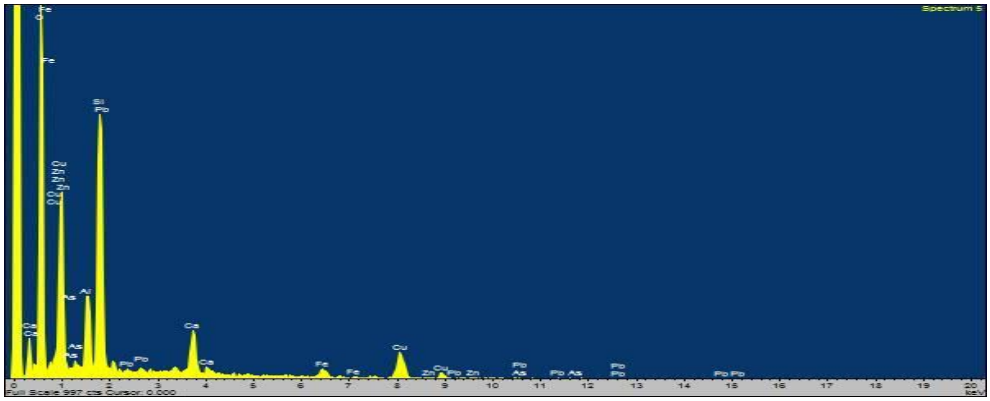

Spectra 39: Fifth measurement of the object BS_10.

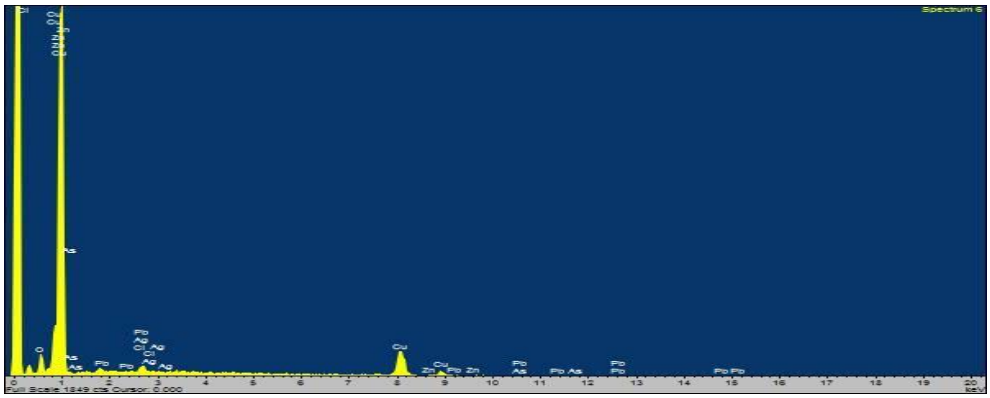

Spectra 40: Sixth measurement of the object BS_10.

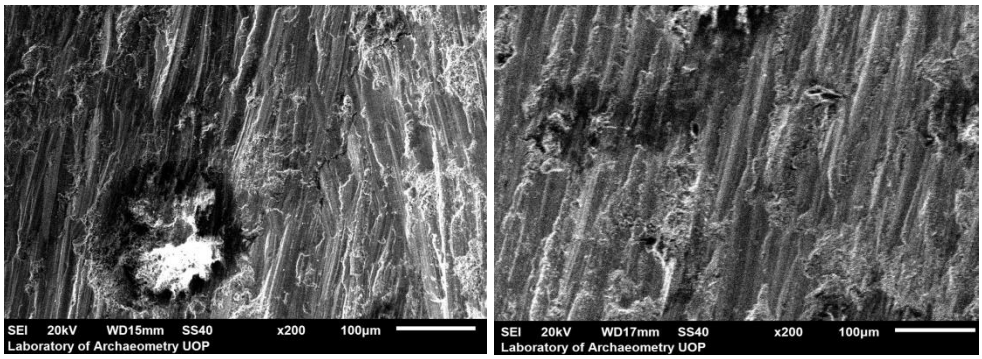

Images 11-12: Backscattered electron images in the SEM for the object BS_10. Magnification 200X. Compositional contrast that results from different atomic number elements and their distribution are displayed.

Left: the highest copper content area, containing also amount of lead (measurement 1 - spectra 35). Right: partially cleaned area with the lowest copper content and without lead (measurement 3 - spectra 37).

Table 8: The performed measurements of the object **KYT_AYV_BS_19** using SEM-EDS expressed in % wt. (m.: measurement, Av.: Average, St. Dev.: Standard Deviation, n.d.: non detected).

BS_19	m.1	m.2	m.3	m.4	m.5	m.6	Av.	St.Dev.
MgO	1,28	0,33	0,92	1,72	1,26	0,61	1,02	0,50
Al_2O_3	n.d.	n.d.	n.d.	4,14	1,76	n.d.	2,95	1,68
SiO_2	2,64	0,57	2,27	8,93	3,33	1,71	3,24	2,94
S	0,52	n.d.	0,46	1,08	n.d.	n.d.	0,69	0,34
CaO	3,84	n.d.	3,00	5,91	2,20	1,70	3,33	1,66
FeO	0,32	n.d.	n.d.	1,35	0,90	0,05	0,66	0,58
Ni	1,99	0,66	1,26	0,98	1,69	2,02	1,43	0,56
CuO	4,67	21,61	9,17	5,58	3,72	7,06	8,64	6,64
ZnO	1,64	1,45	1,68	n.d.	0,80	1,53	1,42	0,36
As_2O_3	0,08	n.d.	n.d.	n.d.	n.d.	0,94	0,51	0,61
Ag	81,84	73,85	80,43	69,41	83,55	83,73	78,80	5,86
SnO_x	1,17	0,67	n.d.	n.d.	n.d.	0,65	0,83	0,29
PbO	n.d.	0,85	0,80	0,89	0,80	n.d.	0,84	0,04

KYT_AYV_BS_19

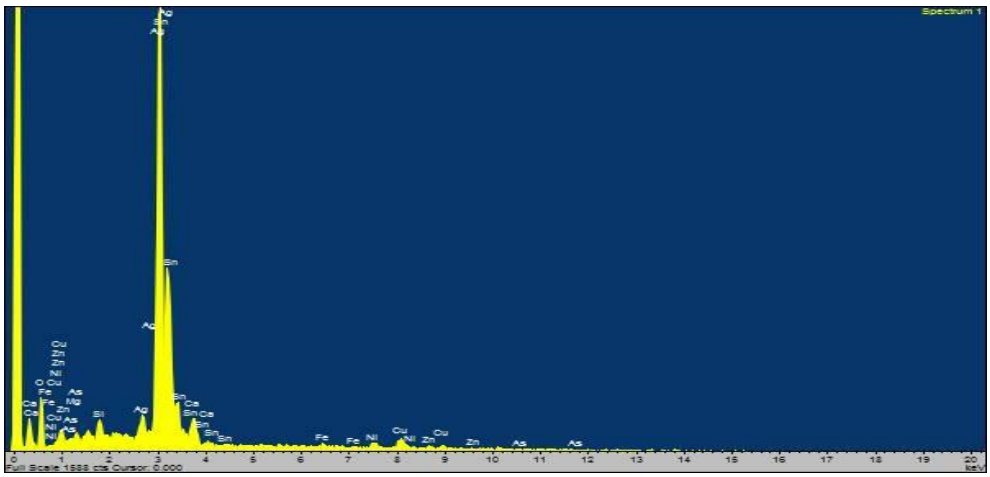

Spectra 41: First measurement of the object BS_19.

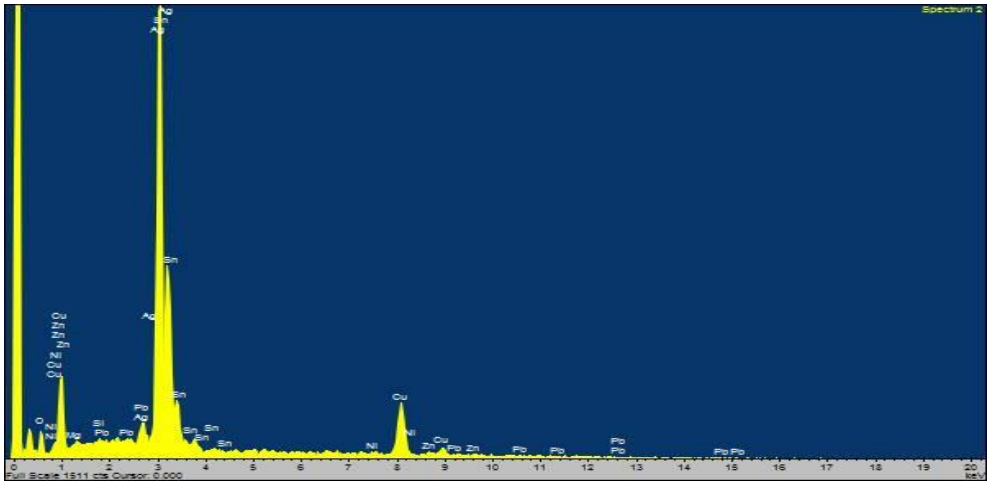

Spectra 42: Second measurement of the object BS_19.

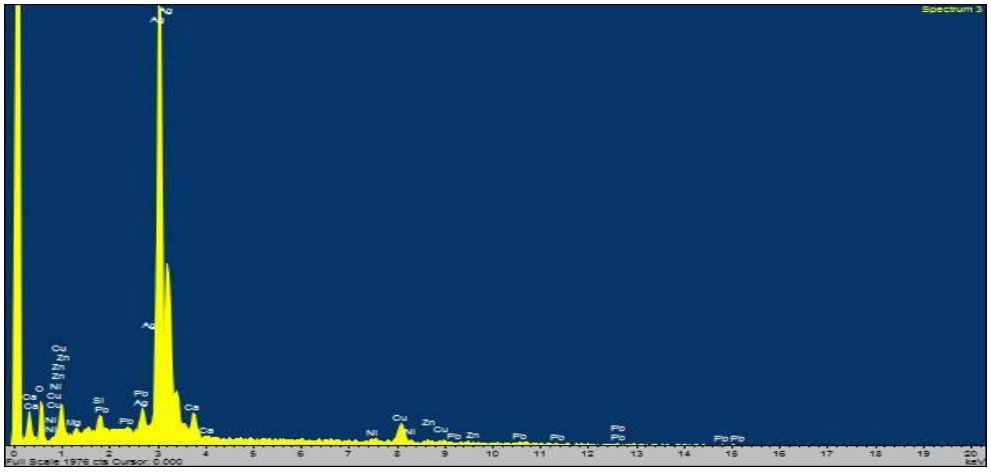

Spectra 43: Third measurement of the object BS_19.

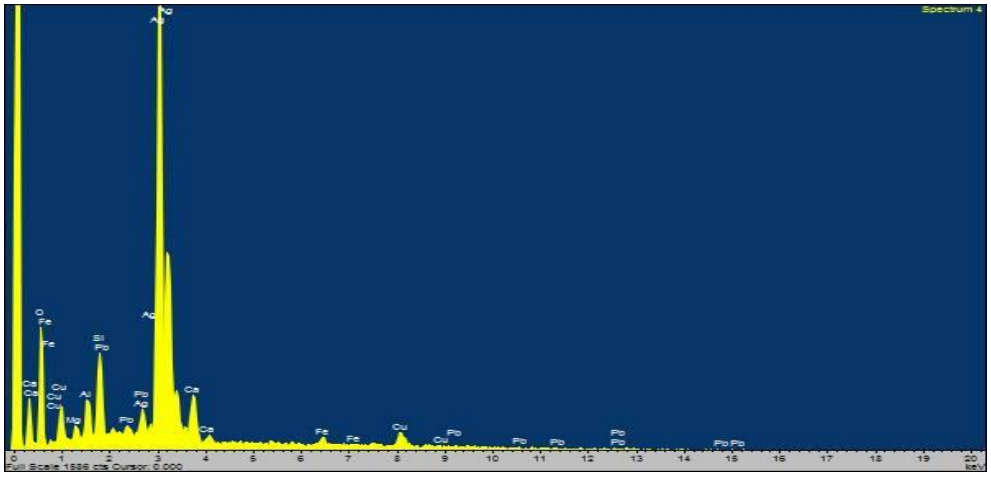

Spectra 44: Fourth measurement of the object BS_19.

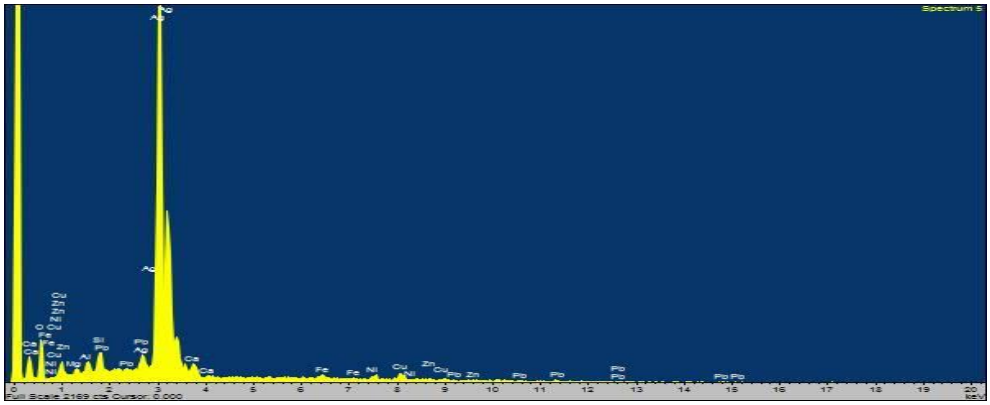

Spectra 45: Fifth measurement of the object BS_19.

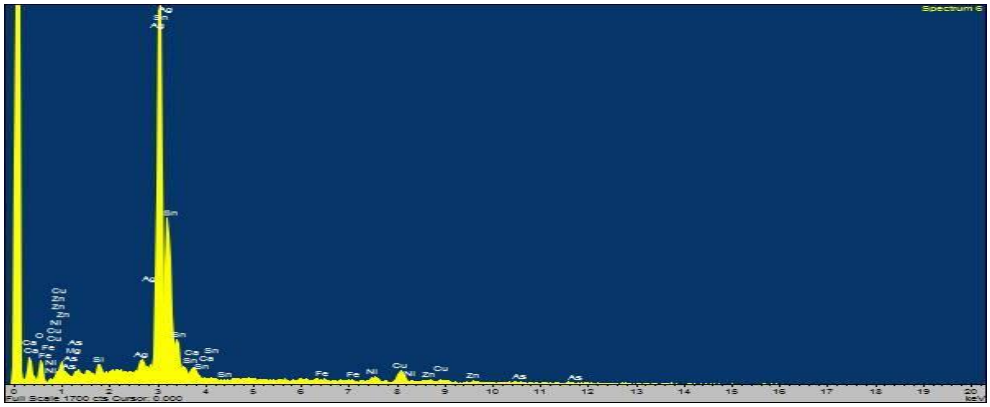

Spectra 46: Sixth measurement of the object BS_19.

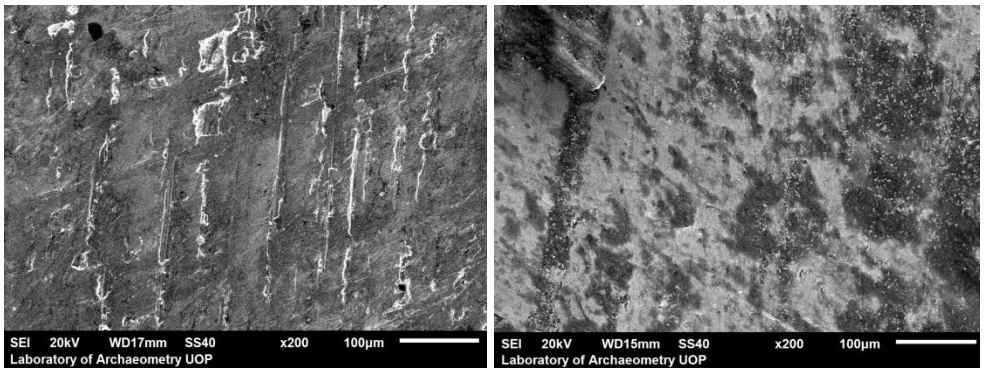

Images 13-14: Backscattered electron images in the SEM for the object BS_19. Magnification 200X. Compositional contrast that results from different atomic number elements and their distribution are displayed.

Left: the highest copper content area (measurement 2 - spectra 42). Right: the lowest silver content area, where the detected elements indicate soil and corrosion encrustations (measurement 4 - spectra 44).

Figurine Base assemblage

Table 9: The performed measurements of the object **KYT_AYV_FB_03** using SEM-EDS expressed in % wt. (m.: measurement, Av.: Average, St. Dev.: Standard Deviation, n.d.: non detected).

FB_03	m.1	m.2	m.3	m.4	m.5	m.6	Av.	St. Dev.
Al_2O_3	1,26	0,75	2,11	n.d.	n.d.	n.d.	1,37	0,69
SiO_2	4,93	17,12	28,51	15,56	n.d.	n.d.	16,53	9,65
P_2O_5	n.d.	1,69	2,34	1,70	n.d.	n.d.	1,91	0,37
Cl	14,22	1,85	1,52	2,32	3,53	5,43	4,81	4,82
CaO	n.d.	1,82	6,97	0,96	n.d.	n.d.	3,25	3,25
CuO	74,04	59,19	42,82	59,84	79,98	68,88	64,13	13,18
ZnO	n.d.	n.d.	n.d.	n.d.	n.d.	0,22	0,22	-
As_2O_3	n.d.	2,85	1,82	2,58	2,64	2,26	2,43	0,40
SnO_x	n.d.	n.d.	n.d.	0,67	0,72	0,34	0,58	0,21
Sb_2O_5	n.d.	n.d.	1,07	n.d.	0,43	n.d.	0,75	0,45
PbO	5,56	14,73	12,85	16,36	12,70	22,87	14,18	5,64

KYT_AYV_FB_03

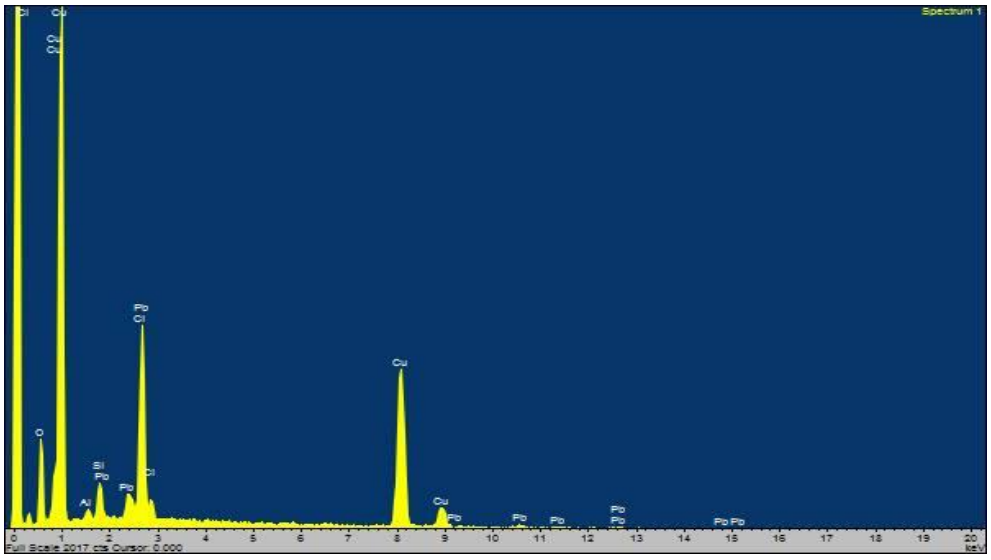

Spectra 47: First measurement of the object FB_03.

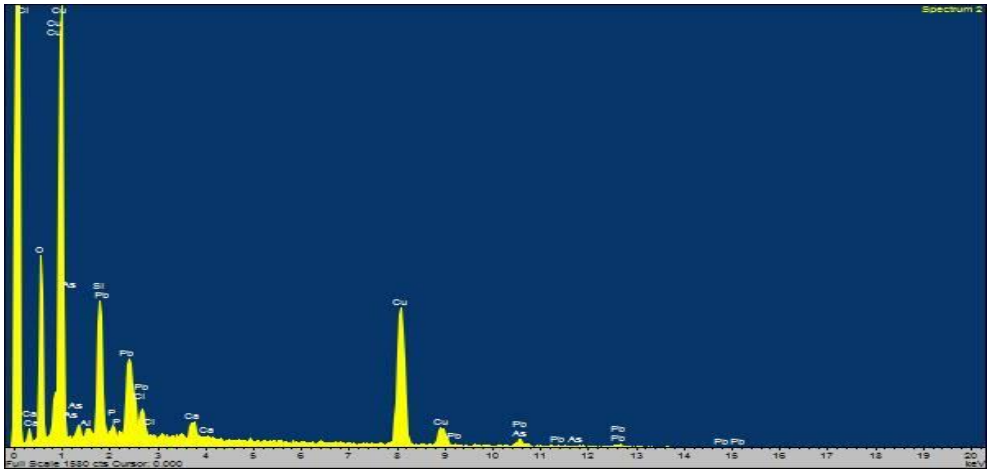

Spectra 48: Second measurement of the object FB_03.

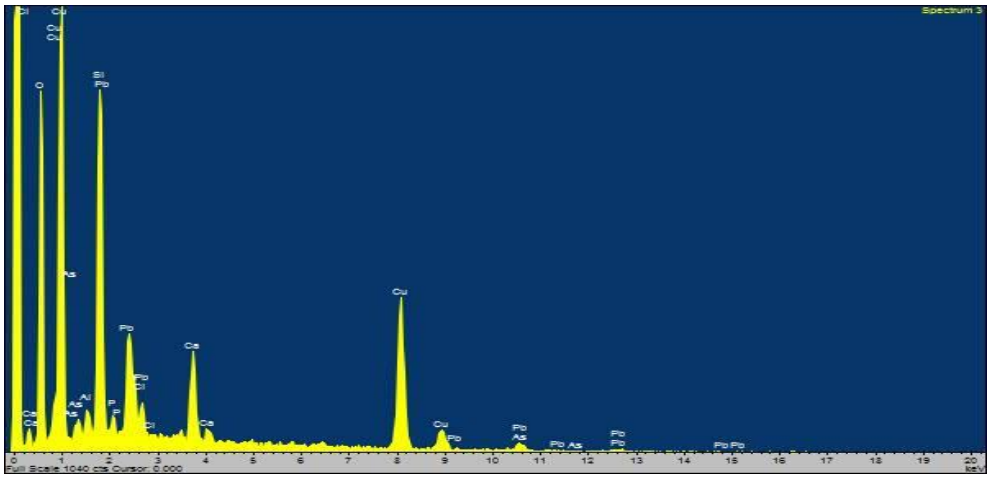

Spectra 49: Third measurement of the object FB_03.

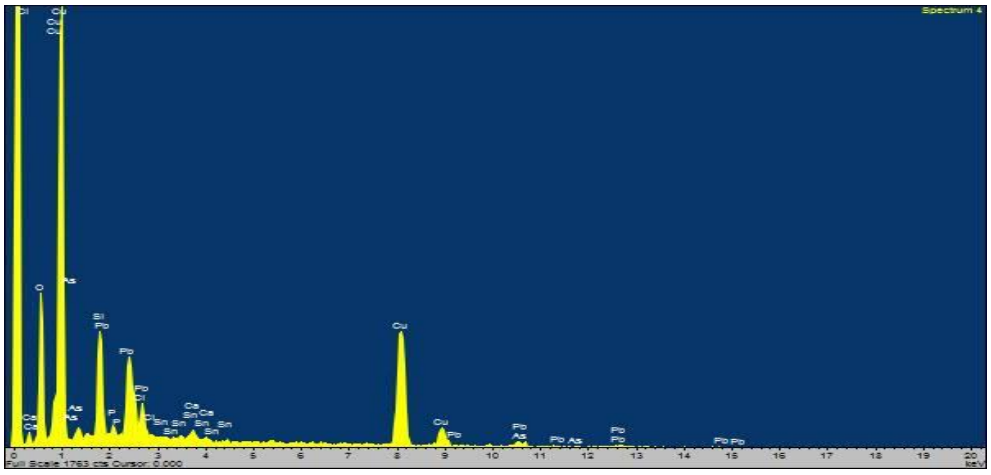

Spectra 50: Fourth measurement of the object FB_03.

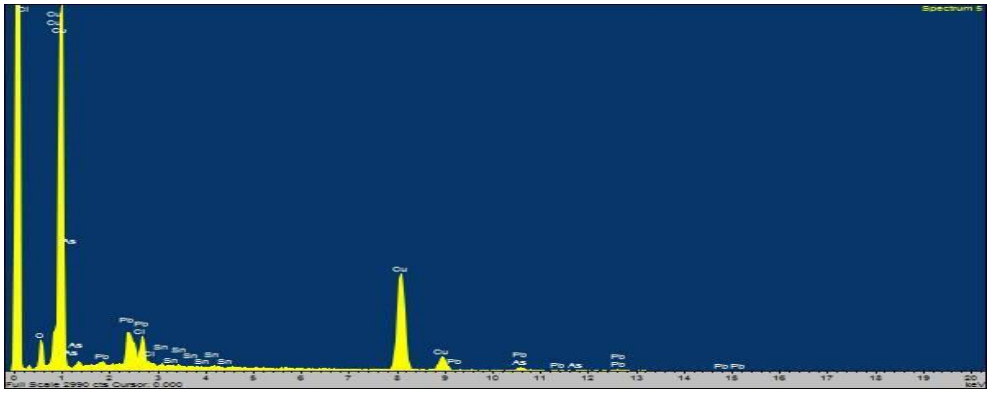

Spectra 51: Fifth measurement of the object FB_03.

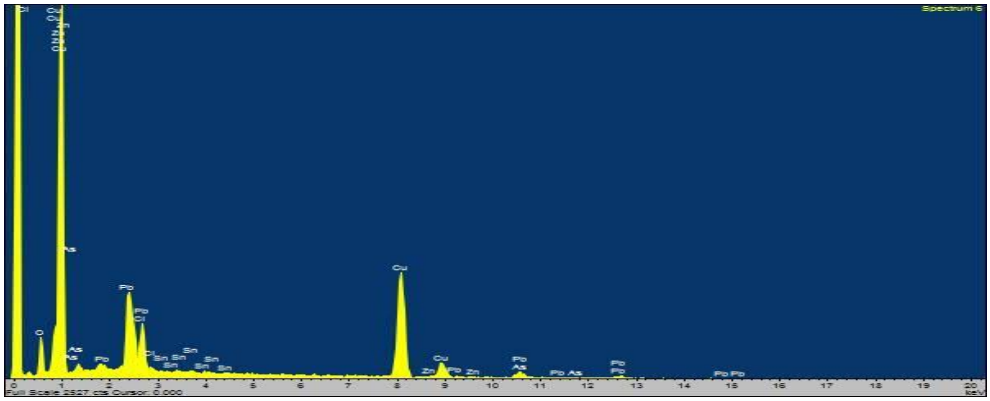

Spectra 52: Sixth measurement of the object FB_03.

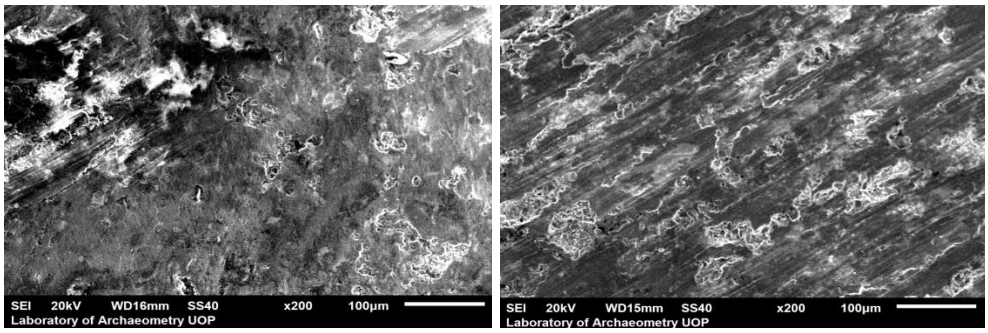

Images 15-16: Backscattered electron images in the SEM for the object FB_03. Magnification 200X. Compositional contrast that results from different atomic number elements and their distribution are displayed.

Left: partially cleaned area containing high amount of lead (measurement 4-spectra 50). Right: the highest copper content area, without residues of soil encrustations but containing amount of chlorine caused by corrosion (measurement 5 - spectra 51).

Bronze Waste assemblage

Table 10: The performed measurements of the object **KYT_AYV_BW_04** using SEM-EDS expressed in % wt. (m.: measurement, Av.: Average, St. Dev.: Standard Deviation, n.d.: non detected).

BW_04	m.1	m.2	m.3	m.4	m.5	m.6	Av.	St.Dev.
Al_2O_3	n.d.	n.d.	3,57	n.d.	n.d.	n.d.	3,57	-
SiO_2	5,65	2,81	39,93	2,44	3,14	10,82	10,80	14,61
Cl	0,65	1,32	n.d	1,26	1,25	6,24	2,14	2,31
CaO	n.d.	n.d.	2,06	n.d.	n.d.	n.d.	2,06	-
FeO	n.d.	0,44	0,54	0,55	0,03	0,94	0,50	0,32
Ni	n.d.	n.d.	0,46	n.d.	n.d.	0,45	0,46	0,01
CuO	92,90	94,23	52,74	94,45	93,71	80,49	84,75	16,57
ZnO	n.d.	n.d.	0,10	n.d.	0,40	n.d.	0,17	0,21
As_2O_3	0,12	0,70	0,40	0,33	0,88	0,57	0,50	0,27
Ag	0,16	n.d.	0,20	0,46	0,05	n.d.	0,22	0,17
SnO_x	0,30	0,41	n.d.	0,48	0,22	0,05	0,29	0,17
PbO	0,23	0,09	n.d.	0,03	0,32	0,46	0,23	0,17

KYT_AYV_BW_04

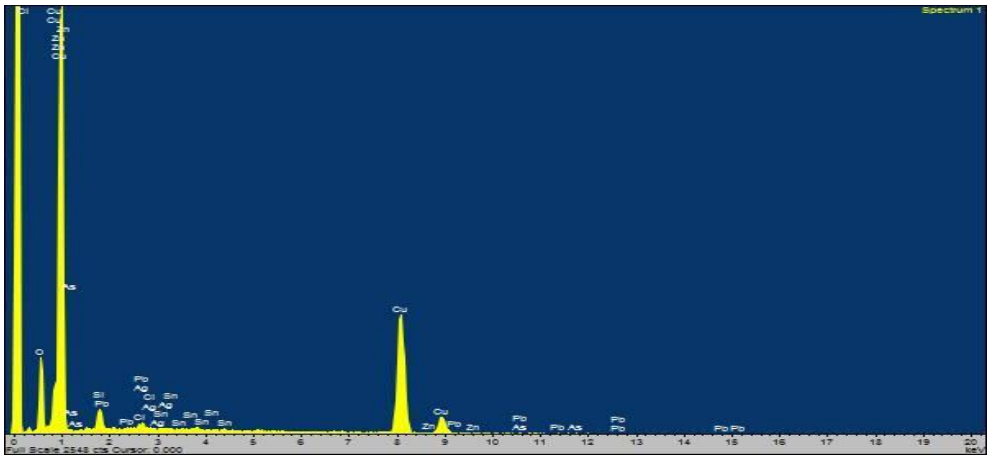

Spectra 53: First measurement of the object BW_04.

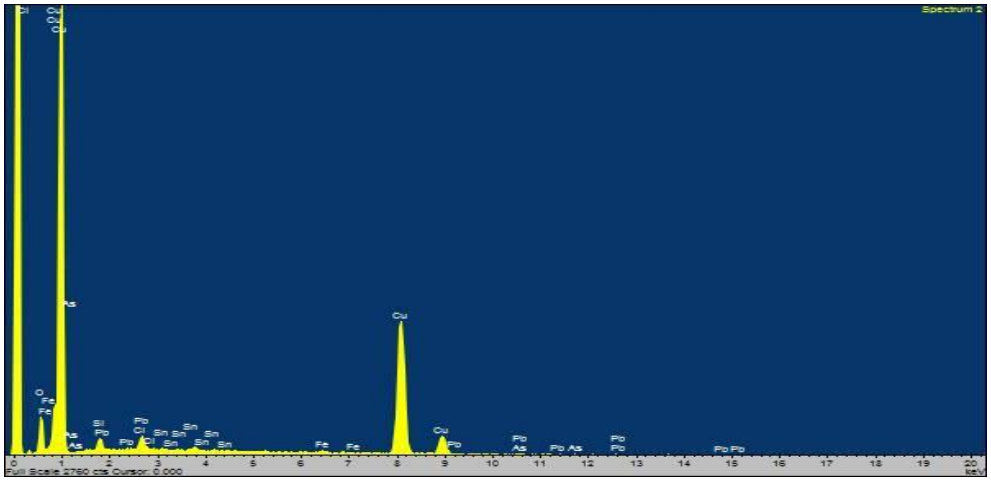

Spectra 54: Second measurement of the object BW_04.

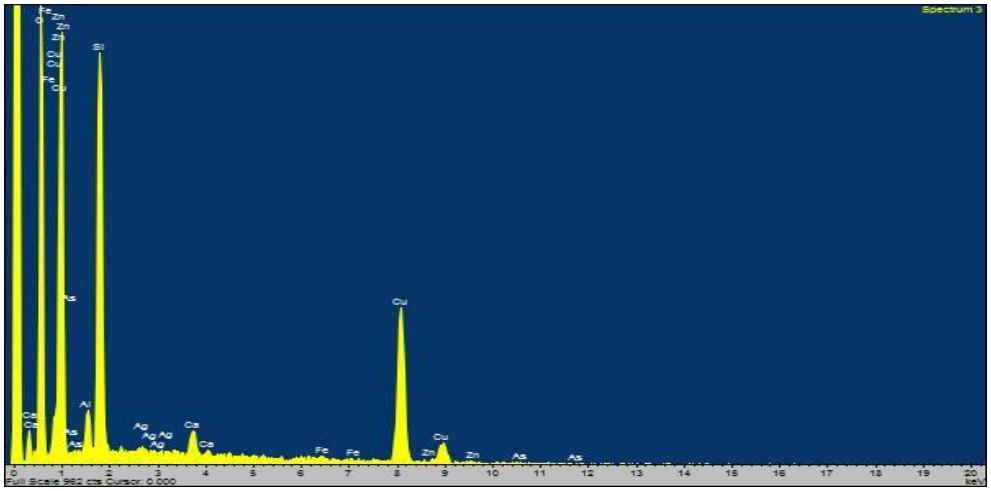

Spectra 55: Third measurement of the object BW_04.

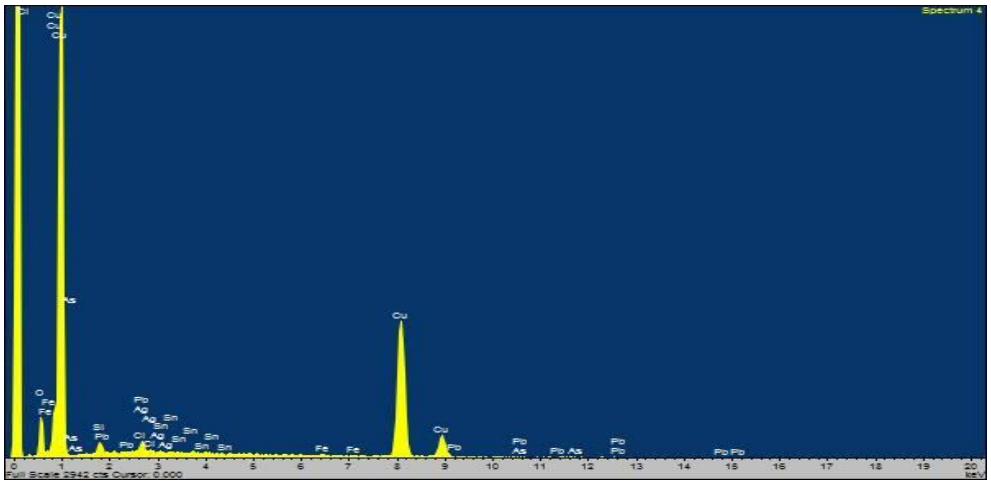

Spectra 56: Fourth measurement of the object BW_04.

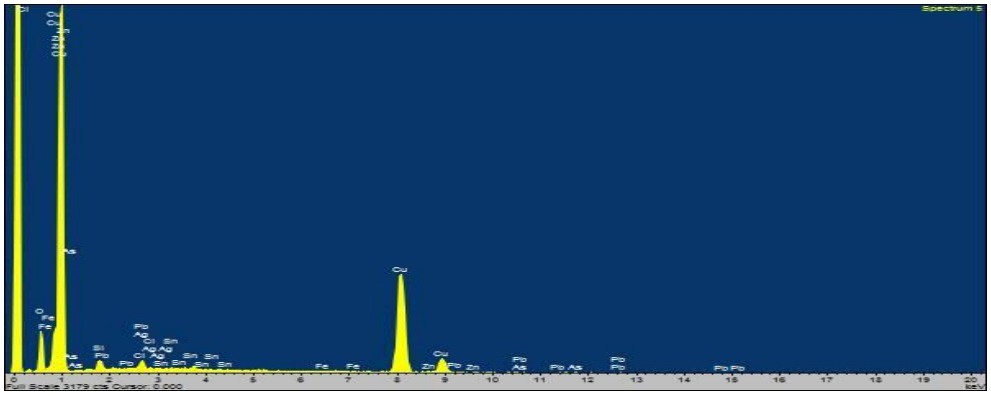

Spectra 57: Fifth measurement of the object BW_04.

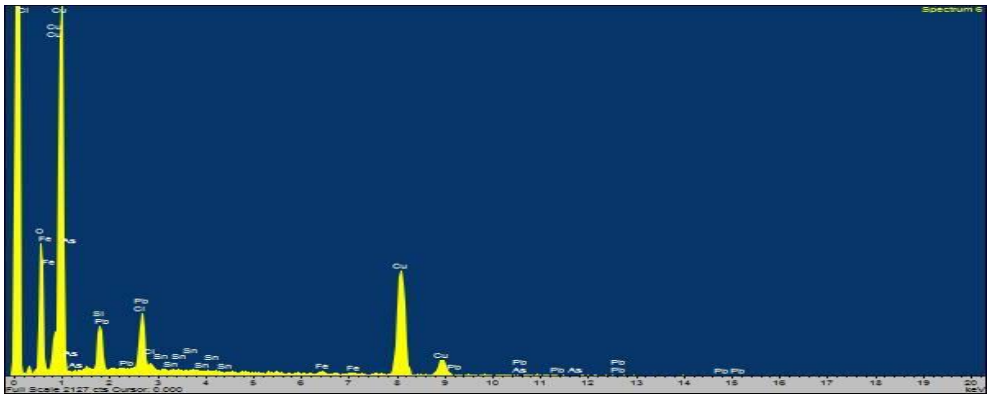

Spectra 58: Sixth measurement of the object BW_04.

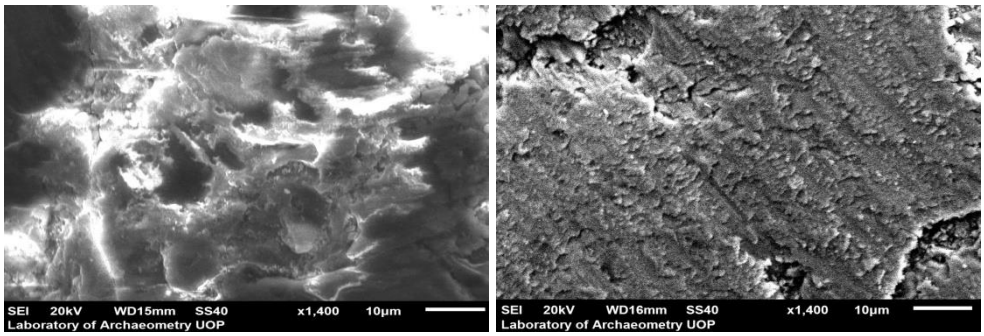

Images 17-18: Backscattered electron images in the SEM for the object BW_04. Magnification 1.400X. Compositional contrast that results from different atomic number elements and their distribution are displayed.

Left: the lowest copper content area, where significant amounts of elements by soil residues have been detected (measurement 3 - spectra 55). Right: the highest copper content area, where the lowest quantity of other elements has been detected (measurement 4 - spectra 56).

Table 11: The performed measurements of the object **KYT_AYV_BW_05** using SEM-EDS expressed in % wt. (m.: measurement, Av.: Average, St. Dev.: Standard Deviation, n.d.: non detected).

BW_05	m.1	m.2	m.3	m.4	m.5	Av.	St. Dev.
MgO	n.d.	n.d.	n.d.	2,43	2,47	2,45	0,03
Al_2O_3	n.d.	n.d.	n.d.	7,80	8,28	8,04	0,34
SiO_2	n.d.	2,52	2,06	33,43	35,30	18,33	18,54
S	n.d.	n.d.	n.d.	0,94	0,75	0,85	0,13
Cl	10,17	3,86	4,43	1,26	0,86	4,12	3,73
CaO	n.d.	1,02	n.d.	14,94	19,24	11,73	9,52
FeO	n.d.	n.d.	n.d.	4,09	3,69	3,89	0,28
CuO	83,30	86,62	87,83	33,00	29,40	64,03	30,04
ZnO	n.d.	n.d.	0,46	2,11	n.d.	1,29	1,17
As_2O_3	0,61	n.d.	n.d.	n.d.	n.d.	0,61	-
SnO_x	5,91	5,98	5,22	n.d.	n.d.	5,70	0,42

KYT_AYV_BW_05

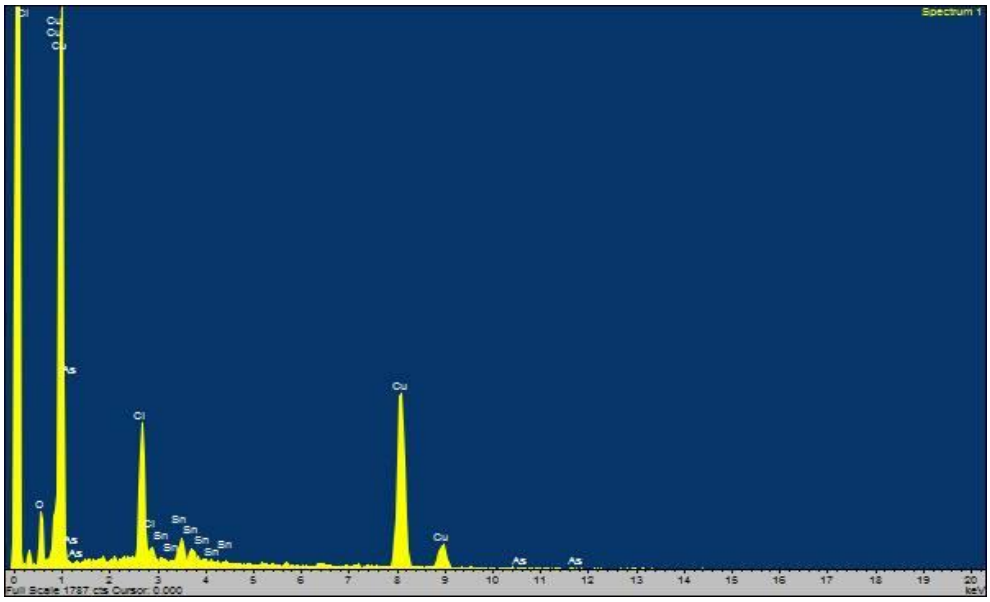

Spectra 59: First measurement of the object BW_05.

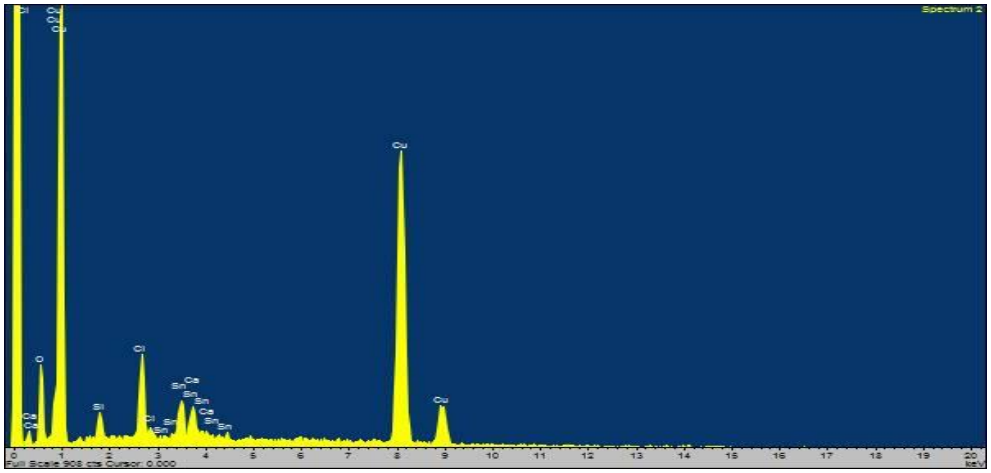

Spectra 60: Second measurement of the object BW_05.

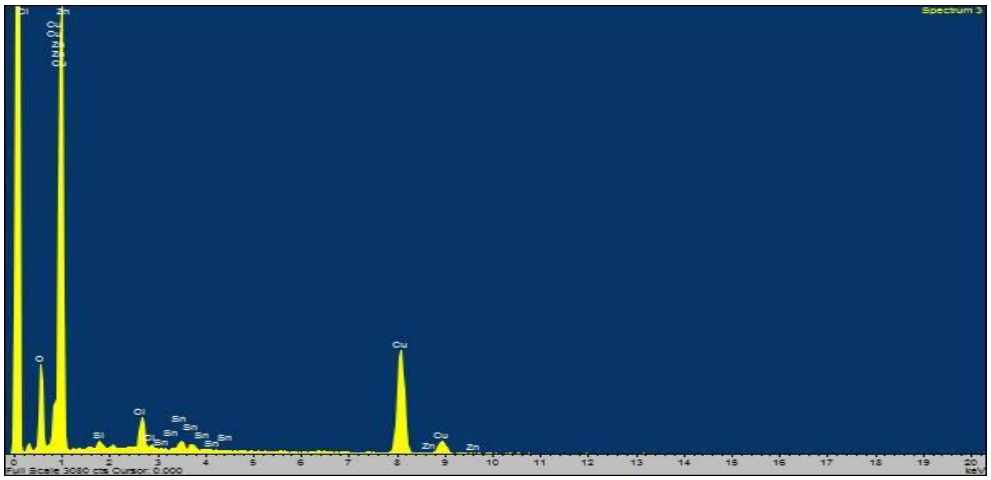

Spectra 61: Third measurement of the object BW_05.

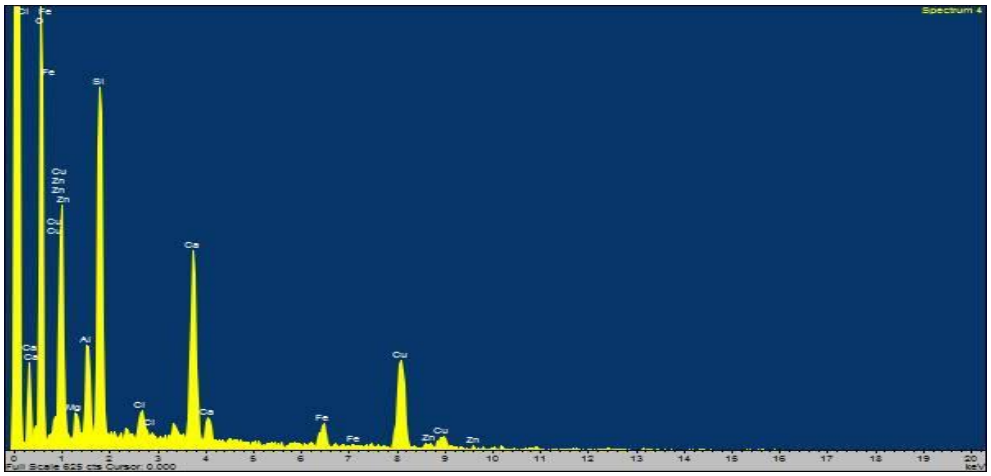

Spectra 62: Fourth measurement of the object BW_05.

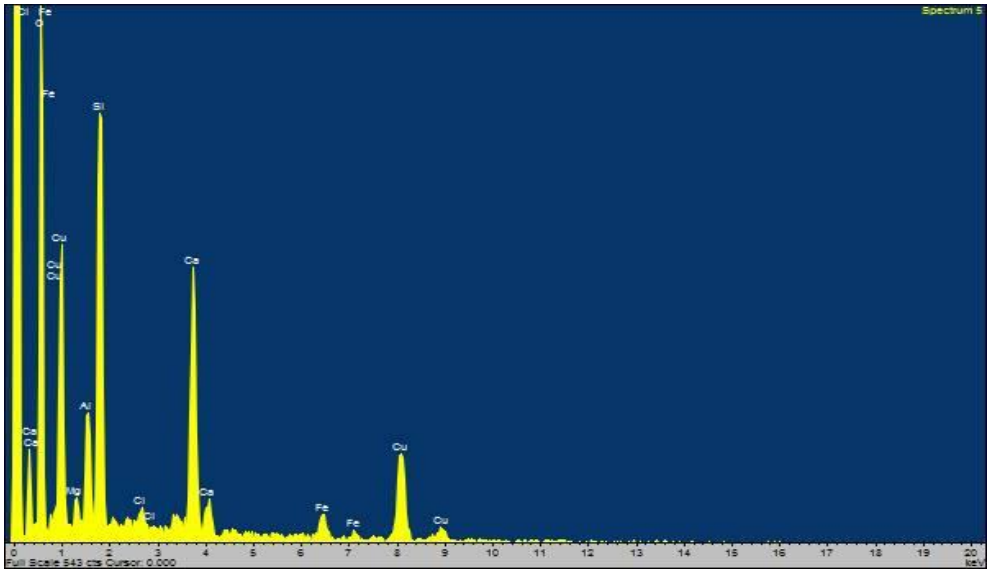

Spectra 63: Fifth measurement of the object BW_05.

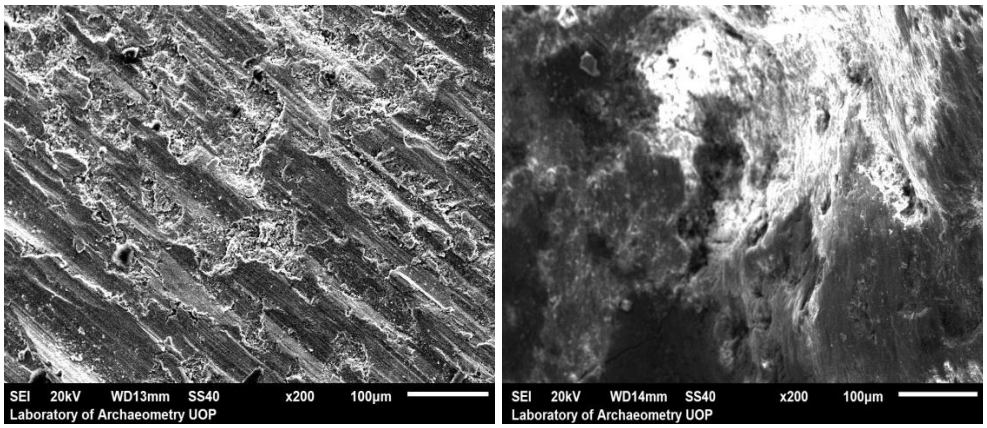

Images 19-20: Backscattered electron images in the SEM for the object BW_05. Magnification 200X. Compositional contrast that results from different atomic number elements and their distribution are displayed.

Left: area where significant amounts only of copper and tin (except from chlorine caused by corrosion) have been detected (measurement 1 - spectra 59). Right: partially cleaned area with encrustations of soil residues and corrosion (measurement 5 - spectra 63).

Table 12: The performed measurements of the object **KYT_AYV_BW_14** using SEM-EDS expressed in % wt. (m.: measurement, Av.: Average, St. Dev.: Standard Deviation, n.d.: non detected).

BW_14	m.1	m.2	m.3	m.4	m.5	m.6	m.7	Av.	St.Dev
Al_2O_3	n.d.	n.d.	n.d.	n.d.	6,17	3,81	n.d.	4,99	1,67
SiO_2	5,78	4,16	2,43	21,63	20,30	13,62	n.d.	11,32	8,40
CaO	2,49	26,14	n.d.	10,48	10,50	12,95	n.d.	12,51	8,58
FeO	10,17	19,81	6,78	41,24	49,43	60,13	14,16	28,82	21,17
Ni	n.d.	n.d.	n.d.	n.d.	0,85	1,88	0,18	0,97	0,86
CuO	79,63	46,97	88,13	23,18	6,43	2,20	83,33	47,12	37,19
ZnO	0,21	n.d.	0,67	n.d.	0,68	1,09	n.d.	0,53	0,43
As_2O_3	0,63	n.d.	1,56	2,13	2,21	1,56	1,50	1,60	0,57
SnO_x	1,08	0,90	n.d.	n.d.	n.d.	0,66	0,60	0,81	0,22
Sb_2O_5	n.d.	1,54	n.d.	1,24	2,80	1,86	n.d.	1,86	0,68
PbO	n.d.	0,48	0,43	0,11	0,62	0,24	0,23	0,35	0,19

KYT_AYV_BW_14

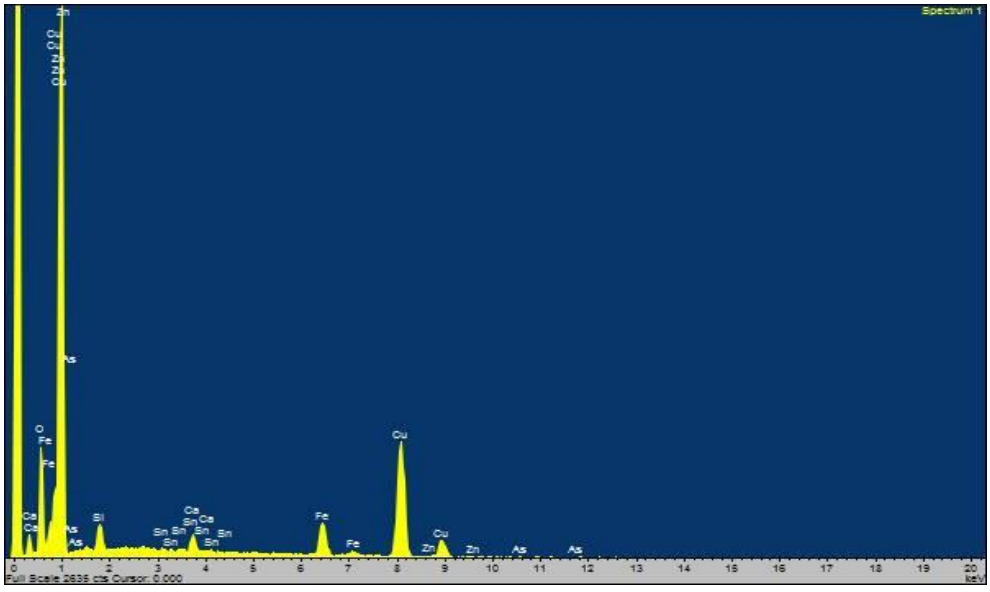

Spectra 64: First measurement of the object BW_14.

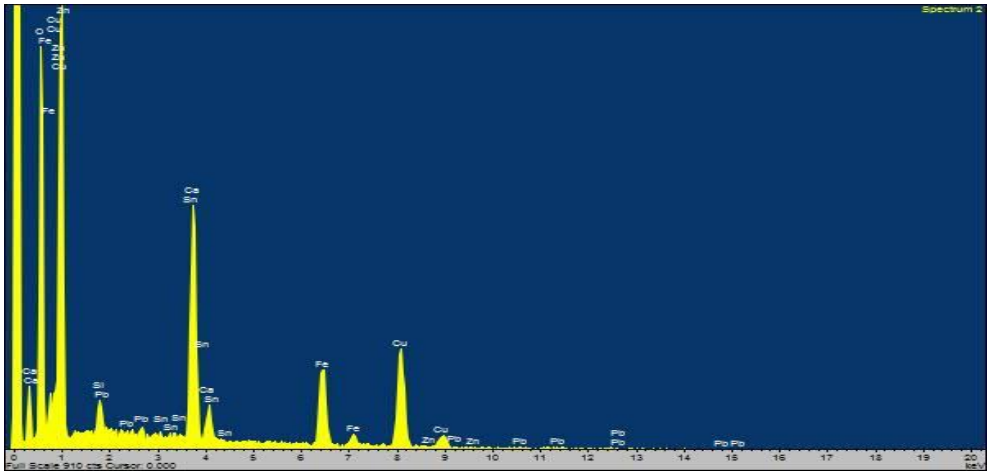

Spectra 65: Second measurement of the object BW_14.

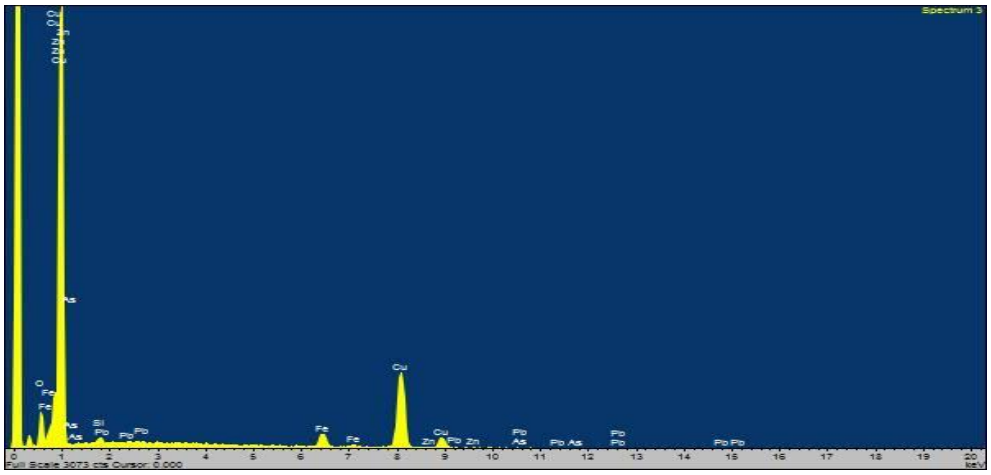

Spectra 66: Third measurement of the object BW_14.

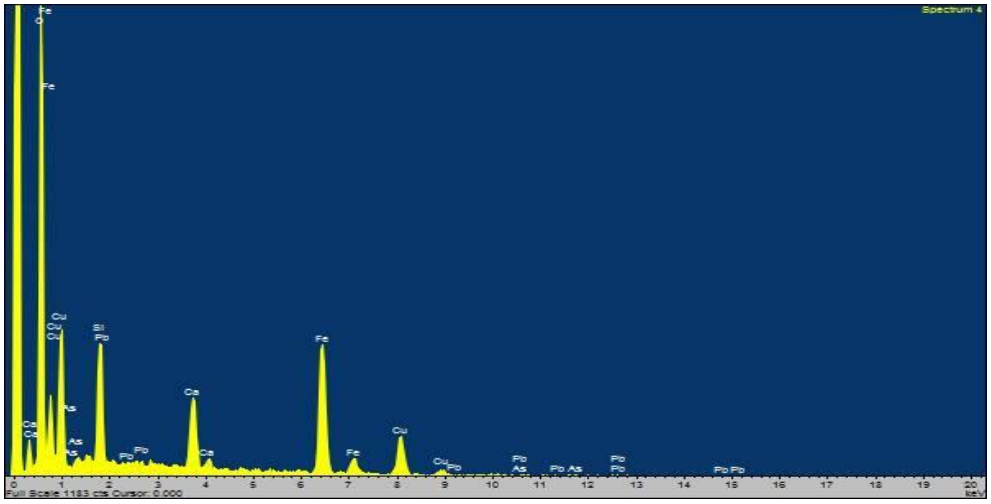

Spectra 67: Fourth measurement of the object BW_14.

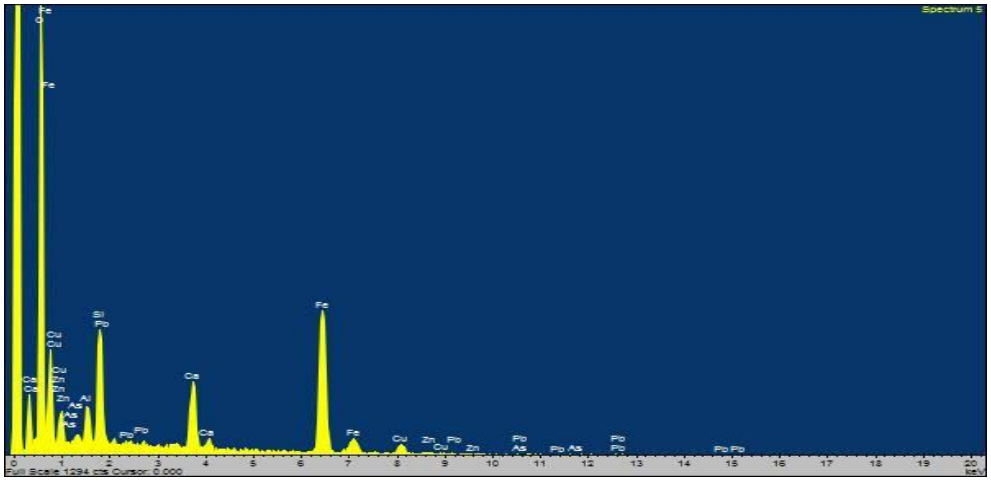

Spectra 68: Fifth measurement of the object BW_14.

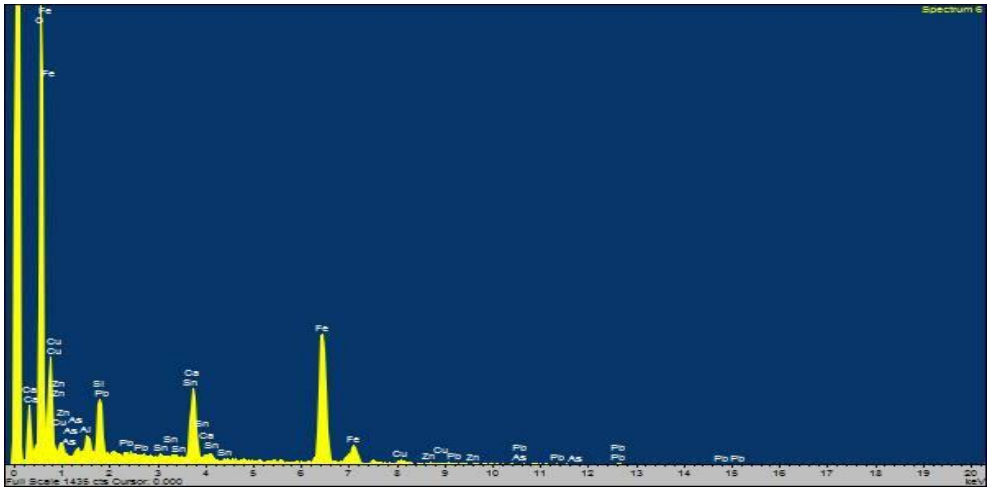

Spectra 69: Sixth measurement of the object BW_14.

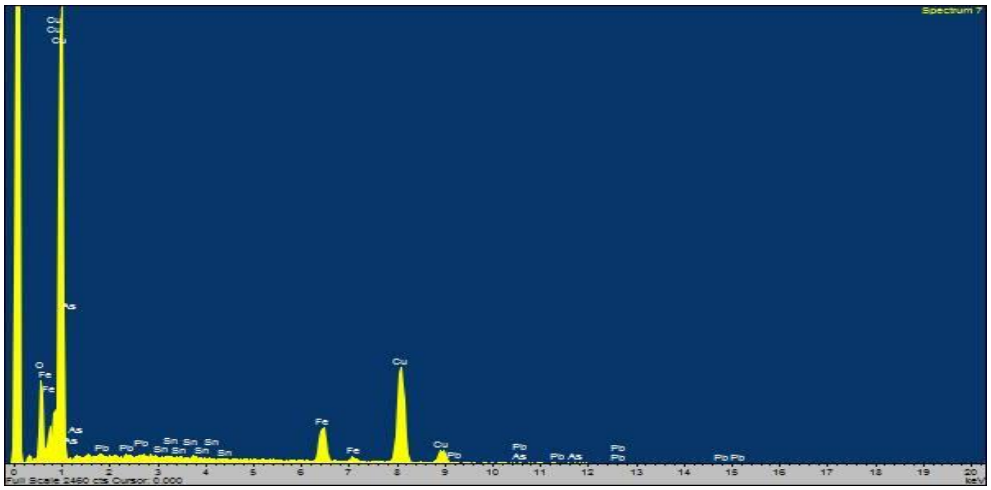

Spectra 70: Seventh measurement of the object BW_14.

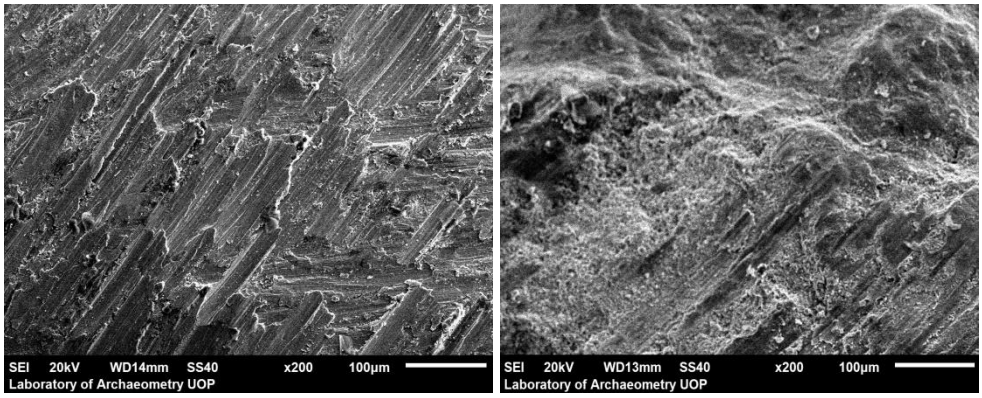

Images 21-22: Backscattered electron images in the SEM for the object BW_14. Magnification 200X. Compositional contrast that results from different atomic number elements and their distribution are displayed.
Left: the highest copper content area (measurement 3 - spectra 66). Right: area where iron is the dominant element with the highest content, while the copper content is extremely low (measurement 6 - spectra 69).

Table 13: The performed measurements of the object **KYT_AYV_BW_15** using SEM-EDS expressed in % wt. (m.: measurement, Av.: Average, St. Dev.: Standard Deviation, n.d.: non detected).

BW_15	m.1	m.2	m.3	m.4	m.5	m.6	Av.	St. Dev.
Al_2O_3	7,65	n.d.	2,15	n.d.	n.d.	n.d.	4,90	3,89
SiO_2	31,52	n.d.	13,41	6,18	12,78	10,71	14,92	9,70
P_2O_5	2,66	n.d.	n.d.	n.d.	n.d.	2,51	2,59	0,11
Cl	n.d.	n.d.	n.d.	0,65	n.d.	n.d.	0,65	-
K_2O	1,62	n.d.	n.d.	n.d.	n.d.	n.d.	1,62	-
CaO	9,21	n.d.	1,43	0,87	4,20	2,17	3,58	3,39
FeO	2,78	n.d.	0,30	n.d.	2,26	1,00	1,59	1,14
CuO	33,83	95,52	79,32	86,84	74,09	71,35	73,49	21,33
ZnO	n.d.	n.d.	n.d.	n.d.	1,89	0,49	1,19	0,99
As_2O_3	0,86	0,24	n.d.	0,09	0,73	0,24	0,36	0,35
SnO_x	2,45	n.d.	0,26	1,87	n.d.	1,52	1,53	0,93
PbO	7,43	4,24	3,14	3,51	4,05	10,02	5,40	2,73

KYT_AYV_BW_15

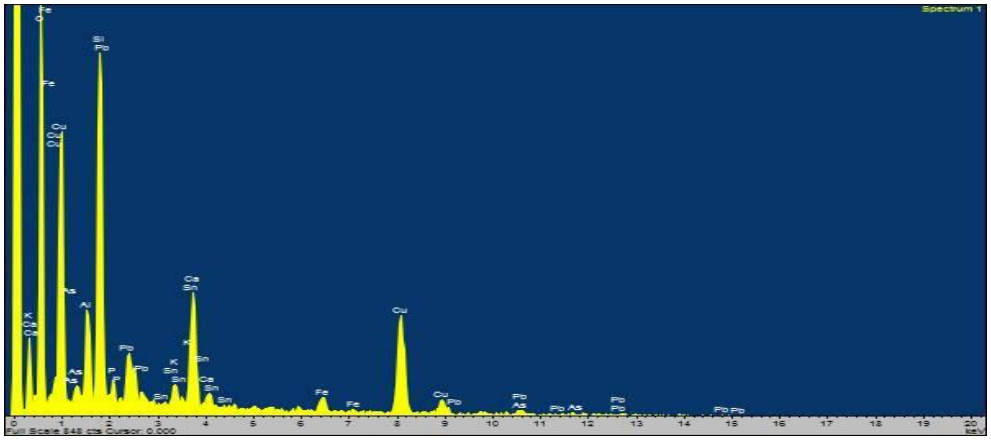

Spectra 71: First measurement of the object BW_15.

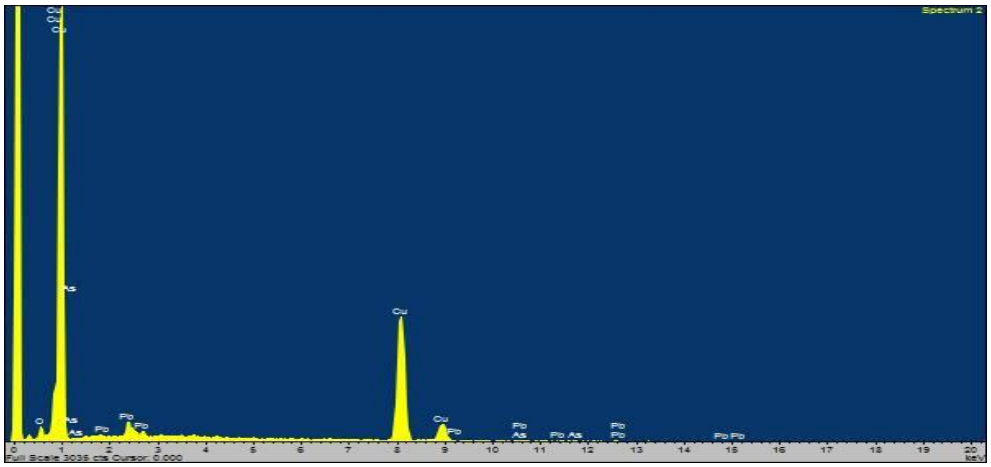

Spectra 72: Second measurement of the object BW_15.

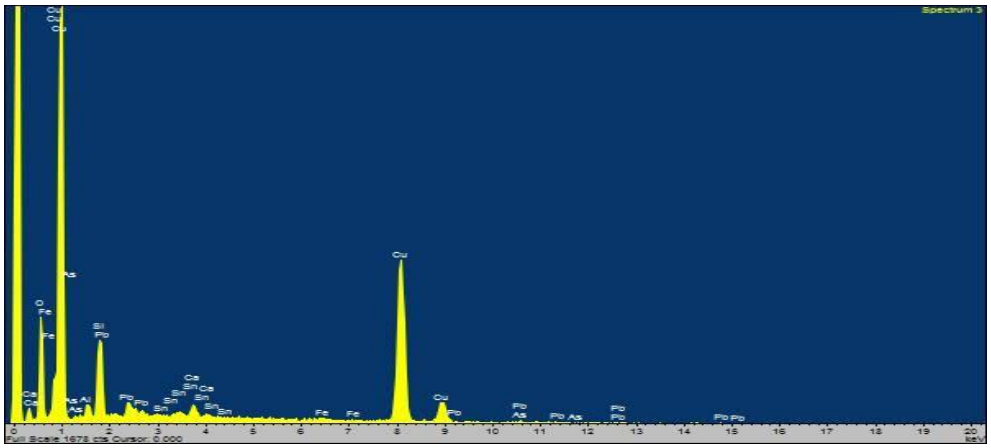

Spectra 73: Third measurement of the object BW_15.

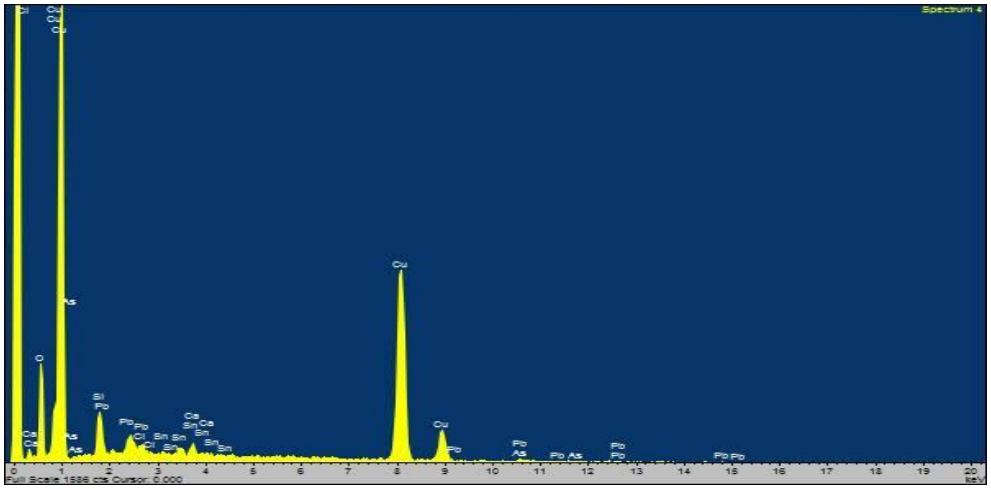

Spectra 74: Fourth measurement of the object BW_15.

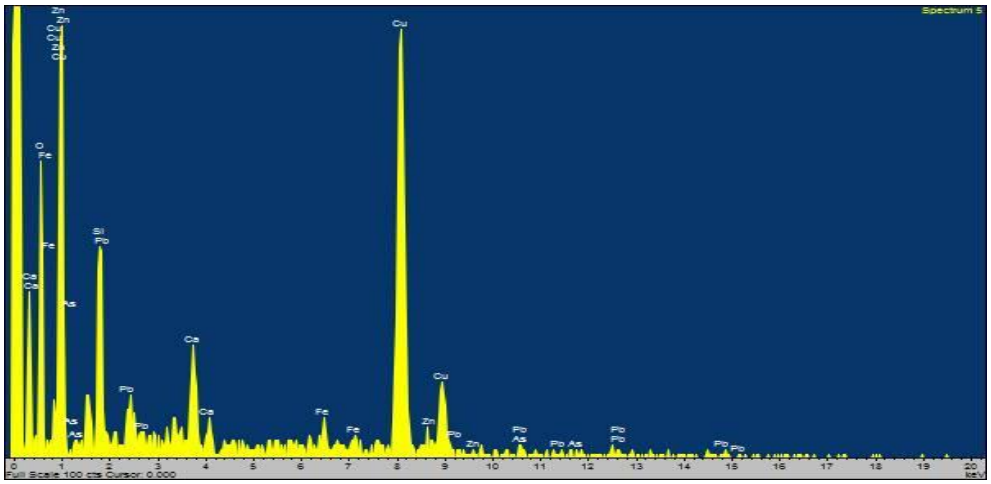

Spectra 75: Fifth measurement of the object BW_15.

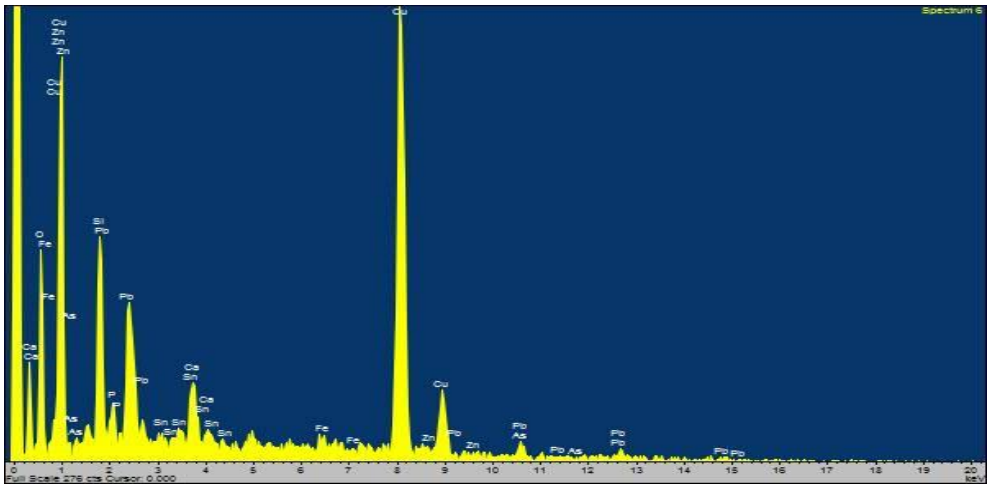

Spectra 76: Sixth measurement of the object BW_15.

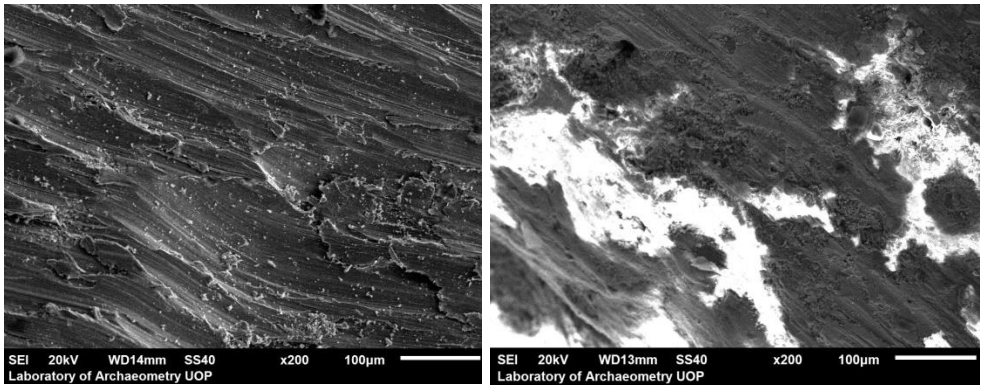

Images 23-24: Backscattered electron images in the SEM for the object BW_15. Magnification 200X. Compositional contrast that results from different atomic number elements and their distribution are displayed.
Left: area where only copper and lead (except from an extremely low arsenic content) have been detected (measurement 2 - spectra 72). Right: the highest lead content area (measurement 6 - spectra 76).

Table 14: The performed measurements of the object **KYT_AYV_BW_16** using SEM-EDS expressed in % wt. (m.: measurement, Av.: Average, St. Dev.: Standard Deviation, n.d.: non detected).

BW_16	m.1	m.2	m.3	m.4	m.5	m.6	m.7	Av.	St.Dev
Al_2O_3	n.d.	n.d.	n.d.	n.d.	n.d.	1,81	1,77	1,79	0,03
SiO_2	n.d.	7,35	n.d.	n.d.	19,13	5,40	6,62	9,63	6,39
Cl	n.d	n.d	0,79	n.d.	n.d.	0,78	1,56	1,04	0,45
CaO	n.d.	n.d.	n.d.	n.d.	1,79	1,55	2,04	1,79	0,25
FeO	n.d.	0,24	0,20	0,22	0,40	0,47	0,48	0,34	0,13
CuO	98,51	89,93	97,51	97,87	75,56	80,00	83,45	88,98	9,44
ZnO	0,23	n.d.	0,71	n.d.	0,99	7,58	2,76	2,45	3,02
As_2O_3	0,71	1,61	0,49	1,05	1,00	1,11	0,63	0,94	0,38
Ag	0,14	0,01	n.d.	n.d.	0,07	0,33	n.d.	0,14	0,14
SnO_x	n.d.	n.d.	0,25	n.d.	n.d.	n.d.	n.d.	0,25	-
Sb_2O_5	0,41	n.d.	n.d.	0,49	0,94	0,28	0,53	0,53	0,25
PbO	n.d.	0,85	0,05	0,37	0,12	0,68	0,15	0,37	0,33

KYT_AYV_BW_16

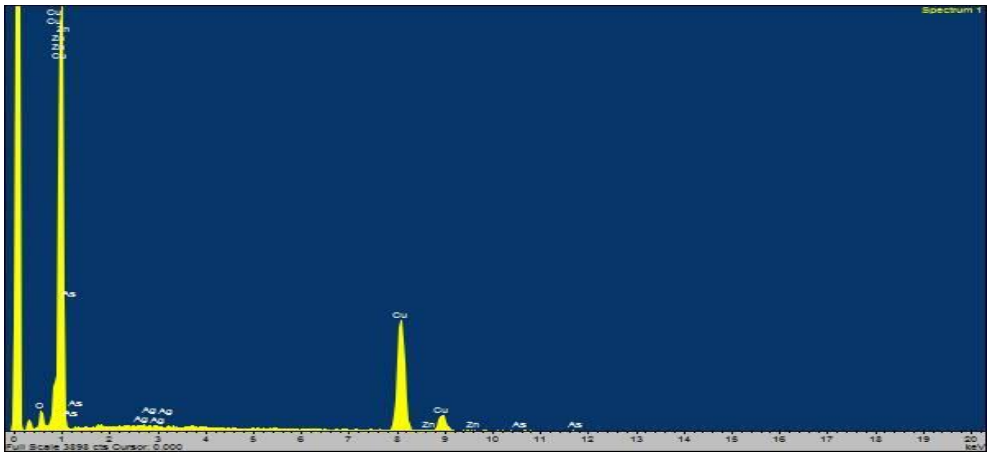

Spectra 77: First measurement of the object BW_16.

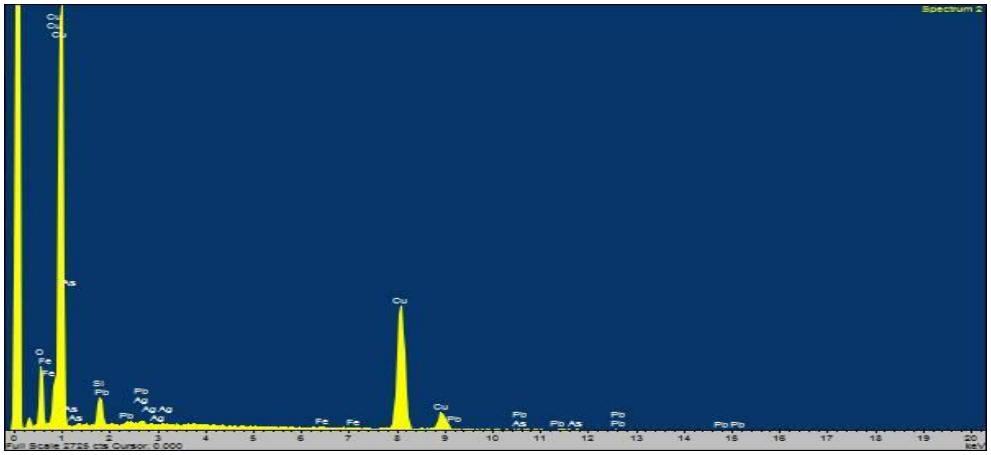

Spectra 78: Second measurement of the object BW_16.

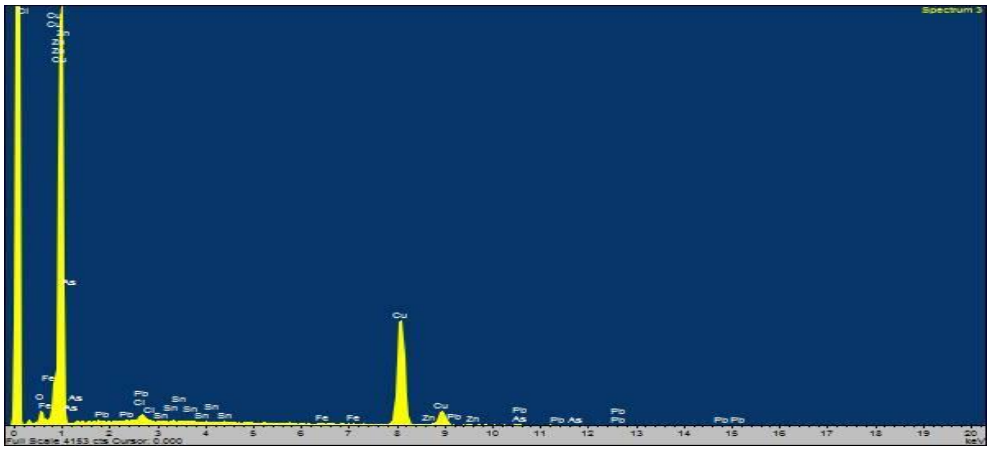

Spectra 79: Third measurement of the object BW_16.

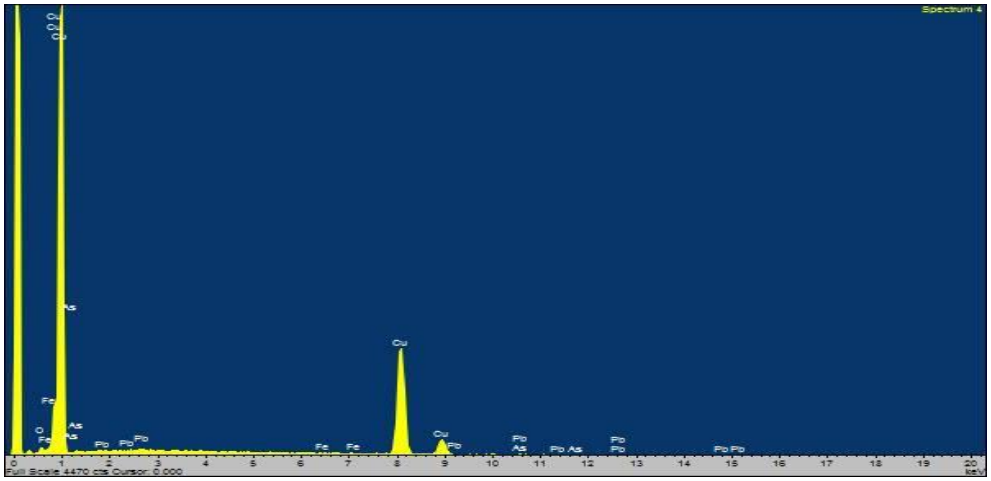

Spectra 80: Fourth measurement of the object BW_16.

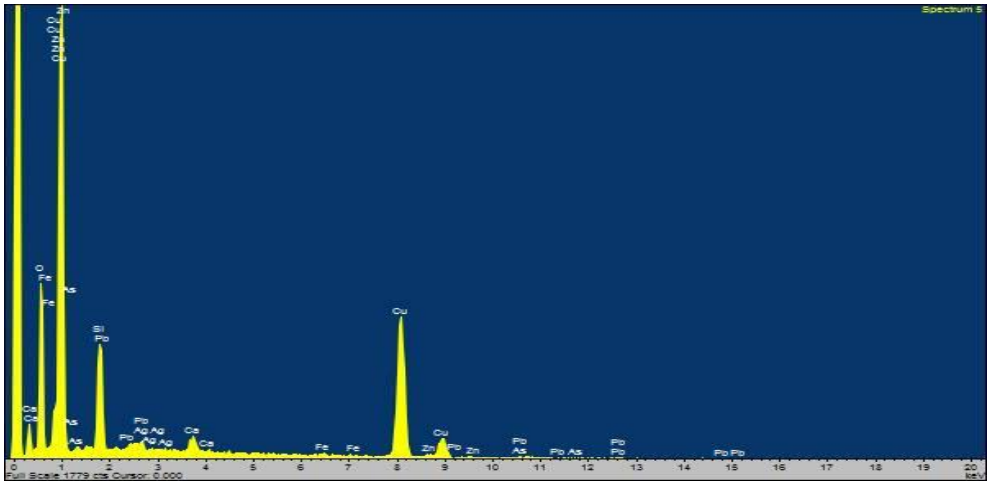

Spectra 81: Fifth measurement of the object BW_16.

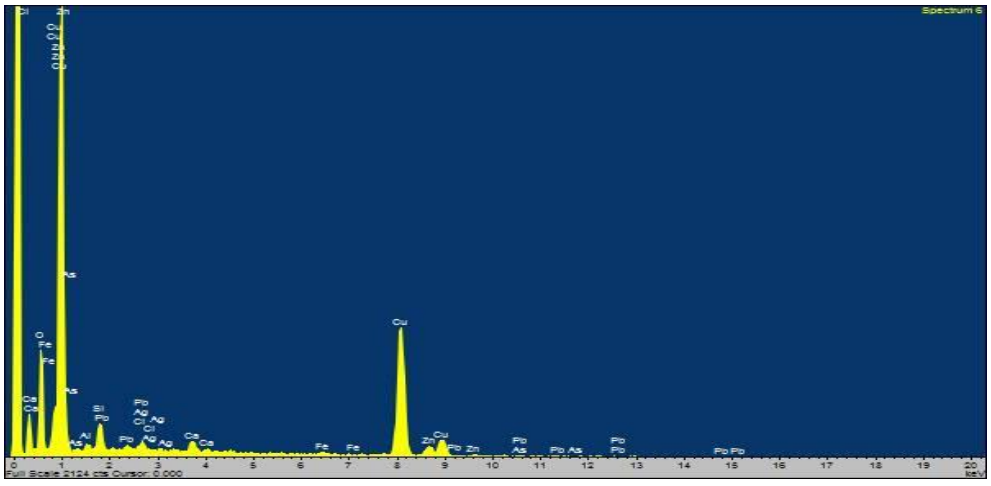

Spectra 82: Sixth measurement of the object BW_16.

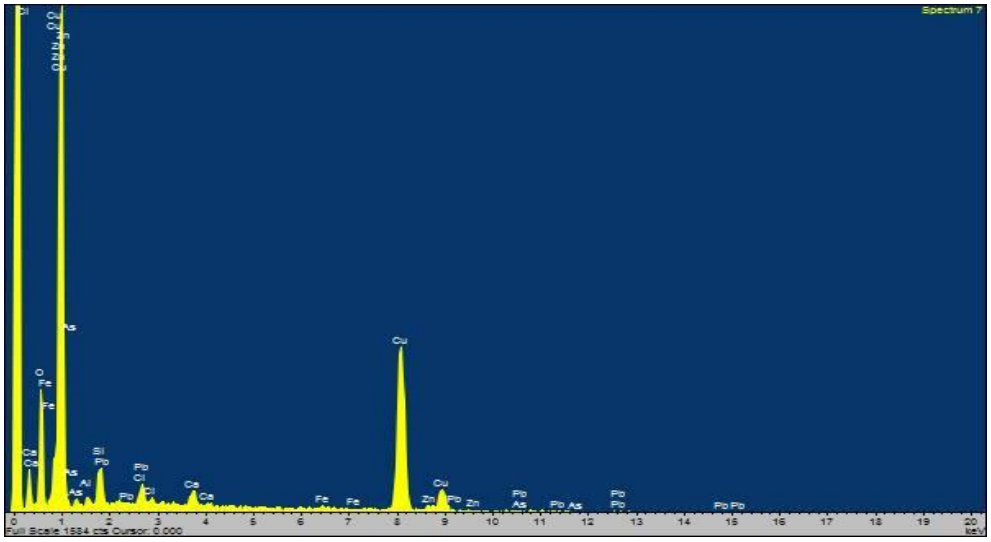

Spectra 83: Seventh measurement of the object BW_16.

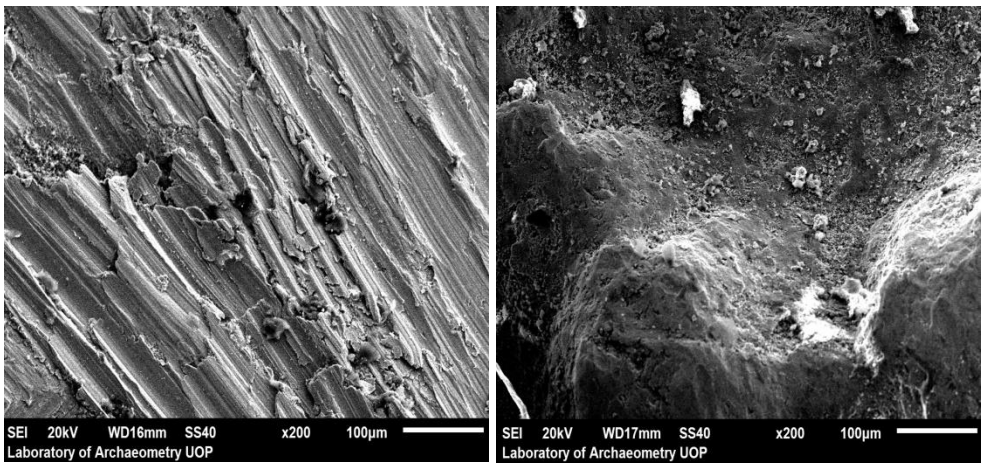

Images 25-26: Backscattered electron images in the SEM for the object BW_16. Magnification 200X. Compositional contrast that results from different atomic number elements and their distribution are displayed.

Left: the highest copper content cleaned area (measurement 1 - spectra 77).

Right: partially cleaned area where the lowest copper content and significant amounts of elements by soil residues have been detected (measurement 6 - spectra 82).

Table 15: The performed measurements of the object **KYT_AYV_BW_17** using SEM-EDS expressed in % wt. (m.: measurement, Av.: Average, St. Dev.: Standard Deviation, n.d.: non detected).

BW_17	m.1	m.2	m.3	m.4	m.5	Av.	St. Dev.
SiO_2	2,22	3,38	n.d.	n.d.	n.d.	2,80	0,82
Cl	7,40	9,99	6,03	3,16	3,79	6,07	2,78
FeO	0,94	0,29	12,46	10,35	8,99	6,61	5,61
CuO	85,94	82,90	78,95	84,01	86,92	83,74	3,11
ZnO	0,85	n.d.	0,43	n.d.	0,23	0,38	0,36
As_2O_3	1,29	0,61	1,19	1,04	0,07	0,84	0,50
Ag	0,45	0,53	0,20	n.d.	n.d.	0,30	0,24
SnO_x	0,51	1,04	n.d.	n.d.	n.d.	0,78	0,37
PbO	0,41	1,25	0,74	1,43	n.d.	0,96	0,47

KYT_AYV_BW_17

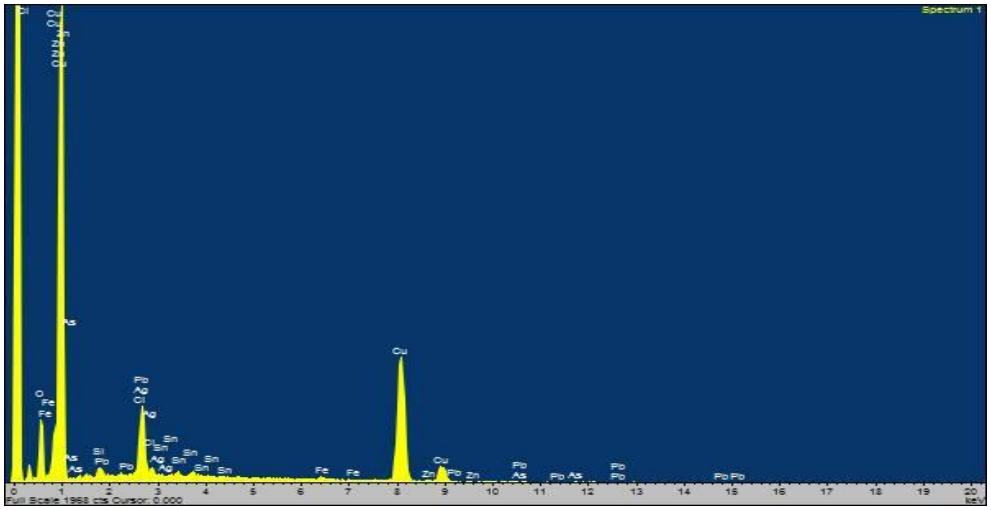

Spectra 84: First measurement of the object BW_17.

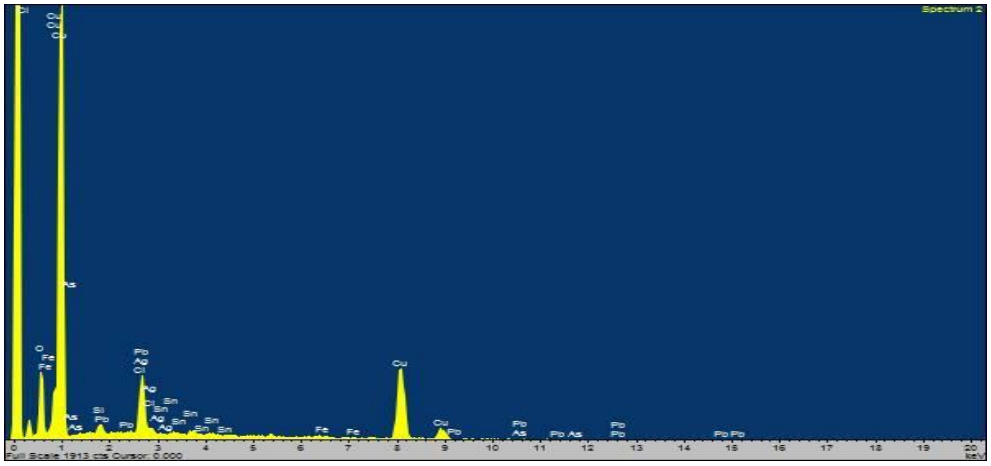

Spectra 85: Second measurement of the object BW_17.

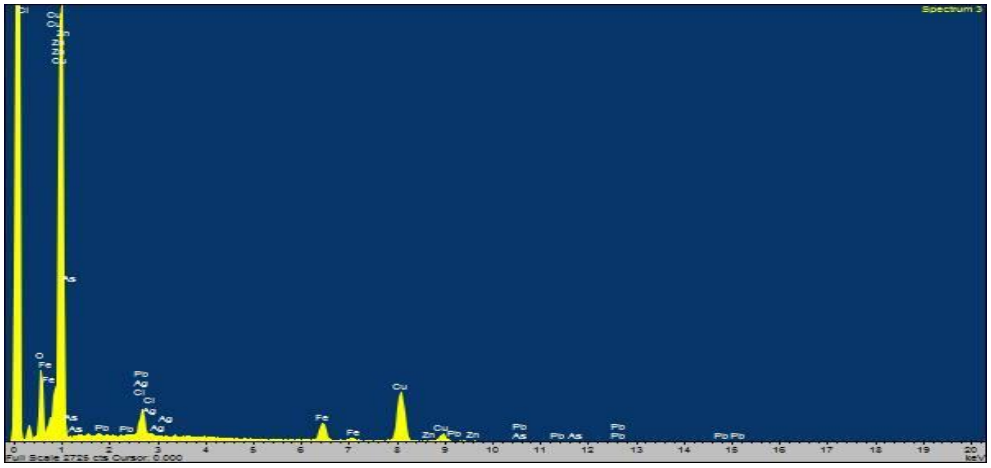

Spectra 86: Third measurement of the object BW_17.

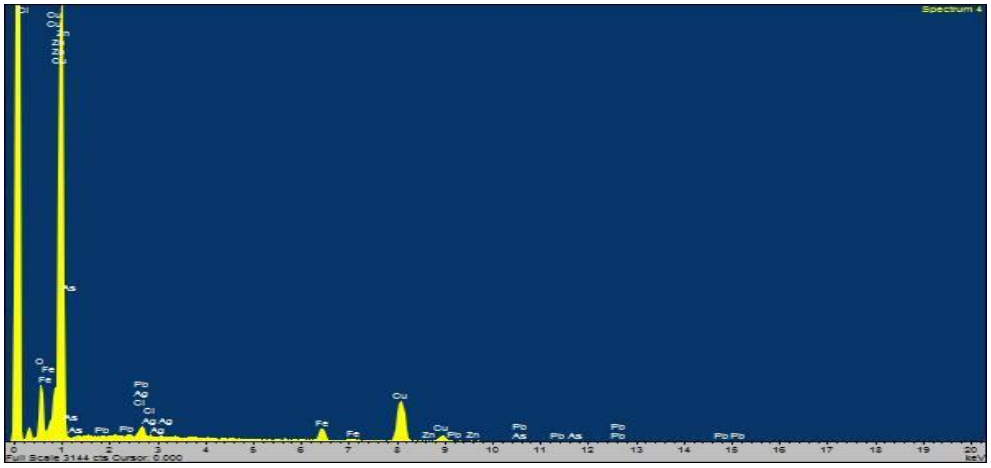

Spectra 87: Fourth measurement of the object BW_17.

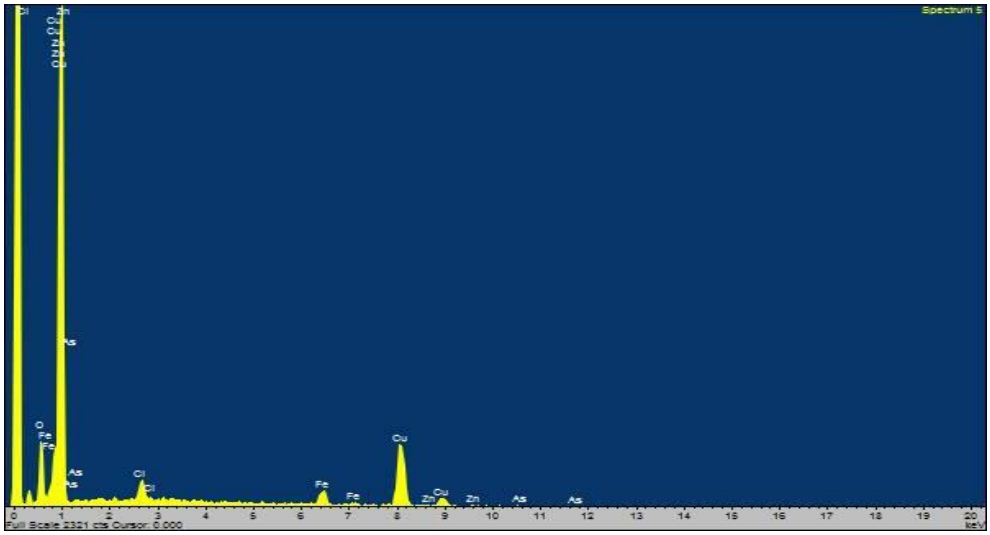

Spectra 88: Fifth measurement of the object BW_17.

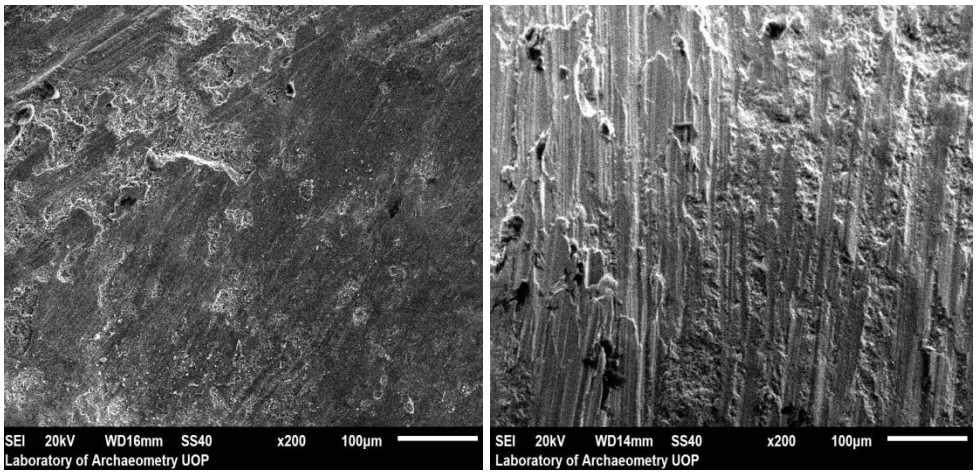

Images 27-28: Backscattered electron images in the SEM for the object BW_17. Magnification 200X. Compositional contrast that results from different atomic number elements and their distribution are displayed.

Left: partially cleaned area containing a high copper content and the lowest iron content. Elements that indicate residues of soil encrustations and corrosion have been detected (measurement 2 - spectra 85). Right: area containing a high copper content and the highest iron content (measurement 3 - spectra 83).

Table 16: The performed measurements of the object **KYT_AYV_BW_18** using SEM-EDS expressed in % wt. (m.: measurement, Av.: Average, St. Dev.: Standard Deviation, n.d.: non detected).

BW_18	m.1	m.2	m.3	m.4	Av.	St. Dev.
Cl	10,65	1,18	1,42	1,93	3,80	4,58
FeO	0,22	n.d.	0,57	0,40	0,40	0,18
CuO	87,59	95,51	95,36	95,83	93,57	3,99
ZnO	n.d.	1,08	0,05	0,26	0,46	0,54
As_2O_3	0,72	0,26	n.d.	0,74	0,57	0,27
Ag	0,20	0,14	1,20	0,83	0,59	0,51
SnO_x	n.d.	0,60	n.d.	n.d.	0,60	-
PbO	0,62	1,23	1,39	n.d.	1,08	0,41

KYT_AYV_BW_18

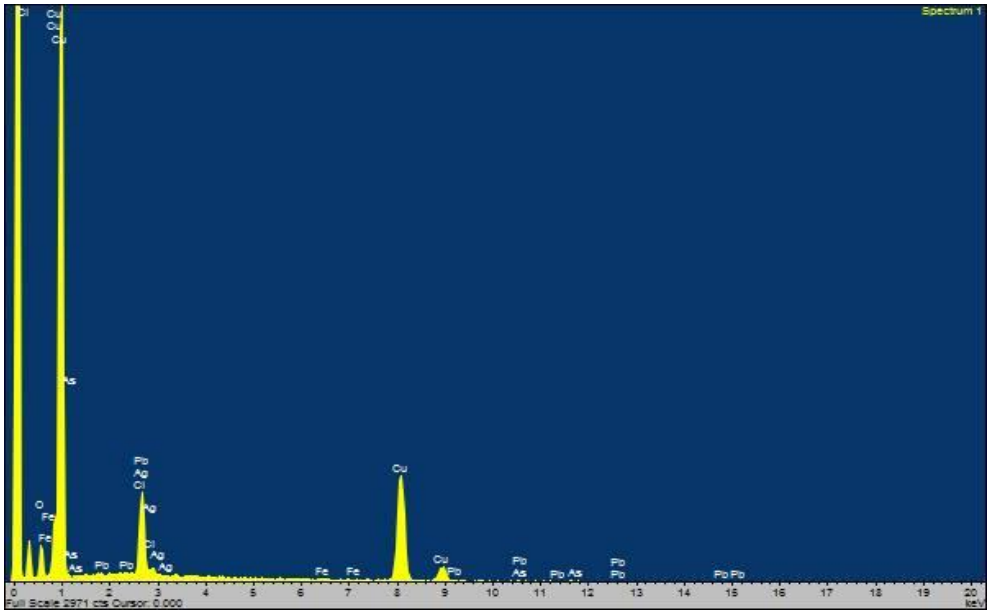

Spectra 89: First measurement of the object BW_18.

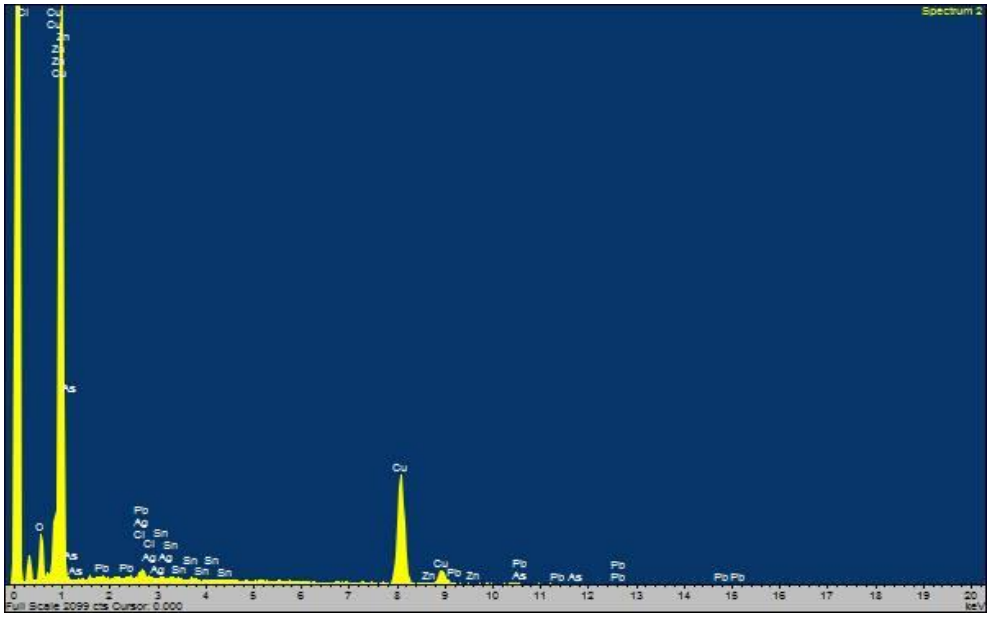

Spectra 90: Second measurement of the object BW_18.

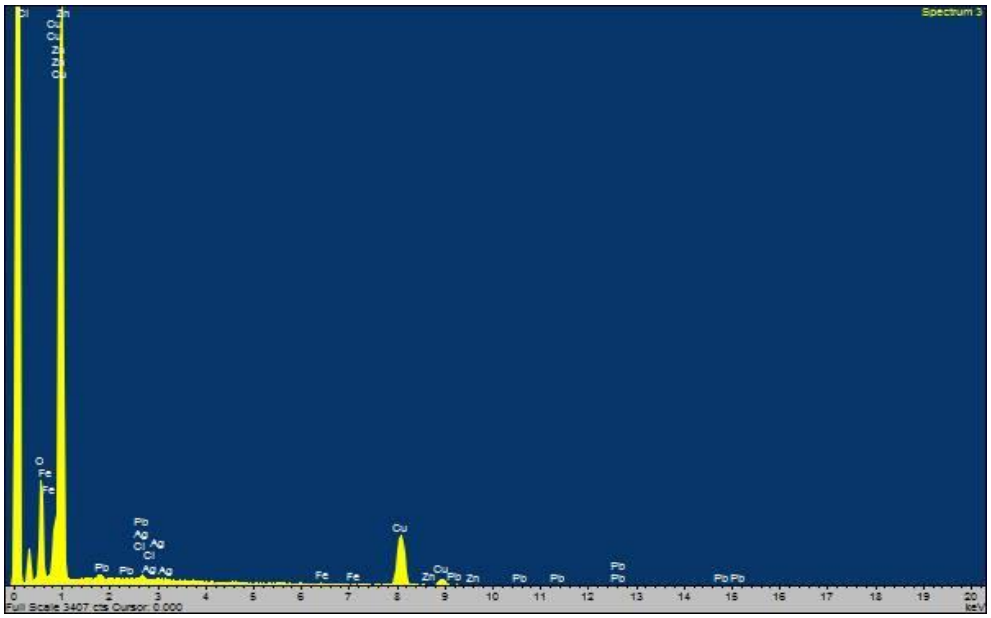

Spectra 91: Third measurement of the object BW_18.

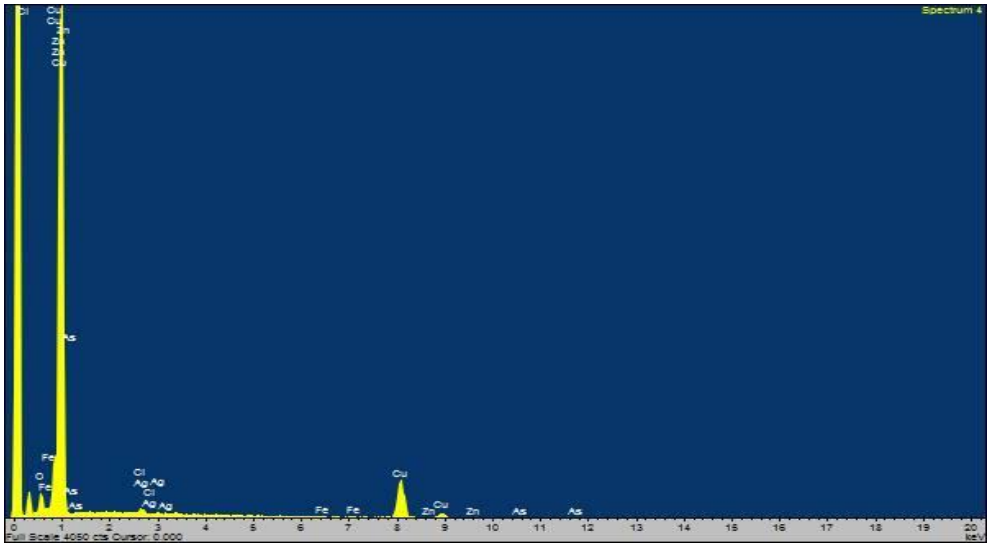

Spectra 92: Fourth measurement of the object BW_18.

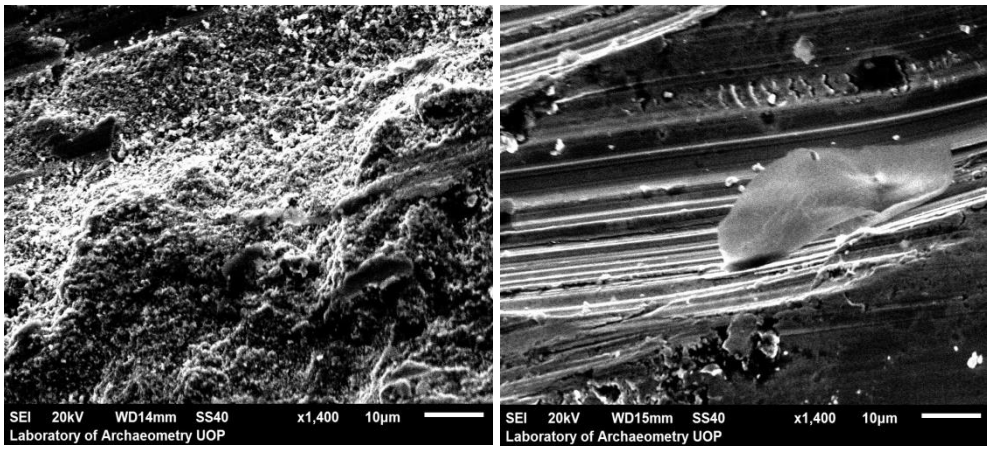

Images 29-30: Backscattered electron images in the SEM for the object BW_18. Magnification 1.400X. Compositional contrast that results from different atomic number elements and their distribution are displayed.

Left: an extremely high copper content area, containing also silver and lead (and chlorine caused by corrosion) (measurement 3 - spectra 91). Right: the highest copper content cleaned area, shown as almost homogeneous, containing also chlorine, caused by corrosion (measurement 4 - spectra 92).

Vessel Fragment assemblage

Table 17: The performed measurements of the object **KYT_AYV_VF_09** using SEM-EDS expressed in % wt. (m.: measurement, Av.: Average, St. Dev.: Standard Deviation, n.d.: non detected).

VF_09	m.1	m.2	m.3	m.4	m.5	m.6	m.7	m.8	Av.	St.Dev
Al_2O_3	n.d.	n.d.	n.d.	n.d.	n.d.	n.d.	n.d.	11,11	11,11	-
SiO_2	7,89	47,25	24,60	51,78	45,83	25,03	12,70	57,58	34,08	18,87
S	0,82	1,67	n.d.	2,83	n.d.	n.d.	n.d.	n.d.	1,77	1,01
Cl	2,48	3,15	2,32	3,41	2,47	2,79	4,37	n.d.	3,00	0,72
K_2O	n.d.	n.d.	n.d.	n.d.	n.d.	n.d.	n.d.	1,76	1,76	-
CaO	n.d.	1,71	n.d.	n.d.	2,67	n.d.	n.d.	7,47	3,95	3,09
FeO	0,40	0,89	0,22	0,56	0,36	0,69	0,46	1,51	0,64	0,41
Ni	n.d.	1,16	n.d.	n.d.	n.d.	n.d.	n.d.	0,68	0,92	0,34
CuO	86,84	41,39	69,30	40,25	44,79	67,81	74,90	13,68	54,87	23,88
ZnO	0,20	0,65	1,02	n.d.	n.d.	n.d.	2,40	n.d.	1,07	0,95
As_2O_3	0,67	1,15	0,55	0,74	n.d.	0,37	0,87	1,87	0,89	0,50
Ag	n.d.	n.d.	0,20	n.d.	0,87	0,12	n.d.	0,54	0,43	0,34
SnO_x	0,70	0,58	0,45	n.d.	1,10	1,70	2,71	2,47	1,39	0,92
PbO	n.d.	0,41	1,34	0,44	1,92	1,48	1,58	1,34	1,22	0,57

KYT_AYV_VF_09

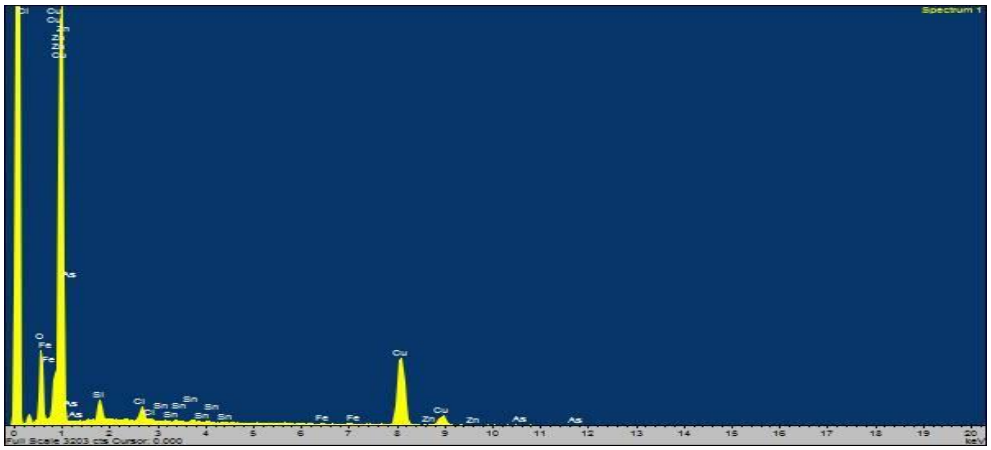

Spectra 93: First measurement of the object VF_09.

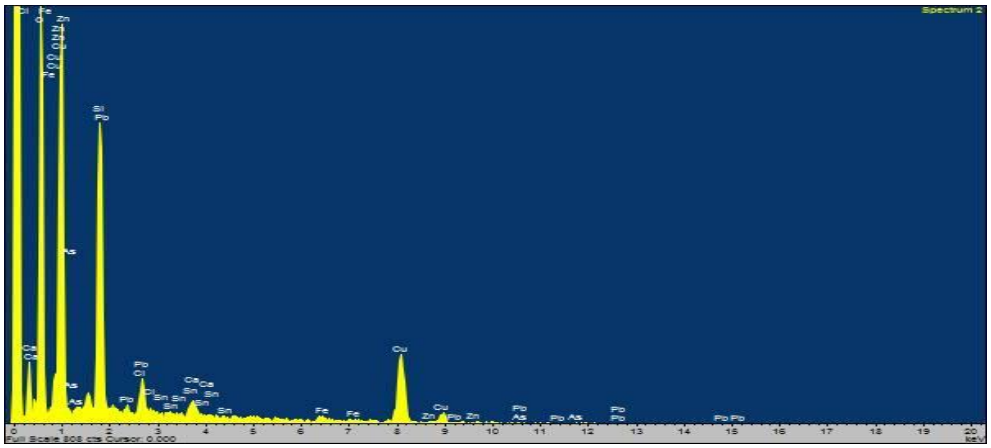

Spectra 94: Second measurement of the object VF_09.

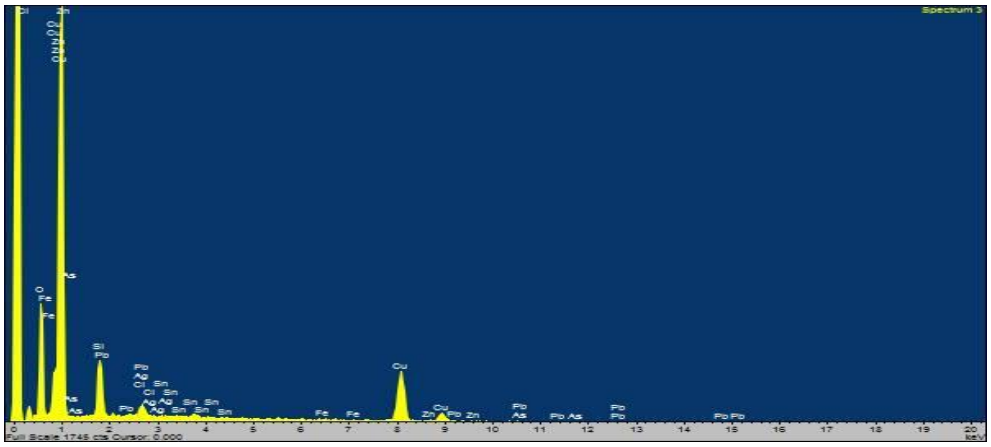

Spectra 95: Third measurement of the object VF_09.

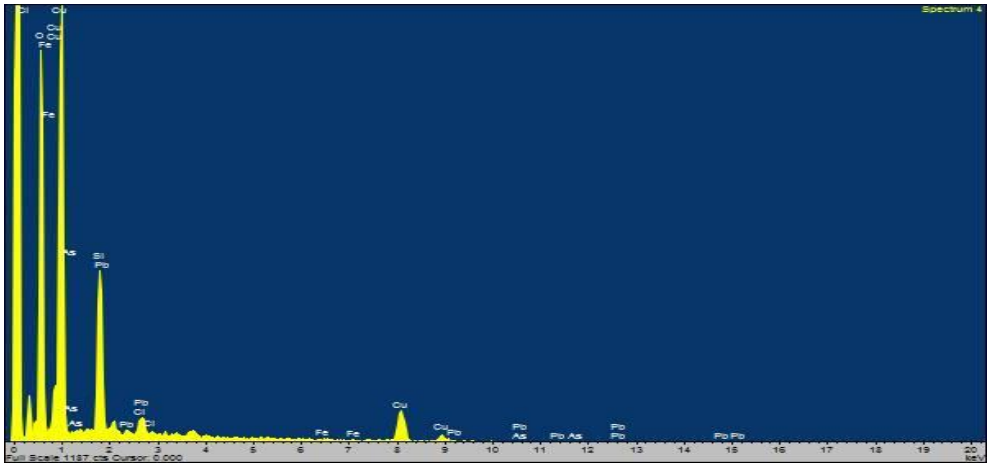

Spectra 96: Fourth measurement of the object VF_09.

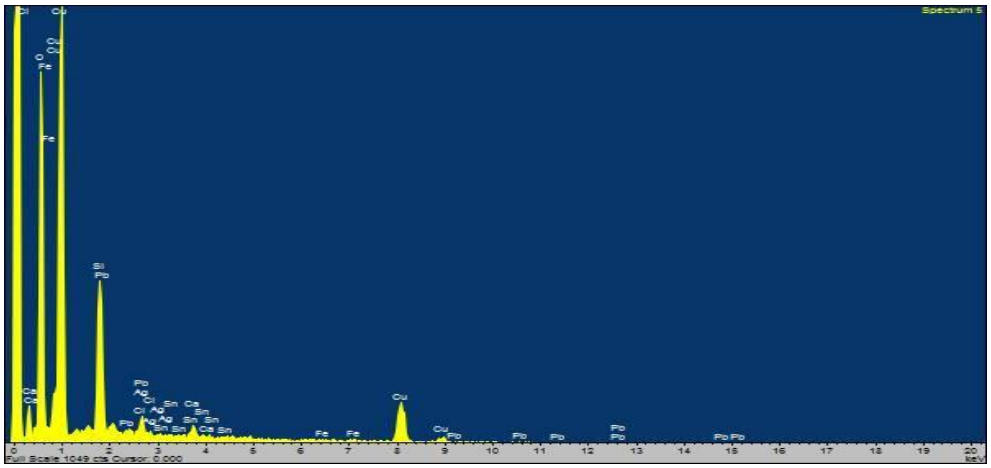

Spectra 97: Fifth measurement of the object VF_09.

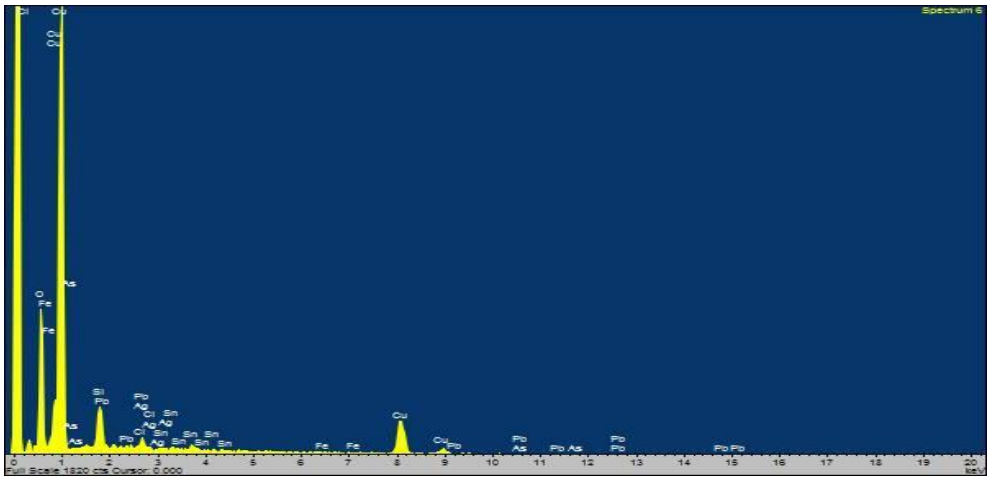

Spectra 98: Sixth measurement of the object VF_09.

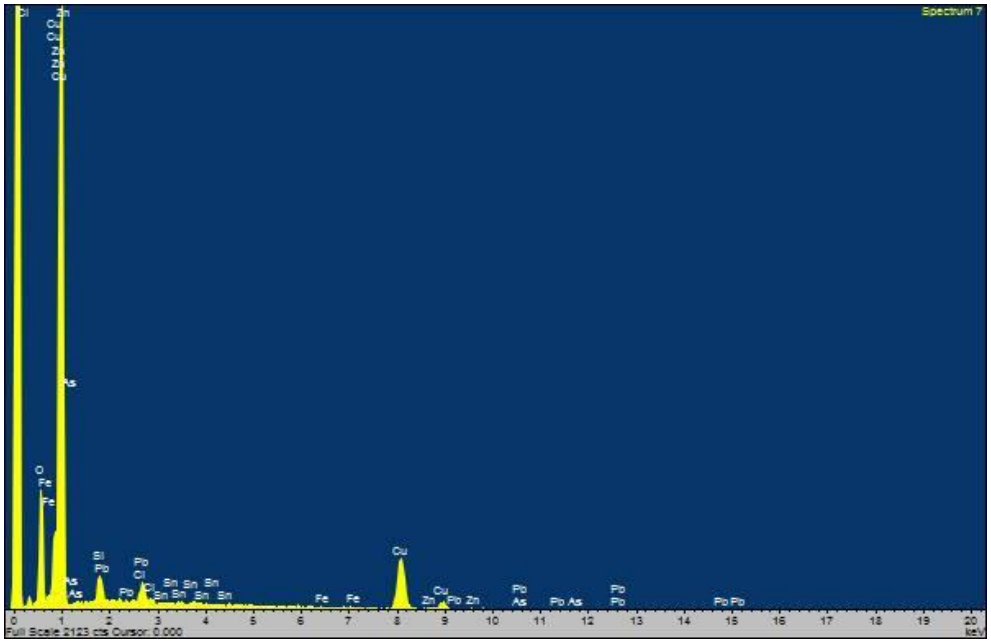

Spectra 99: Seventh measurement of the object VF_09.

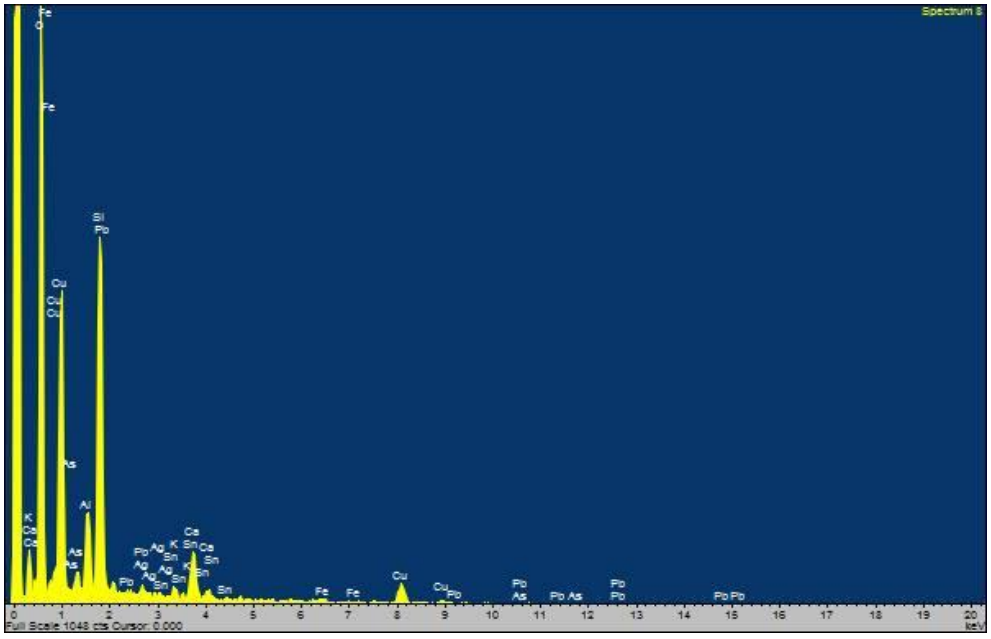

Spectra 100: Eighth measurement of the object VF_09.

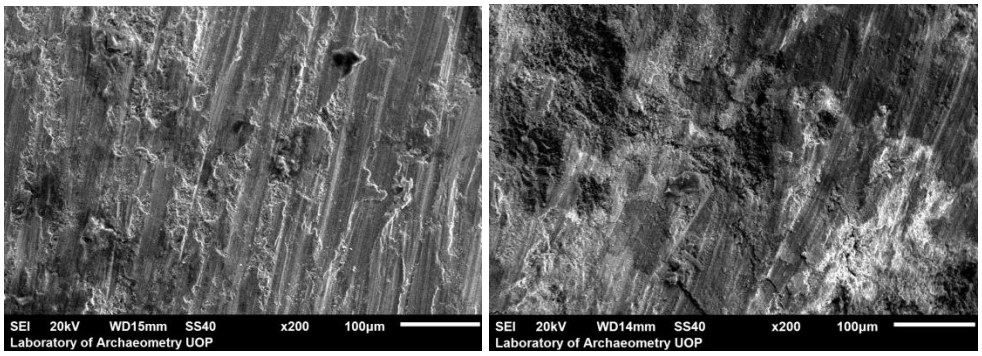

Images 31-32: Backscattered electron images in the SEM for the object VF_09. Magnification 200X. Compositional contrast that results from different atomic number elements and their distribution are displayed.

Left: partially cleaned area where the highest copper content has been detected (measurement 1 - spectra 93). Right: low copper content area where residues of soil encrustations and sulfur have been detected (measurement 4 - spectra 96).

Table 18: The performed measurements of the object **KYT_AYV_VF_11** using SEM-EDS expressed in % wt. (m.: measurement, Av.: Average, St. Dev.: Standard Deviation, n.d.: non detected).

VF_11	m.1	m.2	m.3	m.4	m.5	m.6	m.7	m.8	Av.	St.Dev
Al_2O_3	n.d.	n.d.	n.d.	n.d.	1,98	n.d.	n.d.	n.d.	1,98	-
SiO_2	n.d.	n.d.	n.d.	n.d.	n.d.	5,40	n.d.	n.d.	5,40	-
Cl	n.d.	n.d.	n.d.	1,12	0,83	n.d.	2,32	1,44	1,43	0,65
CaO	n.d.	n.d.	n.d.	n.d.	2,56	6,97	n.d.	n.d.	4,77	3,12
FeO	0,43	1,21	0,48	0,52	1,25	2,48	0,80	0,65	0,98	0,68
Ni	1,67	n.d.	1,70	0,84	1,00	1,85	0,62	0,72	1,20	0,52
CuO	49,58	49,49	46,22	54,47	72,22	51,63	71,35	58,27	56,65	10,01
ZnO	8,40	7,82	8,42	11,04	8,88	5,77	8,93	12,47	8,97	2,03
As_2O_3	0,27	0,47	1,38	0,73	1,03	1,00	0,96	1,19	0,88	0,37
Ag	0,56	n.d.	n.d.	n.d.	0,70	n.d.	n.d.	0,13	0,46	0,30
SnO_x	1,76	1,62	0,82	22,35	0,99	2,26	1,37	14,17	5,67	8,09
Sb_2O_5	6,77	8,36	9,90	2,81	6,10	16,42	4,20	6,73	7,66	4,17
PbO	30,56	31,02	31,08	6,12	2,47	6,22	9,44	4,23	15,14	13,19

KYT_AYV_VF_11

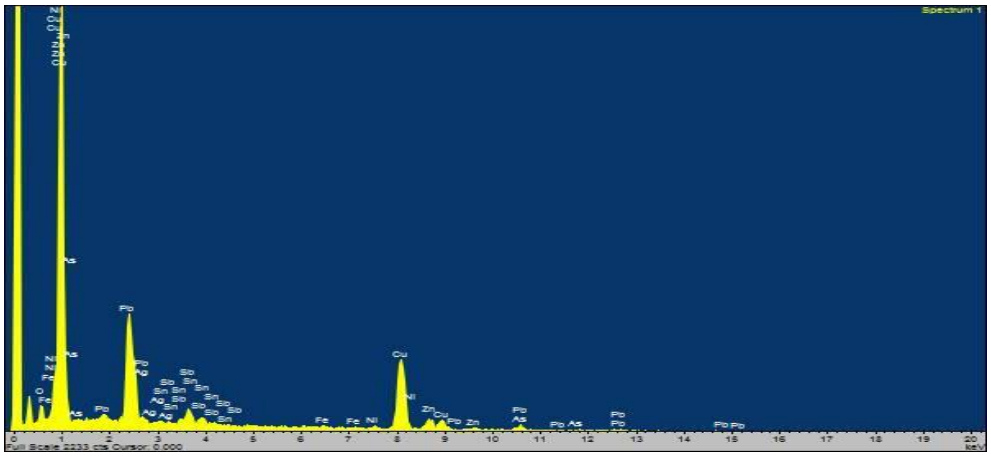

Spectra 101: First measurement of the object VF_11.

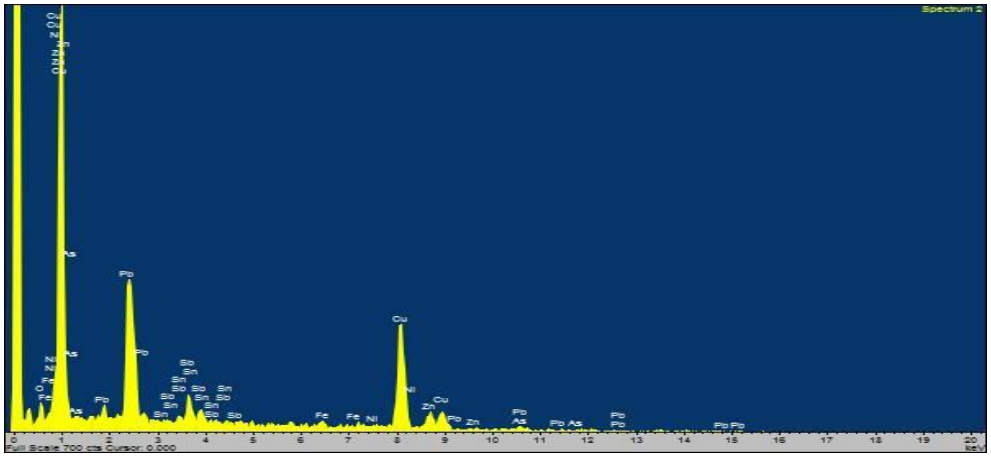

Spectra 102: Second measurement of the object VF_11.

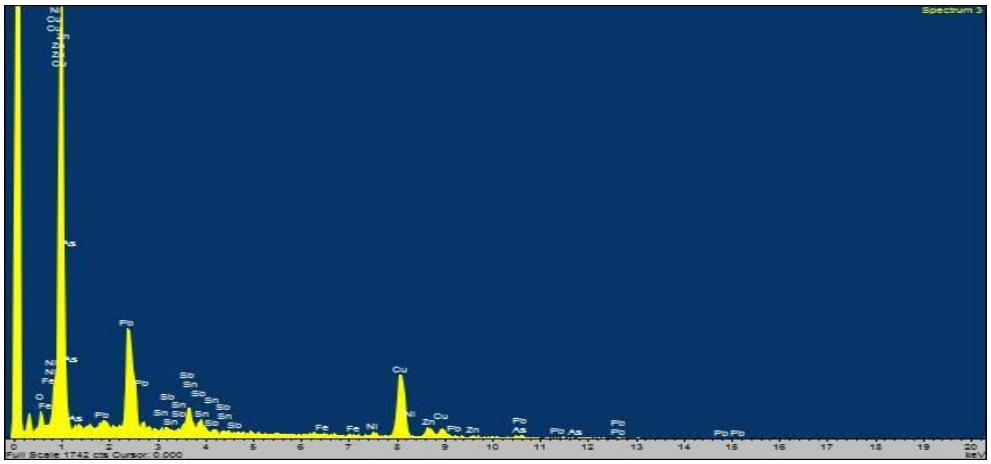

Spectra 103: Third measurement of the object VF_11.

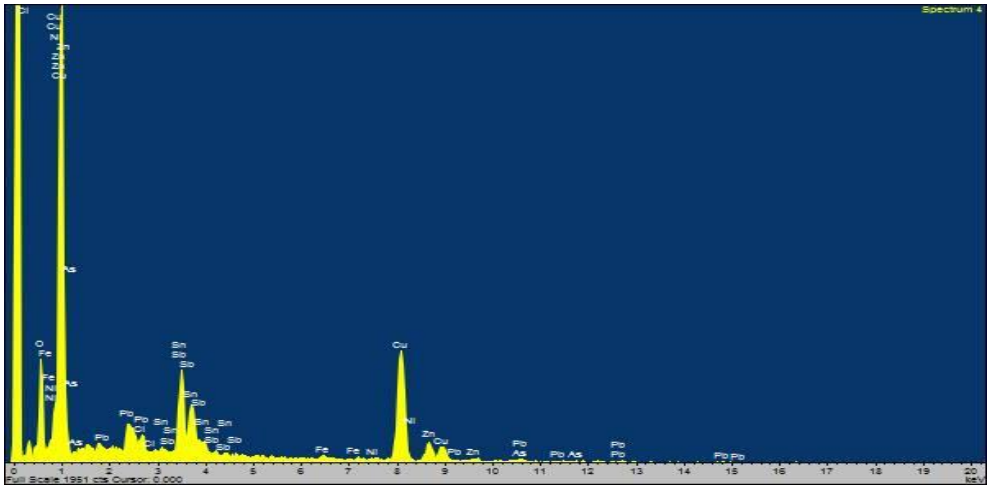

Spectra 104: Fourth measurement of the object VF_11.

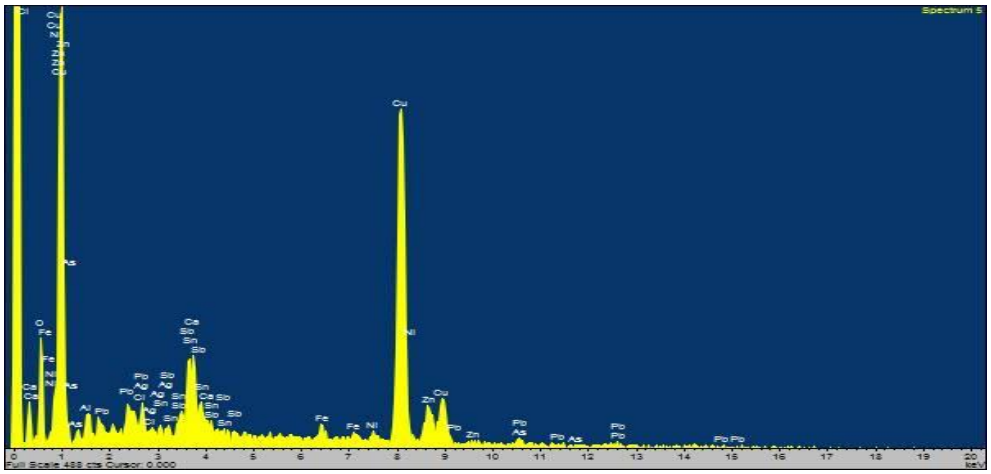

Spectra 105: Fifth measurement of the object VF_11.

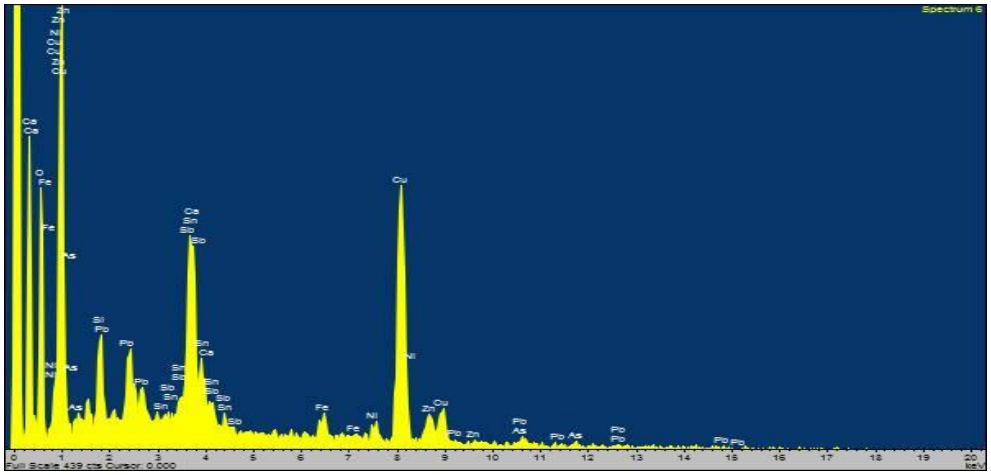

Spectra 106: Sixth measurement of the object VF_11.

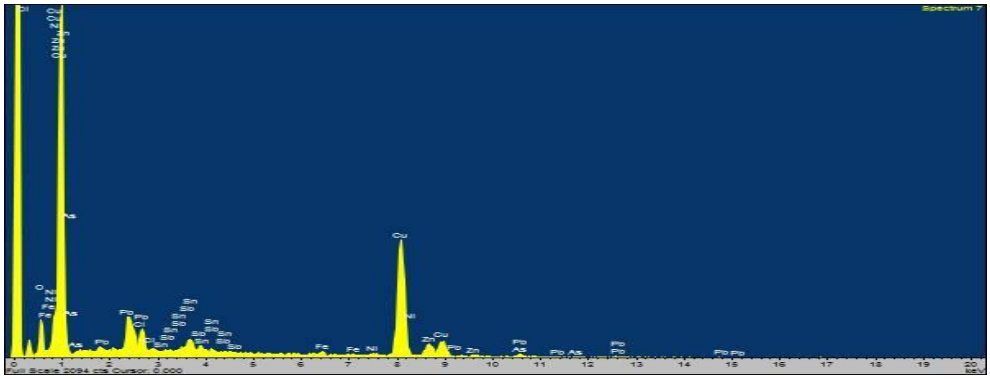

Spectra 107: Seventh measurement of the object VF_11.

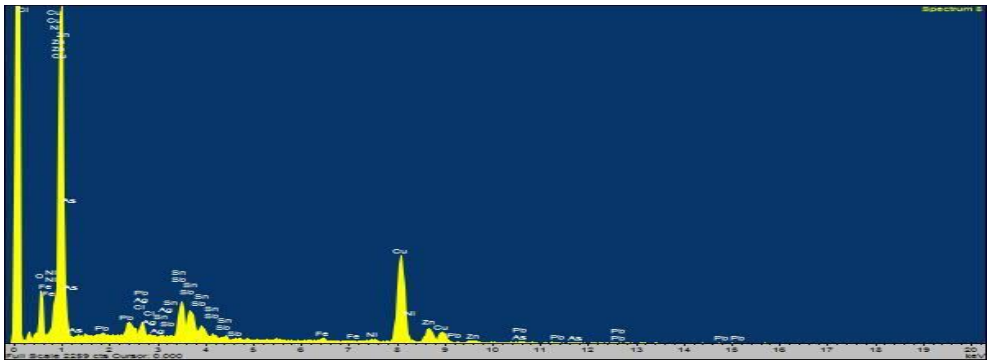

Spectra 108: Eighth measurement of the object VF_11.

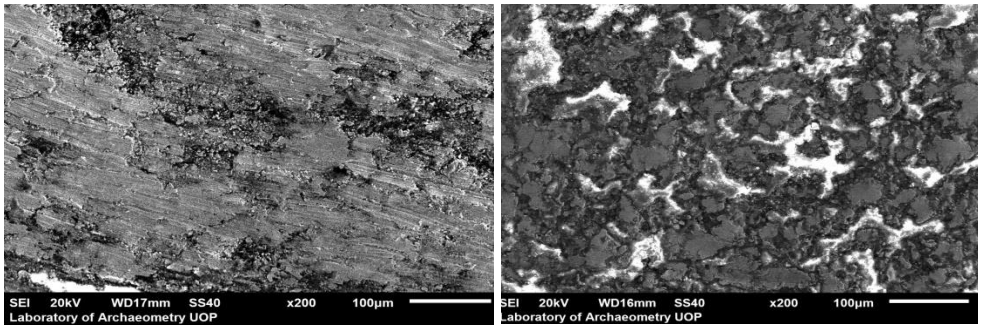

Images 33-34: Backscattered electron images in the SEM for the object VF_11. Magnification 200X. Compositional contrast that results from different atomic number elements and their distribution are displayed.

Left: the highest copper content area where the lowest lead content and a high zinc content have been detected (measurement 5 - spectra 105). Right: low copper content area where the lowest zinc and the highest antimony content have been detected. A significant lead amount also occurs (measurement 6 - spectra 106).

Table 19: The performed measurements of the object **KYT_AYV_VF_12** using SEM-EDS expressed in % wt. (m.: measurement, Av.: Average, St. Dev.: Standard Deviation, n.d.: non detected).

VF_12	m.1	m.2	m.3	m.4	m.5	m.6	Av.	St.Dev
Al_2O_3	n.d.	n.d.	n.d.	5,75	2,46	n.d.	4,11	2,33
SiO_2	n.d.	n.d.	2,06	11,63	6,53	n.d.	6,74	4,79
P_2O_5	0,84	2,29	4,11	5,00	2,81	2,29	2,89	1,47
Cl	2,22	1,59	1,21	1,86	1,31	1,71	1,65	0,37
CaO	n.d.	n.d.	n.d.	8,78	9,81	n.d.	9,30	0,73
FeO	1,10	1,22	2,69	4,92	5,77	2,00	2,95	1,96
Ni	n.d.	0,54	0,97	0,55	1,41	0,83	0,86	0,36
CuO	64,33	66,99	56,11	35,81	43,58	64,16	55,16	12,76
ZnO	11,54	10,53	9,89	8,20	12,51	11,39	10,68	1,51
As_2O_3	1,52	0,67	1,78	1,55	0,91	0,56	1,17	0,52
Ag	n.d.	n.d.	n.d.	0,21	0,33	n.d.	0,27	0,08
SnO_x	4,23	5,64	9,62	5,57	4,29	6,07	5,90	1,97
Sb_2O_5	3,21	3,29	3,96	5,18	5,70	3,13	4,08	1,11
PbO	11,02	7,23	7,61	4,99	2,59	7,87	6,89	2,85

KYT_AYV_VF_12

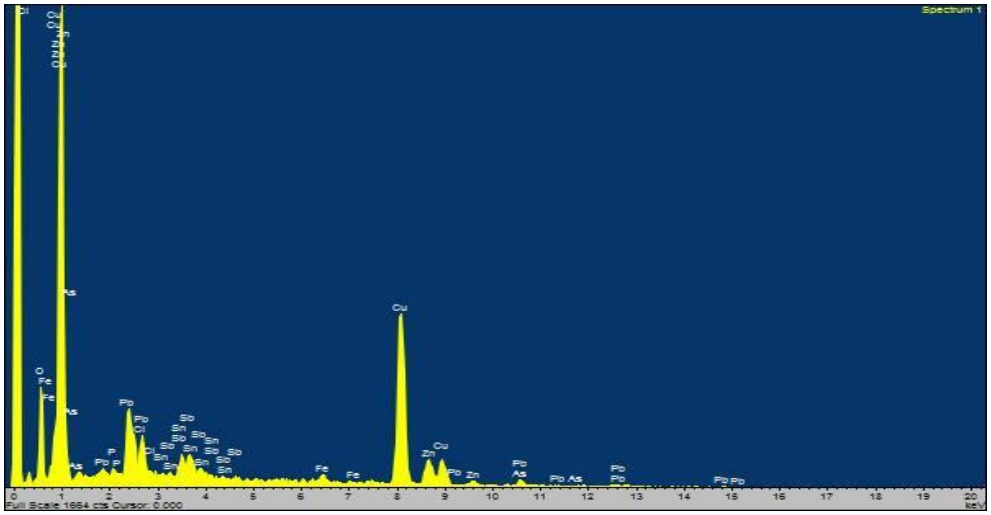

Spectra 109: First measurement of the object VF_12.

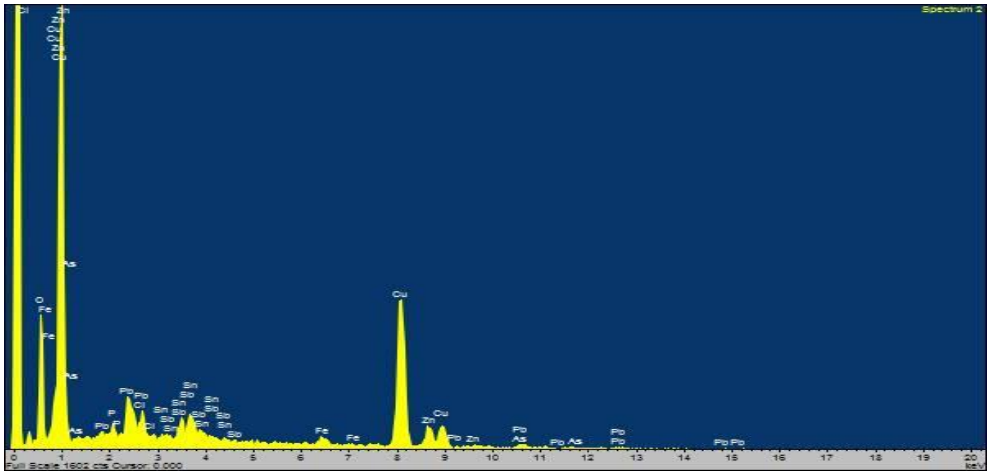

Spectra 110: Second measurement of the object VF_12.

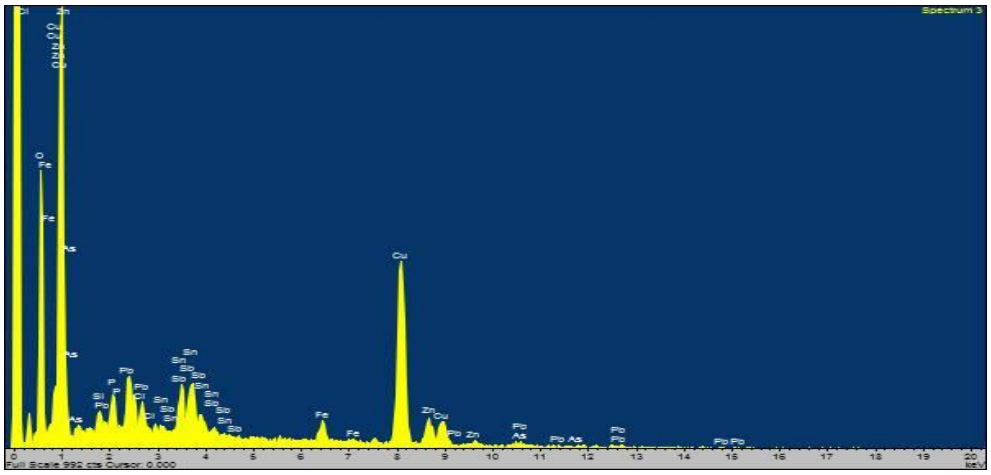

Spectra 111: Third measurement of the object VF_12.

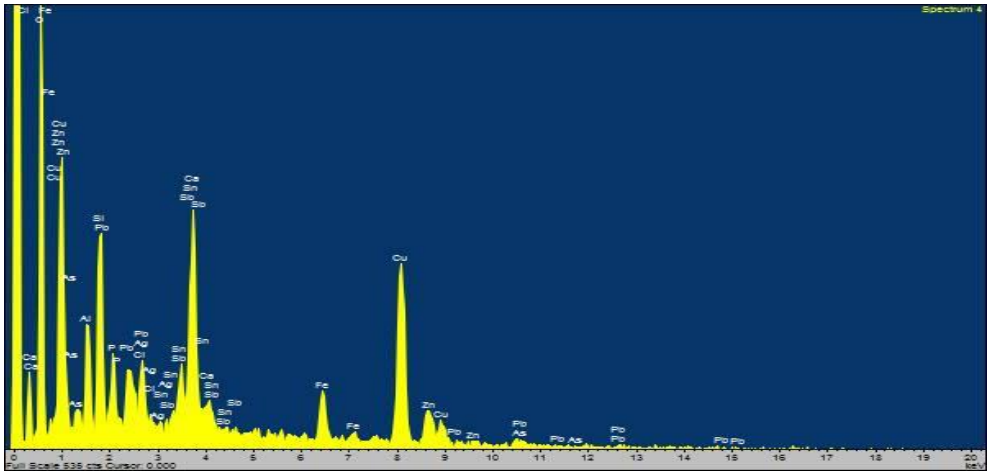

Spectra 112: Fourth measurement of the object VF_12.

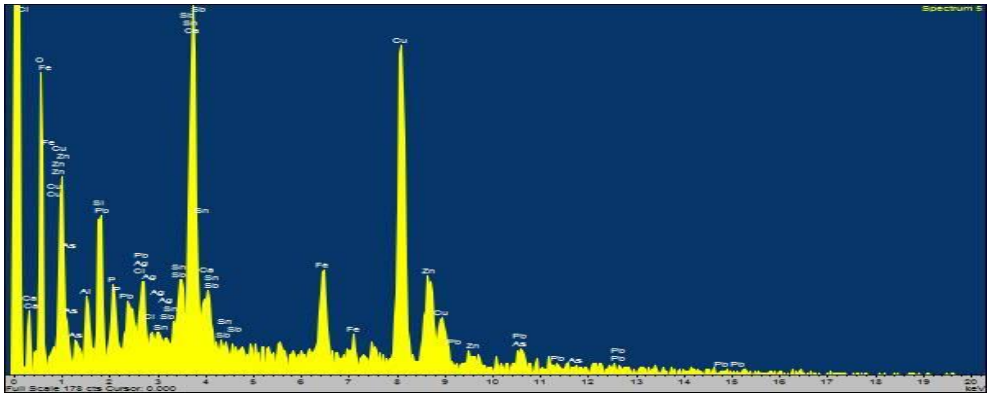

Spectra 113: Fifth measurement of the object VF_12.

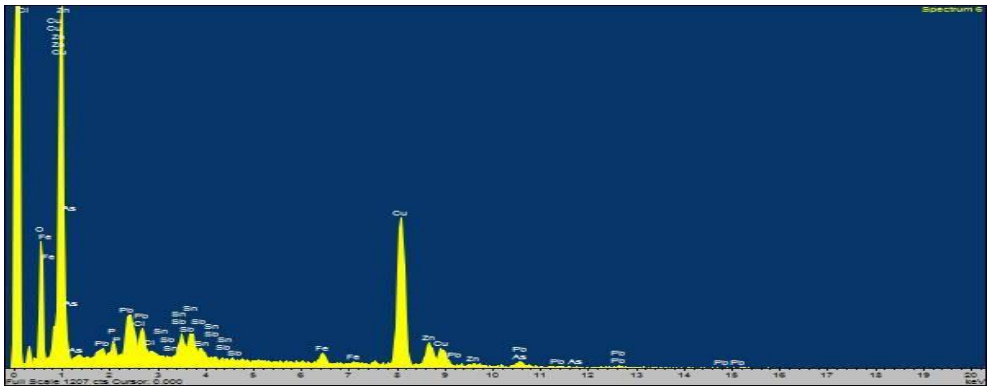

Spectra 114: Sixth measurement of the object VF_12.

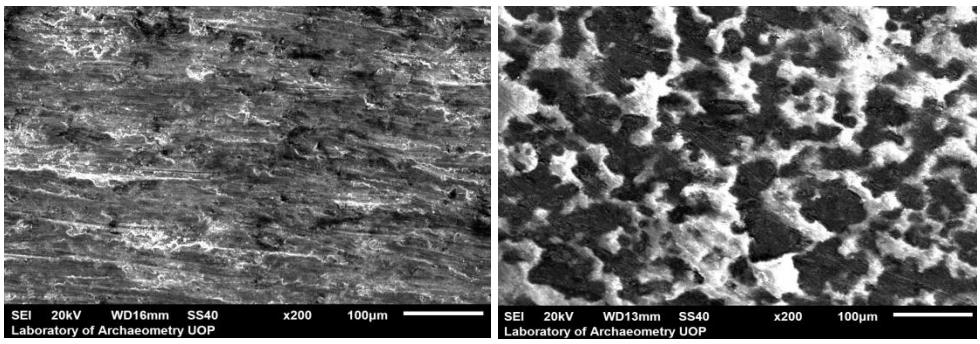

Images 35-36: Backscattered electron images in the SEM for the object VF_12. Magnification 200X. Compositional contrast that results from different atomic number elements and their distribution are displayed.

Left: the highest copper content area where amounts of zinc, tin, antimony and lead have been detected (measurement 2 - spectra 110). Right: partially cleaned low copper content area where the highest zinc content and amounts of tin, antimony and lead have been detected (measurement 5 - spectra 113).

Table 20: The performed measurements of the object **KYT_AYV_VF_13** using SEM-EDS expressed in % wt. (m.: measurement, Av.: Average, St. Dev.: Standard Deviation, n.d.: non detected).

VF_13	m.1	m.2	m.3	m.4	m.5	Av.	St. Dev.
FeO	0,35	n.d.	0,17	0,26	0,38	0,29	0,09
CuO	93,96	92,21	94,95	93,80	98,23	94,63	2,24
ZnO	4,67	6,79	4,43	5,26	0,51	4,33	2,33
As_2O_3	0,30	0,04	0,14	0,68	0,24	0,28	0,24
Ag	0,04	0,73	0,01	n.d.	n.d.	0,26	0,41
SnO_x	0,08	n.d.	0,29	n.d.	0,09	0,15	0,12
PbO	0,60	0,22	n.d.	n.d.	0,55	0,46	0,21

KYT_AYV_VF_13

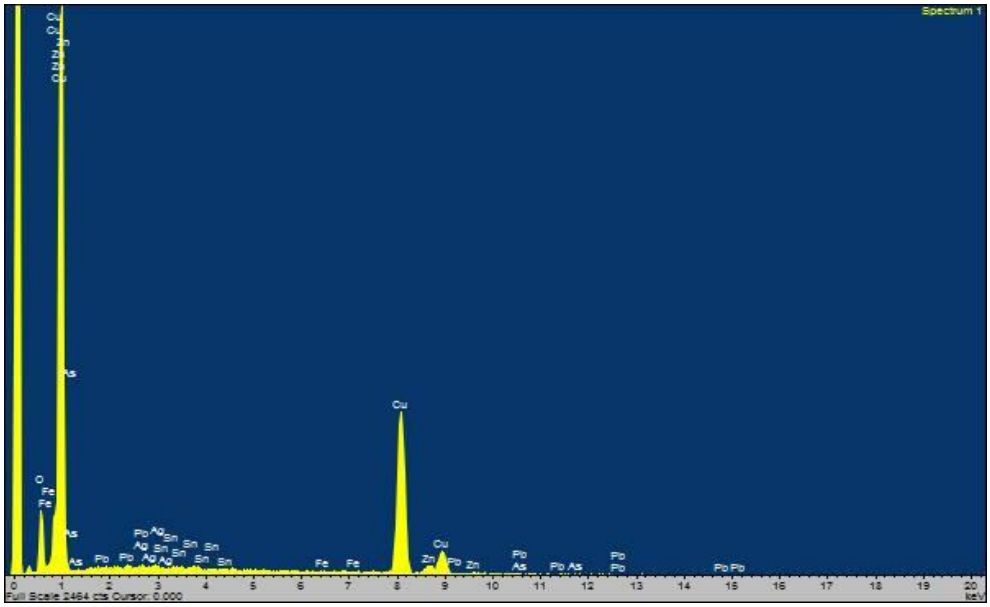

Spectra 115: First measurement of the object VF_13.

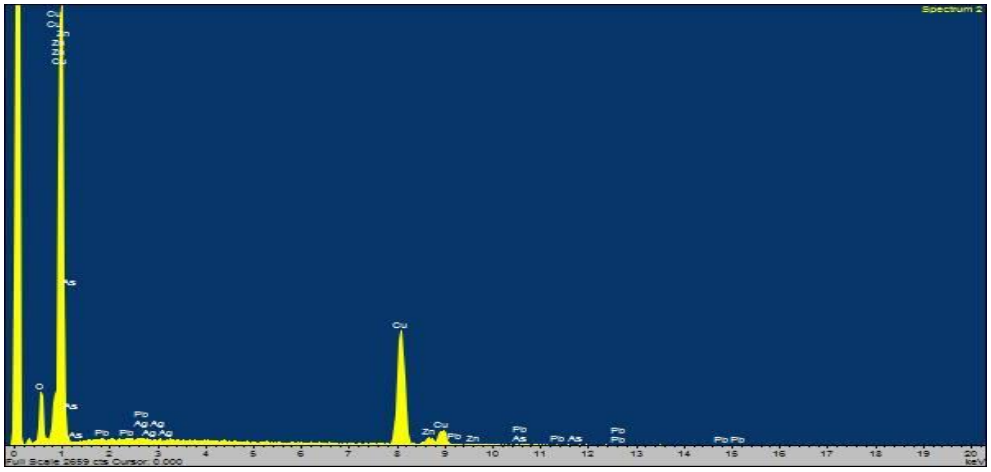

Spectra 116: Second measurement of the object VF_13.

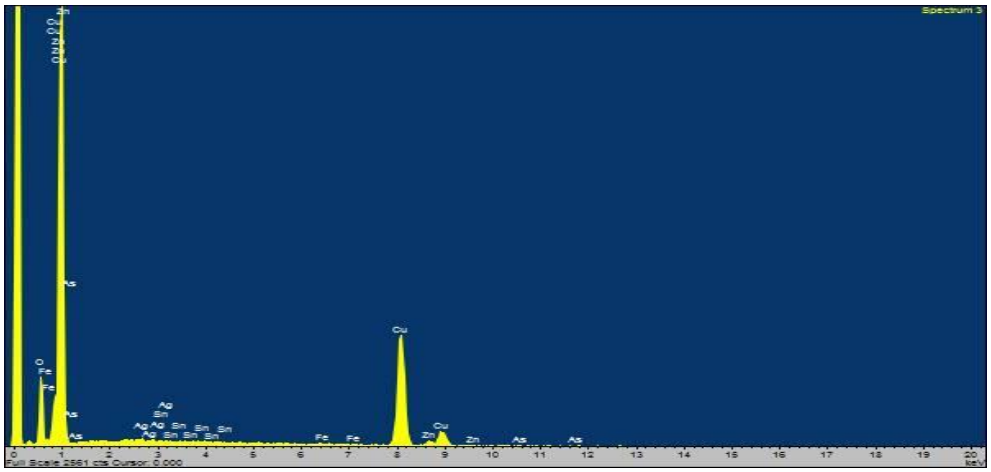

Spectra 117: Third measurement of the object VF_13.

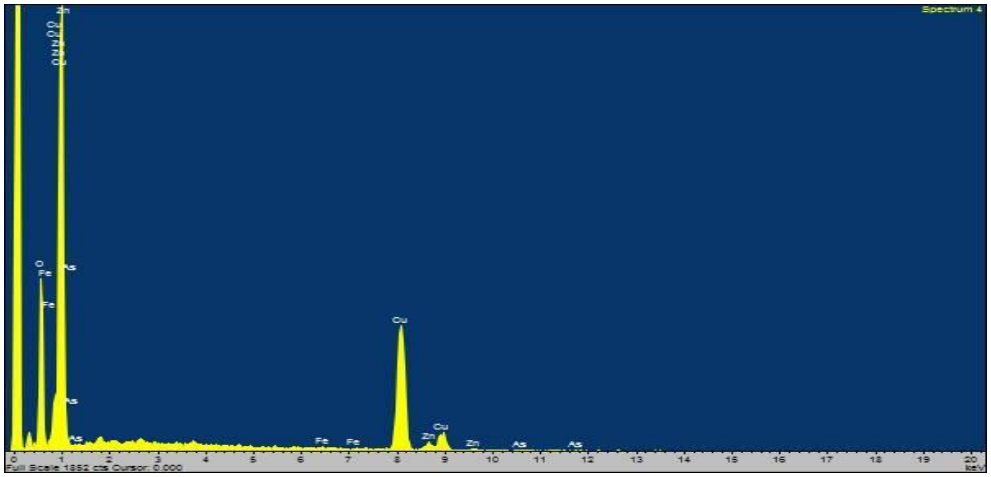

Spectra 118: Fourth measurement of the object VF_13.

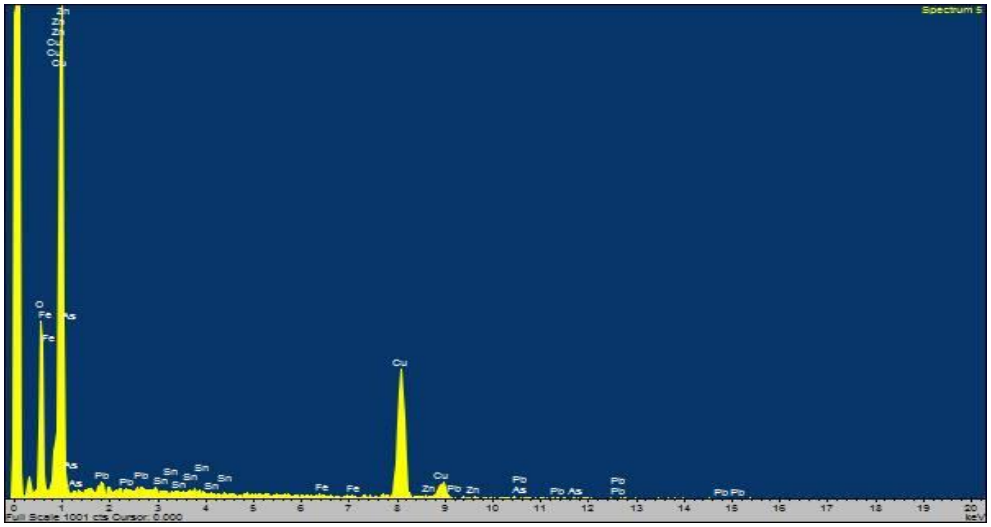

Spectra 119: Fifth measurement of the object VF_13.

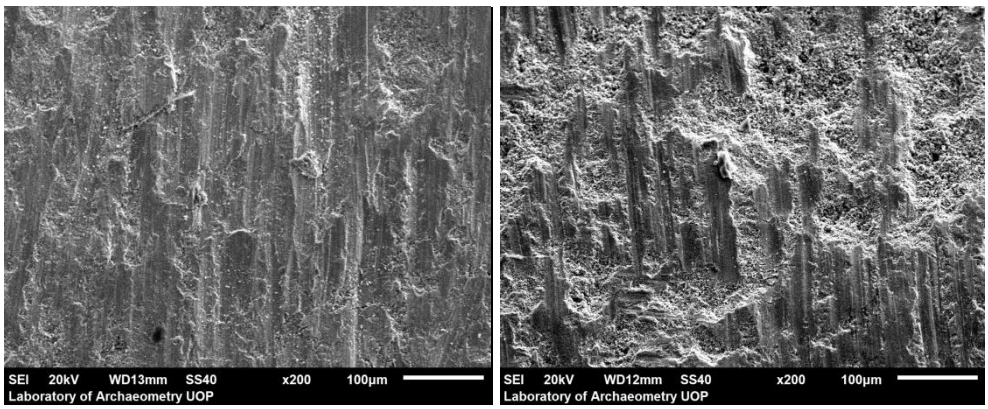

Images 37-38: Backscattered electron images in the SEM for the object VF_13. Magnification 200X. Compositional contrast that results from different atomic number elements and their distribution are displayed.

Left: high copper content area where the highest zinc amount occurs (measurement 2 - spectra 116). Right: the highest copper content area where the lowest zinc amount has been detected (measurement 5 - spectra 119).

Bibliography

Banou E. in press, The Sacred Land- and Seascape of Kythera: The Minoan Peak Sanctuary at Ayios Yeoryios sto Vouno, in Chr. Gallou, W. Cavanagh, J. Roy and L. Cavanagh, *From Prehistory to Post-Byzantine Times, 3rd CSPS International Conference, Sacred Landscapes in the Peloponnese,* Sparti,30 March - 1 April 2012.

Banou E. in press, Το Μινωικό Ιερό Κορυφής στον Άγιο Γεώργιο στο Βουνό Κυθήρων: Τα Νεότερα Αποτελέσματα της Αρχαιολογικής Έρευνας (2011-2013), in *Ι΄ Πανιώνιο Συνέδριο, Κέρκυρα 1-4 May 2014.*

Banou E. 2007, Μινωικά Ιερά Κορυφής: Η Περίπτωση του Αγίου Γεωργίου στο Βουνό Κυθήρων, in Ε. Κονσολάκη – Γιαννοπούλου, *Έπαθλον, Αρχαιολογικό Συνέδριο προς τιμήν του Αδώνιδος Κ. Κύρου,* Αθήνα, Α. Ε. Μπουλούκος & Σ^{ΙΑ} Ο.Ε., 285-291.

Bassiakos Y. and Tselios Th. 2012, On the Cessation of Local Copper Production in the Aegean in the 2nd Millennium BC, in V. Kassianidou and G. Papasavvas, *Eastern Mediterranean Metallurgy and Metalwork in the Second MillenniumBC, A Conference in Honour of James D. Muhly, Nicosia Cyprous 2009,* UK, Oxbow Books, 151-161.

Betancourt P. 2008, The Copper Smelting Workshop at Chrysokamino: Reconstructing the Smelting Process, in I. Tzachili *Aegean Metallurgy in the Bronze Age, Proceedings of an International Symposium Held at the University of Crete, Rethymnon, Greece, 2004*, Ta Pragmata, 105-111.

Broodbank C. and Kiriatzi E. 2007, The First 'Minoans' of Kythera Revisited:Technology, Demography, and Landscape in the Prepalatial Aegean, in *American Journal of Archaeology,* Vol. 111, 241-274.

Broodbank C., Rehren T. and Zianni A-M. 2007, Scientific Analysis of Metal Objects and Metallurgical Remains from Kastri, Kythera, *Annual of the British School at Athens 102,* 219-238.

Charalambous A., Kassianidou V. and Papasavvas G. 2015, A comparative Study of Cypriot Bronzes Dated to the Late Bronze and the Early Iron Age, in E. Photos-Jones *Proceedings of the 6th Symposium of the Hellenic Society for Archaeometry,* United Kingdom, British Archaeological Reports Ltd, 95-100.

Doonan R., Day P. M. and Dimopoulou-Rethimiotaki N. 2007, Lame excuses for emerging complexity in Early Bronze Age Crete: the metallurgical finds from Poros Katsambas and their context, in M. P. Day and R. Doonan, *Metallurgy in the Early Bronze Age Aegean, Sheffield Studies in Aegean Archaeology*, Great Britain, Oxbow, 98-122.

Ferretti M. 2014, The investigation of ancient metal artefacts by portable X-ray fluorescence devices, *J. Anal. At. Spectrom. 29,* 1753-1766.

Gale N., Papastamataki A., Stos-Gale Z. A. and Leonis K. 1985, Copper sources and Copper Metallurgy in the Bronze Age, in T. P. Craddock and M. Hughes *Furnaces and Smelting Technology in Antiquity,* London, British Museum Occasional Paper no 48, 81-102.

Gale H. N. and Stos-Gale Z. A. 1986, Oxide Copper Ingots in Crete and Cyprous, in *The Annual of the British School at Athens*, Vol. 81, 81-100.

Gale H. N., Kayafa M. and Stos-Gale Z. A. 2008, Early Helladic Metallurgy at Raphina, Attica, and the Role of Lavrion, in I. Tzachili, *Aegean Metallurgy in the Bronze Age, Proceedings of an International Symposium Held at the University of Crete, Rethymnon, Greece, 2004,* I. Ta Pragmata, 87-104.

Gale H. N., Kayafa M. and Stos-Gale Z. A. 2009, Further Evidence for Bronze Age Production of Copper from Ores in the Lavrion Ore District, Attica, Greece, *Proceedings of the 2nd International Conference Archaeometallurgy in Europe, Aquileia 2007*, Milan, 158-176.

Gale H. N., Stos-Gale Z. A. 2012, The role of Apliki Mine Region in the Post c. 1400BC Copper Production and Trade Networks in Cyprus and in the Wider Mediterranean, in V. Kassianidou and G. Papasavvas *Eastern Mediterranean Metallurgy and Metalwork in the Second MillenniumBC, AConference in Honour of James D. Muhly, Nicosia Cyprous 2009,* UK, Oxbow Books, 70-82.

Georgakopoulou M. 2004, Examination of Copper Slags from the Early Bronze Age Site of Daskaleio-Kavos on the island of Keros (Cyclades,Greece), *Institute of Archaeo-Metallurgical Studies 24,* 3-12.

Georgakopoulou M. and Bassiakos Y. 2010, Η Παραγωγή των Αρχαίων Μετάλλων και η Μελέτη των Αντίστοιχων Καταλοίπων, in Ι. Λυριτζής and Ν. Ζαχαριάς, *ΑρχαιοΥλικά,*Αθήνα, Παπαζήση, 419-442.

Georgakopoulou M. and Bassiakos Y. 2015, Μεταλλουργικές δραστηριότητες και χρήση των μετάλλων στο Παλαμάρι, in Λ. Παρλαμά, Μ. Θεοχάρη, Χ. Ρωμανού and Στ. Μπονάτσος, *Ο Οχυρωμένος Προϊστορικός Οικισμός στο Παλαμάρι της Σκύρου, Διεπιστημονική Συνάντηση για το Έργο Έρευνας και Ανάδειξης,* 23-24 Οκτωβρίου 2012,. Αθήνα, Υπουργείο Πολιτισμού, Παιδείας και Θρησκευμάτων, Γενική Διεύθυνση Αρχαιοτήτων και Πολιτιστικής Κληρονομιάς, Διεύθυνση Προϊστορικών και Κλασικών Αρχαιοτήτων, Επιστημονική Επιτροπή Έργου Παλαμαρίου Σκύρου, 347-366.

Gillis C. and Clayton R. 2008, Tin and the Aegean in the Bronze Age, in I. Tzachili, *Aegean Metallurgy in the Bronze Age, Proceedings of an*

International Symposium Held at the University of Crete, Rethymnon, Greece, 2004, Ta Pragmata, 133-142.

Giumlia-Mair A., Kassianidou V and Papasavvas G. 2011, "Miniature Ingots from Cyprus" in Ph.P. Betancourt and S.C Ferrence, *Metallurgy: Understanding How, Learning Why*, Philadelphia: INSTAP Academic Press, 11-19.

Hafner B., Energy Dispersive Spectroscopy on the SEM; A Primer, in http://www.charfac.umn.edu/instruments/eds_on_sem_primer.

Hatsisavvas S. 2011, Broken Symbols: Aspects of Metallurgy at Alassa, in Ph.P. Betancourt and S.C Ferrence, *Metallurgy: Understanding How, Learning Why*, Philadelphia: INSTAP Academic Press, 21-27.

Karydas A.G. 2007, Application of a portable XRF Spectrometer for the non-invasive analysis of museum metal artefacts, *Annali di Chimica 97*, 419-432.

Karydas A.G., Katzamani D., Bernard R., Barrandon J. N. and Zarkadas Ch. 2004, A composition study of a museum jewellery collection (7th-1st BC) by means of a portable XRF spectrometer, Nuclear Instruments and Methods, in *Physics Research B*, 226, 15-28.

Katapotis M. and Bassiakos Y. 2007, Copper smelting at the Early Minoan Site of Crysokamino on Crete, in P. Day and R. Doonan, *Metallurgy in the Early Bronze Age Agean*, Great Britain, *Oxbow* books, 68-83.

Kourkoumelis D. 2011, Θαλάσσιοι Ορίζοντες του Αγίου Γεωργίου στο Βουνό, in Γ. Σακελλαράκη, *Κύθηρα το Μινωικό Ιερό Κορυφής στον Άγιο Γεώργιο στο Βουνό 1: Τα Προανασκαφικά και η Ανασκαφή*, Αθήνα, Η εν Αθήναις Αρχαιολογική Εταιρεία αρ.271, 75-111.

Liritzis I. and Zacharias N. 2011, Portable XRF of Archaeological Artifacts: Current Research, Potentials and Limitations, ch.6, in M. S. Shackley, *X-Ray Fluorescence Spectrometry (XRF) in Geoarchaeology*, USA, Springer, 109-142.

Lytitzis I. 2007, *Φυσικές Επιστήμες στην Αρχαιολογία*, Αθήνα, Γ. Δαρδάνος, Τυπωθήτω.

Mangou E. and Ioannou P. 1997, On the Chemical Composition of Prehistoric Greek Copper-based Artefacts from the Aegean Region, *The Annual of the British School at Athens*, Vol. 92, 59 – 72.

Mangou E. and Ioannou P. 2000, Studies of the Late Bronze Age copper-based ingots found in Greece, *The Annual of the British School at Athens*, Vol. 95, 207-217.

Muhly J. 2004, Chrysokamino and the Beginnings of Metal Technology on Crete and in the Aegean, in P. Day, M. Mook and J. Muhly, *Crete Beyond the Palaces: Proceedings of the Crete 2000 Conference*, USA, INSTAP Academic Press, 283-290.

Muhly J. 2006, Chrysokamino and Early Metallurgy, in P. Betancourt, *The Crysokamino Metallurgy Workshop and its Territory,* Hesperia ch.36, The American School of Classical Studies at Athens, 155-177.

Musilek L., Cechak T. and Trojek T. 2012, X-ray fluorescence in investigations of cultural relics and archaeological finds, *Applied Radiation and Isotopes 70*, 1193-1202.

Palmieri A., Begemann F., Schmitt-Strecker S. and Hauptmann A. 2002, Chemical Composition and Lead Isotopy of Metal Objects from the "Royal" Tomb and Other Related Finds at Arslantepe, Eastern Anatolia, in *Paléorient,* vol. 28, n°2, France, CNRS, 43-69.

Papadimitriou G. 2001, Simulation Study of Ancient Bronzes: Their Mechanical and Metalworking Properties, in I. Μπασιάκος, Ε. Αλούπη and Γ. Φακορέλλης, *Αρχαιομετρικές Μελέτες για την Ελληνική Προϊστορία και Αρχαιότητα,* Αθήνα, ΕΑΕ and ΕΜΑΣ, 713-733.

Papadimitriou G. 2008, The Technological Evolution of Copper Alloys in the Aegean During the Prehistoric Period, in I. Tzachili, *Aegean Metallurgy in the Bronze Age, Proceedings of an International Symposium Held at the University of Crete, Rethymnon, Greece, 2004,* Ta Pragmata, 271-287.

Sakellarakis Y. 2013, *Κύθηρα ο Άγιος Γεώργιος στο Βουνό Μινωική Λατρεία και Νεώτεροι Χρόνοι,* Αθήνα, Η εν Αθήναις Αρχαιολογική Εταιρεία αρ.287.

Sakellarakis Y. 2011, Η Ανασκαφή, in Γ. Σακελλαράκη, *Κύθηρα το Μινωικό Ιερό Κορυφής στον Άγιο Γεώργιο στο Βουνό 1: Τα Προανασκαφικά και η Ανασκαφή,* Η εν Αθήναις Αρχαιολογική Εταιρεία αρ.271,145-345.

Sakallarakis Y. 1996, Minoan Religious Influence in the Aegean: The Case of Kythera, *Annual of the British School at Athens 91,* 81-99.

Sapouna-Sakellaraki E. 2012, Χάλκινα Ειδώλια, in Γ. Σακελλαράκη, *Κύθηρα το Μινωικό Ιερό Κορυφής στον Άγιο Γεώργιο στο Βουνό 2: Τα Ευρήματα,* Αθήνα, Η εν Αθήναις Αρχαιολογική Εταιρεία αρ.276, 1-212.

Smith D. 2012, Handheld XRF analysis of Renaissance bronzes: Practical approaches to quantification and acquisition, in A. Shugar and J. Mass, *Handheld XRF for Art and Archaeology*, Studies in Archaeological Sciences, 37-74.

Soles J. 2008, Metal Hoards from LM IB Mochlos, Crete, in I. Tzachili, *Aegean Metallurgy in the Bronze Age, Proceedings of an International Symposium Held at the University of Crete, Rethymnon, Greece, 2004,* Ta Pragmata, 143-156.

Stos-Gale S. 2000, Trade in metals in the Bronze Age Mediteranean: an overview of Lead Isotope data for provenance studies, in *Metals Make the World Go Round. The supply and circulation of metals in Bronze Age Europe, Proceedingsof a Conference Held at the University of Birmingham 1977,* Great Britain, Oxbow books, 56-69.

Stos-Gale Z. A. and Gale N. H. 2006, Lead Isotope and Chemical Analyses of Slags from Chrysokamino, in *The Chrysokamino Metallurgy Workshop and Its Territory,* Hesperia Supplements, Vol. 36, American School of Classical Studies at Athens, 299-319.

Tselios Ch., Filippaki E. and Korres G. 2015, Selective use of arsenical copper during the Mycenaean period: the evidence from Pylia, in Messenia, Greece, *Proceedings of the 6th Symposium of the Hellenic Society for Archaeometry* 40, 81-88.

Tselios T. 2008, *Η Μεταλλουργία του Χαλκού στην Προανακτορική Κρήτη*, Αθήνα, Καρδαμίτσα.

Tzachili I. 2008, Aegean Metallurgy in the Bronze Age: Recent Developments, in I. Tzachili, *Aegean Metallurgy in the Bronze Age, Proceedings of an International Symposium Held at the University of Crete, Rethymnon, Greece, 2004,* Ta Pragmata, 7-34.

Webb J., Frankel D., Stos- Gale Z. A. and Gale N. H. 2006, Early Bronze Age Metal Trade in the Eastern Mediterranean. New Compositional and Lead Isotope Evidence from Cyprus, in *Oxford Journal of Archaeology 25(3)*, UK, Blackwell, 261–288.

https://hellenicum.wordpress.com

http://kalamata.uop.gr/~archaeolab